Imperial College London

PROCESSING THE PROBLEMATIC FINE FRACTION OF INCINERATOR BOTTOM ASH INTO A RAW MATERIAL FOR MANUFACTURING CERAMICS

PhD Thesis

ATHANASIOS BOURTSALAS

August 2015

Faculty of Engineering

Department of Civil and Environmental Engineering

I, ATHANASIOS BOURTSALAS, confirm that the work presented in this PhD thesis is my own original work

Signature: ATHANASIOS BOURTSALAS

Date:

ABSTRACT

The aim of this research was to develop a novel thermal treatment technology able to transform the problematic fine fraction of incinerator bottom ash (IBA) into an inert material suitable for the production of ceramics.

In this project two different problematic fractions of fine IBA have been used. The less than 1mm fraction of processed fine IBA dust was obtained from the dry discharge system for IBA used in the Energy from Waste (EfW) plant at Monthey, Zurich. The dry discharged fine IBA dust from the Monthey plant is currently disposed of to landfill at high cost. The second fine IBA fraction was supplied by Day Group who process wet discharge IBA from the Lakeside and the Newhaven EfW facilities in the South of England. There are currently no beneficial uses for the fine fraction which is either blended back into coarser fractions or disposed of to landfill.

The conclusion from the research is that the fine fractions of IBA generated from both discharge techniques can be transformed into an inert material suitable for the production of hard, dense ceramics. Processing involves the addition of glass, wet ball milling and calcining, pressing and sintering. The addition of glass aids liquid phase sintering and improves the appearance of the ceramic body formed, milling increases sintering reactivity and calcining limits the loss of volatiles and shrinkage during firing. This transforms the major crystalline phases present in the fine IBA fraction from quartz (SiO_2), calcite ($CaCO_3$), gehlenite ($Ca_2Al_2SiO_7$) and hematite (Fe_2O_3), to the pyroxene group minerals diopside ($CaMgSi_2O_6$) and clinoenstatite ($MgSi_2O_6$), together with some andradite ($Ca_3Fe_2Si_3O_{12}$). Processed calcined powders can be pressed and sintered to form dense (>2.5 g/cm^3), hard ceramics that exhibit low firing shrinkage (<7%), zero water absorption and minimal leaching. Calcining the IBA: glass powders before processing was able to minimize the linear shrinkage observed compared to samples produced using uncalcined powders. Calcining also had the effect of reducing the leaching of metals of environmental concern present in the fine IBA fraction by over 95%. These are encapsulated within the glassy phases present in the calcined and sintered materials.

ACKNOWLEDGEMENTS

I cannot find the right words to describe my sincere gratitude to Prof. Chris Cheeseman. He has been a wonderful supervisor and has guided me in all situations and hard times during this project. Thank you for everything, and thank you for always being there every day to discuss. It has been a life changing experience for me here in London and you have contributed greatly into that. I would like to thank Prof. Nickolas Themelis for his constant support and encouragement and Prof. Sue Grimes and Dr. Luc Vandeperre for their invaluable input throughout my studies.

My sincere thanks to Dr. Ralf Koralewska and the team of Martin Gmbh for giving me strength and support to fulfil the expectations of my PhD.

I am also grateful to Martin Gmbh, the Waste-to-Energy Research and Technology Council (GWC), Wheelabrator Technologies for financially supporting this research, Day Group for their support and the Civil &Environmental Engineering Department for supporting my studies with the Dixon Scholarship.

I would like to thank Dr. Geoff Fowler, Mrs. Carol Edwards and Dr. Karl Smith in the Roger Perry laboratory for their technical help and support.

My special thanks to my 307A friends who are still here and who have already left to business. Every one of you has contributed in this thesis with their sincere advice and guidance, thank you for everything.

I would like to thank Hara (kommati), George, Gregory, Elias, Toni, Korina, Marielena, Filipos, Andreas, Rhea, Titikou, Thanos, Nicolas, Rob, Kostis, Charis, and Petros for their support and good times outside the lab.

Finally I am grateful to members of my family, particularly my parents Christos and Dimitra and my sister, Athina for their care, concern and support. Many thanks to Maria, Kotsos,

Fifi, Charitini, Tomaso, Efi, Alexandros, Froso, Kostas (who has also served as my spiritual father), Kiki, Vasilis and Marcia. They were the source of my inspiration, strength and encouragement.

TABLE OF CONTENTS

LIST OF FIGURES

LIST OF TABLES

LIST OF ABBREVIATIONS

ANC	Acid Neutralization Capacity
ANOVA	Analysis of Variance
APC	Air Pollution Control Residues
ASTM	American Standard for Testing and Materials
BSI	British Standards Institution
CCGT	Combined Cycle Gas Turbine
CEN	European Committee for Standardization
DEFRA	Department of the Environment, Food and Rural Affairs
DOE	Design of Experiments
DOM	Desirability Optimization Methodology
DTA	Differential Thermal Analysis
ECS	Eddy current separation
EfW	Energy from Waste
ESP	Electrostatic Precipitator
IA	Incinerator Ash
IAWG	International Ash Working Group
IBA	Incinerator Bottom Ash
ICP-AES	Inductively Coupled Plasma Atomic Emission Spectroscopy
ISS	Induction Sorting System
ISWA	International Solid and Waste Association
MACT	Maximum Achievable Control Technology
MSW	Municipal Solid Waste
MWC	Municipal Waste Combustors
PEG	Polyethylene Glycol

RSM	Response Surface Methodology
SCR	Selective Catalytic Reduction
SELCHP	South East London Combined Heat and Power
SEM	Scanning Electron Microscopy
TCLP	Toxicity Characteristic Leaching Procedure
TEQ	Toxic Equivalency
TGA	Thermogravimetric Analysis
TOC	Total Organic Carbon
VLN	Very Low NOx
VOC	Volatile Organic Compounds
WID	Waste Incineration Directive
XRD	X-Ray diffraction

CHAPTER 1 INTRODUCTION

1.1 ENERGY FROM WASTE TECHNOLOGY

The only proven alternative to landfilling for residual municipal solid waste (MSW) is thermal treatment involving incineration/combustion to recover electricity, heat, metals and secondary aggregates. Waste combustion on a moving grate is the dominant technique applied in most Energy from Waste (EfW) facilities in Europe, the USA and Asia. It is estimated that ~165 million tonnes of MSW per year is currently thermally treated world- wide. It is used not only in large-scale applications, but also in small EfW plants that serve communities as small as 10,000 inhabitants.

The feedstock to the EfW with moving grate can include all non-radioactive and non-explosive materials. These include residential and commercial wastes remaining after recycling and composting, combustible industrial wastes that are currently disposed in regulated or non-regulated landfills and are mixed with the MSW in the storage bunker, post-recycling combustible construction and demolition wastes, shredded rubber tires, mattresses and post-recycling furniture wastes that are contained in sealed thick plastic bags, such as are used in medical incinerators. Forty-one plants of the over 800 EfW plants in the world are co-combusting medical wastes. On an average, 1.8% of the initial feedstock corresponds to medical wastes (Themelis et al., 2012).

A typical EfW plant with moving grate is presented in Figure 1.1. The building is fully enclosed and the collection vehicles (1) discharge MSW bags and other wastes into the waste bunker (2), which is large enough to hold the waste generated in one week. An overhead claw crane (3) loads the waste into the feed hopper (4) of the EfW furnace and a hydraulic ram feeder (5) at the bottom of the hopper drives the wastes onto the moving grate (6), which is either inclined or horizontal. The grate is either air or water-cooled (7) and the solids are moved slowly through the combustion chamber (9), via the mechanical motion of the grate, and the gravity force in the case of an inclined grate. Another fan (8) is used to prevent the egress of unpleasant odours from the plant. The combustion chamber reduces wastes to ash residues, due to the high temperature oxidation, and this is discharged at the lower end of the grate (18-21). There are currently two types of discharge systems, the wet and dry, which are explained in 1.4. The water-

cooled furnace water wall (9) and super-heater tubes (10), transfer the heat contained in the combustion gases to the high-pressure steam that drives the turbine generator (15). The low-pressure steam from the generator exhaust is typically used for district heating. The most efficient EfW facilities are co-generators of electricity (> 0.6 MWh per tonne of MSW) and district heating (> 0.5 MWh per tonne of MSW).

Nitrogen oxides are reduced to nitrogen and water by the injection of dilute ammonia solution inside the combustion chamber at a temperature between 850 and 1000 °C. Lime, stored in a silo (22), and water are introduced with a semi-dry scrubber (12) into the acidic flue gases, and results to neutralisation. Dioxins and heavy metals that may be present are eliminated by the use of activated carbon, injected into the scrubbing chamber. The bag house filters (13) have the ability to remove the particulate matter from the gas stream and the clean flue gases are ejected to the atmosphere. The residues from the flue gas treatment are stored in the ash silo (23), until they are transferred to treatment facilities (Brunner and Rechberger, 2015).

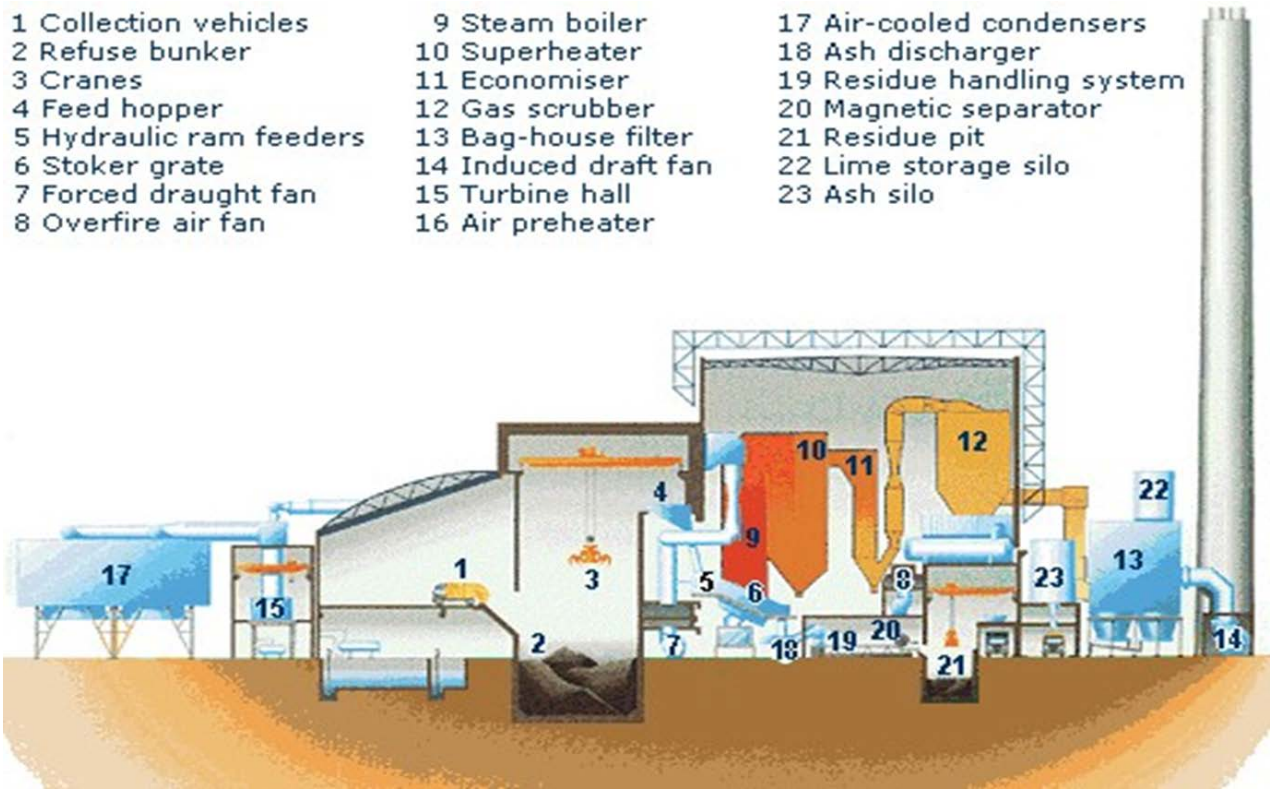

Figure 1.1: Schematic diagram of an EfW facility (SELCHP plant East London website)

Table 1.1 presents the technologies used for the treatment of the waste incineration flue gases (Vehlow, 2015).

Table 1.1: Main Air Pollution Control systems in EfW plants

Parameter	Used abatement technology
Suspended solids	Cyclones
	Electrostatic precipitator (wet-dry)
	Bag filters
Acid gases	Dry sorption mainly with activated carbon
	Semi dry sorption
	Wet scrubbers
Nitrogen oxides	Selective non-catalytic reduction
	Selective catalytic reduction

The chemical formula $C_6H_{10}O_4$ closely approximates the mix of organic compounds in MSW. Similar molecular formula can be found in ten organic compounds, such as adipic acid and ethylene glycol diacetate, with a heat of formation of about 960 MJ/kilomol. The equation $C_6H_{10}O_4 + 6.5O_2 = 6CO_2 + 5H_2O$, corresponds to the full combustion of these organic compounds in MSW, which is a highly exothermic reaction and at the combustion temperature of 1000°C the calculated heat of combustion is 2.7 MJ/kilomol of organic compound. The molecular weight of $C_6H_{10}O_4$ is 146 kg/ kilomol and therefore, the "theoretical" heat of reaction (i.e. in the absence of non-combustible materials and moisture) is calculated to be 18.5 MJ/kg (Tchobanoglous et al., 1993; Matthews and Themelis, 2007). The calorific value of MSW treated in EfW plants range from 7 to 14 MJ/ kg, which is similar or higher than the calorific value of lignite coal, still used in many parts in the world. The high values correspond to plants burning a mix of MSW and industrial wastes; the low values to high moisture MSW. The value of 9 MJ/kg corresponds to about 2.5 MWh (megawatt-hours) of thermal energy per tonne (Themelis et al., 2012).

Typical EfW plants exhibit up to 80% to 90% thermal efficiency and 14% to 27% electrical efficiency (Defra, 2013; Reitman, 2013). The European Union to promote high thermal efficiencies in EfW plants introduced the R1 thermal efficiency factor. The R1 formula is calculated according to the equation:

$$R1 = (2.6\ MWh_{elec.} + 1.1\ MWh_{heat}) / 0.97\ MWh$$

The energy required for the production of electricity and heat is expressed by the factors 2.6 and 1.1, respectively. The 3% expected heat loss in transforming chemical to thermal energy is associated with the factor 0.97. According to R1 formula, an EfW plant is considered as a recovery facility when the R1 formula is greater than 0.6 (> 0.65 for recently built EfW plants), otherwise is considered as disposal facility. In all recent EfW projects in Europe, the R1 criteria are mandatory and must be guaranteed by the companies bidding for such projects.

1.2 ENERGY FROM WASTE RESIDUES

The management of EfW residues depends on the material properties, which depend directly on the composition of feed waste and, to a lesser extent, on the type of combustion chamber. Significant differences exist between the ashes generated at modern EfW plants and the ashes produced in older plants. The modern plants have improved design of the combustion chamber and generally achieve better burn rate and lower organic content in the ash produced (ISWA, 2006).

Energy from Waste solid residues, the residual by-product from MSW incineration, is composed of Bottom Ash (IBA) and Air Pollution Control (APC) Residues. IBA, accounts for 80 to 90% of the total IA, is a granular material, intermingled with ferrous and non-ferrous metals and other incombustibles. IBA consists of glass, ceramics, ferrous and non-ferrous metals and inorganic materials and corresponds to the residues occurring during MSW combustion in the grate furnace. The molten aluminium, zinc, copper and lead can drip down into the hoppers and agglomerate as small stalagmites. These molten metals, together with fine glass and stones comprise the bulk of grate siftings, normally enriched in Al, Cu, Pb, Zn and Si. IBA appearance is similar to porous sand with larger grey gravels and contains small amounts of unburned organic matter and metal pieces. (Sabbas et al., 2003; ISWA, 2006; Themelis et al., 2013). According to the EU legislation, IBA should have a total organic carbon content of less than 3%.

APC residues generally refers to Boiler Ash, Economizer Ash, and Electrostatic Precipitator (ESP) Ash or their combination. Boiler ash and economizer ash are the fume dust in the heat exchange and economizer system. They are dust-like or fine granular materials, ranging from black-grey to beige-tan in colour. The particle sizes range from submicron to millimetre in

diameter. ESP ash freshly collected from dry or semi-dry process appears as very fine, dusty materials with practically no water content. The colour may vary from almost white through various shades of grey and brown to almost black, depending on the composition and the combustion efficiency. Dry process air pollution control systems usually produce a fine-powdered mixture of APC residues, reaction products (predominantly calcium chloride) and unreacted lime, and is thus highly hygroscopic and soluble. Sometimes sodium sulphide or activated carbon is also added to the air pollution control system to remove mercury. APC residues are classified as hazardous waste according to the European Waste Catalogue (EWC, 2000; Sabbas et al., 2003; Porteous, 2005; ISWA, 2006; Rani et al., 2008; Themelis et al., 2013).

1.3 EMISSIONS FROM ENERGY FROM WASTE

The negative public perception of EfW plants is often associated with emissions of incinerators that stopped operating two decades ago. Opponents of EfW, picture modern EfW plants as major polluters but there is no credible data to back up these claims. The existing EfW facilities are in full compliance with the established limits. In addition, studies of people living around EfW facilities have found no evidence of health effects caused by EfW plant emissions.

The EU, the Directive 2000/76/EC on the incineration of waste (WID) imposes strict operating conditions and technical requirements on waste incineration plants and waste co-incineration plants to prevent or reduce air, water and soil pollution. The Directive requires a permit for EfW and co-incineration plants, and emission limits are introduced for certain pollutants released to air or to water. In USA, the Maximum Achievable Control Technology (MACT) standards for Large Municipal Waste Combustors (MWC), issued by the U.S. EPA under the requirements of the Clean Air Act, established mandatory emissions limitations that are protective of human health and the environment. European limits, which are similar to the USEPA standards and are the most stringent standards applied to high temperature industrial sources, including coal-fired power plants, cement plants, and metal smelters are presented in Table 1.2. Typically, Requests for Proposals for a new EfW are based on Air Pollution Control equipment that can result in emissions lower than the legislative limits, even if some of the current national standards allow for higher emissions than those shown in Table 1.2.

Table 1.2: Emission standards as issued by the European Waste Incineration Directive (WID) and the USA Environmental Protection Agency Maximum Achievable Control Technology (MACT) for Large Municipal Waste Combustors (MWC).

Pollutant	E.U. WID limits	U.S.A. MACT limits
	11% O_2 dry basis (mg/ Nm^3)	
TOC	10	15
HCl	10	29
HF	1	N.D.
SO_2	50	61
NO_x	200	219
Cd		0.008
Cd, Ti	0.05 total	N.D.
Hg	0.05	0.04
Pb	N.D.	0.11
Pb, As, Sb, Cr, Cu, Mn, Ni, V	0.5 total	N.D.
CO	50	89
Dioxins and furans	0.1 ng/ Nm^3 TEQ	9.9 ng total dioxins = 0.1 ng TEQ

TEQ: Toxic Equivalency
N.D.: Not defined.

In the UK, all the major pollutants of environmental concern are significantly below the WID limit and significantly reduced by the UK 1991 emissions, as shown in Table 1.3. Particulates and Hydrogen Chlorides (HCl) are reduced by 99.8 and 97.1% since the 1991 EfW emissions, respectively. Sulphur dioxide (SO_2) and carbon monoxide (CO) are reduced by 89 and 98%, accordingly. Hg and Cadmium (Cd) are reduced by 99 and 99.8%, respectively. Heavy metals are reduced by 99% since 1991 and dioxin emissions by 99.9%. EfW facilities indicated 686, 261 and 136 g of $CO_{2\text{-eq}}$ savings/ $kWh_{\text{-el}}$ generated compared to $CO_{2\text{-eq}}$ emitted by coal, gas and combined cycle gas turbine (CCGT) power plants, accordingly (Porteous, 2005).

In the USA, a comparison of the pre and post-MACT emissions from EfW combustion showed that emissions of environmental concern from EfW facilities were reduced by 90% since 1990. Dioxins and furans were reduced by 99.9% compared to facilities operated in 1990. Dioxin emissions from EfW facilities operating in the USA have been reduced to 0.045 nanograms toxic equivalency (TEQ), which is one tenth of the USEPA and one third of the EU WID standards,

respectively. This number corresponds to 6 grams TEQ from all the EfW facilities operating in the USA, which is significantly lower than the estimated 500 grams TEQ per year generated from the uncontrolled burning of MSW. According to USEPA estimation, approximately 78% of the U.S.A. total dioxin emissions is associated with landfill fires, forest and brush fires, and uncontrolled burning of MSW. Dioxins are very long-lived organic substances that can bioaccumulate in the food chain and may cause cancer and other illnesses. According to the 'European Dioxin Emission Inventory', EfW facilities has exhibited a rapid decrease of dioxin and furan emissions of about 99.1% from 1990 to 2007 due to efficient abatement measures (EPA website).

Table 1.3: A comparison of UK and European mean Energy from Waste emissions and percentage improvement over UK 1991 performance (Porteous, 2005).

Component	Emission to air in mg/Nm^3 – dioxins in ng/Nm^3- dry gas 11% O_2			UK 1991	% Reduction
	Measured UK	European (mean)	Waste Incineration Directive	Mean emissions mg/Nm^3	Measured UK over UK 1991
Particulates	0.9	2.2	10	500	99.8
HCl	20	1.6	10	689	97.1
HF	< 0.1	0.03	1	N.A.	-
SO_2	36	7.2	50	338	89
NO_x as NO_2	274	29	200	N.A.	-
CO	5	-	50	220	98
VOC	< 5	-	10	N.A.	-
Hg	< 0.02	< 0.001	0.05	0.26	99
Cd	< 0.001	< 0.001	0.05 (Cd and Ti)	0.6	99.8
Heavy metals summation	< 0.1	0.16	0.5	> 11.0	99
Dioxin TEQ ng/Nm^3	0.006	< 0.01	0.1	> 225	99.9

TEQ: Toxic Equivalency
N.A.: Not available

The potential impact of EfW emissions per MWh of electricity produced have been compared with other sources of electrical energy. Only natural gas and nuclear power plants have lower stack carbon emissions per MWh, as shown in Figure 1.2. Furthermore, when the avoided landfill emissions of methane are taken into account, EfW actually results in net reductions in GHG emissions for every MWh generated or tonne of MSW processed (Kaplan et al., 2009).

An analysis of the operating data of over two hundred grate combustion plants concluded that dioxin emissions were in the order of 0.02 nanograms TEQ per standard cubic meter, which corresponds to only 0.1 grams of TEQ dioxins emitted per million tonnes of MSW processed. Very low NOx emissions can also be obtained by grate combustion facilities that use selective catalytic reduction (SCR) or the Very Low NOx (VLN) process developed by Covanta Energy and Martin GmbH (Kaplan et al., 2009; Themelis et al., 2012).

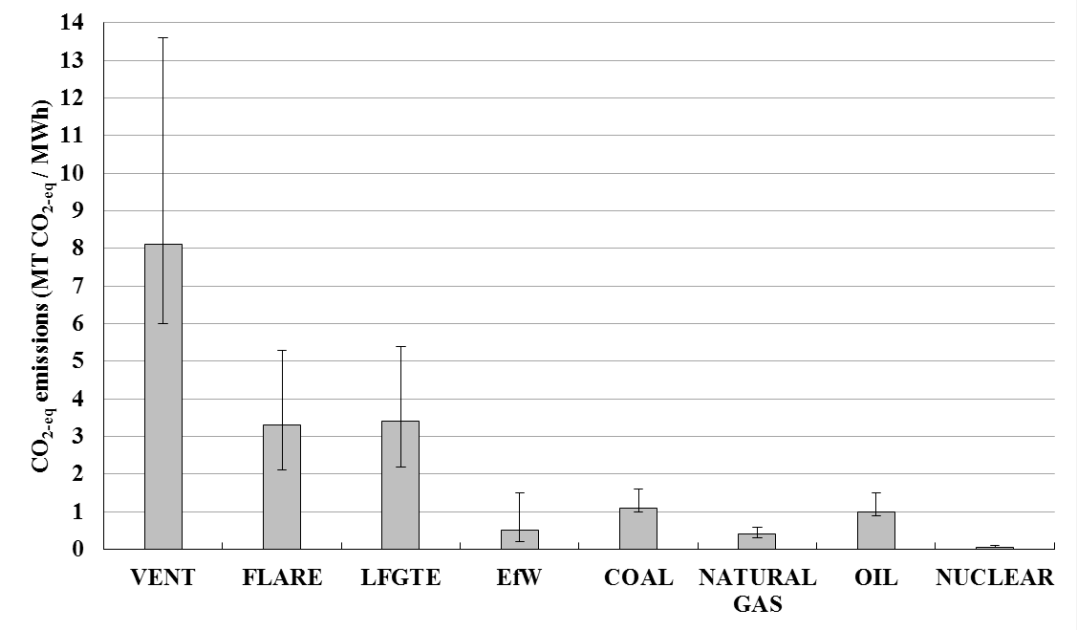

Figure 1.2: Carbon dioxide emissions (tonnes CO2/MWh) of various energy sources. Landfill gas to energy (LFGTE), Flaring (FLARE) and Venting (VENT) represent alternative MSW techniques (Kaplan et al., 2009).

1.4 INCINERATOR BOTTOM ASH DISCHARGE METHODS

IBA drops from the end of the moving grate into a water tank below the furnace, wet discharging the IBA, as shown in Figure 1.3. Temperature and water absorption of IBA control the water consumption. The amount of water provided to the discharger is sufficient to quench the IBA and recirculation or overflow of water is not required. The discharger is usually filled with water and a constant amount of bottom ash up to the level of the front air sealing wall. This creates an air seal against the furnace and therefore preventing flue gas and thermal pollution in the basement and false air ingress into the boiler. The discharge rate ranges within 4.5 to 12.0 m^3/h. The discharging ram forces IBA under the air sealing wall towards the drop-off edge without creating any dust or odours. There is a drain-off section before the drop-off edge where excess water is extracted by the compressing action of the discharging ram. IBA is therefore moist rather than wet when discharged. The discharger is driven either by a separate or a central hydraulic unit. A pressure piston is typically pushes the quenched IBA out of the discharge system and onto conveyor belts leading to an IBA bunker/silo. The cadence of the pressure piston can be regulated by timer or by the height of IBA in the shaft using sensor techniques. Some instalments use a metal belt conveyor or chain belt conveyor to continuously remove the quenched slag. When the water comes in contact with the heterogeneous IBA, there are many uncontrolled chemical reactions which result in poor quality of IBA. The energy requirements of the wet discharged process is 2 MWh/ 1,000 tons IBA and the water used is 50,000 litres / 1,000 tonnes IBA discharged (ISWA, 2006; Cleary, 2009; Muchova, 2010; Allegrini et al., 2014).

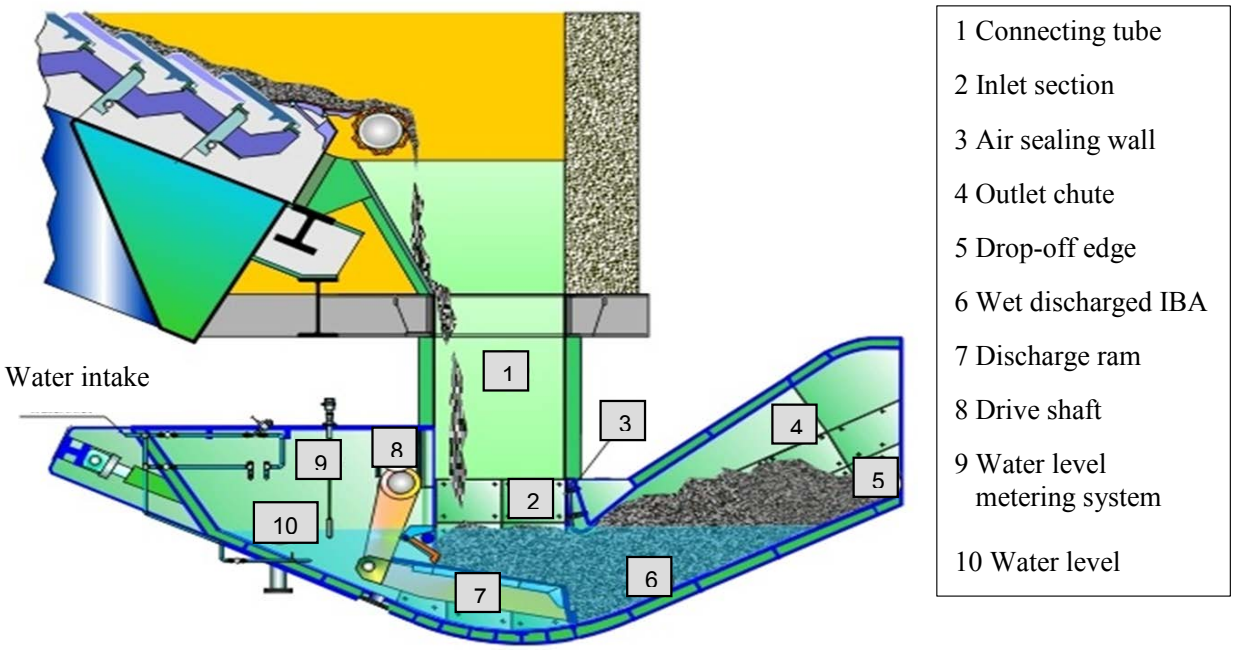

Figure 1.3: Cross-sections of combustion chamber and wet discharge system. Drive shaft, which is typically a pressure piston pushes the quenched IBA out of the discharge system and onto conveyor belts leading IBA to a bunker/silo (ISWA, 2006).

Martin GmbH applied a dry ash discharge technology (Figure 1.4) at the Iwaki Nanbu EfW plant in Japan. Currently there are six EfW plants in Japan using the dry discharge technology; it is also used at the KVA Monthey EfW plant in Switzerland and in KEZO plant in Switzerland. IBA passes through an ash drum and falls onto a baffle plate to comminute further. In front of this equipment there is a set of flaps, that serve to reduce the flow of air through the system, and a water sprinkler used to quench any still burning embers, if necessary. The ash is discharged onto a vibrating conveyor, designed to withstand temperatures up to 400 °C. The ash discharge is monitored with a camera and has a 2-way diverter for the removal of the material in emergency. Any pieces that are too big can be removed through an electrically operated hood. The ashes are air-cooled during discharge by injecting tertiary air, which is an additional process variable for dry discharge. However, it should be noted that the total air input to the furnace is not increased; the secondary air is reduced by the amount of tertiary air used in the dry

quenching process. The tertiary air also supports afterburning of any organic compounds remaining in the dry –discharge ash, which can be as much as 0.3% of the ash. Very fine particles entrained in the tertiary air are returned to the furnace. A conveyor belt transports the crushed ashes at the end of the discharge to a screen that separates oversize particles (>9mm). The undersize ash is then processed, as described in a following section. The energy use of the dry discharge system is 0.2 MWh/ 1,000 tonnes IBA, while the use of water is negligible (KEZO, 2011; Koralewska et al., 2014; Bourtsalas et al., 2015).

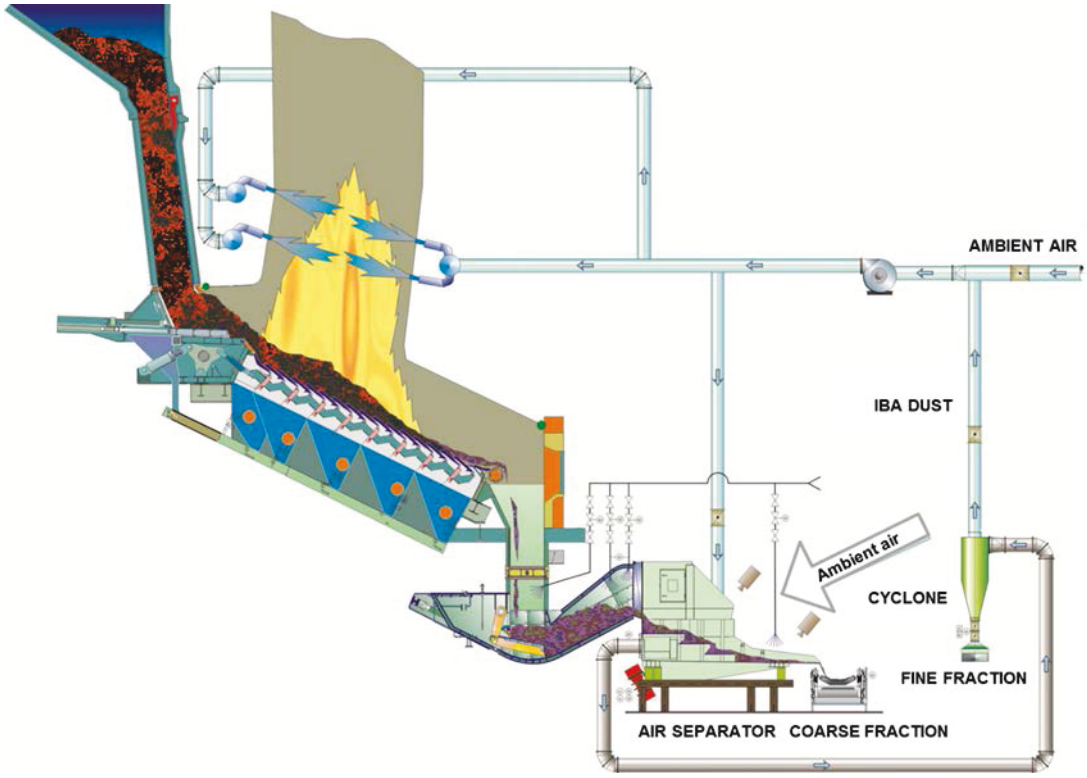

Figure 1.4: Cross-sections of combustion chamber and dry discharge systems of Monthey EfW plant in Switzerland. IBA is sieved in an enclosed vibrating screen into the fractions < 1 and > 1 mm and results in a metal enriched coarse fraction (> 1 mm) and a nearly metal free fine fraction (< 1 mm) for reuse. The fine IBA dust fraction (< 1mm) is the material used in this research (Koralewska et al, 2014).

The IBA discharge system has an influence on metal recovery from the IBA, as the system design has an effect on the degree of oxidation and the subsequent metal sorting process and performance. An image of the metals in wet and dry discharged IBA is shown in Figure 1.5 (KEZO, 2011; Morf et al., 2013; Koralewska et al., 2014).

Because water is not used, the weight of ash to be disposed is 10 to 20% wt. less, and consequently, the cost of disposal (including transportation), is considerably less. In addition, dry discharge exhibits higher energy efficiency, lower total organic carbon (TOC) in the IBA, significant reduction of the leaching of metals of environmental concern from IBA. The dry discharge method has shown 45% increase in ferrous metal recovery and 50% in non-ferrous metals recovery over the wet-discharge method (Morf et al., 2013). The main disadvantage of this process is the generation of dust emissions of very fine dry IBA particles, which needs special treatment. However, many industries, e.g. flour mills, cement plants and others, can manage dust issues in a sustainable manner. Prerequisite is a sealed transport system, in which many EfW industries are unfamiliar (KEZO, 2011; Koralewska et al., 2014).

Figure 1.5: Difference between metals sorted from a wet and dry bottom ash. The discharge system of IBA has an effect on the degree of oxidation and the subsequent metal sorting process and performance (photos taken from ISWA-WGER).

1.5 WEATHERING

Weathering or aging is a relatively simple treatment completed prior to or after metal separation. Weathering is the combination of CO_2 uptake from the atmosphere and chemical reactions following contact with water. Contact with water is associated to the wet slag extraction or wetting after dry slag extraction. Proper weathering can effectively be achieved by storing the bottom ashes with good access to air, water and occasional turning.

Weathering is strongly associated with the reactivity of the IBA and the leaching of metals are reduced. This is due to:

- Mineralogical and geochemical changes due to uptake of CO_2 (carbonation) and thereby lowering of pH (typical from pH 11-12 to pH 8-10)
- Hydration and other changes in the mineral phases in the bottom ash
- Binding/sorption of dissolved elements (especially heavy metals) to the matrix of the bottom ash
- Removal or transformation of available organic ligands, e.g. by evaporation, leaching, or changes in the binding characteristics
- Leaching of highly dissolvable salts

Research has shown, that the concentration of various components in leachate follows the pH value of the leachate (Zhang et al., 2008). Leachate collected during weathering has a high concentration of highly soluble salts, such as chlorides and sulphates, and minor amounts of metal, primarily copper. Typically, the bottom ashes are weathered until the chemical reaction with water goes from strongly alkaline to somewhat neutral. It takes 6-20 weeks of weathering before the ash is chemically stable and suitable for utilization or landfilling (Hjelmar et al., 1998; ISWA, 2006). Besides improving the leaching properties of the bottom ash, weathering improves the mechanical properties as the bottom ash becomes more chemically stable.

1.6 PROCESSING OF INCINERATOR BOTTOM ASH

IBA processing typically uses standard drum or flat screen decks with mesh sizes to sort different size fractions and further metal recovery using magnetic and eddy current separators, as explained in detail in the following section. These techniques are low cost methods and improve

the chemical composition, resource quality and structural strength of IBA aggregates before reuse. For example, the presence of metallic Al in IBA may generate H^+ or form hydroxides during cement hydration under alkaline conditions, and subsequent volume increase and cracking of concrete (Pecquer et al., 2001). The mitigation of this effect is possible if IBA is treated with sodium hydroxide. In addition, the high angularity and brittle nature of IBA may create problems in the workability of concrete products. IBA contains relatively high sulphate and chloride concentrations, and this may lead to sulphate attack and reinforcing steel corrosion problems (Berg and Neal, 1998; Bertolini et al., 2004). The removal of metals and efficient IBA aggregates sorting techniques may alleviate these effects. The metal recovery and fractioning techniques are presented in the following section.

1.6.1 Metal recovery and fractioning techniques

Magnetic separation. Magnetic separation is typically applied for the removal of ferrous metals in the IBA recycling plants. Stainless steel, which is also present in the total ferrous fraction of IBA, cannot be removed by magnetic separation. There are many different types and setups of magnetic separation. The most common in IBA sorting are magnetic drum and overhead suspension magnets. The setup of the magnets varies depending on the material flow, particle size, magnet strength and size and material velocity. The advantages and suggested setup is beyond the scope of this research.

Sieving. A very important step in the removal of metals is an efficient fractioning system of IBA. Sorting of metals is strongly dependent on the accurate definition of fractions. The sieve type in the sorting system depends on the sizing.

The oversized items are typically removed using a finger sieve and are normally manually sorted, since the metal items in this size range are in a relatively small amount and easily identified. Drum sieves are used for intermediate size fractioning, and consist of a rotating perforated steel cylinder. Flip flow screens are commonly used for the fine fractioning of wet IBA. A flexible perforated rubber screen moves in an oscillating manner, while the material travels across the screen. Shaking ensures that the material is mixed and allows the fine fraction to pass through the perforations. Similar to the flip flow screen is the vibrating screen, where the

sieve vibrates instead of oscillating. Both the flip-flow screen and the vibrating screen can have multiple fractioning stacked above each other, minimizing space requirement.

Sieving and transport of wet IBA can generally be done in open systems, although this approach is associated with emissions of dusty material. Wet sorting systems aim to ensure a water content of 10-20 %. If the water percentage is higher, sieving and therefore metal sorting is difficult to control due to strong agglomerations of the bottom ash. This is especially the case for the fine fraction, where the high value metals are present. If the water percentage is lower than 10 %, dust will likely escape. Sieving can be carried out enclosed to avoid dust. Enclosed vibrating screens are typically used in dry discharge and sorting system. In order to have an effective sorting of non-ferrous metals, it is important to have an accurate and effective fractioning of IBA.

Eddy Current Separation. Eddy current separation (ECS) is a technique for separating non-magnetic metals from a material stream. The eddy current machine consists of a conveyor with a non-magnetic drum. The drum is equipped with an internal rotating set of magnets. The magnets inside the drum create repulsive forces, pushing non-ferrous metals on a path away from the drum (Figure 1.6).

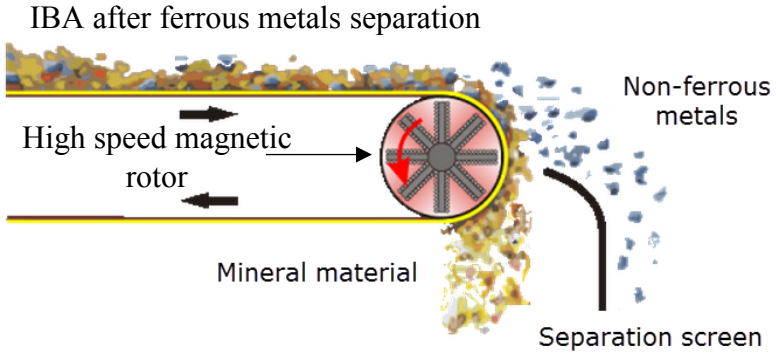

Figure 1.6: Schematic diagram of Eddy current separator.The drum is equipped with an internal rotating set of magnets. The magnets inside the drum create repulsive forces, pushing non-ferrous metals on a path away from the drum (ISWA-WGER).

The ballistic curve of non-metallic objects results from the gravitational, centrifugal, friction (with belt) and drag force (air resistance). Metallic objects are also affected by a magnetic deflecting force that is caused by the interaction of eddy currents induced in conductive materials. The eddy currents result from the internal rotating magnets. Metals will have a more flat ballistic curve than the non-metallic material. Separation of the two types can thus be done by a screen set in a proper distance.

The theoretical curve of different objects is difficult to predict. However, the magnitude of the magnetic deflection force is highly related to the ratio of electrical conductivity and density, referred to as repulsiveness. The ballistic curves are therefore more predictable for equal sizes. For this reason, a precisely defined interval in the fractioning and a properly chosen dimension span, is the most important factor on the effectiveness of the ECS. Furthermore, having multiple ECSs in series will increase the overall effectiveness. Experiences at the ZAR facility showed, that two ECSs in series installed in an inclined angle increased the overall sorting efficiency of 75% to 82% (Stiftung Zentrum Für Nachhaltige Abfall- Und Ressourcennutzung (ZAR), 2011). Modern ECS machinery can therefore be very effective.

Induction Sorting System. Stainless steel is a non-magnetic material. In addition, the conductivity of steel is low, resulting in a low repulsiveness. Stainless steel cannot be sorted using magnets or ECS. Stainless steel can, however, be sorted using sensor technology. Induction Sorting System (ISS) are used for the detection of metallic objects by applying magnetic induction. When a metallic object is located on the conveyor belt in the ISS, the object is removed from the stream by a pulse of compressed air and the object is thrown over the conveyor belt edge. The ISS is typically applied after magnetic separation and ECS.

X-ray sorting. The working principle of X-ray sorting is very similar to the ISS sorting system. Instead of a sensor detecting metallic items, an X-ray module is installed, recognizing specific shapes that most likely will be metallic, such as flat round objects (coins, washers etc.). The recognized objects are mechanically removed from the stream using a pulse of compressed air.

Crushing/milling. Some sorting plants improve their metal separation performance by crushing/milling the bottom ash. This technique enables the removal of mineral fractions

strongly bonded with metal pieces and the pulverization of large pieces of minerals. The drawback of crushing and milling is the alteration of the mechanical characteristics of IBA. Crushing and milling is only applied to a small extent, typically when the mineral fraction is used for road construction.

Other separation techniques. The Dutch company INASHCO has in collaboration with the Delft University of Technology (TÜ Delft) developed a separation technique, in which ballistic separation is used to separate the fine, soft and light minerals with the hard and coarse metals/rocks. The separation apparatus used by INASHCO deals with the fraction typically < 2 mm size. The principle of the apparatus is depicted in Figure 1.7.

The apparatus lets the bottom ash stream fall onto a turning bladed drum. As the bottom ash is struck by the drum blades, the different components of the bottom ash (mineral fraction, rocks and metals) will obtain different ballistic paths. Furthermore, the different ballistic paths are assisted by a downward blowing jet stream. The light components (mineral fraction) will fall down to the first conveyor belt exiting the apparatus. The heavy components (rocks and metals) will experience a more flat ballistic curve and therefore land on the second conveyor belt. The air jet separation is repeated to increase purity of the separated stream. The fine, light and soft components and the hard and coarse components will be separated. The INASHCO Company operates their metal separation technique at many plants in Europe and recently expanded its activities in North America.

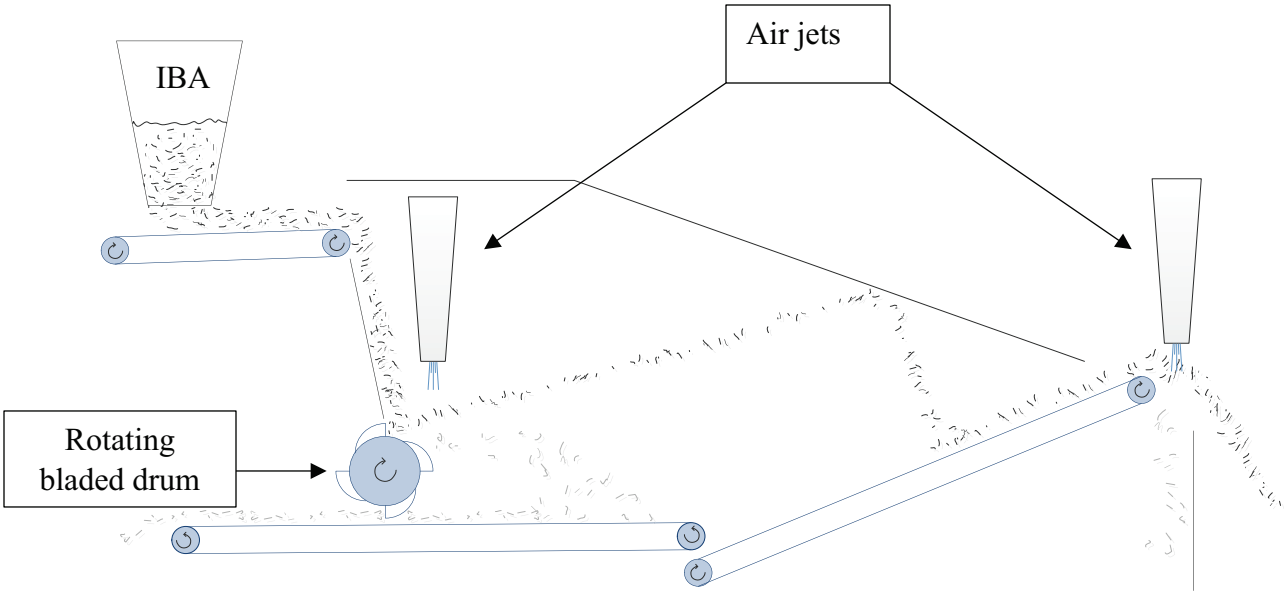

Figure 1.7: Schematic diagram of the separation technique used by INASHCO. IBA falls onto a rotating bladed drum, separating hard heavy objects (dark blue colour) from the porous mineral fraction (light blue colour). Air jets assist the separation (ISWA-WGER).

1.6.2 Examples of modern metal sorting systems

In this project two different IBA materials were used and obtained from modern sorting facilities in Switzerland and England.

The dry discharged fine IBA used in this research was produced in Monthey EfW plant in Switzerland. Monthey plant is located in the Industrial Zone of Boeuferrant and serves 250,000 inhabitants from 57 villages. The average calorific value of the residual MSW is 12.9 to 13.1 MJ/ kg, and the operated two line furnaces, both Martin reverse moving grate, have an operating capacity of 10.5 tonnes of MSW/ hour (SATOM Monthey website). A Sankey diagram of the IBA streams produced and utilised in Monthey EfW plants is presented in Figure 1.8. The main components and particle sorting system are a discharger, an air separator, a dust removal system and an air system; and are operated without the use of water. IBA is dry discharged and is directly transferred by means of gravity and mechanical vibration to an air separator. Martin dry discharge and treatment system uses a fully sealed air separator area applying negative pressure through the air supply system, to prevent air leakage into the furnace and dust emission into the

combustion chamber. An ash removal system, e.g. a cyclone separator, is used to separate the fine fraction from the air separators' exhaust air. As part of the secondary air system, the exhaust air and its dust content are fed into the combustion process. IBA is sieved in an enclosed vibrating screen into the fractions < 1 and > 1 mm and results in a metal enriched coarse fraction (> 1 mm) and a nearly metal free fine fraction (< 1 mm) for reuse. The fine (< 1 mm) IBA dust represents 7.0 to 10.6 wt. % of the total IBA produced and is used as cement substitute for the stabilisation of neutral washed filter ashes prior to disposal in a hazardous landfill (Koralewska et al., 2014).

The > 1 mm fraction first undergoes removal of ferrous metals by the use of magnets. After removal of the magnetic iron, the stream undergoes screening and this results to separation of dry discharge IBA in three product streams, the coarse (> 9 mm), the 2-9 mm and the 1- 2 mm fraction. These fractions are subject to ECS and ISS for removal of non-ferrous metals and stainless steel. Each of the 1-2 mm and 2-9 mm streams are fed into separating tables, which are able to separate the non-ferrous metal into aluminium and a mixture of other non-ferrous metals, primarily Cu and some Zn, Au, Ag etc. The separation tables separate the metals based on density. The sorting system is fully enclosed and kept in a slight vacuum, ensuring that the working environment is practically dust free. Ferrous metals represent 10.3 to 10.6 wt. % of the total IBA and non-ferrous metals 3.3 to 4.4 wt. % of the total IBA. The mineral IBA fraction represents approximately 74.4 to 79.4 wt. % of the total IBA, is stored in a silo, and is typically landfilled.

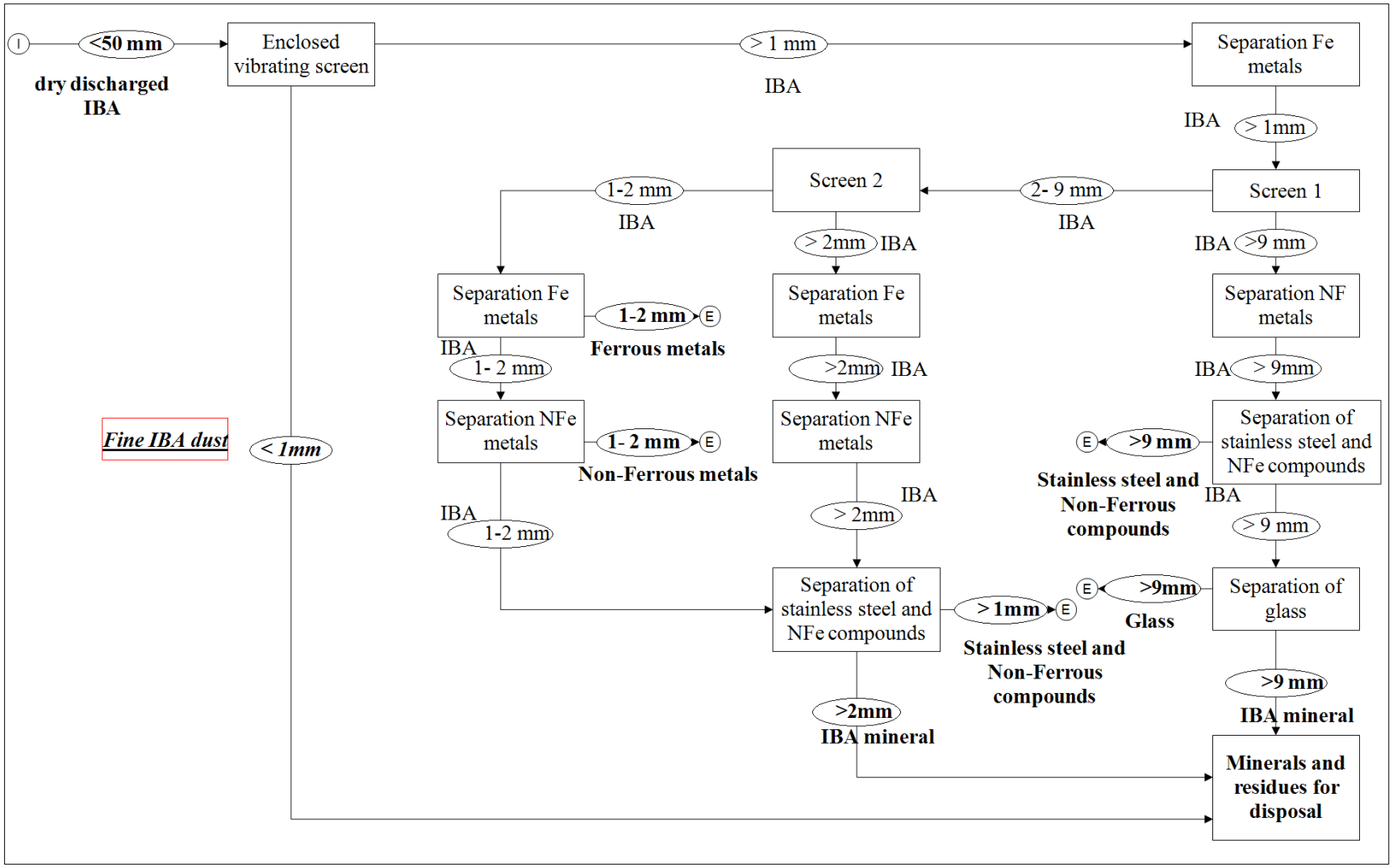

Figure 1.8: Sankey diagram of dry discharged IBA processing. The red box refers to the dry discharged fine IBA dust fraction used in this research.

The second fine IBA fraction was supplied by Day Group who manage the wet discharged material from the Lakeside and the Newhaven EfW facilities in the UK. The Lakeside EfW facility at Colnbrook near Slough has been operational since 2010. This plant processes 410,000 tonnes of MSW per year, and generates approximately 37 MW of electricity (Viridor website; Defra 2013). The Newhaven EfW in the South of England was built in 2011 with total capacity 210,000 tonnes per year and ability to produce 36 MW of electricity. The average calorific values of the treated MSW ranges from 7.5 to 14 MJ/ kg (Hitachi Zosen Inova website; Defra, 2013). A Sankey diagram of the wet discharged IBA processed in Day Group recycling facility is shown in Figure 1.9. IBA is aged for 1 to 2 months prior to sorting. Bulky and oversized objects (> 100mm) are removed from the stream and manually sorted. IBA is then sieved at 32 mm. The 32-100 mm interval undergoes magnetic sorting and some degree of crushing, in order to liberate metals embedded in larger chunks of solidified mineral material. The fraction below 32 mm is sieved to 12-32, 4-12 and < 4 mm. The medium (4-12 mm) and coarse (12-32 mm) fractions are subject to magnetic separation and ECS for ferrous and non-ferrous metals removal, respectively. The plant has a metal sorting efficiency of about 75-80%. The metals extracted have significant value and the processed IBA mineral fraction greater than 4 mm is extensively used as secondary recycled aggregate, predominately as a sub-base and capping material and aggregate replacement in hydraulically bound mixtures and asphalt. Processed wet discharged IBA also contains approximately 40-45 wt. % of fine material, most of which is significantly less than 4 mm in diameter, which is not ideal for use as aggregate. There are currently limited alternative beneficial reuse options for this material which is typically either blended back into IBA aggregate or disposed of to landfill, neither of which is ideal (Day, 2012; Day Group website).

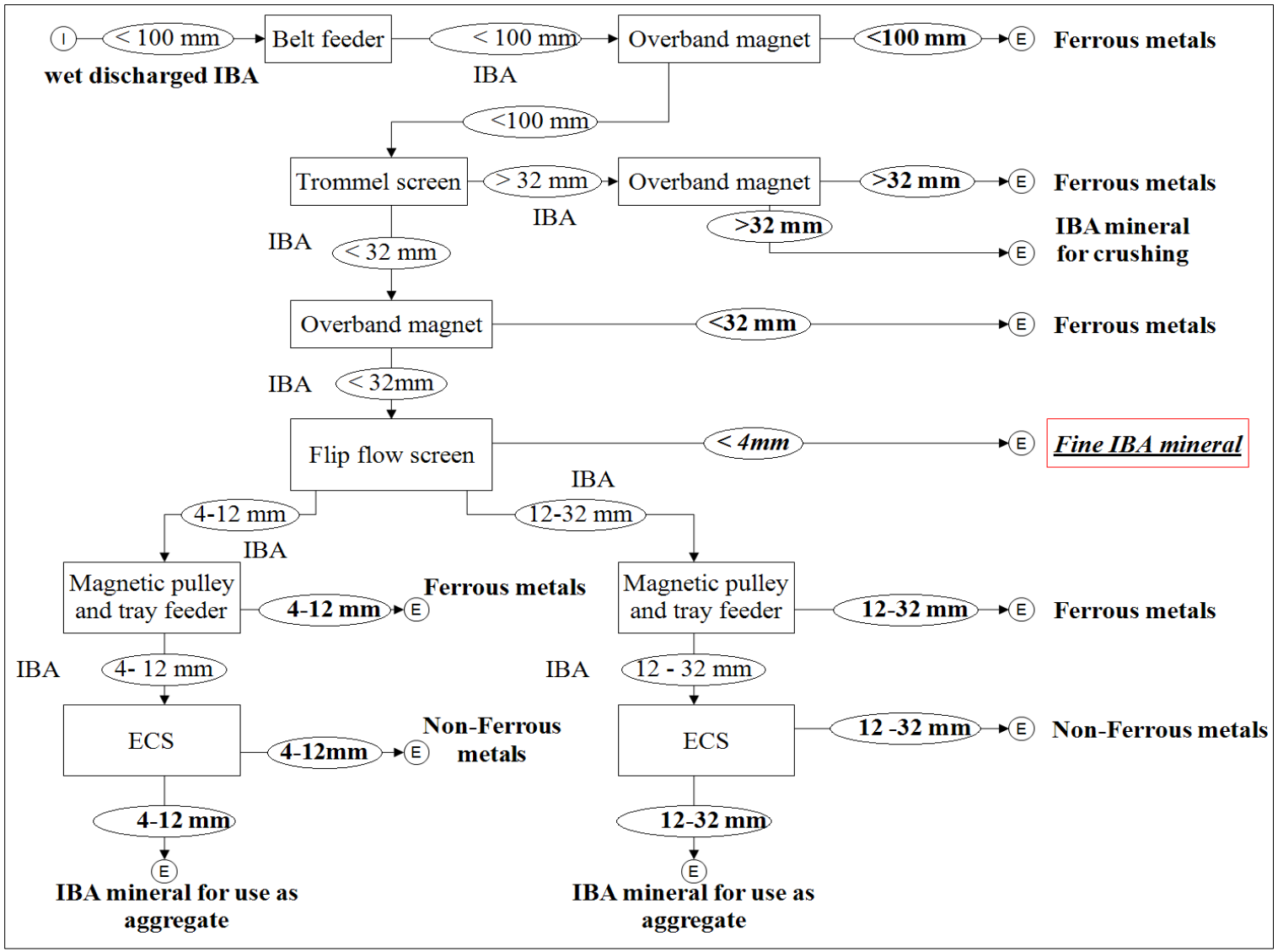

Figure 1.9: Sankey diagram of wet discharged IBA processing. The red box refers to the wet discharged fine IBA used in this research.

1.7 BOTTOM ASH UTILIZATION

The physical and chemical characterisation and the potential leaching of metals and soluble salts of waste materials are essential in order to identify appropriate management techniques and possibilities for reuse by achieving minimum environmental impact. The properties and potential applications of processed IBA minerals have been extensively studied (IAWG, 1994; Rivard-Lentz, 1998; Chimenos et al., 1999; Schreurs et al., 2000; Belevi and Langmeier, 2000; Bruder-Hubscher et al., 2001; Pecquer et al., 2001; Barbieri et al., 2002; Bethanis et al., 2002; Sabbas et al., 2003; Appendino et al., 2004; Bethanis et al., 2004; Bertolini et al., 2004; Reijinders, 2005; ISWA, 2006; Hu et al., 2008; Hjelmar et al., 2010; Rambaldi et al., 2010; Schabbach et al., 2012; Morf et al., 2013).

This section presents the mechanical properties of processed IBA minerals, its current uses and some environmental considerations.

1.7.1 Mechanical properties

For all possible types of utilization, it is beneficial for the mechanical properties that the metal sorting prior to utilization is as efficient as possible. Removing all metals creates a very homogenous and mechanically strong material. The mechanical properties of IBA have been thoroughly studied. Table 1.4 shows examples of test values from different countries.

Table 1.4: Characterisation data of IBA (Wiles and Shepherd, 1999; ISWA, 2006)

Properties	**IBA**
Gradation (% passing)	
Coarse fraction, > 4.75 mm	30-45
Fine fraction, < 4.75 mm	42-50
Silt fraction < 0.075 mm	9-16
Relative Density (g/cm^3)	
Fine particles (< 4.75 mm)	1.70-1.81
Coarse particles (> 4.75 mm)	2.11-2.23
Water Absorption (%)	
Fine particles (< 4.75 mm)	12-16
Coarse particles (> 4.75 mm)	5-7
Moisture content,% Dry weight	14-30
Specific Gravity, kg/m^3	960-1400
Loss on ignition (L.O.I.) at 550 °C in%	1.0-2.0

The particle size distribution plays an important role for the utilization possibilities of processed IBA minerals. A typical particle size distribution curve of processed IBA after removal of the oversized material is shown in Figure 1.12. Experience has shown that the mechanical properties are linked to the grain size distribution curve. Fractioning and/or crushing the bottom ash influence the mechanical properties. Utilization techniques are typically the driver for the treatment process applied. However, in all cases the disposal and utilization of the fine fraction of IBA is a challenge for the IBA recycling plants operators.

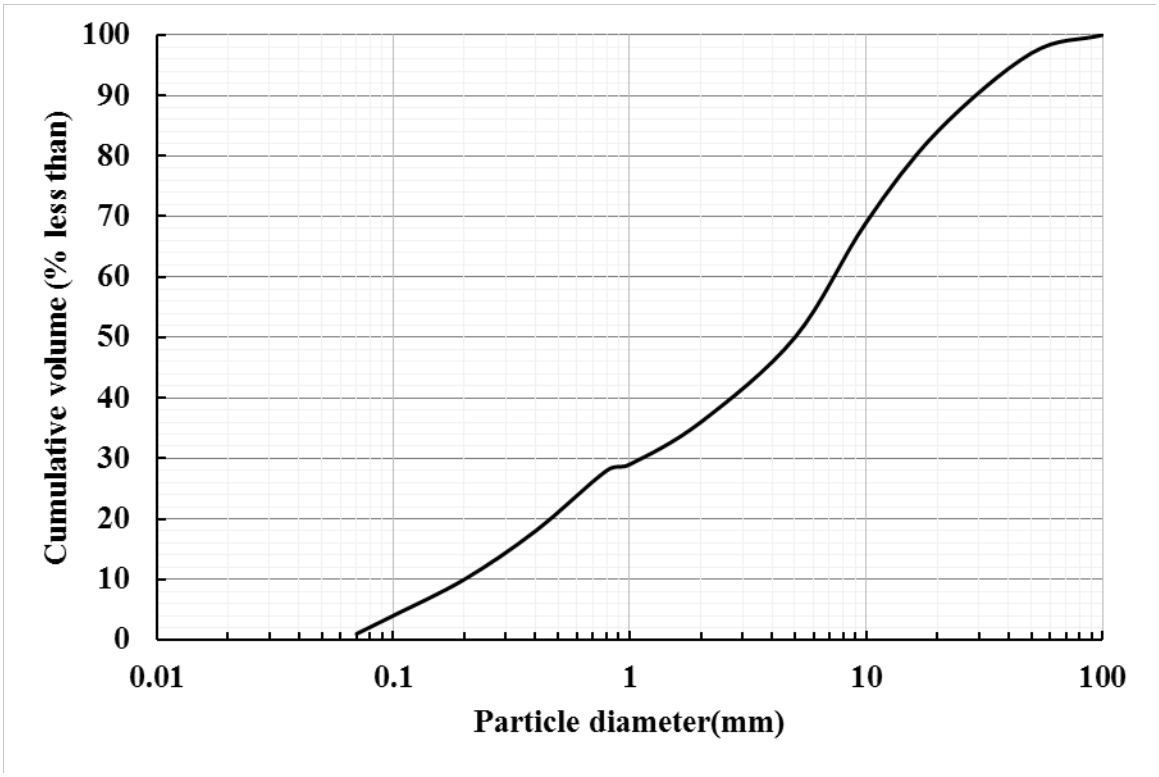

Figure 1.10: Typical average particle size distribution by volume for IBA (ISWA, 2006)

1.7.2 Examples of utilization and environmental considerations

Processed IBA minerals have the greatest potential for reuse, because it has relatively low concentration of metals that can leach (e.g. lead, cadmium, mercury etc.), and soluble salts (Schneider et al., 1994; Wunsch et al., 1996; Wang et al., 1998; Wang et al., 2001; Van der Sloot, 2001; Hjelmar et al., 2010). IBA is typically weathered (or aged) for 6 to 20 weeks prior to

metal separation, in order to reduce the reactivity of processed IBA minerals and the leaching of metals. While the utilisation of processed IBA mineral fraction is very high in some European countries, e.g. the UK, Denmark, Germany and the Netherlands, with utilisation rates up to 98%, other countries do not obtain the full benefits of this resource, which is instead landfilled (ISWA, 2006). However, recent regulations in many countries enforce resource efficiency of IBA as a way of preserving natural resources.

Processed IBA minerals have been extensively used as a sub base material for road construction, substituting primary/ virgin gravel and sand material. The application of this technique has been standardized in EN 13285 and EN 13242, to ensure that there is no hydraulic contact with the surface layer, eliminating the leaching potential of processed IBA minerals. For example, in the UK processed IBA minerals can be used as a secondary aggregate if complying with the Standards for Highways (SHW) C803 Type 1 or as a capping material in accordance with SHW 600 series. It may also be used as a constituent of a granular material compliant to the same SHW 600 and 800 series. Processed IBA minerals have also been used for the production of concrete products with low tensile strength, the manufacture of embankments and as sound or wind barriers (ISWA 2006). Other uses of processed IBA minerals involve land reclamation, as pavement base and as landfill cover (Garrick and Chan, 1993; Alkemade, 1994; Eymael et al., 1994; Zhang et al. 1999; Estarkhri and Saylak, 2000; Francois et al., 2000; Bruder-Hubscher et al., 2001; Rendek, 2006; Lin et al., 2012; Valle-Zermeño et al., 2014). Processed IBA mineral have also been used for the production of bricks, paving stones and lightweight aggregates for subsequent use in geotechnical applications (Wiles, 1999; Cheeseman et al., 2003; Cheeseman et al., 2005; Muller and Rubner, 2006; Stegemann, 2006; Qiao et al., 2008a; Qiao et al., 2008b; Rambaldi et al., 2010; Schabbach et al., 2013). In some cases, processed IBA minerals have been utilized for the manufacture of blended cement and concrete products (Polletini et al., 2000; Quenee et al., 2000; Bertolini et al., 2004; Ferraris e t al., 2009; Onori et al., 2011; Kuo et al., 2013; Song et al., 2015).

Denmark has for many years used processed IBA minerals as a sub base material in road construction. Since 2012, Danish legislation has allowed for EfW IBA to be used in roads with a high load. Research is being carried out, aiming to allow for incineration ashes to be used in road construction without load restrictions. In Denmark, roughly 3 million tonnes of concrete products are produced annually. It is estimated that for this amount of concrete products, 1.3 million

tonnes of virgin cement production can be avoided by utilizing bottom ash (Kallesøe, 2012). France, Germany and the Netherlands are examples of European countries that also utilize bottom ash from waste incineration as a sub base material for road construction. In all countries, the degree of contamination of the leachate is tested prior to utilization and the degree of utilization is high in all cases. For example, along the A12 highway in the Netherlands, processed IBA minerals from Dutch incineration plants are the primary material for more than 1 km of noise barrier.

In Switzerland processed IBA minerals are generally landfilled and therefore not utilized. However, the finer fraction of processed IBA minerals is in some cases utilized in APC stabilization. In APC stabilization, cement and water is mixed with the APC, creating a solid chemically inert concrete block. By mixing the fine IBA fraction with the APC, less cement must be added in order for the mixture to solidify and stabilize the APC. The demand for virgin produced cement is thereby lowered (Koralewska et al., 2014).

The drivers for IBA utilisation are typically associated with the cost of processing and the demand for the final product. However, long term environmental effects must also be evaluated to ensure the sustainability of the IBA upcycling technique. The major environmental concerns are associated with the potential leaching of processed IBA minerals constituents, such as heavy metals and soluble salts. With regard to toxicity to water and soil, the environmental impact of using processed IBA minerals in road construction has been shown to be comparable with disposal of processed IBA minerals in controlled landfills. By taking into account the natural aggregates and fossil fuels savings, IBA utilisation is demonstrated superior (Olsson et al., 2006; Birgisdóttir et al., 2007; Toller et al., 2009; Blengini et al., 2012; Beylot and Villeneuve, 2013; Boesch et al., 2014). However, the leaching potential is directly linked with the particle size of the processed IBA mineral, which affects the permeability of the sample. In addition, the significant high costs for disposal and the high volumes of IBA production has lead scientists to identify alternative utilisation techniques with main objective the elimination of environmental impacts. These methods target to the decontamination and/ or inertization of processed IBA minerals and normally involve chemical and thermal methods (Eusden et al., 1999; Cheeseman et al., 2005; Park et al., 2007; Xiao et al., 2008; Polettini et al., 2009; Jing et al., 2013; Santos et al., 2013; Lancellotti et al., 2015).

The most efficient alternative methods include thermal treatments of processed IBA minerals, by sintering and vitrification. These techniques have the ability to completely destroy the organic pollutants and encapsulate metals of environmental concern into the new crystalline phases formed, and therefore, the leaching potential is normally extremely low. Sintering is a thermal treatment process that has the ability to improve the mechanical and other engineering properties of compacted materials and promote the densification of the body (German et al., 1985). Sintering cycles generally consist of three phases: gradual heating of the 'green' body to the soak temperature, which typically is approximately two-thirds of the melting point of the material at ambient pressure; a soak period of constant, peak temperature (soak temperature), where the bond between the material grains is formed and a gradual cooling down of the fired material. Sintering is normally used for the production of ceramics, metals and composites. High temperature sintering has been used for the conversion of inorganic waste materials, including processed IBA minerals, into products with minimal adverse environmental effects and improved properties for potential reuse. The waste derived products have been used in several applications, such as ceramics for construction, bricks and other civil engineering applications.

Previous research has focused on the effect of sintering conditions on the properties of sintered processed IBA minerals samples. The results were consistent and indicated that the sintering time and temperature are directly proportional to the density, linear shrinkage and compressive strength of the sintered samples, and inversely proportional to the water absorption. Processed IBA minerals have also been used as sintering promoter in ceramic manufacture and has been mixed with other waste materials and sintered for the production of construction materials, such as ceramics and aggregates (Sorensen et al., 2000; Barbieri et al., 2002; Bethanis et al., 2004; Cheeseman et al., 2005; Baruzzo et al., 2006; Rambaldi et al., 2010; Schabbach et al., 2013). The properties of the sintered products were in compliance with the requirements for the conventional building materials. Sintering has also been applied by many researchers to reduce the leaching of processed IBA minerals and other waste materials. As received and sintered processed IBA minerals were subjected to the acid neutralisation capacity (ANC) test and leachate analysis. The results were similar from most studies and indicated a significant reduction in ANC and leaching of most metals of concern examined, at all pH conditions, but especially at alkali pH levels. The only exception was Na leaching which was only reduced at alkali pH levels (Van der Sloot et al., 2001; Bethanis et al., 2004).

Vitrification is a thermal process where raw materials are melted to form a glass at relatively high temperatures and then held at lower temperatures to promote crystallisation and form an amorphous, homogeneous phase solid. Vitrification results in a glass-ceramic material, which incorporates complex chemical compositions into materials with advanced properties. Typical vitrification temperatures are much higher than sintering temperatures, and range between 1100 and 1500 °C (Rawlings et al., 2006).

A significant amount of research has involved melting processed IBA minerals to form a glass which is then ground, compacted and sintered for the production of glass-ceramics. Glass-ceramics have been manufactured by a variety of silicate based waste materials, such as coal fly ash (Boccaccini et al., 1996; Kumar et al., 2000; Zhang et al., 2007; Yoon et al., 2013) , metallurgical slag (Ponsot and Bernardo, 2013; Rozenstrauha et al., 2013), blast furnace slag (Lin et al., 2009; Wang et al., 2010; Zhao et al., 2012; Francis et al., 2013) slag from steel production (He et al., 2012), ash and slag from waste incinerators (Tang et al., 2014), red mud from aluminium production (Yang et al., 2008), waste glass from lamp and other glass products (Lin et al., 2009; Cicek et al., 2014; Fan and Li , 2014) and electric-arc furnace dust and foundry sands (Pelino et al., 2002). The manufacture of glass-ceramics has also been reported from IBA mixed with glass cullet (Barbieri et al., 2008) and other waste materials, such as fly ashes and fine corundum-based waste from an aluminium foundry (Ferraris et al., 2001; Appendino et al., 2004; Aloisi et al., 2006; Andreola et al., 2008; Xiao et al., 2008; Karamanov et al., 2014; Zhang et al., 2015). Vitrified processed IBA mineral has also been used as feldspar substitute for the production of porcelain stoneware, and this resulted in a 20 °C reduction in the sintering temperature (Barbieri et al., 2006).

These processes clearly produce high quality glass-ceramics but involve melting at high temperatures and therefore high energy consumption. They have also used all the mineral fraction of processed IBA remaining after metal extraction, whereas industrial applications already exists for much of this material as secondary aggregate. The only fraction in terms of high leaching potential and limited utilisation techniques is the fine fraction of processed IBA.

1.8 LEACHING TESTS AND REGULATIONS

1.8.1 Leaching tests

Leaching can be broadly defined as the mobilization, extraction or washing of soluble constituents from a solid phase by a contacting solvent. Leaching tests are typically used to provide information about the constituent concentration or the constituent release from a waste material under reference test conditions, or under conditions that more closely approximate the actual disposal site. This information may subsequently be used in computer models to predict long term leaching behaviour. They are useful tools for the assessment and regulation of waste materials, and the legislation for utilization is usually based on leaching criteria. Some of the factors which may influence the leaching of granular waste materials are particle size of the waste, pH in the liquid phase, contact time between waste and leachant, chemical/ mineralogical composition of waste and buffering capacity of the liquid solution (Astrup et al., 2010; Van der Sloot and Kosson, 2012).

Waste materials contain a variety of heavy metals and salts which, if managed inappropriately, may spread via leaching during utilization or disposal, and eventually lead to soil and water pollution. This can occur in stockpiles, landfills, and utilization fields. Leaching of waste materials is a highly complex subject which requires substantial background knowledge to interpret leaching data adequately. The selection of the appropriate leaching test depends on the general objective and/ or more specific questions that need to be addressed.

Leaching tests vary from batch or flow-through, static or agitated, and depend on the information needed in each case. There is not a single answer as to which leaching method is more appropriate for the characterisation of waste materials, therefore, there should be a case by case evaluation. For example, the EU Directives and most of the national regulations advocate the use of processed IBA minerals as secondary aggregates. However, the problem fraction in terms of leaching is the fine fraction, for which alternative sustainable uses are not available.

Batch Leaching Test. The objective of this test is to simulate accelerated leaching of trace elements over a time interval up to 30 years with certain precipitation conditions and IBA layer thickness in the field.

The test sample is mixed with DI water at a liquid to solid ratio of 10 l/kg on an end-over-end tumbler for 24 hours. The eluate is then analysed using ICP-OES for its trace element contents (Van der Sloot, 2015).

pH-dependence Leaching Test. The results of pH-static leaching offer an informative reference for estimating the variation of test sample leaching level under different environmental pH and the availability of leaching for each element.

In this test, separate test portions are leached at a fixed L/S ratio with leachants containing pre-selected amounts of acid or base in order to reach stationary pH values at the end of the extraction period. Each leachant is added in three steps in the beginning of the test. At least 8 final pH-values are required, covering at the minimum the range pH 4 to pH 12. The tests are carried out at a fixed contact time of 48h, at the end of which equilibrium condition can be assumed to be reached for most constituents in test sample (Van der Sloot, 2015).

Column Leaching Test. This test resembles the percolation scenario after test sample has been placed in the field and allows modelling of this situation, although the test is typically carried out under water saturated conditions which is a worst case leaching scenario. Whether the test sample is saturated in real application depends on the groundwater table and the permeability of the materials around the test sample.

This test is designed to provide the release of substances as a function of L/S under specified conditions intended to ensure local equilibrium between the substances in the solid and aqueous phases and at the pH imposed by the waste itself. In this test, IBA is packed in a column in a standardised manner. The leachant is percolated in up-flow through the column at a specified flow rate up to a fixed L/S ratio. The eluate is collected in several separate fractions. Both deionised water and seawater can be used in this test. The execution time of the test is approximately 30 days for L/S = 10 l/kg (Van der Sloot, 2015).

Compacted Granular Leaching Test. The purpose of the test is to simulate the diffusion-controlled leaching of inorganic components from granular test sample that has been compacted in the field, as a function of time over a period of 64 days.

In the test the diffusion controlled leaching of IBA is simulated by compacting a quantity of it in a cylindrical vessel and then exposing it on one side to a leaching fluid and refreshing the eluates at set times. The concentrations of the leached components in the successive eluate fractions obtained are measured. The pH value under which the leaching is carried out is

imposed by the test sample. Based on the results of the test the leached quantity per unit area of each component analysed is calculated both per fraction and cumulatively (Van der Sloot, 2015).

1.8.2 Environmental standards

There are significant differences in the approaches used by countries to develop leaching test methods and the acceptable leaching limit values could vary up to three orders of magnitude (Van der Sloot, 2015).

Europe: The EU members are required by EU legislation to follow the standards provided by CEN/TC 292 for the management of waste. CEN/TC 292, established in 1992, is a technical committee in the European Committee for Standardization (CEN) for the characterisation of waste. The objective of CEN/TC 292 is to provide a standardized methodology for waste characterisation, which will help to improve comparability of results and ensure uniformity in waste practice. However, the responsibility in setting the limit values for beneficial use of residues is out of the scope of CEN/TC 292. Thus, it is at individual countries' discretion to set up their own regulations and criteria for waste utilization according to their specific situation. Waste acceptance criteria (WAC) for hazardous and inert landfill sites came into force in the EU in July 2005, with the end of co-disposal, and set leaching limit values that must be achieved if a particular pre-treated waste is to be acceptable for landfill disposal. In the UK the BS EN 12457 parts 1-4:2002 'Leaching – compliance test for leaching granular materials and sludges' is used for the characterization of all waste types. BS EN 12457 is a one stage batch leaching test at a liquid to solid ratio of 10 l/kg for materials with high solid content and with particle size below 4 mm. In addition, the BS EN 14899:2005 'Characterisation of waste – Sampling of waste materials -Framework for preparation of a sampling plan'. Testing is therefore to demonstrate that variability is within an acceptable range, which has been set up by the Council Decision 2003/33/EC (Table 1.5). The Council Decision requires that compliance testing is carried out at least once per year and to the scope and frequency determined by the Basic Characterisation for regularly generated wastes (Environment Agency, 2013). For use of waste materials as aggregates, the producer must comply with all the requirements of a BS EN aggregates standard appropriate to the use for which the aggregate is destined for at the time it is produced to comply

with the Quality Protocol. There are various BS EN standards, however, the documentation is out of the scope of this research.

Table 1.5: Leaching limits as set out in Council Decision 2003/33/EC (European Union).

Element or substance	Inert Wastes			Non-hazardous wastes			Hazardous waste acceptable at non-hazardous waste landfills			Hazardous waste acceptable at hazardous waste landfills		
	L/S = 2 L/kg	L/S = 10 L/kg	C_0 percolation test	L/S = 2 L/kg	L/S = 10 L/kg	C_0 percolation test	L/S = 2 L/kg	L/S = 10 L/kg	C_0 percolation test	L/S = 2 L/kg	L/S = 10 L/kg	C_0 percolation test
	mg/kg	mg/kg	mg/L	mg/kg	mg/kg	mg/L	mg/kg	mg/kg	mg/L	mg/kg	mg/kg	mg/L
As	0.1	0.5	0.06	0.4	2	0.3	0.4	2	0.3	6	25	3
Ba	7	20	4	30	100	20	30	100	20	100	300	60
Cd	0.03	0.04	0.02	0.6	1	0.3	0.6	1	0.3	3	5	1.7
Cr (total)	-	-	-	4	10	2.5	4	10	2.5	25	70	15
Cu	0.9	2	0.6	25	50	30	25	50	30	50	100	60
Hg	0.003	0.01	0.002	0.05	0.2	0.03	0.05	0.2	0.03	0.5	2	0.3
Mo	0.3	0.5	0.2	5	10	3.5	5	10	3.5	20	30	10
Ni	0.2	0.4	0.12	5	10	3	5	10	3	20	40	12
Pb	0.2	0.5	0.15	5	10	3	5	10	3	25	50	15
Sb	0.02	0.06	0.1	0.2	0.7	0.15	0.2	0.7	0.15	2	5	1
Se	0.06	0.1	0.04	0.3	0.5	0.2	0.3	0.5	0.2	4	7	3
Sn	-	-	-	-	-	-	-	50	-	-	-	-
Zn	2	4	1.2	25	50	15	25	50	15	90	200	60
Cl	550	880	450	10000	15000	8500	10000	15000	8500	17000	25000	15000
F	4	10	2.5	60	150	40	60	150	40	200	500	120
SO_4	560	1000	1500	10000	20000	7000	10000	20000	7000	25000	50000	17000

USA: One of the most widely known and used leaching tests is the US EPA Toxicity Characteristic Leaching Procedure (TCLP). TCLP is a leaching test used to determine if a waste is hazardous before acceptance into a landfill. It is developed based on the co-disposal of industrial waste in a municipal solid waste (MSW) landfill without management: a worst-case (mismanagement) scenario. The leachant used in TCLP is acidic to reflect the condition at a MSW landfill with organic biodegradable matter, which will produce acids, leading to a much higher leaching of heavy metals compared to other leaching standards. This scenario is totally different from an IBA utilization scenario, where the amount of organic degradable matter is very low, and pH is unlikely to drop below 7 (particularly in a marine environment), even with excessive carbonation. The TCLP is therefore not applicable to risk and impact assessments related to the use of IBA (or any other waste materials, for that matter) under natural conditions. The limit values normally used with the TCLP test are not risk-related, but simply based on drinking water standards multiplied by 100. Because of its availability, the TCLP has been widely used out of its scope, and as such, adopted for regulatory use by several countries, but providing results that in general are not related to the risk it is meant to assess. As a consequence, the US EPA has developed a set of new tests (Methods 1314 to 1316) which are to be included in "Test Methods for Evaluating Solid Waste – Physical/Chemical Methods" (SW-846), issued by the US EPA. The three first methods are practically the same methods as the European CEN methods (EPA, 2014).

1.9 CERAMICS

The term 'ceramic' is derived from the Greek word 'keramikos', meaning burned substance, since the desired properties are obtained with high temperature heat treatment (sintering). It is one of the most ancient industries, since first hand made pottery were discovered in Japan and dated back to 9,000 BC (Virta, 2003). Ceramics are defined as inorganic and non-metal behaviour materials, made up of metal and non-metal elements with ionic or covalent bonds. The ceramics industry can be separated into seven sectors: Bricks and roof tiles, wall and floor tiles, vitrified clay pipes, refractory products, table and ornamental ware (household ceramics) and sanitary ware and technical ceramics (EU BREF, 2007). The global ceramics market reached a value of £95 billion in 2013 with EU accounted for approximately 23% of the

global ceramic market. The tile industry dominates the sector, accounting for 32% of the total ceramic industry production (Cerame-Unie, 2013).

In most cases readily available, cheap, abundant, local materials are used to make ceramics. Naturally- occurring raw materials used to manufacture ceramics include a variety of clays (including ball clay, kaolin, fire clay, and common clay), feldspar, talc, silica, and nepheline syenite. Silica can be in the form of silica sand, quartz, or flint. Extracting and processing these resources is very demanding and polluting to the natural environment (scarred landscape, noise, dust, energy usage etc.). For example, for the production of roof and wall tiles, 30 to 35% of the production costs are associated with the production of raw materials, corresponding to the highest share of the production costs, as explained in section 1.11 (EU BREF, 2007; Cerame-Unie, 2013). To alleviate these bottlenecks of production, legislative bodies place a lot of pressure on the use of waste materials in construction industry, in the general concept of circular economy. Therefore, one approach for relieving pressure on the demand for ceramics is to provide an opportunity for artificially manufactured raw materials suitable for ceramic manufacturing to be considered. These are materials that would otherwise need to be extracted from the environment, at great cost and potential for environmental damage, or to be imported from remote locations. This, together with the economic burden of waste disposal and associated adverse environmental impacts, have made it highly desirable to develop alternative techniques for converting wastes into revenue-earning products that reduce the demand for less accessible non-renewable materials. Processing mineral wastes and combustion ashes to produce ceramics is one of the most attractive reuse applications with particular benefits both in terms of resource recovery and protection of the environment. One way to offer a product competitive on cost with the materials already used (terrazzo, pavers, natural stones, etc.) but providing full value of the ceramics is the use of high proportions of waste to obtain these products, not only the wastes generated in the ceramic tile manufacturing process but also wastes from high thermal processes.

1.10 CERAMIC TILES

The European standard for ceramic tiles BS EN 14411 defines ceramic tiles as: “Thin slabs made from clays and/or other inorganic raw materials, generally used as coverings for floor

and walls, usually shaped by extruding or pressing at room temperature but may be formed by other processes, then dried and subsequently fired at temperatures sufficient to develop the required properties, tiles can be glazed or unglazed and are incombustible and unaffected by light". Ideally ceramic tiles should have:

- a strong but high density, sintered ceramic core;
- a dense continuous surface layer to inhibit ingress of water and enhance strength;
- low shrinkage to prevent deformation and cracking during sintering

Typical water absorption values and uses of tiles are given in Table 1.6 (Cerame-Unie, 2013; EU-BREF, 2007).

Table 1.6: Water absorption and uses of wall and floor tiles (EU-BREF, 2007; Cerame-Unie, 2013)

	Water absorption of tile (%)	**Uses**
Impervious tiles	< 0.5	All interior and exterior
Vitreous tiles	< 3	Outdoor rooms and all interior
Semi-vitreous tiles	3-7	Only interior
Non-vitreous tiles	> 7	Only interior

Ceramic tiles are important external and internal covering products used in the building and housing industry. Other applications include external facades, swimming pools and public areas. Ceramic tiles can be shaped, sized, styled and finished (glazed) in a variety of ways to enhance the final product, as well as being physically strong, long-lasting and aesthetically pleasing. The most common tile shapes are squares and rectangles, but other polygonal shapes are also available. As for size, tile sides range from only a few centimetres to slabs with 60 to 100 cm sides and thicknesses range from around 5 mm to over 25 mm (EU BREF, 2007; Cerame-Unie, 2013).

1.11 CERAMIC PROCESSING

Ceramic manufacturing involves the processing of raw materials, which are normally crushed, ground and classified in sizes. Except for the raw materials, binders are used, such as clays and other materials that facilitate processing or impart specific properties to the final product. The processed materials are then wet or dry milled for the production of a more chemically and physically uniform material suitable for forming. Wet milling is typically used when the ceramic products are formed by slip casting, while dry milling is used when the products are dry-pressed. The most common technique for the manufacture of ceramics is wet milling followed by spray drying and pressing.

The forming step allows the production of a cohesive material with specified shape and dimensions. Forming techniques can be either dry or wet. The most common technique of dry forming is pressing in a rigid die or mould. Prior to pressing, spray drying is typically used to produce a free-flowing powder suitable for further processing. In spray drying, the ceramic powder is mixed with water to from a slurry, which is injected into a drying chamber with hot gases at temperatures between 70° to 570°C. The produced granulated powder is then collected in a cyclone or fabric filter. Other dry forming techniques involve isostatic pressing, vibratory compaction and jiggering by plastic or injection mouldings. The dry pressing technique applied is associated with the shape and the complexity of the ceramics to be produced. Wet forming is usually applied by slip casting and to a lesser extent by gel or tape casting. In slip casting, the ceramic mix with a moisture content of 20 to 35% is placed into a porous mould. Capillary suction of the mould draws the liquid from the mould, thereby consolidating the cast ceramic material. After a fixed time, the excess slurry is drained, and the cast shape is dried.

The next step of processing involves drying of the formed material to eliminate the moisture content and therefore, prevention of differential shrinkage, distortion, cracking, and spilling when the material is fired for the production of ceramics. Drying is typically performed in continuous or periodic dryers at temperatures ranging from 80°C to 120°C. The tile bodies are then fired in tunnel kilns and roller hearth kilns (roller kilns) at temperatures between 900°C and 1400°C. Firing cycle times range from less than 1 hour to 48 hours.

Additional processing techniques involve glazing, to provide a smooth, shiny surface that seals the ceramic body and grinding, polishing, sand blasting, drilling, sawing, or lathing, to enhance ceramic characteristics or to meet dimensional tolerances (Virta, 2003; EU BREF, 2007; Cerame-Unie, 2013).

The total cost of raw materials for the production of floor tiles amount to 374£/1000 m^2. A breakdown of the costs associated with the manufacture of floor and wall tiles is presented in Table 1.7. The manufacturing of wall and floor tiles include energy costs, which are the costs of electricity and fuels used in the production of clay ceramic products; labor costs which are the costs associated with wages and benefits; and the cost of materials which are the costs of tangible inputs. (Cerame-Unie, 2013).

Table 1.7: Breakdown of wall and floor tiles production (Cerame-Unie, 2013)

	Production costs (%)
Energy	25-30
Labour	25-30
Raw materials	30-35
Other production costs	10-15
Total	100

A range of sintered ceramics have been produced by a variety of waste materials, including IBA mixed with clay and other waste materials, such as marine dredging spoil, water treatment sludge cake; thermal power station ash; incinerated sludge ash and other waste materials (Rawlings et al., 2006).

During the formation of monolithic samples sintering occurs in three overlapping stages (German, 1985):

- Rearrangement of the initial particles occurs as the material is heated in two stages, and it is due to the melting of the glass and the formation of liquid within the particles. Primary rearrangement takes place from the spreading of the liquid and depends on the melt spreading rate, whereas secondary rearrangement includes clustering from the expansion of the melt zone through the un-wetted particles; and penetration, which leads to disintegration of the solid and rearrangement of fragments. Typically, fine particles give better rearrangement and if enough liquid is formed, full density is possible by rearrangement.
- Solution-precipitation is the second stage of liquid phase sintering, which relies on solid solubility in the liquid and greatly depends on the grain size and shape. Diffusion leads

small grains to large, causing growth of the large grains. Furthermore, diffusion alters the grain shape, resulting in pore elimination and the formation of a rigid skeleton of solid.

- The final stage of the liquid phase sintering involves an extension of the second stage, where the rigidity of the solid skeleton decelerates the densification rate, although diffusion continues microstructural coarsening. The diffusion events lead to contact growth between solid grains, while the porosity may stabilize or totally eliminated, unless an insoluble gas is trapped in the pores, causing compact swelling.

1.12 THE PROBLEM IN PERSPECTIVE

Estimated urban population in the year 2050 will be 6 billion, which is equal to the population of the world in 2000 (World Economic Forum, 2015). This growth will challenge cities to move towards sustainable management of MSW and to develop alternative techniques for producing secondary raw materials, since the availability of natural/ virgin raw materials will decline rapidly.

In 2010, global MSW generation amounted at about 1.3 billion tonnes (Hoornweg and Bhada, 2012), and this is projected to reach about 4.5 billion tonnes by 2100 (Hoornweg et al., 2013). Landfilling have been a cost-effective option for MSW, and an estimated two thirds of global MSW is disposed of in landfills that range from highly engineered landfills to waste dumps. However, lack of available void space, concerns about the leaching potential of wastes and the long-term environmental burdens mainly associated with the emissions of methane, have lead communities to consider alternative, more sustainable integrated options for the disposal of MSW, with extensive recycling, composting and EfW of the residual waste. Proper planning and political will and commitment is needed to accelerate these actions. The EU, these efforts are aided by the implementation of legislation, such as the landfill tax, which provide incentives for people and businesses to move towards a ‘do more with less’, circular economy approach. A circular economy is restorative and regenerative by design, and aims to keep products, components and materials at their highest utility and value at all times, distinguishing between technical and biological cycles (Ellen Mac Arthur, 2014). It aims in ‘closing the loops’ of processes, and therefore, processes indicate no losses of materials and resources.

Energy from Waste (EfW) involving combustion is a sustainable waste management technology used in many countries throughout Europe and world-wide. It is estimated that 80 million tonnes of residual municipal solid waste (MSW) is combusted annually in the EU with the energy released producing steam and electricity in approximately 430 EfW facilities. EfW is a proven and dominant alternative to landfill for the disposal of MSW and is expected to increase in most countries due to legislative pressures. However, the main by-product from the combustion of MSW, the incinerator bottom ash, which amounts for 250 to 320 kg per tonne of thermally treated input waste, needs to be properly disposed or utilised. IBA is normally processed for the recovery of ferrous and non-ferrous metals by dry physical separation (magnetic and eddy current separators) and the production of mineral aggregates for use in construction. IBA also contains a significant amount of fine material, the size and quantity of which depends on the technology used. There are currently limited alternative beneficial reuse options for this material which is typically either disposed of directly to landfill, or in some cases such as Switzerland, where dry discharge systems are gaining popularity, is reused as a cement substitute for stabilizing neutral washed filter ashes prior to disposal in a hazardous landfill at a significant high cost. Concerns over the potential adverse environmental effects of the fine fraction, has lead scientists to identify more sustainable processing techniques, but further research is still needed (Bio Intelligence Service, 2012; CEWEP, 2012).

In order to accelerate the adaptation of cities to the climate change, there is a global trend dealing with the identification of bottlenecks in processes and the development of circular economy techniques able to recycle or upcycle the produced wastes. Making use of IBA shows resource savings in virgin materials and fossil fuels. In addition, the depletion in world natural resources such as clay and the production of ceramics for construction purposes is an ever-increasing problem, since it involves environmental intense processes. Therefore, two opportunities co-exist, the upcycling of wastes and the provision of ceramic materials.

CHAPTER 2 RESEARCH AIM AND OBJECTIVES

2.1 RESEARCH AIM AND OBJECTIVES

The aim of this research is to develop processing technology to produce an inert material from the fine fraction of processed IBA produced by either wet or dry discharge technology. The work investigates how this material can be transformed into a viable raw material for manufacturing sintered ceramics with high density and hardness that exhibits low shrinkage during firing. The research aim will be achieved by meeting the following objectives:

- Characterizing the physical and chemical properties of the fine fraction of processed IBA;
- Understanding the effect of processing parameters on the properties of the end-product;
- Developing a laboratory process for the production of an inert material containing a significant fraction of fine processed IBA;
- Developing a laboratory technology for manufacturing ceramics produced from the inert raw material, by characterising relevant physical, mechanical, chemical properties and leaching potential according to the legislative standards. The optimum ceramics should have a density of > 2.1 $g.cm^{-3}$, negligible water absorption and hardness > 4.0 MPa.

2.2 EXPERIMENTAL APPROACH

The experimental approach is presented in Figure 2.1. The research has been divided in four parts as follows:

Part 1: Investigation of the ash characteristics and processing effects on product properties

The as-received fine IBA dust from dry discharge technology has been characterised in terms of the chemical composition, mineralogy and leaching behaviour. The effects of processing parameters on the materials produced have been examined. The effect of adding glass to the dry discharged fine IBA dust has been investigated. The materials produced have been characterised, for chemical composition, physical and mechanical properties, mineralogy, microstructure and leaching behaviour.

Part 2: Effect of calcining to obtain an inert material suitable for the production of dense ceramics that exhibit low firing shrinkage

The produced powder and ceramics have been characterised and compared with commercially available ceramic tiles, with respect to their physical and mechanical properties. The mineralogy and leaching behaviour has also been investigated.

Part 3: Process envelopes- optimisation and boundaries of the system

This research involved the use of statistical models and response surface methodology to determine the boundaries of the system developed and optimise further the process. This step was critical to obtain the optimum conditions, for which the dry discharged fine IBA dust can be processed to form an inert material and up-cycled for the production of ceramic tiles.

Part 4: Effect of IBA discharge technique

This research involved the effect of wet discharged fine IBA in the process developed. The material has been fully characterised, following the techniques used in Part 1 of the research. The repeatability of the process has been examined and the materials produced were characterised, in terms of physical, chemical and mechanical properties and compared with the ceramics produced by the dry discharged fine IBA dust and commercially available ceramics. The mineralogy and leaching behaviour of wet discharged fine IBA-derived ceramic has been also characterised and compared with the dry discharged fine IBA dust-derived ceramic.

Now that the aims and objectives of the research have been defined the next chapter outlines the materials and methods used for the completion of this research.

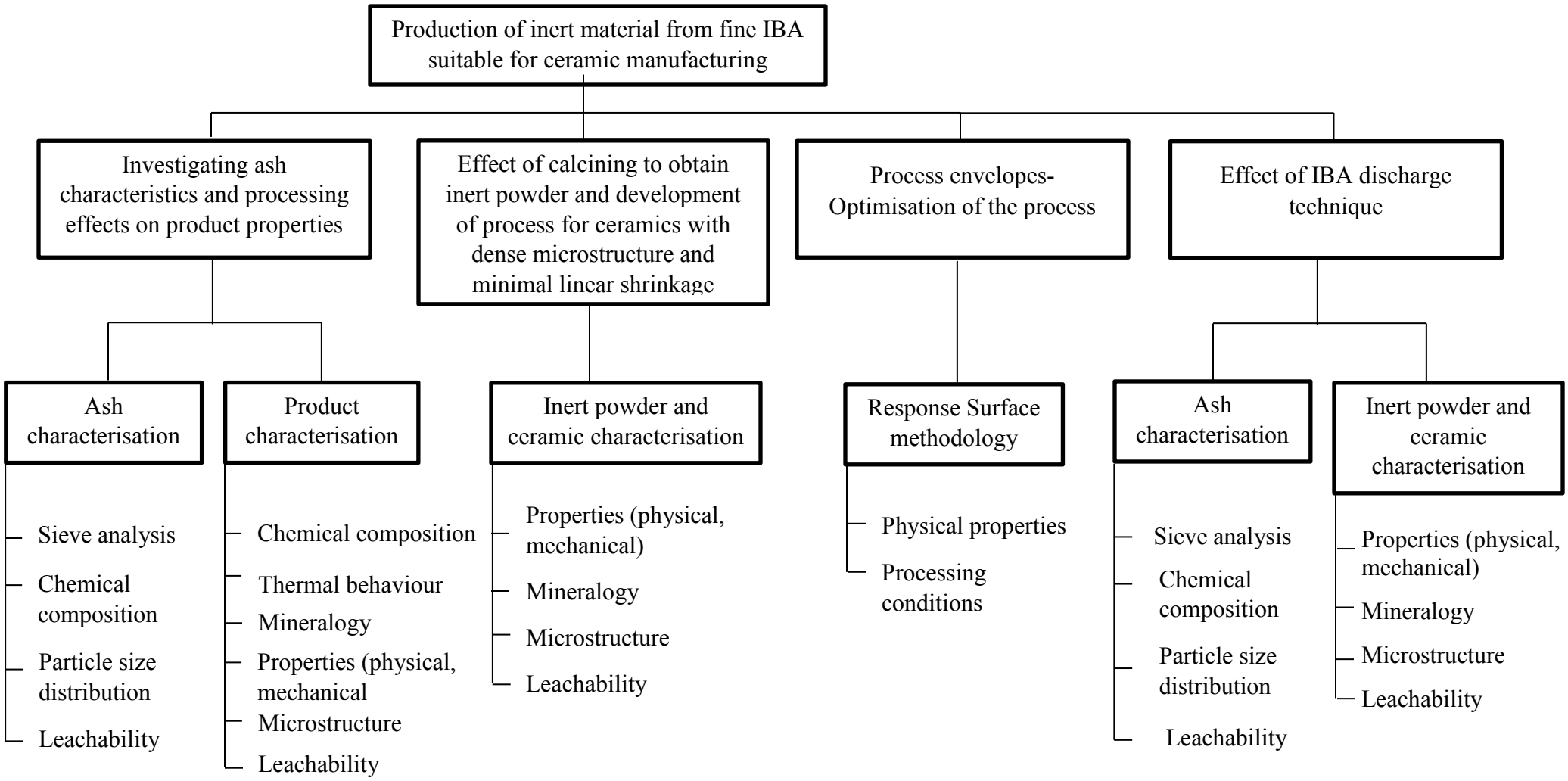

Figure 2.1: Schematic diagram of the scope of the work

CHAPTER 3 MATERIALS AND METHODS

This chapter describes the materials and methods used in the processing of the fine IBA samples. In addition, it describes the methodologies used to characterize the produced materials.

3.1 MATERIALS

3.1.1 Fine IBA

In this project fine fraction of IBA has been obtained from two different sources. The less than 1 mm dry discharged IBA dust fraction was supplied by Martin Gmbh. Martin Gmbh have recently developed a dry discharge system for IBA which is used in the EfW plant at Monthey, Switzerland. IBA had been pre-treated, as described in section 1.6.2. This material is challenging because it is currently used as cement substitute for the stabilisation of filter ashes and disposed of in hazardous landfills at significant high costs, an option which is not ideal.

The second fine IBA fraction was obtained from Day Group (Brentford facility, SE England) who manage the wet discharged material from the Lakeside and the Newhaven EfW facilities in the UK. This had previously been treated, as explained in section 1.6.2. This material is because it is currently landfilled at high costs, a solution which is not sustainable.

3.1.2 Glass

Glass is an amorphous solid material that is produced from inorganic materials, fused together at high temperatures and cooled rapidly to form a rigid structure. However, the cooling time is not adequate to enable the formation of a crystalline regular structure. Most of inorganic glasses comprise of a network of covalently bonded silica (SiO_2) tetrahedral, while other oxides may be added to alter glass structure and give glass properties suitable for its applications, which range from packaging to medical equipment and building products. For example, Aluminium oxide (Al_2O_3) may be added to improve glass durability or sodium (Na_2O) and calcium oxides (CaO) to decrease glass viscosity (Lenntach, 2014). Soda-lime glass is the most common marketable glass, corresponding to approximately 90% of the total glass production. It is prepared by melting the raw materials, such as silicon oxide (silica, sand), limestone (lime),

sodium carbonate (soda), dolomite, and aluminium oxide. Other forms of glass which are commonly used are lead glass and borosilicate glass (Alim 2009).

It is estimated that approximately 17 million tonnes of glass containers were consumed throughout the European Union in 2012, with about 71% being recycled. In the UK, of the 2.7 million tonnes of glass consumed, approximately 61% was recycled (FEVE 2014). The recycling of glass typically involves sorting, crushing, removal of metals and other impurities, such as paper and plastics and reuse in a variety of applications. By substituting 1 tonne of recycled glass for virgin raw materials, 1.2 tonnes of virgin raw materials can be saved and 670 kg of CO_2 emissions are avoided in a cradle to cradle scope (FEVE, 2014). The use of glass as sintering promoter for the production of construction materials has had promising results (Ducman et al., 2002; Kourti and Cheeseman, 2010). In addition the high content of SiO_2, which exhibit low melting point, has the ability to generate more viscous phases with lower viscosity, and subsequently improve the strength and reduce the water permeability of the materials produced.

The glass which used in the experiments is EcoSand, a mixture of various glass containers and bottles such as wine bottles and jam jars, with an average price of £15 in 2014 (WRAP, 2014). EcoSand corresponds to approximately 25% of the weight of the average household waste. This glass has been collected by local authorities and processed by Day Group Ltd. The process involves crushing, grading to size and washing to produce a glass sand. It is typically used as a paving sand under block paving and concrete slabs and has density that range from 1.45 to 1.56 $g.cm^{-3}$ (Day Group website: EcoSand). For the purpose of the research the less than 1 mm mixed-colour glass cullet free of any significant contamination was used. Chemical composition data for recycled glass were determined by X-ray fluorescence (XRF Spectro 2000 Analyser) as shown in Table 3.1.

Table 3.1: Chemical composition of glass. Data obtained by XRF analysis and expressed as oxides.

Major oxides	**Weight %**
SiO_2	70-73
Na_2O	13.8-14.4
CaO	9.1-9.8
Al_2O_3	1.7-2.0
MgO	1.1-1.7
K_2O	0.55-0.68
Fe_2O_3	0.06-0.24

3.1.3 Binders

Polyethylene glycol (PEG-8000) available as powder was used in the experiments as binder to aid pressing of samples before sintering and this was provided by The Dow Chemical Company with trade name: CARBOWAX. It is commonly used in agglomeration applications, and is extensively used in the ceramic manufacturing. Typical physical properties are presented in Table 3.2.

Table 3.2: Physical properties of Carbowax Polyethylene glycol binder

Range of Avg. Molecular weight	7,000 - 9,000
Range of Average Hydroxyl Number, mg KOH/ g	12 - 16
Density, $g.cm^{-3}$	1.085
Solubility in water at 20°C, % by wt	63
pH at 25°C, 5% Aqueous Solution	5.0 – 6.0

3.1.4 Water

Degassed tap water was used for density and water absorption determination. Tap water was used for the wet ball milling.

3.2 PROCESSING TECHNIQUES

The key objective of this research is to develop a processing technology to transform the fine fraction of IBA, into a raw material suitable for the production of ceramic products. The processing procedure investigated involved the following key stages:

a) Wet ball milling
b) Sieving
c) Calcining
d) Powder compaction, and
e) Sintering

3.2.1 Wet ball milling

In order to reduce the particle size distribution of the fine fraction of IBA: glass mixtures, ball milling was used. Wet ball milling is widely used in the ceramics industry to reduce powders to a fine particle size. During milling, particles are fractured by the mechanical impact of the grinding media against them. Wet milling has the advantage that in addition to reducing particle size, it produces a homogeneous slurry suitable for subsequent processing. In the laboratory, ball milling involves placing the material in a closed cylindrical container with grinding media and rotating the cylinder horizontally so that the media cascade. The material particles move between the larger media and between the media and the wall of the mill and are effectively broken into smaller particles (Richerson, 1982).

The apparatus used consisted of a 3-litre porcelain ball mill (Pascal Engineering Co. Ltd., Model No. 21589) containing approximately 2.255 kg high-density alumina sphere milling media (19 mm size). A milling media to charge ratio of 5 and a water to charge ratio of 2 was defined as standard milling conditions, as used in previous work to process wastes into ceramics (Cheeseman et al., 2003).

3.2.2 Sieving and pressing

The milled slurries obtained were dried overnight at 105 °C and ground in a pestle and mortar to produce a fine, homogeneous grey powder. This was passed through a 500 μm sieve to remove coarse particles unsuitable for further processing. The sieving was performed by shaking stainless steel mesh screens (ASTM standard sieves). 'Green' tile samples (110 m × 55 mm × 20 mm) and 'green' disc samples (40 mm diameter) were formed by uniaxial pressing (Nannetti S hydraulic press) in a steel die. The pressing pressure was fixed at 48 MPa, as suggested by other researchers for the processing of waste materials in ceramic manufacturing.

3.2.3 Calcining and sintering

After wet ball milling, drying and sieving to less than 500μm, the milled powder was heated in an alumina crucible to different temperatures to investigate the effect of calcining temperature. Calcining is the process of heating the powders before processing, to eliminate the volatiles present in the material. The volatile compounds are responsible for the high firing shrinkage associated with deformation and warping during firing, and therefore sintering that is difficult to control. By calcining the powders, dense ceramics are formed after sintering. After calcining, the powders were lightly ground using a mortar and pestle to produce calcined powders suitable for processing into ceramics using the same procedures as for un-calcined powders.

Pressed samples were fired in an electric furnace (Lenton, Model no. UAF 14/5), at different temperatures, with a ramp rate of 6 °C/ min and a dwell time of 60 minutes at maximum temperature. These were identified as optimum sintering conditions by other researchers (Cheeseman et al., 2003; Appendino et al., 2004; Rawlings et al., 2006; Rambaldi et al., 2010; Schabbach et al., 2012).

3.3 MATERIALS CHARACTERISATION

3.3.1 Particle size distribution of raw materials

A laser diffraction analyser (Beckman Coulter, LS-100 Series) with a particle size range between 0.4 and 900 μm was used to determine the particle size distribution of the as-received and milled fine IBA powders. The analyser uses a low power laser source, sample cell and an

array of concentric diodes to detect diffracted light, mounted on an optical bench. The sample was dispersed in clean water and the suspended particles diffract the incident light through a range of diffraction angles related to the particle size.

3.3.2 Loss on ignition of raw materials

Samples were first oven-dried at 105 °C to eliminate residual moisture. The loss on ignition was measured by heating dried samples to 550 °C, and was calculated by the percentage loss in mass of each sample (Chandler et al., 1997; ISWA, 2006; BS EN 15169:2007). 10 samples were tested to determine the loss on ignition.

3.3.3 Thermal behaviour of raw materials

The weight and energy changes of the sample when heated were measured by a differential thermal analyser (Stanton Redcroft, STA-1500 Series). The analyser is a high temperature microbalance used for the characterisation of the thermal stability of solids and liquids when heated in various temperatures and in different gas atmospheres. Both weight, Thermogravimetric analysis- TGA, and energy, differential thermal analysis- DTA, changes occurring in the samples can be measured. TGA was conducted on 25µg samples of milled powders using a ramp rate of 10 °C.min^{-1}.

3.3.4 pH measurement

The pH measurements of supernatants were made using a glass probe pH meter (Fisherbrand Hydrus series, Model 500) calibrated with standard pH buffer solutions at pH 4.00, 7.00 and 10.00 (Merck UK Limited).

3.3.5 X-ray fluorescence

X-ray fluorescence (XRF) was carried out at the Chemistry Department at Imperial College London in order to determine the major elements present in both SBE and CKD. Samples were pressed into discs and then analysed. Results were expressed as oxide % of total sample weight

3.3.6 Elemental analysis of raw materials by inductively coupled plasma atomic emission spectroscopy

ICP-AES is an analytical technique used to determine the concentrations of elements in inorganic solutions. It allows the simultaneously determination of many elements from a single sample. In ICP-AES, atoms are excited with sufficient energy to excite electrons to higher energy levels, which emit characteristic radiation on relaxing to lower energy states. The emitted energy is at specific wavelengths, which are detected simultaneously through photomultiplier tube detectors. The resulting spectrum is characteristic of the emitting element and the intensity is proportional to the concentration of the element (Thompson and Walsh, 1989). ICP-AES had to be performed on liquid samples so solids were digested prior to analysis using lithium metaborate fusion, as described below.

Lithium metaborate digestion

Lithium metaborate and tetraborate flux fusion was used to determine the major, minor and trace elements of the as-received and processed fine IBA. Lithium metaborate is a powerful flux, widely used in the characterisation of elemental composition. It has the ability to attack all major silicates and most minerals (Ingamells, 1970; Chandler et al., 1997).

Mixtures of 0.25 g of samples and 0.75 g of lithium metaborate and lithium tetraborate flux were poured into a graphite crucible and heated to 1000 °C for 20 minutes. The molten mixture is then transferred into a plastic beaker and mixed with 25 ml 1M nitric acid and 150 ml deionised water. A magnetic stirrer is used to dissolve the solution, which is then poured into a 250 ml volumetric flask and made up to volume. The solution is then shaken and filtered through a 0.45µm filter membranes into a plastic bottle. The filtrates are then analysed by ICP-AES (BS ISO 14869-2:2002).

The sulphate and chloride contents were characterised gravimetrically, by the use of $BaCl_2$ and $AgNO_3$ as precipitating agents, accordingly (APHA- AWWA-WEF, 1992).The sulphates and chlorides analysis was carried out at MEDAC Ltd, Surrey, UK.

3.3.7 Crystalline phases of raw and processed materials

X-ray diffraction (XRD) was used to characterise the crystalline phases of the as-received fine IBA and the processed materials. Representative samples were dried at 105 ºC and disc milled (Gy–Ro, Glen Creston Ltd., UK) to form powders with a mean particle size of 35 μm.

A crystal consists of a regular arrangement of atoms, ions or molecules, which produce a lattice structure with regular repeating distances, between crystallographic phases. The distances between atoms in crystals are comparable with the wavelengths of X-rays, while according to the Bragg's law, the wavelength of incident X-rays, the inter-planar spacing and the angle between the planes and the X-ray beam are connected with the following equation:

$$2d \sin \theta = n\lambda$$

where n: the order of diffraction, λ: the wavelength of incident X-rays, d: the inter-planar spacing, θ: the diffraction angle

In order to identify the crystalline phases in samples a Philips PW 1830 diffractometer system fitted with a PW1820 goniometer, an automatic divergence slit and a graphite mono-chromator using CuKalpha radiation with an accelerating voltage of 40 kV was used. A parallel beam is produced by the X-rays, which is directed at the sample, while it is rotated and scanned though a range of angles between 0 and 80˚. The diffracted beam is passed through the crystal mono-chromator and then to the detector, whereas the signal produced by the X-ray photons on the detector was amplified and recorded. For the characterisation of the diffraction patterns a comparison is being made with standard diffraction patterns (Whiston, 1987).

3.3.8 Micro structural assessment of processed materials by Scanning Electron Microscopy (SEM) and optical microscopy

In SEM a beam of electrons strikes the specimen and penetrates into a depth; depending on the energy of the beam and the nature of the sample. The interaction produces various emissions, which can provide different types of data depending on the detector used. Backscattered electrons are highly energetic electrons, while secondary electrons can knock electrons out of their orbits around an atom, with enough energy to escape from the sample. The backscattered detectors produce an electron micrograph that indicates the difference in average atomic mass between the phases, while secondary detectors produce topographical micrographs

of the sample (Bowen and Hall, 1975). Prior to testing fracture surfaces were coated with a thin layer of gold.

Microstructural analysis was characterised by the use of optical microscopy (Olympus, BX 51TRF) of polished samples. Prior to examination samples were polished to 1μm.

3.4 PHYSICAL AND MECHANICAL PROPERTIES OF PROCESSED MATERIALS

3.4.1 Density

The dimensions of the disc samples were measured using a micrometre and the weight was recorded to calculate the 'green' density of the samples.

The relative density of the sintered samples was measured according to the Archimedes principle using the formula:

m_{dry} / V_{dry} (g/cm^3)

where m_{dry} is the mass and V_{dry} is the volume of the sintered samples.

According to this principle, the apparent weight of an object immersed in a liquid decreases by an amount equal to the weight of the volume of water that it displaces ($W_{displaced}$), and is given by the product of the density of water (ρ_{water}), the volume of water displaced (V displaced) and the acceleration due to gravity (g).

$W_{displaced} = \rho_{water} V_{displaced} g$

$m_{displaced} = \rho_{water} V_{displaced}$

The mass of water displaced by the samples ($m_{displaced}$) is equal to the difference between the mass of the saturated surface-dry (m_{sat}) and the mass of the pellet in water (m_{wet}). The density of water is taken to be 1.00 g/cm^3.Therefore, the volume of the dry pellet is calculated as follows:

$m_{displaced} = m_{sat} - m_{wet}$

$V_{displaced} = m_{displaced}$

$V_{dry} = m_{sat} - m_{wet}$ (cm^3)

Therefore, the relative density is:

$m_{dry} / (m_{sat} - m_{wet})$ (g/cm^3)

3.4.2 Linear shrinkage

The linear shrinkage LS occurring during sintering was calculated from disc samples by comparing the diameter before and after firing using (BS EN 10545-8):

$$LS = (Do - Ds)*100/ Do$$

where Do is the diameter of the green disc and Ds the diameter of the sintered disc.

3.4.3 Water absorption

According to B.S 10545-3: 1997, the water absorption capacity of a sintered sample is determined by the apparent increase in weight of a dried sample when immersed for 24 hours. The following formula was used for the calculation of the water absorption:

$$(m_{sat}- m_{dry})*100/m_{dry}$$

3.4.4 Hardness

The property of a material to resist deformation by applying techniques that scratch or dent the surface is called hardness. Diamond indenters are normally used for the hardness characterisation of ceramics. The diamond pyramid Vickers test involves the measurement of the diagonals of the residual pyramidal impression after removing a given applied load (Morell, 1985; Green, 1998). Micro-hardness tests apply loads in the range of 10 to 1,000 g and macro-hardness tests use loads ranging from 1,000 to 30,000 g (Morrell, 1985).

Prior to hardness testing the samples were diamond polished to a 1 μm finish. The Vickers micro-hardness of sintered samples was measured with a Leitz Wetzlar 8423 microhardness tester using a 25 g load. The indenter employed is a square-based pyramid whose opposite sides meet at the apex at an angle of 136 °. The diamond is pressed into the surface of the material, and the size of the impression is measured with the aid of a calibrated microscope. Average hardness values were calculated from five measurements on five different samples with the Vickers number (HV) calculated from:

$$HV= 1.854 (F/ D^2)$$

where F is the applied load (kg-force) and D is the length of the diagonal of the indentation measured in mm (Ullner et al., 2001).

The main advantage of the Vickers indenter over other indenters is that it does not deform over time and use. The impression left by the Vickers indenter is a dark square on a light

background, which is easier to measure than other types of impressions. When applied on uniform materials, repeat loadings give practically identical hardness numbers. The superiority of the Vickers hardness test is associated with the accuracy of the measurements and that just one type of indenter is used for all metals and surface treatments (Quinn, 1998).

3.4.5 Young's modulus

The stiffness of an elastic material is normally characterised by the Young's modulus, also known as the tensile or elastic modulus, E. The Young's modulus of the optimum ceramics was determined by using a rectangular bar of known mass and dimensions, and applying the equation:

$$E = 0.9465*(m*f_l^2/w)*(L^3/t^3)*T_l$$

where m: mass of sample (g), w: width of sample (mm), t: thickness of sample (mm), L: length of sample (mm), f_l: flexural resonant frequency (Hertz), T_l: correction factor

The flexural resonant frequency is measured by a linear amplifier, and corresponds to the vibration excitation of the rectangular test bar resulting from an external mechanical impulse (BS EN ISO 12680-1:2007). The correction factor, T_l, for the fundamental flexural mode is used to include various factors, such as the finite thickness and Poisson's ratio. T_l is 1, when the ratio t/L approaches zero, and is calculated according to the equation:

$$T_l = 1+ 6.585*(1+ 0.0752\mu+0.8108\mu^2)*(t/L)^2 - 0.868*((t/L)^4 – J$$

where μ is Poisson's ration

The apparatus used was a GrindoSonic MK5 'Industrial' Instrument. A ball hammer of about 9 mm diameter was used to strike and excite the rectangular test bars. A transducer converts the mechanical vibration to an electrical signal, which is then analysed to give the fundamental vibration, R, for a duration of two periods. R is expressed in microseconds and the flexural resonant frequency is given by:

$$f_l = 2{,}000{,}000/R$$

3.4.6 Thermal conductivity

Thermal conductivity of the optimum ceramic samples was determined using a TT–TC Probe (Therm Test Inc.). The non-destructive technique followed is based on the Mathis modified hot-wire method, which allows the measurement of the temperature increase at a

defined distance from a linear heat source in contact with the test material. It is assumed that the heat source has a constant and uniform output along the length of the test sample. The thermal conductivity is then obtained from the change in temperature over a known time interval (Ferrandiz-Mas et al., 2014).

3.5 LEACH TESTING OF AS-RECEIVED AND PROCESSED MATERIALS

One of the most dominant factors affecting the solubility of most elements from waste materials is the pH of the leaching environment (Van der Sloot et al., 1997; Kosson and Garrabrants, 2002; Astrup et al., 2010; Van der Sloot and Kosson, 2012). The leaching characteristics of the raw and processed materials have been evaluated using the pH dependence leaching test using a liquid to solid (L/S) ratio of 10 (CEN/ TS 14429). The ability of a material to resist changes in pH is related to the buffer capacity. The CEN standard allows characterisation of leaching under different pH conditions covering a wide range from basic to acidic. The concept of buffer capacity of a material is widely used in the study of water and wastewater chemistry and hazardous waste stabilisation (Van der Sloot and Kosson, 2012). It is an important leaching characteristic of these materials that affects the ability to retain inorganic contaminants, especially heavy metals.

Samples for leaching were dried and ground to pass through a 150 μm sieve and 2 g of solid samples were mixed with 20 ml of aqueous acid solutions that varied in concentration between 0 and 100% 1.0 N nitric acid over 15 equal increments. The slurries obtained were mixed for 48 hours in a rotary extractor. The leachate was extracted and filtered through a 0.45 μm membrane filter, acidified with 10% nitric acid (HNO3) and diluted with deionised water when necessary to bring the concentrations of the elements of interest within the detection range of the instrument. The samples were then analysed by ICP-AES for a range of elements including Al, Ca, Cd, Cr, Cu, Fe, K, Mg, Mn, Na, Ni, Pb and Zn.

CHAPTER 4 PRODUCTION OF CERAMICS FROM DRY DISCHARGED INCINERATOR BOTTOM ASH DUST

4.1 INTRODUCTION

In this chapter the <1 mm dry discharged fine IBA dust fraction produced in Monthey EfW plant in Switzerland has been characterised and processed for the production of ceramics, using standard ceramic processing. This involved wet ball milling to increase sintering reactivity, drying and sieving the milled material to obtain a homogenised powder suitable for pressing and sintering. The addition of glass as sintering promoter was also investigated and liquid phase sintering was achieved at temperatures significant lower than those needed for vitrification.

The produced specimens had rectangular and cylindrical shapes, so that the effects of processing parameters on samples of a consistent 'green' state could be determined. The effects of particle size distribution, glass addition and sintering temperature on the physical and mechanical properties, mineralogy and microstructure of sintered samples have been investigated. The effect of sintering temperature on the acid neutralisation capacity and the leachability of fine IBA constituents has been studied.

4.2 AIM AND OBJECTIVES

The aim of this research is to develop a processing technology for the production of ceramic tiles from the fine IBA fraction. The primary objective of the work demonstrated in this chapter is to understand the inter-relations of the dry discharged fine IBA dust characteristics and processing variables on the performance of sintered materials. This step would also allow the identification of the bottlenecks in the processing of the dry discharged fine IBA dust for the production of ceramics by the conventional method, with respect to the desired properties of the final product. The as-received and sintered materials characterisation would allow the understanding of the influence of the dry discharged fine IBA dust characteristics and processing parameters on the properties of the sintered products.

4.3 MATERIAL PROCESSING AND CHARACTERISATION

4.3.1 Characterisation of dry discharged fine IBA dust

A representative 50 kg batch of the dry dishcarged < 1mm processed IBA, obtained from Monthey facility in Switzerland and supplied by Martin Gmbh, has been used. This represents about 10 wt. % of the total IBA produced from the plant (section 1.6.2). The major, minor and trace elements were determined by digestion using lithium metaborate and tetraborate flux fusion (section 3.3.5). The pH of the sample was determined using a glass probe pH meter, as described in section 3.3.4, and the moisture content was identified as the weight loss at 105 °C. X-ray diffraction (XRD) was used to characterise the crystalline phases in the dry discharged fine IBA dust (section 3.3.6). The energy and mass loss of the dry discharged fine IBA dust heated from 25 to 1100 °C at a ramp rate of 10 °C.min^{-1} in air, using calcined alumina as reference material, has been characterised by TGA (section 3.3.3).

4.3.2 Ceramic processing of as-received powders

The flow diagram of the process is presented in Figure 4.1.Initial experiments were conducted to identify the optimum milling time able to produce a fine powder suitable for subsequent processing. 500 g dry discharged fine IBA dust sample batches were wet milled in a

porcelain ball mill rotating at 50 rpm using high-density alumina milling media, a water to charge ratio of 2 and a milling media to charge ratio of 5. Dry discharged fine IBA dust was milled for 2, 8, 24 and 32 hours and the particle size distribution of the milled slurries was determined by laser diffraction (section 3.3.1).

After optimising the milling time, samples of 500 g of dry discharged fine IBA dust and different additions of waste soda lime silica glass were wet milled for 24 hours using the same conditions as for the milling of the dry discharged fine IBA dust. Batches with dry discharged fine IBA dust/ glass ratios of 100/0, 90/ 10, 80/ 20 and 70/ 30 by weight were milled and the particle size distribution was characterised by laser diffraction. 1 wt. % of polyethylene glycol (PEG-8000) was added as a binder to aid pressing.

Milled slurries were dried overnight at 105 °C and passed through a 500 μm sieve to form powder suitable for pressing. The > 500 μm fraction contains mainly coarse glass and stones and corresponds to 1 to 2 wt. % of the total material milled. 'Green' tile samples (110 m × 55 mm × 20 mm) and 'green' disc samples (40 mm diameter) were formed by uniaxial pressing at 48 MPa in a steel die. Pressed samples were then sintered in an electric furnace at a heating rate of 6 °C.min-1 to temperatures between 1020 and 1100 °C using a dwell time of 1 hour at peak temperature.

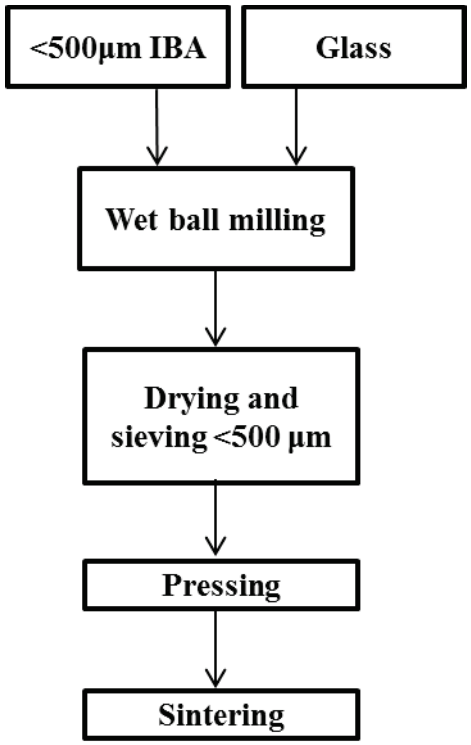

Figure 4.1: Flow diagram of ceramic processing of dry discharged fine IBA dust

4.3.3 Characterisation of sintered samples

The density, linear shrinakge and water absorption of sintered samples were characterised as explained in section 3.4. X-ray diffraction used the same procedures as for the dry discharged fine IBA dust to determine the crystalline phases present in milled and sintered samples. Polished surfaces of selected sintered samples were examined by optical microscopy (section 3.3.7).

4.3.4 Metal leaching from as-received and sintered samples

The acid neutralisation capacity and leaching characteristics of the dry discharged fine IBA dust, and the processed dry discharged fine IBA dust have been evaluated using the pH dependence leaching test using a liquid to solid (L/S) ratio of 10 (section 3.5). Samples for leaching were dried and ground to pass through a 150 µm sieve.

4.4 RESULTS AND DISCUSSION

4.4.1 Characterisation of dry discharged fine IBA dust

Chemical analysis and loss on ignition data is given in Table 4.1. Reported values represent the average measurements from 5 samples. Approximately 77% w/w of the fine fraction of dry discharged IBA dust consists of oxides of Si, Ca, Fe and Al. These data are in agreement with IBA composition data presented by other researchers (IAWG, 1994; Cheeseman et al., 2003; Bethanis et al., 2004; ISWA, 2006; Qiao et al., 2008b; Hjelmar et al., 2010; Yiao et al., 2010; Onori et al., 2011; Cheng, 2012; Lin et al., 2012;Schabbach et al., 2011; Schabbach et al., 2012; Morf et al., 2013; Liu et al., 2014). The dry discharged fine IBA dust contains significant amounts of potassium, sodium, magnesium, titanium, zinc, copper and phosphate. Heavy metals of environmental concern present in the dry discharged fine IBA dust at high concentrations, include Ba (500-550 mg/ kg), Ni (180- 210 mg/kg) and Pb (300-350 mg/kg).

The moisture content was 0.01%, as attenuated, since the material is produced in a dry process and there is no contact with water. The pH of the dry discharged fine IBA dust ranged from 11.5 to 12.5, indicating the alkaline nature of the material, mainly occuring from the presence of alkali and alkali-earth elements and metal oxides (ISWA, 2006).

Table 4.1: Chemical composition of the as-received dry discharged fine IBA dust obtained from Monthey EfW facility in Switzerland. Representative samples were dried at 105 ºC and disc milled (Gy–Ro, Glen Creston Ltd., UK) to form powders with a mean particle size of 35 μm. The powders were then pressed into discs and analysed by XRF. Results are expressed as oxides.

Oxide	Major elements % (dry basis)	Minor and trace elements (mg/kg)	
SiO_2	36.3	Ba	520
Fe_2O_3	18.4	Be	1.2
CaO	15.7	Cd	60
Al_2O_3	6.4	Co	17
K_2O	3.7	Cr	170
MgO	3.4	Mn	24
Na_2O	2.0	Ni	195
P_2O_5	1.9	Pb	350
ZnO	1.9	Sr	320
CuO	1.8	V	40
TiO_2	1.8	Y	8
		Zr	95

XRD data given in Figure 4.2 shows that the major crystalline phases present were quartz (SiO_2), calcite ($CaCO_3$), gehlenite ($Ca_2Al_2SiO_7$) and hematite (Fe_2O_3). These minerals has also been reported by other scientists as major crystalline phases found in IBA (Cheeseman et al., 2003; Bethanis et al., 2004; Polettini and Pomi, 2004; Park et al., 2007; Qiao et al., 2008a; Hjelmar et al., 2010; Yiao et al., 2010; Schabbach et al., 2011; Liu et al., 2014; Lancelloti et al., 2015). The crystalline pattern of five as-received dry discharged fine IBA dust samples from different batches was reproducible, indicating that the dry discharged fine IBA dust was homogeneous.

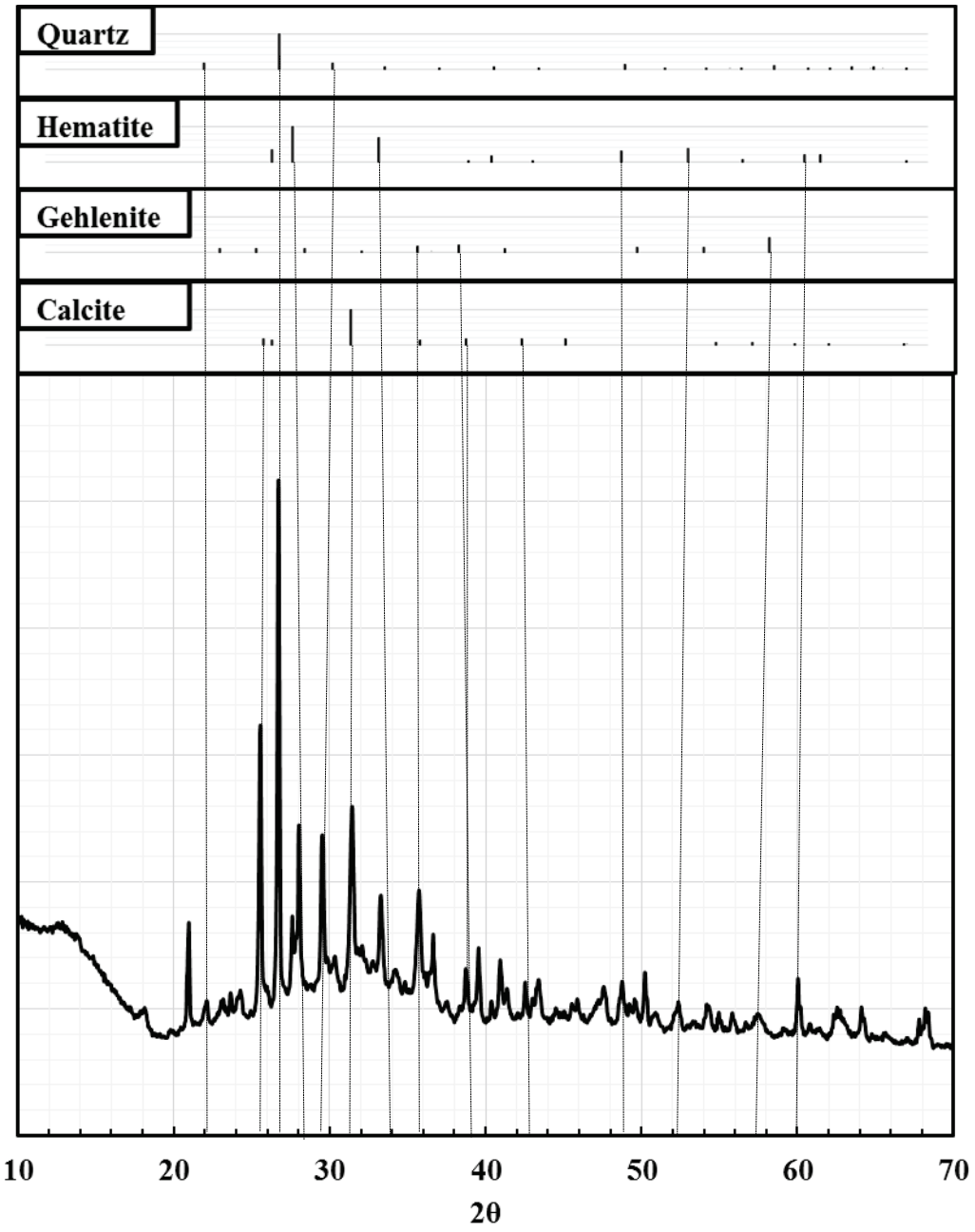

Figure 4.2: X-ray diffraction traces for the as-received dry-discharged fine IBA dust. Representative samples were dried at 105 ºC and disc milled (Gy–Ro, Glen Creston Ltd., UK) to form powders with a mean particle size of 35 μm. Schematic X-ray powder diagrams are included for relevant phases. Quartz (SiO_2), Hematite (Fe_2O_3), Gehlenite ($Ca_2\ Al[AlSiO_7]$) and Calcite (CaO) are the major crystalline phases present.

Thermogravimetric analysis data in Figure 4.3 shows that from ambient temperature to 120 °C weight loss is due to evaporation of residual moisture. Significant weight loss occurs between 550 and 850 °C due to decomposition of calcite ($CaCO_3$) to CaO and CO_2 and other volatile phases (Slavo et al., 2000; Bethanis et al., 2004; Qiao et al., 2008b). The decomposition of trace levels of alkali metal sulphates with the evolution of SO_2 is also reported to occur at temperatures between 950 and 1000 °C (Stern and Weise, 1966; Mangialardi et al., 1998).

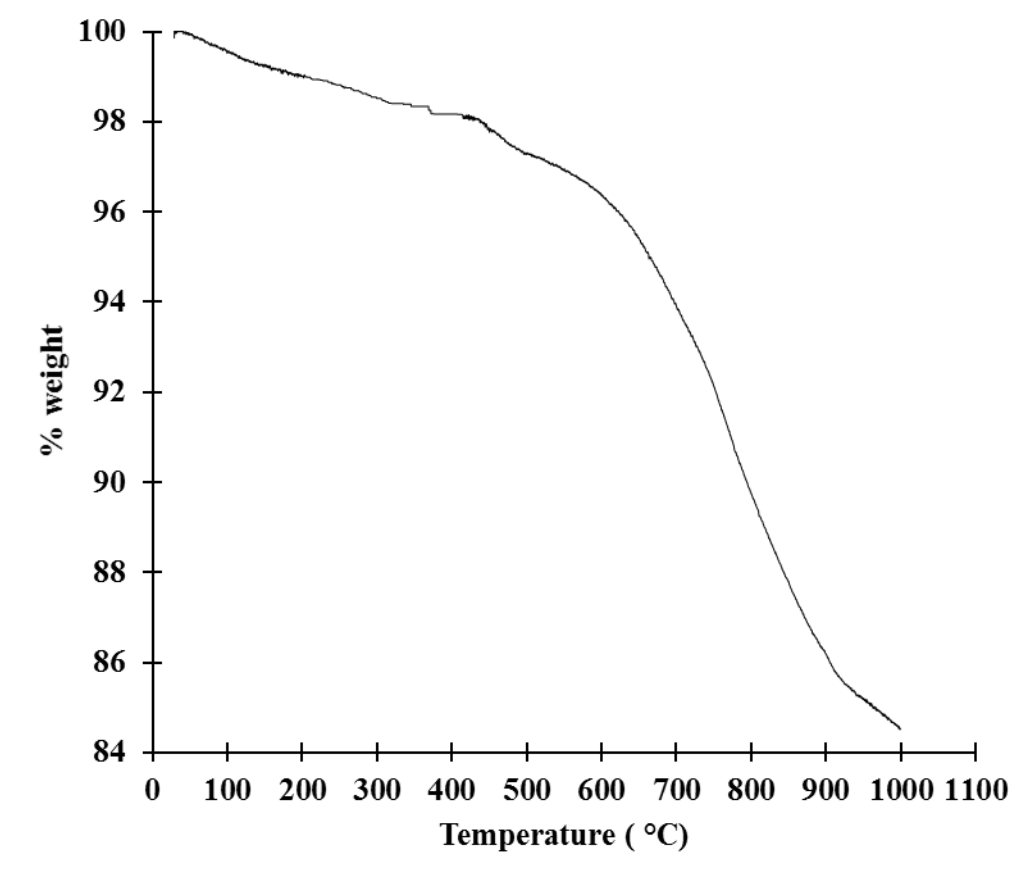

Figure 4.3: Thermogravimetric curve for the as-received dry discharged fine IBA dust. 25µg of milled powders were used and heated to 1000 °C with a 10 °C.min^{-1} ramp rate.

4.4.2 Effect of milling time on dry discharged fine IBA dust particle size distribution

The effect of milling time on the particle size distribution of the dry discharged fine IBA dust fraction using standard milling conditions is presented in Figure 4.4. The distribution curves represent an average from 10 analysis. The particle size distribution of the as-received dry

discharged fine IBA dust is also presented for comparison. The data clearly indicate that the particle size reduction of milled IBA occurs initial rapidly with increasing time, but decreases as IBA becomes finer. Fifty percent of the volume (d_{50} value) of the dry discharged fine IBA dust consists of particles finer than 112 μm, and this decreased to 13.8, 4.7, 2.3 and 1.9 μm after milling for 2, 8, 24 and 32 hours, respectively. The corresponding d_{95} values were 117.4, 36.1, 9.9 and 8.9 μm, accordingly. The 24 hours milling seemed to give reasonably effective particle size reduction as suggested by other researchers and this was used for subsequent experiments (Cheeseman et al., 2003).

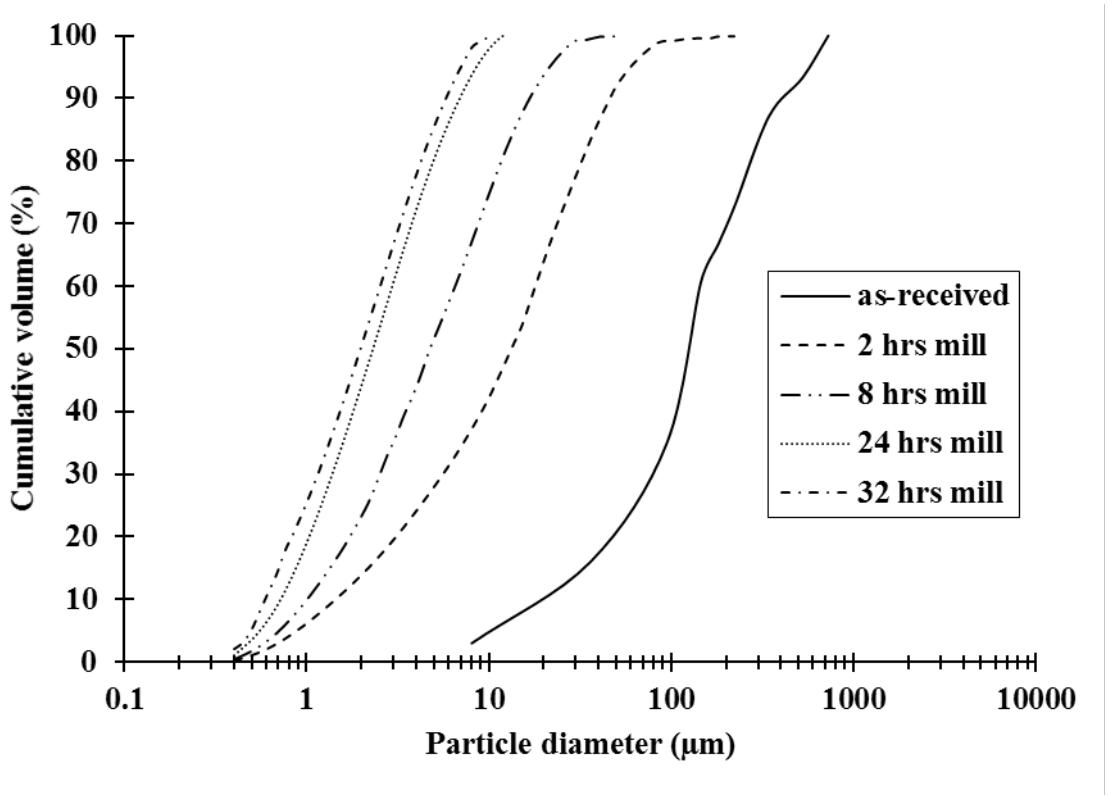

Figure 4.4: Particle size distribution of as-received and milled at different time dry discharged fine IBA dust. The 24 hours milling seems to give reasonable particle size.

4.4.3 Effect of glass addition on particle size distribution of milled powders

The effect of glass addition on the particle size distribution of dry discharged fine IBA dust: glass powders wet milled for 24 hours is presented in Figure 4.5. The results indicate that glass addition had little or no effect on the particle size distribution of milled powders. The d_{50}

values of mixture compositions containing 100wt. % dry discharged fine IBA dust, 90wt.% dry discharged fine IBA dust and 10wt. % glass, 80 wt.% dry discharged fine IBA dust and 20wt. % glass and 70 wt.% dry discharged fine IBA dust and 30wt. % glass were 2.3, 2.4, 2.5 and 2.8 μm, respectively. The corresponding d_{95} values were 8.9, 9.9, 13.7, 12.4 μm, accordingly.

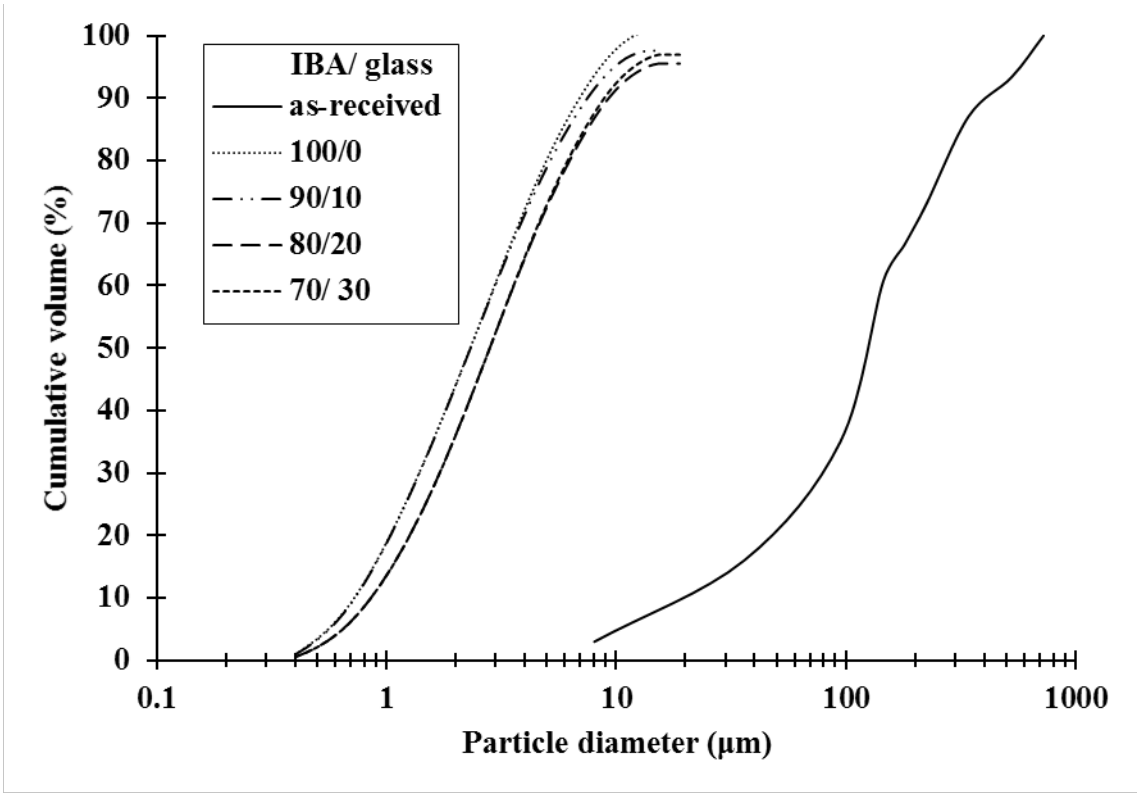

Figure 4.5: Particle size distribution of as-received dry discharged fine IBA dust and milled fine IBA dust with different amounts of soda lime recycled glass for 24 hours.

4.4.4 Density and linear shrinkage of sintered fine IBA dust: glass ceramics

The effect of sintering temperature and glass addition on the densities and linear shrinkage of dry discharged fine IBA dust: glass samples are shown in Figures 4.6 and 4.7, respectively.

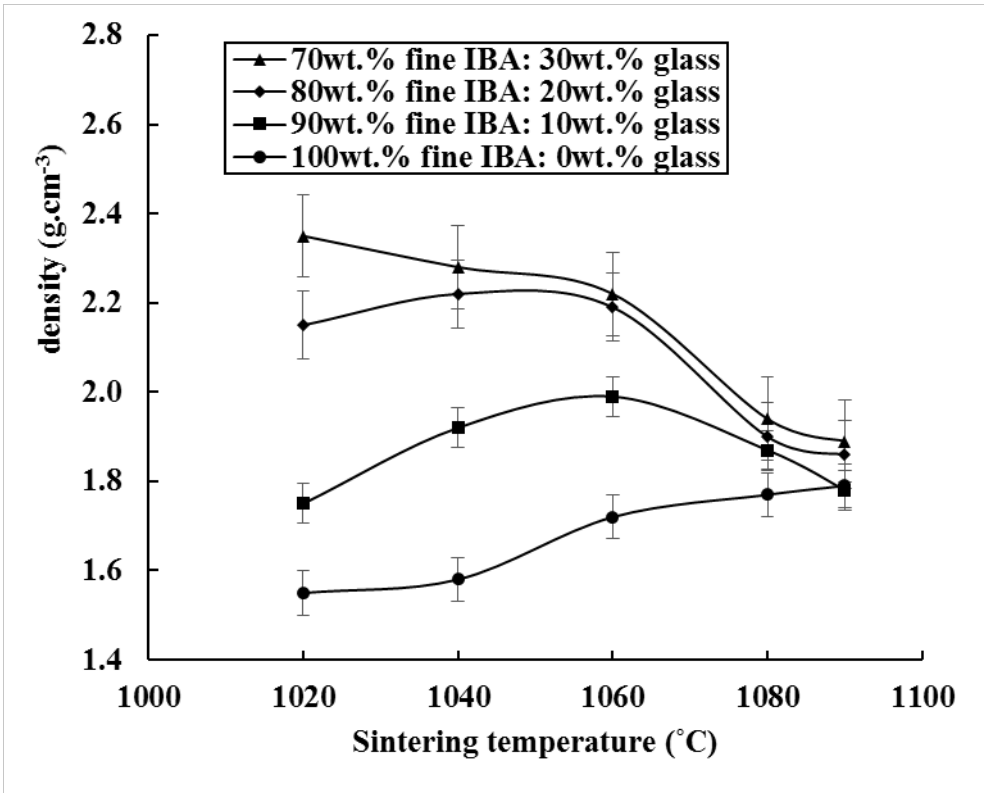

Figure 4.6: Effect of sintering temperature (1 hour dwell) on the density of ceramics produced with dry discharged fine IBA dust and glass powders. Error bars: +/- 1 std.

It is clear that as the glass content in the mixture composition increases, the densification point decreases. The addition of glass accelerates liquid phase sintering. The increase in density and linear shrinkage and the decrease in water absorption is associated with the elimination of pore volume that occurs during sintering. (German, 1985; Wang et al., 1998; Cheeseman et al., 2003). Dry discharged fine IBA dust: glass samples containing 20wt. % and 30wt. % glass fired at temperatures below 1020 °C indicated chalky surface with extremely weak structure. Samples sintered at temperatures above 1100 °C were melted and deformed and properties measurements were not possible.

The addition of 20 wt. % and 30 wt. % glass resulted in significant higher densities than samples produced with 10 wt. % or no glass. Maximum densities between 2.20 and 2.40 g/cm^3 were obtained when sintering between 1020 and 1040 °C for a mix containing 30 wt. % glass. These samples exhibited high (~20%) linear shrinkage and this tended to cause deformation and warping of tile samples. Mixture compositions with 20 wt. % and 30 wt. % glass fired above

1060 °C resulted in a rapid decrease in density. At these temperatures melting and softening of the powder compact occurs. The decomposition of trace components results in pore formation, which is associated with the entrapment of gaseous emissions within the glassy matrix of the samples and the subsequent formation of a vesicular, lower density, bubbled microstructure.

Dry discharged fine IBA dust samples containing 10 wt. % glass and no glass produced significant lower maximum densities of 1.9 and 1.8 g/cm^3, respectively. The produced samples appeared to be relatively weak with chalky surface, especially at the low temperatures examined. The increase in density associated with increased sintering temperature was much lower than the samples produced with higher glass addition.

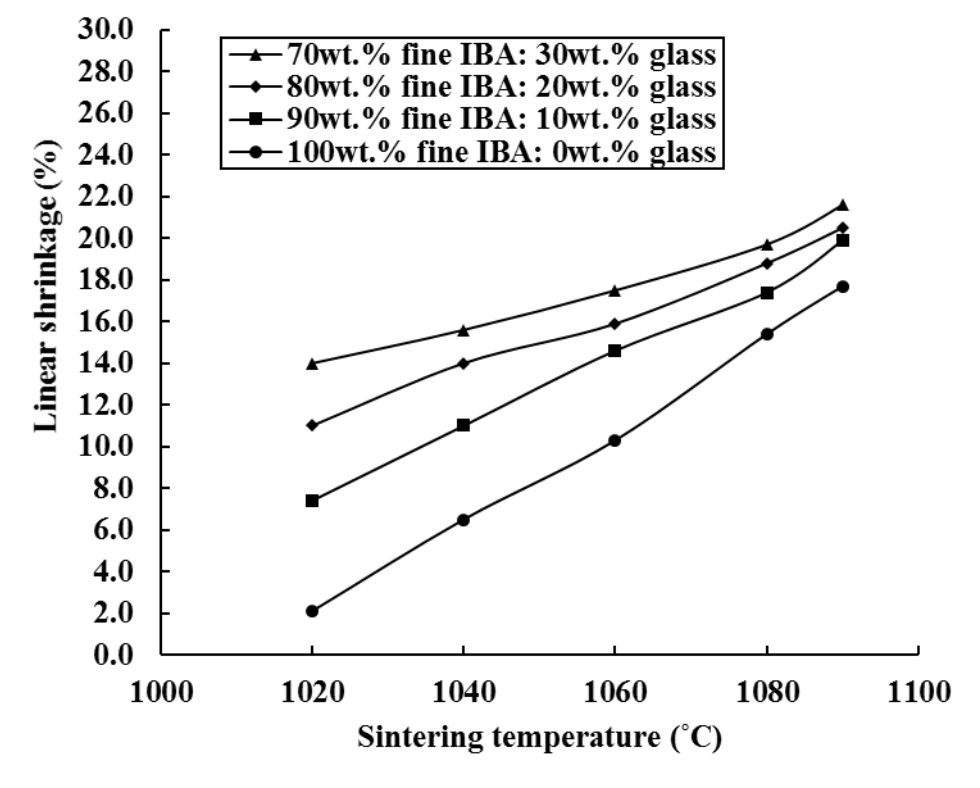

Figure 4.7: Effect of sintering temperature (1 hour dwell) on the linear shrinkage of ceramics produced with dry discharged fine IBA dust and glass powders. Increasing the sintering temperature results in a significant increase in the linear shrinkage, associated with warping and deformation of the produced ceramics. Error bars: negligible.

4.4.5 Water absorption of sintered fine IBA dust: glass ceramics

The effect of sintering temperature and glass addition on water absorption is shown in Figure 4.8. Increasing sintering temperature is associated with decrease in water absorption, due to a reduction in the open, water accessible porosity also linked with an increase in density. Rearrangement and solution-precipitation stages of liquid phase sintering are responsible for pore reduction at temperatures of maximum densification (German, 1985; Cheeseman et al., 2003).

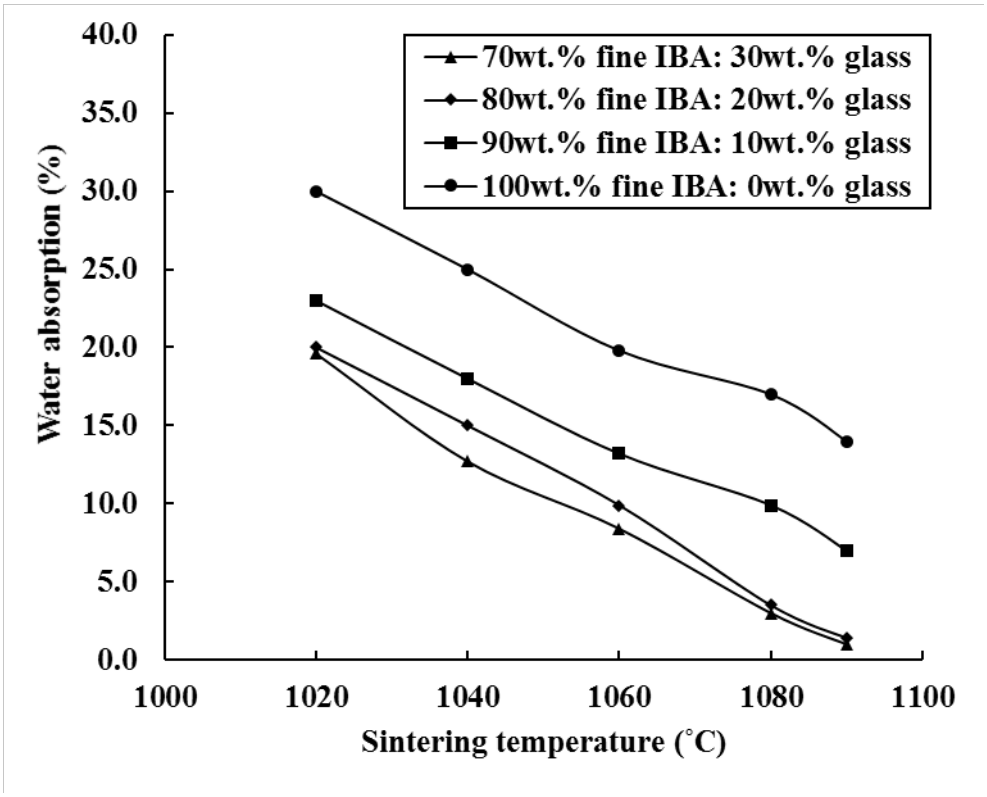

Figure 4.8: Effect of sintering temperature (1 hour dwell) on the water absorption of ceramics produced with dry discharged fine IBA dust and glass powders. Increasing the sintering temperature results in a decrease in water absorption. Error bars: negligible.

The water absorption of the 20 wt. % and 30 wt. % glass samples sintered between 1020 and 1040 °C was between 10 and 20%. Water absorption significantly reduced to 1 to 5% for samples sintered above 1080 °C. Samples produced with 10 wt. % or no glass exhibited high water and this is associated with a lower density, highly porous microstructure.

Samples containing 20 wt. % and 30 wt. % glass showed lower water absorption and had improved appearance. It must be pointed out, however, that there is always a trade-off between the amount of waste recycled and the optimisation of properties of the new products. In general, since the main objective is to reutilise the fine IBA fraction, the quantity of pure materials or non-waste additions introduced for improving performance must be kept as low as possible. Therefore, the addition of 20 wt. % glass and sintering at 1080 °C were selected as the optimum processing conditions and this mixture composition was characterised further, although sintering at 1080 °C resulted in an additional mass loss of 16 wt. %.

4.4.6 Effect of pressing pressure on physical properties of optimum sintered ceramics

The effect of pressing pressure on both 'green' and sintered density and linear shrinkage after firing bodies containing 80 wt.% dry discharged fine IBA dust and 20 wt.% glass is presented in Figure 4.9 . Fired samples were sintered at 1080 °C.

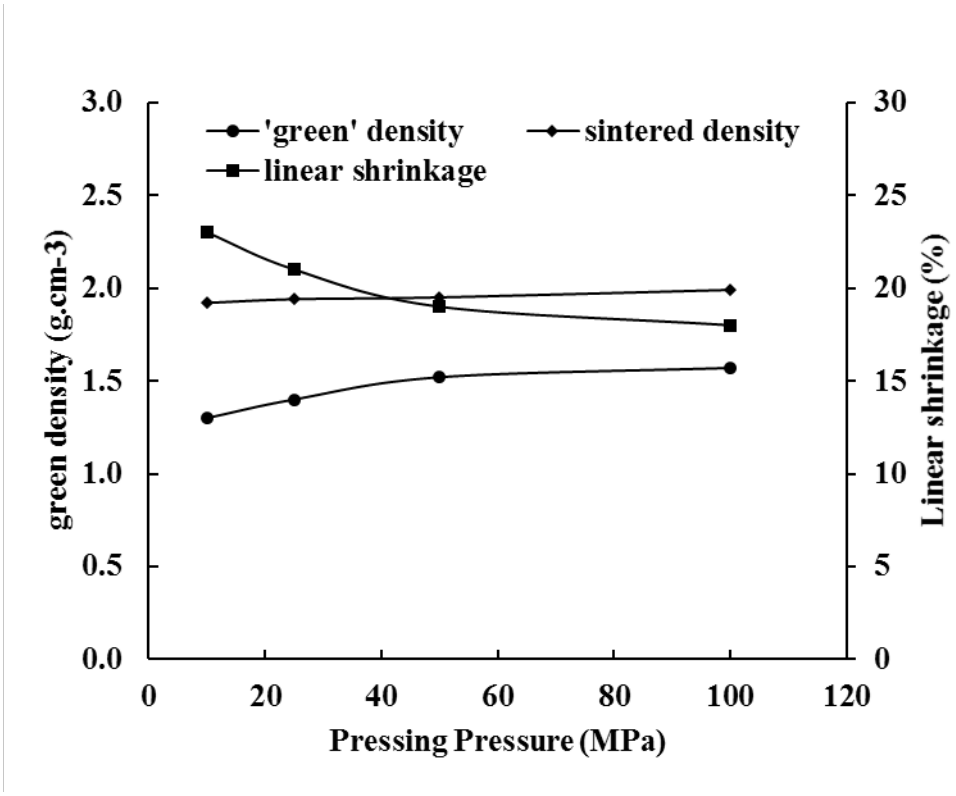

Figure 4.9: Effect of pressing pressure on 'green' and sintered density and linear shrinkage of samples produced with 80 wt.% dry discharged fine IBA dust and 20 wt.% glass.

Increasing the pressing pressure have negligible effect on the density of sintered samples. However, 'green' density affects the firing shrinkage, with samples produced with higher pressing pressure exhibiting increased 'green' densities and subsequent lower linear shrinkage. This has also been observed by other researchers (Bethanis et al., 2002).

4.4.7 Mechanical properties of ceramics produced with optimum conditions

The polished surfaces of the materials sintered with optimum glass addition (20 wt. % glass) has been subjected to Vickers micro hardness testing by applying a 25 g load and the results are presented in Figure 4.10 . Measurements correspond to average values from 10 samples.

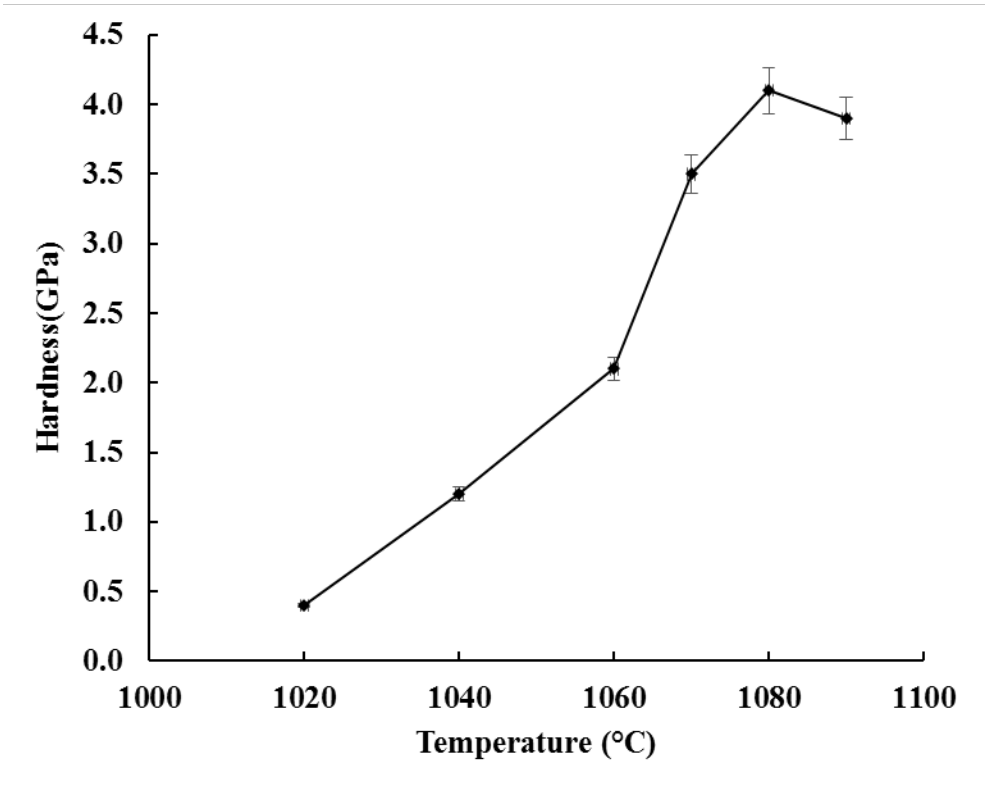

Figure 4.10: Effect of sintering temperature (1 hour dwell) on the Vickers micro hardness of mixture containing 80 wt. % dry discharged fine IBA dust and 20 wt. % glass. Increasing the sintering temperature results in an increase in Vickers microhardness. Error bars: +/- 1 std.

The average micro-hardness values increases rapidly from 1020 °C to 1080 °C. Maximum Vickers micro hardness values of 4.0 GPa were obtained for materials sintered at 1080 °C, and this is associated with the complete melting of glass and the production of a hard, well sintered ceramic. This value is similar or slightly lower than the values achieved from ceramics produced by coal fly ash and waste glass, and mixtures of IBA, incinerator fly ash and other waste materials (Boccaccini et al., 1997; Romero et al., 1999; Boccaccini et al., 2000; Ferrarris et al., 2001; Appendino et al., 2004; Cheng et al., 2007; Yoon et al., 2013). Sintering the material above 1080 °C, slightly decreases the hardness of the material, resulted from the softening of the glass matrix and the evolution of gases contained in the dry discharged fine IBA dust. The low hardness observed for materials sintered at 1020 °C is due to the poorly sintered, low density material obtained at this temperature.

4.4.8 Mineralogy of processed dry discharged fine IBA dust: glass powders

X-ray diffraction data for the 24 hour milled 80wt. % dry discharged fine IBA dust, 20wt. % glass and the corresponding sintered ceramic fired at 1020, 1040, 1060 and 1080 °C is shown in Figure 4.11.

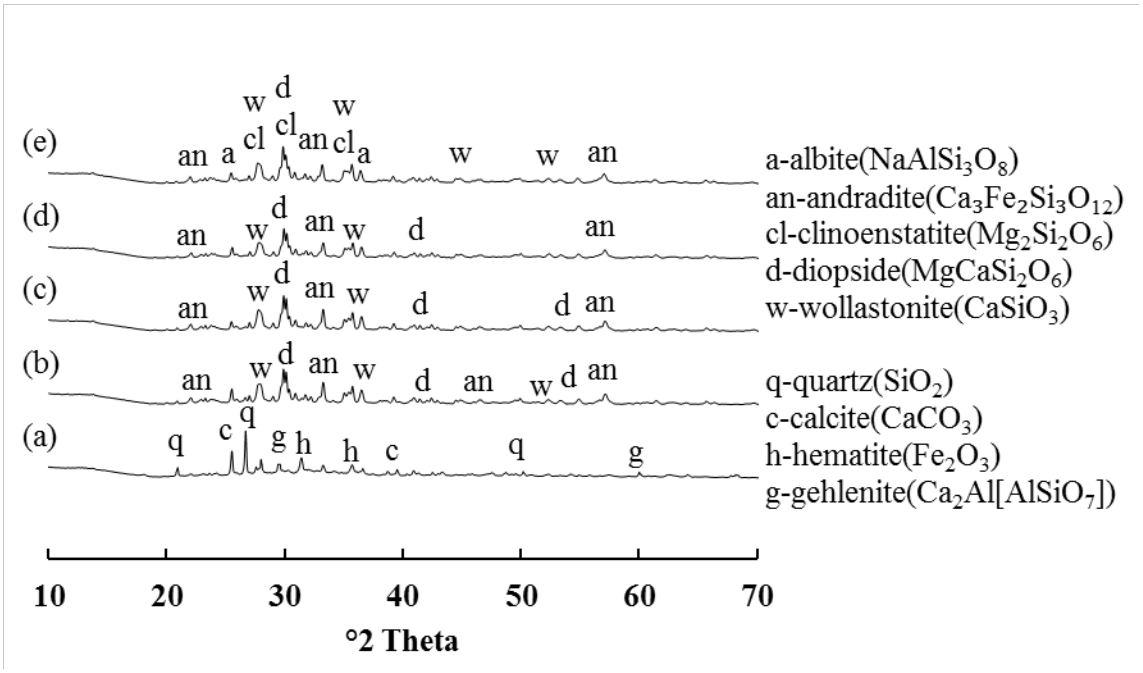

Figure 4.11: XRD data of: (a) 24 hours milled, and sintered at (b) 1020 °C, (c) 1040 °C, (d) 1060 °C and (e) 1080 °C samples containing 80 wt. % dry discharged fine IBA dust: 20 wt. %

glass. Representative samples were dried at 105 ºC and disc milled (Gy–Ro, Glen Creston Ltd., UK) to form powders with a mean particle size of 35 μm.

Quartz (SiO_2), calcite ($CaCO_3$), hematite (Fe_2O_3) and ghelenite ($Ca_2Al_2SiO_7$) are the major crystalline phases in the milled fine IBA dust: glass, and these were transformed into the pyroxene minerals diopside ($CaMgSi_2O_6$), clinoenstatite ($MgSi_2O_6$) and wollastonite ($CaSiO_3$) together with some albite ($NaAlSi_3O_8$) and andradite ($Ca_3Fe_2Si_3O_{12}$) in the sintered at 1080 °C product.

XRD data of dry discharged fine IBA dust: glass samples sintered at 1020 °C revealed that diopside ($MgCaSi_2O_6$) and andradite ($Ca_3Fe_2Si_3O_{12}$) were the principal crystalline phases, together with significant amounts of wollastonite ($CaSiO_3$). Similar crystalline phases were identified for samples sintered at 1040 and 1060 °C, with the presence of wollastonite and andradite being less significant. Analysis of dry discharged fine IBA dust: glass samples sintered at 1080 °C showed that diopside ($CaMgSi_2O_6$), clinoenstatite ($MgSi_2O_6$) and wollastonite ($CaSiO_3$) together with some albite ($NaAlSi_3O_8$) and andradite ($Ca_3Fe_2Si_3O_{12}$) were present in the sintered product. Quartz and calcite peaks found in the as-received and milled dry discharged fine IBA dust had completely disappeared by 1020 °C, since these were replaced by pyroxene group crystals, such as diopside and clinoenstatite.

Diopside is a calcium pyroxene, while clinoenstatite is a magnesium pyroxene. Pyroxenes are an important group of rock-forming silicate minerals of variable composition typically containing Ca, Mg and Fe. They occur as stable phases in almost every type of igneous rock and are found in rocks of widely different composition (Deer et al., 1992).

The presence of both clinoenstatite and diopside has previously been identified in ceramics produced from processed IBA minerals. They form from solid-phase reactions between liberated alkaline-earth oxides and quartz at temperatures above 600 to 700 °C. Diopside is also reported to be the major crystalline phase in ceramics formed from vitrified municipal incinerator fly ash, filter dusts, bottom ash and thermal power plant fly ash. Andradite and clinoenstatite were identified in ceramics obtained from vitrification of incinerator bottom and fly ash. Andradite has also been reported in crystalline phases formed from the vitrification of electric arc dust (Romero et al., 2001; Rawlings et al., 2006).

4.4.9 Microstructure of processed dry discharged fine IBA dust: glass samples

SEM micrographs of fracture surfaces of 80 wt. % dry discharged fine IBA dust: 20 wt. % glass samples sintered at 1020, 1040, 1060 and 1080 °C are shown in Figure 4.12. The effect of sintering temperature on the pore formation is in agreement with the density data. SEM images of samples sintered at 1020 °C indicated a microstructure of an intermediate stage of densification, with continuous channels of pores at particle boundaries. Samples fired at 1040 and 1060 °C resulted in a relatively dense material inhibiting irregularly shaped dispersed pores. Increasing the sintering temperature to 1080 °C resulted in increased closed porosity of a more spherical shape, typically with a wide diameter size distribution, ranging from ~ 5 to 50 μm.

The fracture surfaces of dry discharged fine IBA dust: glass samples containing 20wt. % glass sintered at 1020 °C showed a poorly sintered material with a granular surface associated with high, interconnected porosity. Samples sintered at 1040 and 1060 °C appeared to be well sintered with dense microstructure. The high water absorption of these samples is associated with the elongated cavities, responsible for the open pores, which are accessible to water.

The microstructure of the samples sintered at 1080 °C was very different. At these temperatures the decomposition of alkaline metal sulphates results in evolution of SO_2, which in combination with the melting of the glass, lead to the formation of a foamed internal microstructure (Stern and Weise, 1996; Cheeseman et al., 2003). The materials formed approximately spherical closed pores associated with a reduction in density and water absorption. It has been shown that ceramic materials containing closed porosity associated with gas evolution and entrapment inside the pyroplastic mass, exhibit high thermal insulation and thermal shock resistance, and could be used for thermal insulation purposes (Boccaccini, 1999; Boccaccini et al., 2001).

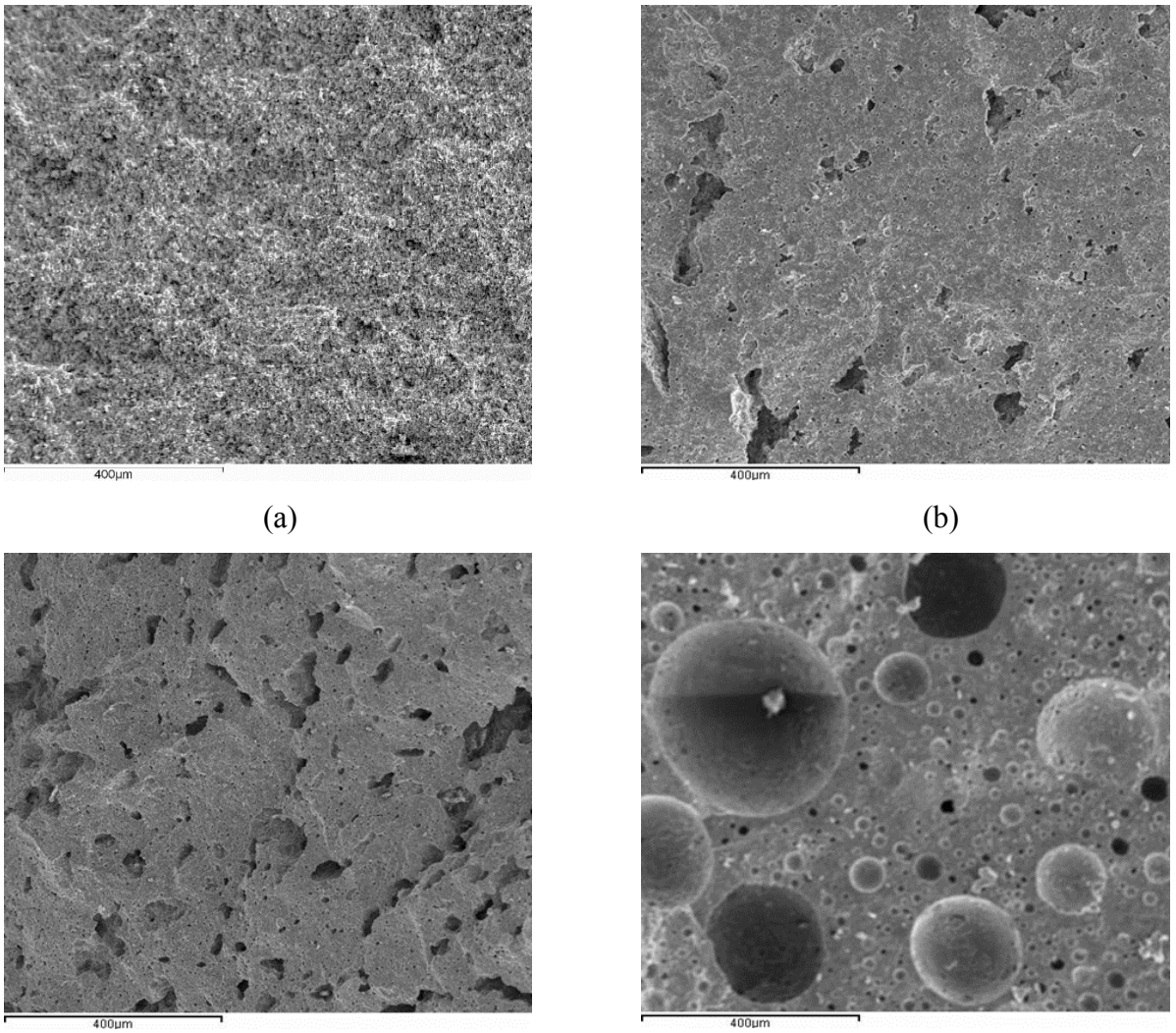

(a) (b)

(c) (d)

Figure 4.12: SEM micrographs of fracture surface of samples containing 80 wt. % dry discharged fine IBA dust: 20 wt.% glass and sintered at: (a) 1020°C, (b) 1040 °C, (c) 1060 °C, (d) 1080 °C

4.4.10 Leaching properties of as-received and processed dry discharged fine IBA dust

The leaching behaviour of the as-received dry discharged fine IBA dust derived from Martin's dry discharge system, 24 hours milled 80wt. % dry discharged fine IBA dust: 20 wt. % glass and dry discharged fine IBA dust: glass sintered at 1020, 1040, 1060 and 1080 °C have been assessed applying the pH dependence leaching test using a liquid to solid (L/S) ratio of 10 (CEN/ TS 14429). The CEN standard allows characterisation of leaching under different pH conditions covering the range from basic to acidic.

Acid Neutralisation Capacity

The effect of processing dry-discharged fine IBA dust on the acid neutralisation capacity (ANC), expressed as final leachate pH as a function of acid addition in equivalents of acid per kg of solid is shown in Figure 4.13.

The as-received dry discharged fine IBA dust exhibited a relatively constant rate of pH decrease with acid addition. Carbonation during ageing of the fine IBA dust, leads to the formation of $CaCO_3$, which provides significant buffering capacity (Van der Sloot et al, 2001; Bethanis et al., 2004; Guimaraes et al, 2006; Van der Sloot et al., 2012). The solubilisation and removal of alkali metal and alkali metal earth elements occurring during wet milling, is responsible for the reduction of ANC in the milled dry discharged fine IBA dust: glass mixture. The presence of water is associated with the formation of Ca^{2+}, HCO_3^- and OH^- ions, which provide significant buffering capacity to acid addition. The addition of glass, alters the composition of the as-received dry discharged fine IBA dust, and this advocates the reduction of ANC in the milled dry discharged fine IBA dust: glass samples.

Sintered dry discharged fine IBA dust: glass samples showed rapid decline in leachate pH with acid addition, indicating reduced ANC compared to the as-received dry discharged fine IBA dust and the milled material. Increasing the sintering temperature results in a decrease in ANC, and this has also been reported by other researchers (Selinger et al., 1997; Bethanis et al., 2004; Boccaccini et al.; Van der Sloot et al., 2012). Sintering decomposes $CaCO_3$ to CaO and CO_2 and

the CaO then forms new amorphous and crystalline phases in the processed dry discharged fine IBA dust: glass mix (Van der Sloot et al, 2001; Guimaraes et al, 2006; Van der Sloot et al., 2012).

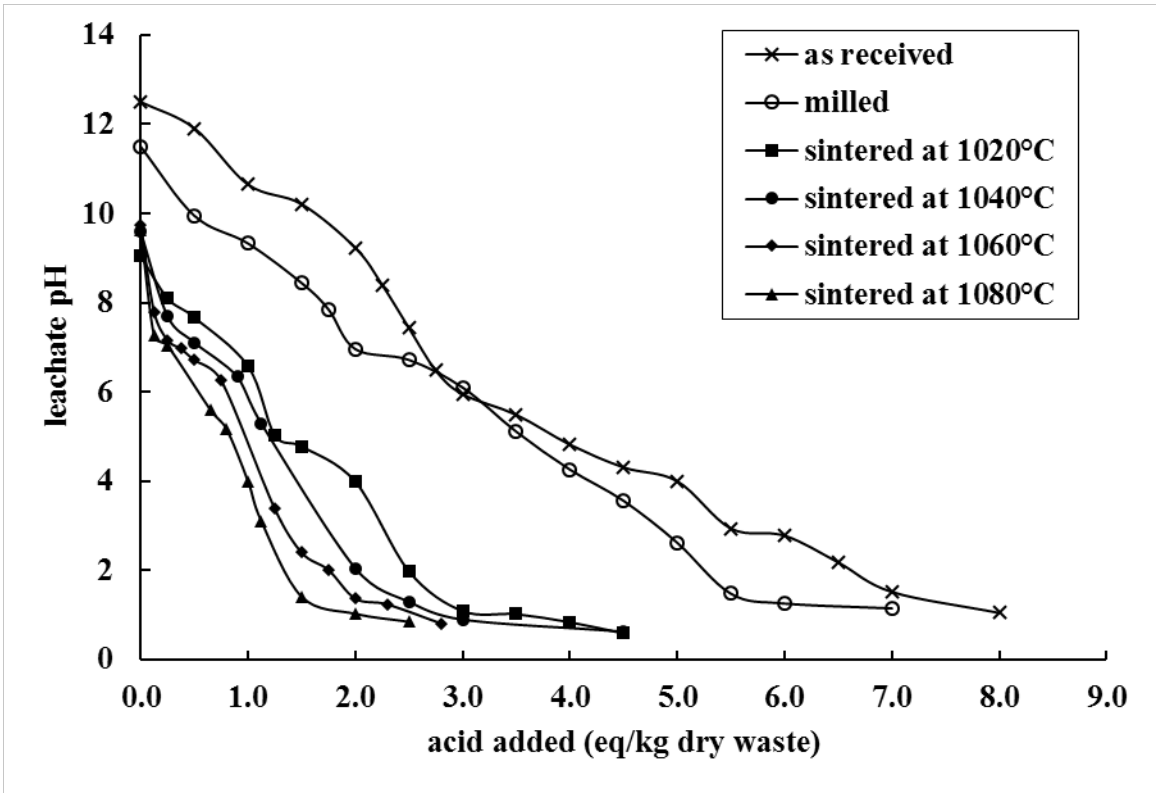

Figure 4.13: Acid Neutralisation capacity of the as-received dry discharged fine IBA dust, milled 80 wt.% dry discharged fine IBA dust: 20 wt.% glass and samples sintered at 1020 °C, 1040 °C, 1060 °C and 1080 °C. Increasing the sintering temperature resulted in a decrease in ANC curve.

Leachate analysis data

The concentrations of selected alkali and alkali earth metals and heavy metals leached from the as-received dry discharged fine IBA dust, 24 hours dry discharged fine IBA dust: glass milled and sintered at 1020, 1040, 1060 and 1080 °C have been plotted as a function of leachate pH and presented in Figures 4.14 to 4.18. Sintering of dry-discharged fine IBA dust significantly reduced leaching of all elements contained in the as-received fine IBA dust.

(a) Leaching of alkali metals and alkali metal earth ions

Leaching data for Ca, Mg, Na and K in mg/kg are presented in Figures 4.14 and 4.15. Soluble mineral phases, such as $CaCO_3$, $CaSO_4$, $CaCl_2$, CaO and Ca-silicates present in the as-received dry discharged fine IBA dust and milled dry discharged fine IBA dust: glass samples, are released with acid addition. Numerous studies of IBA leaching behaviour have reported similar observations (Kida et al., 1996; Van der Sloot et al., 2001a; Van der Sloot et al., 2013). Ca leaching of the as-received dry discharged fine IBA dust increased with acid addition from 500 mg/kg at pH 12.5 to about 9,700 mg/kg at pH 6.0 and was significant increased to 40,000 mg/kg at pH 1.1. The milled dry discharged fine IBA dust: glass samples indicated lower Ca release with acid addition than the as-received dry discharged fine IBA dust. The reported values showed that Ca concentration leached from the milled dry discharged fine IBA dust: glass materials was about 330 mg/kg at pH and this was increased to 7,000 mg/kg at pH 6.1 and approximately 7,000 mg/kg at pH 1.2. It should be noted, however, that strongly acidic conditions are not typically present in the environment. In addition, as noted earlier, the milled mixture contains 20 wt. % glass, therefore the metals leached from the milled material are expected to be lower than the processed 100wt. % dry discharged fine IBA dust, as suggested by other researchers (Bethanis et al., 2004; Van der Sloot et al., 2012).

Analysis of data for dry discharged fine IBA dust: glass samples sintered at 1020 °C reveals that metal ion release with acid addition has partially occurred and this is associated with the poorly sintered material obtained. Ca leached concentration was reduced with increasing sintering temperature. The ceramics produced by sintering at 1040 and 1060 °C exhibited slightly lower Ca leached concentration than samples sintered at 1020 °C. Sintering the dry discharged fine IBA dust: glass samples at 1080 °C significantly reduced Ca leaching due to the more dominant presence of low solubility calcium silicates, such as diopside, wollastonite or andradite (Selinger et al., 1997; Van der Sloot et al., 2012).

Na and K leach from the as-received dry discharged fine IBA dust over a wide pH range and this is also reduced after wet milling. These metals are present as soluble salts in the as-received dry discharged fine IBA dust and are dissolved rapidly when the material contacts water (Bethanis et al., 2004; Van der Sloot et al., 2012).

Na concentrations leached of samples sintered at 1020 °C were similar to the concentrations found in the as-received dry discharged fine IBA dust and the milled dry discharged fine IBA dust: glass samples. This is associated with the partial sintering of the produced materials, and also indicates the presence of readily soluble phases containing this ion at this sintering temperature. The concentrations of K leached under acidic conditions are significantly reduced at all sintering temperatures.

The similarity in the leaching behaviours of Mg and Ca from the as-received dry discharged fine IBA dust, is in accordance with the role of calcite in controlling Mg leaching (Van der Sloot et al, 2012). Sintering at 1020 °C produced samples with reduced Mg leached concentration than the as-received dry discharged fine IBA dust and the milled material. This was slightly decreased with increasing sintering temperature at 1040 and 1060 °C, and was significantly reduced when sintering at 1080 °C.

(b) Leaching of heavy metals

Leaching data for Cr, Cu, Ni, Zn, Cd and Pb in mg/kg for the as-received dry discharged fine IBA dust, the milled dry discharged fine IBA dust: glass and the sintered materials are presented in Figures 4.16, 4.17 and 4.18.

The as received dry discharged fine IBA dust and the milled material indicated similar Cr leaching curve, which is in accordance with the literature (Van der Sloot et al., 2001; Bethanis et al., 2004). This is reduced with increasing sintering temperature. Sintering at 1020 °C produced samples with lower Cr concentration leached in highly acidic environment, but similar to the as-received and milled materials values at pH > 4. This is due to the relatively poor sintering of the samples at these temperatures. Sintering at 1040 and 1060 °C produced samples with reduced Cr leached concentrations and this was further decreased when sintering at 1080 °C associated with the encapsulation of Cr into non-leachable phases.

Cu leaching of the as-received dry discharged fine IBA dust and the milled material exhibited similar behaviour with low concentration values, typically <10 mg/kg at pH > 6. This is believed to be due to the sorption processes and the formation of more stable insoluble mineral phases occurred during aging (Zevenbergen et al., 1994; Chimenos et al., 2000; Bethanis et al., 2004; ISWA, 2006; Van der Sloot et al., 2012). Cu leaching concentrations are significantly reduced with increasing sintering temperature and very low levels are achieved at pH > 5 at all

sintering temperatures. Cu is incorporated within the stable and less soluble phases formed during sintering.

Ni leached concentration is at low levels for the as-received dry discharged fine IBA dust and the milled material over the entire pH range examined. Sintering at 1020 and 1040 °C results in a reduction on Ni leached concentration by approximately an order of magnitude for the entire pH range examined, compared to the as-received and milled material. This is further reduced, especially at pH > 3, when sintering at 1060 °C. Sintering at 1080 °C resulted in a significant reduction on Ni leached compared to the as-received material over the range of leachate pH values examined. This is also associated with the entrapment of Ni within the stable phases formed during sintering.

Zn curves for the as-received and milled materials are similar and in accordance with the results presented by other researchers (Eighmy et al., 1994, Bethanis et al., 2004, Van der Sloot et al., 2012). Zn is very sensitive to acid addition and this metal has been reported to be present in as-received dry discharged fine IBA dust as zinc silicates and aluminates (Eighmy et al., 1994; Van der Sloot et al., 2012). A significant increase in Zn leached concentration is observed for the as-received and milled materials as the pH falls below 6 (Eighmy et al., 1994, Bethanis et al., 2004, Van der Sloot et al., 2012). Sintering the dry discharged fine IBA dust: glass samples resulted in a gradually reduction in Zn leaching. Sintering at 1020 °C produced samples with Zn leaching about an order of magnitude lower than the as-received and milled material under extreme acidic conditions. This was further decreased for samples sintered at 1040 and 1060 °C. Sintering at 1080 °C resulted in Zn leached concentration of about an order of magnitude lower than the sintered at 1020 °C materials, associated with the inertization of Zn to compounds of low solubility, also reported by other researchers (Selinger et al., 1997; Reich et al., 2002).

Pb leaching was significantly reduced with sintering, and was not detectable at pH > 4 for all the sintering temperatures examined. The concentration of Pb leached was decreased with sintering to over an order of magnitude compared to the as-received and milled materials under highly acidic environment.

Cd leached concentrations of the as-received dry discharged fine IBA dust and milled material were at low levels, especially for pH > 5, and this has also been reported by other researchers (Van der Sloot et al., 2001; Bethanis et al., 2004; Van der Sloot et al., 2012). Carbonation occurring during aging is responsible for the sorption of Cd minerals on the surface

of calcite, and this is associated with the non-solubility of Cd at high leachate pH. Sintering reduces the Cd leached concentration by approximately a factor of 10 under highly acidic conditions.

(c) Leaching of Al and Fe

Leaching data for Al and Fe in mg/ kg for the as-received dry discharged fine IBA dust, the milled dry discharged fine IBA dust: glass and the sintered materials are presented in Figure 4.19.

The Al leaching curve for the as-received dry discharged fine IBA dust is characterised by a V-shaped curve, also reported by other researchers (Eighmy et al., 1994; Bethanis et al., 2004; Van der Sloot et al., 2012). Aging of the dry discharged fine IBA dust results in the formation of Al $(OH)_3$ and amorphous aluminosilicates (Eighmy et al., 1994; Meima et al., 2002; Bethanis et al., 2004; Van der Sloot et al., 2012). Pecquer et al. (2001) reported that Al leaching is associated with swelling and cracking problems when processed IBA minerals are used in the production of concrete. Sintering reduces Al leached concentration, since Al ions have been encapsulated in more stable crystalline phases.

Fe leaching from the as-received dry discharged fine IBA dust and milled dry discharged fine IBA dust: glass is at very low levels, especially at pH > 5, and this has also been reported by other researchers. Aging of the as-received material results in the formation of ferrihydrite ($Fe(OH)_3$) associated with the low values of Fe leached concentration. Sintering significantly reduces Fe leaching under acid conditions for all sintering temperatures examined. Under mild and alkaline conditions the Fe leached concentrations of the sintered at 1020 and 1040 °C materials were similar or slightly lower than the as-received dry discharged fine IBA dust. This was reduced by a factor of 10 for materials sintered at 1060 and 1080 °C at a pH > 5, as the sintered at these temperatures materials form less soluble phases.

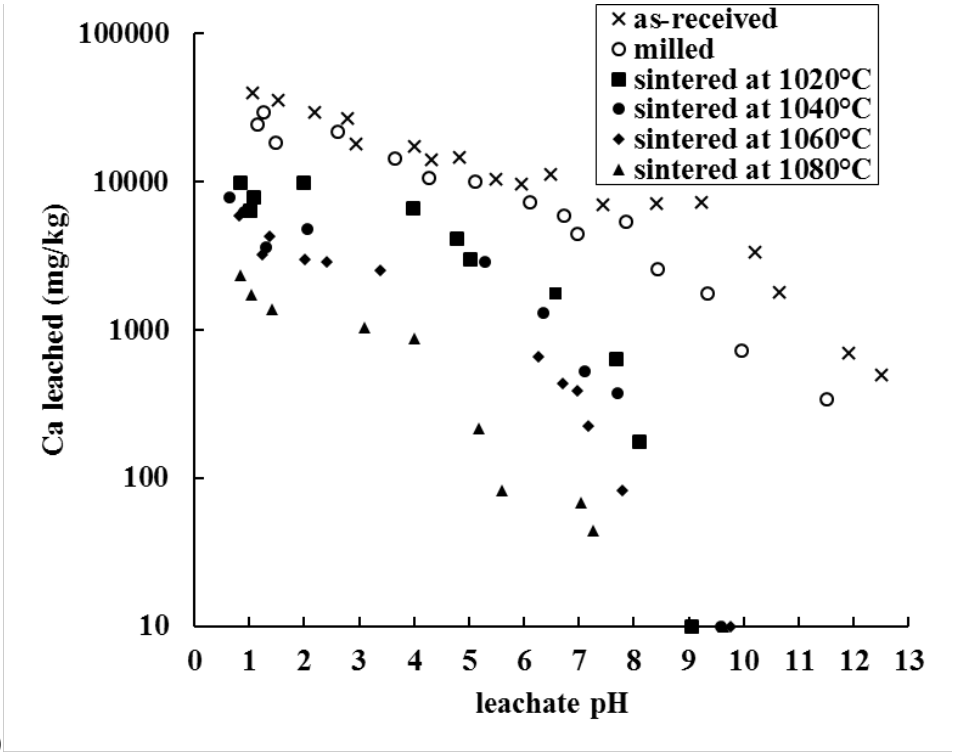
as-received
milled
sintered at 1020°C
sintered at 1040°C
sintered at 1060°C
sintered at 1080°C
Ca leached (mg/kg)
100000
10000
1000
100
10
0
1
2
3
4
5
6
7
8
9
10
11
12
13
leachate pH

(a)

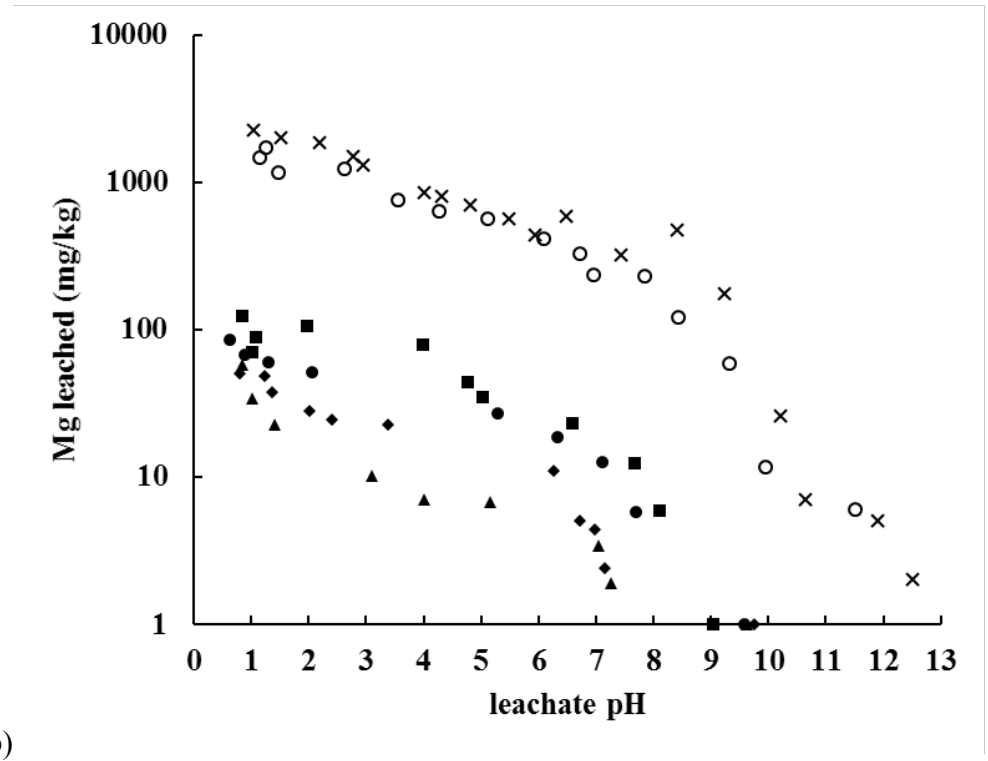

(b)

Figure 4.14: Leaching data for (a) Ca and (b) Mg as a function of leachate pH for aged dry discharged fine IBA dust, 80wt. % fine IBA dust: 20wt. % glass milled and sintered fine IBA dust: glass powders

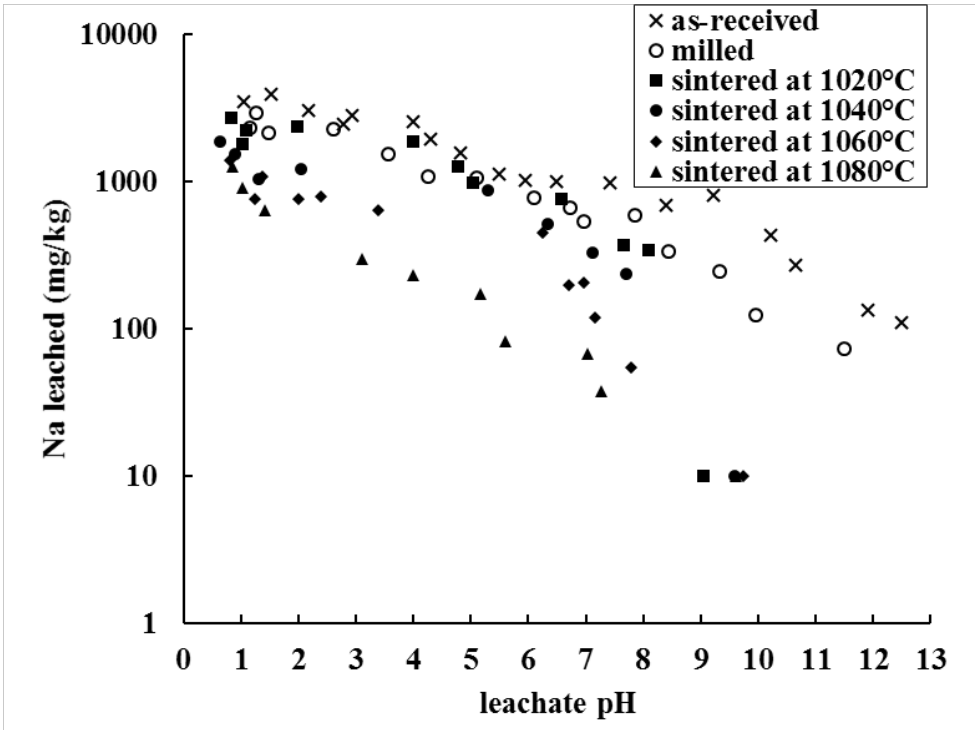

(a)

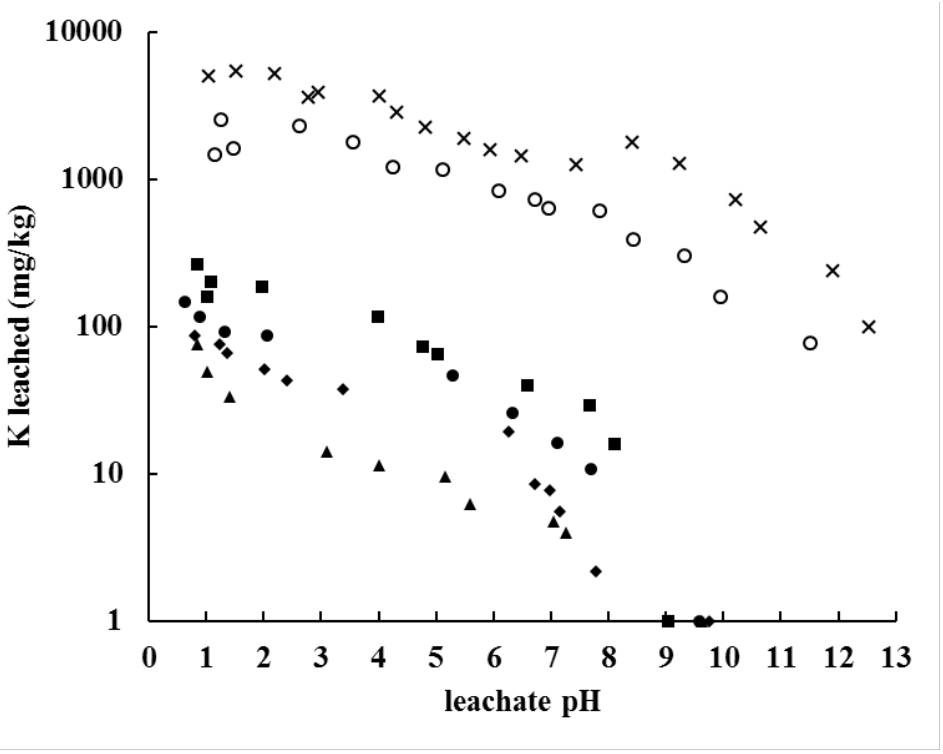

(b)

Figure 4.15: Leaching data for (a) Na and (b) K as a function of leachate pH for aged dry discharged fine IBA dust, 80wt. % fine IBA dust: 20wt. % glass milled and sintered fine IBA dust: glass powders

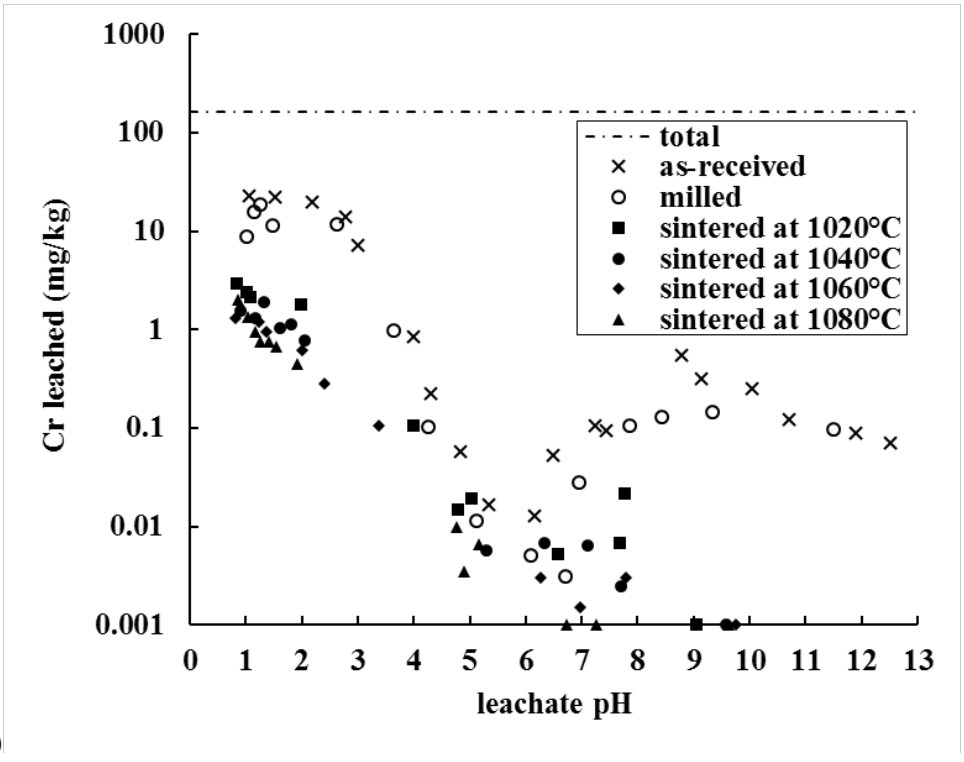

(a)

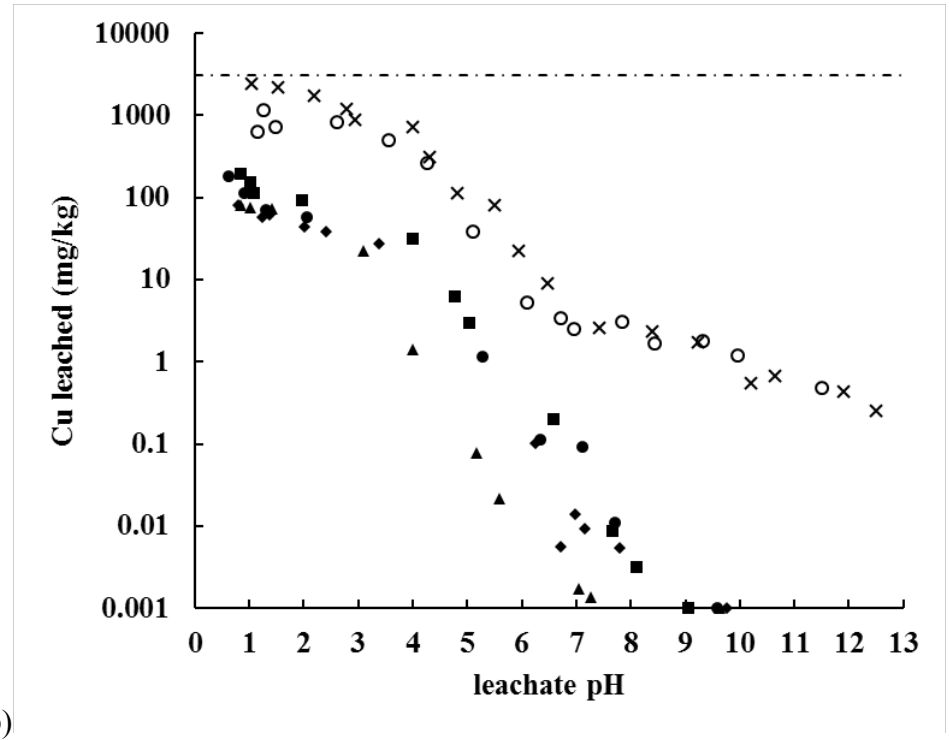

(b)

Figure 4.16: Leaching data for (a) Cr and (b) Cu as a function of leachate pH for aged dry discharged fine IBA dust, 80wt. % fine IBA dust: 20wt. % glass milled and sintered fine IBA dust: glass powders

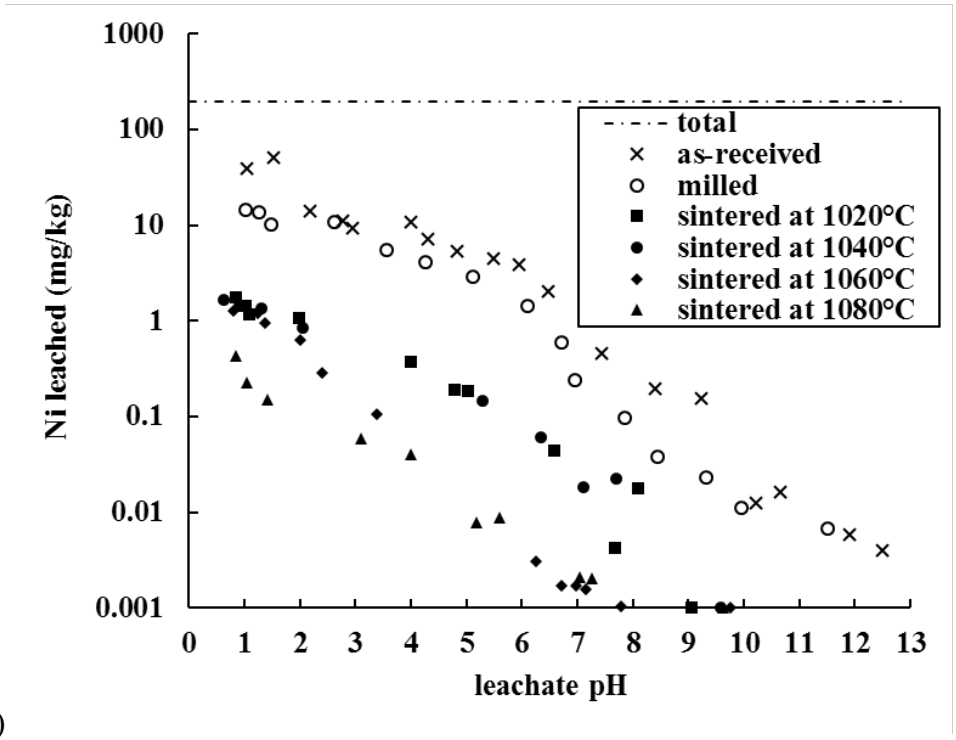

(a)

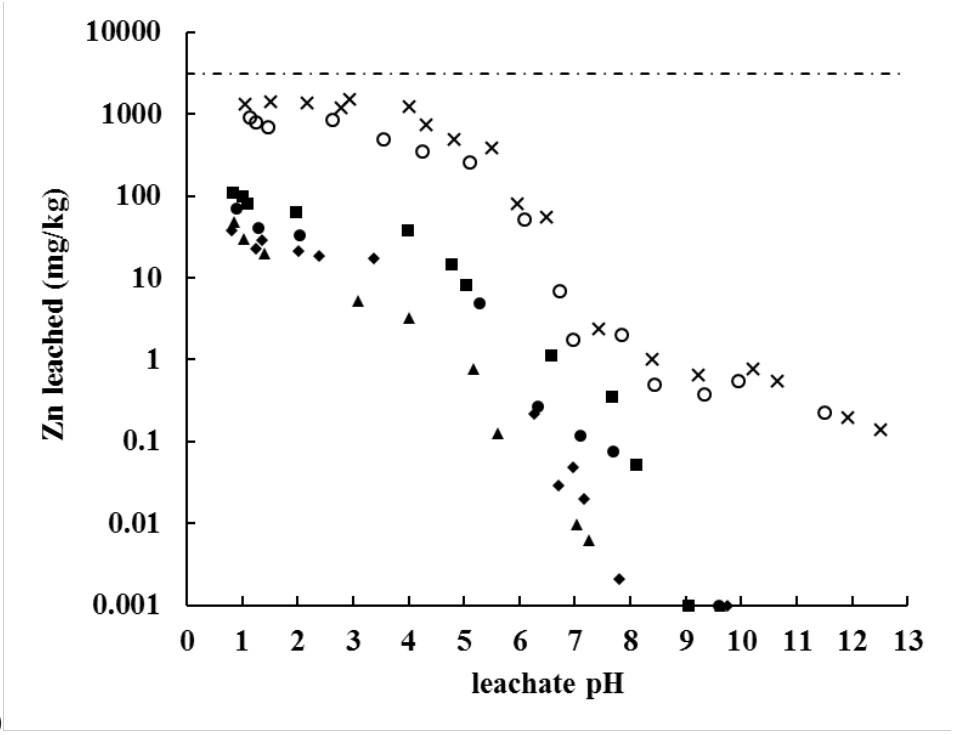

(b)

Figure 4.17: Leaching data for (a) Ni and (b) Zn as a function of leachate pH for aged dry discharged fine IBA dust, 80wt. % fine IBA dust: 20wt. % glass milled and sintered fine IBA dust: glass powders

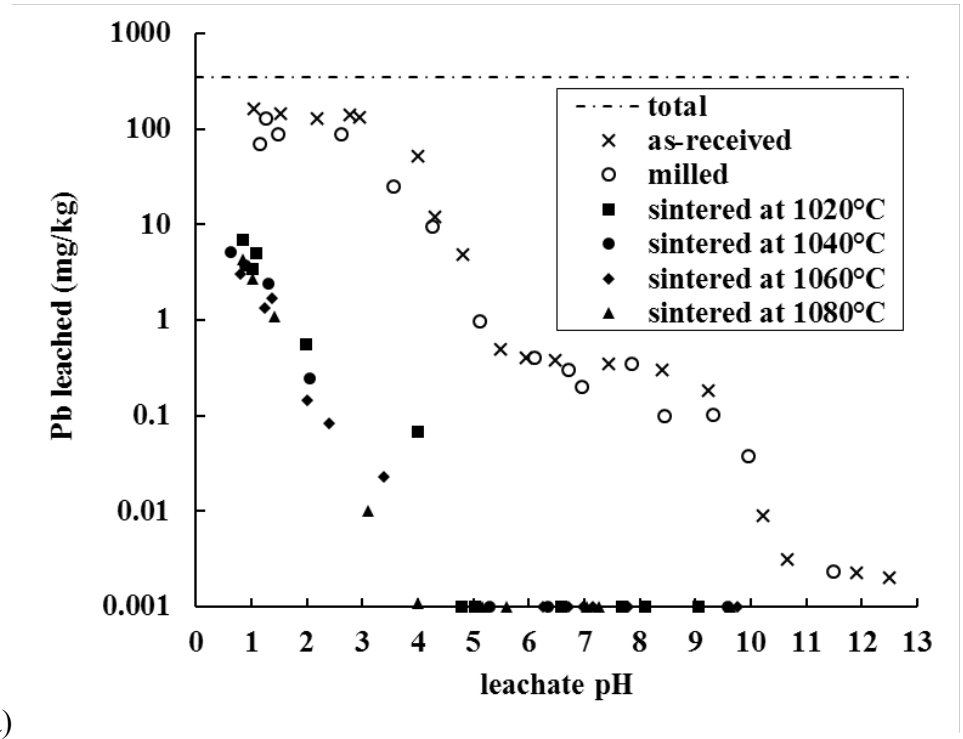

(a)

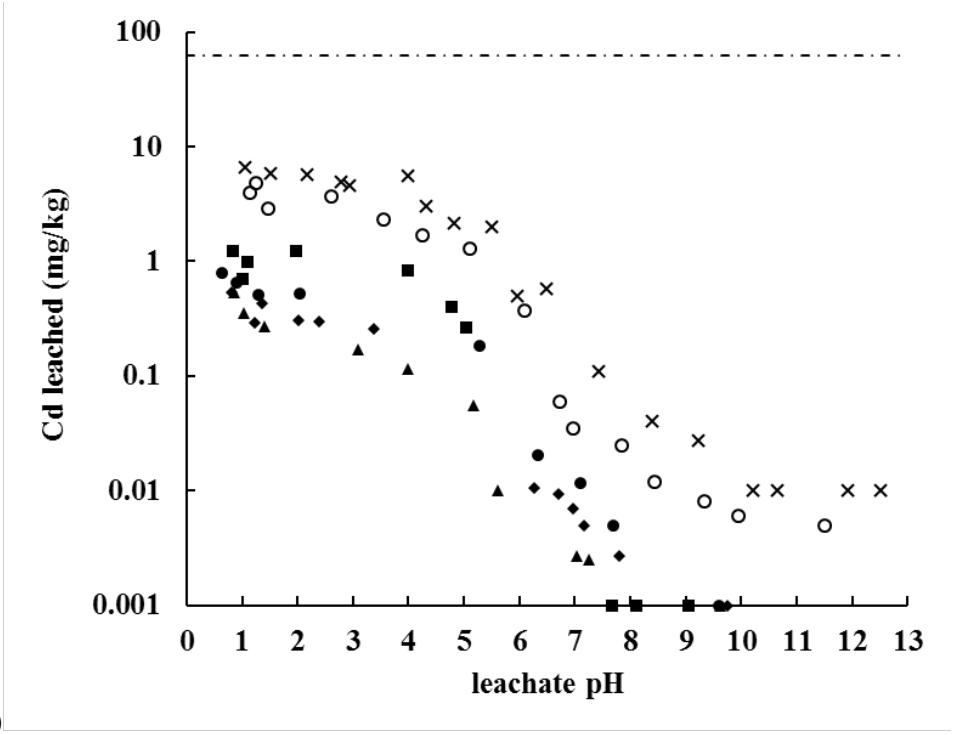

(b)

Figure 4.18: Leaching data for (a) Pb and (b) Cd as a function of leachate pH for aged dry discharged fine IBA dust, 80wt. % fine IBA dust: 20wt. % glass milled and sintered fine IBA dust: glass powders

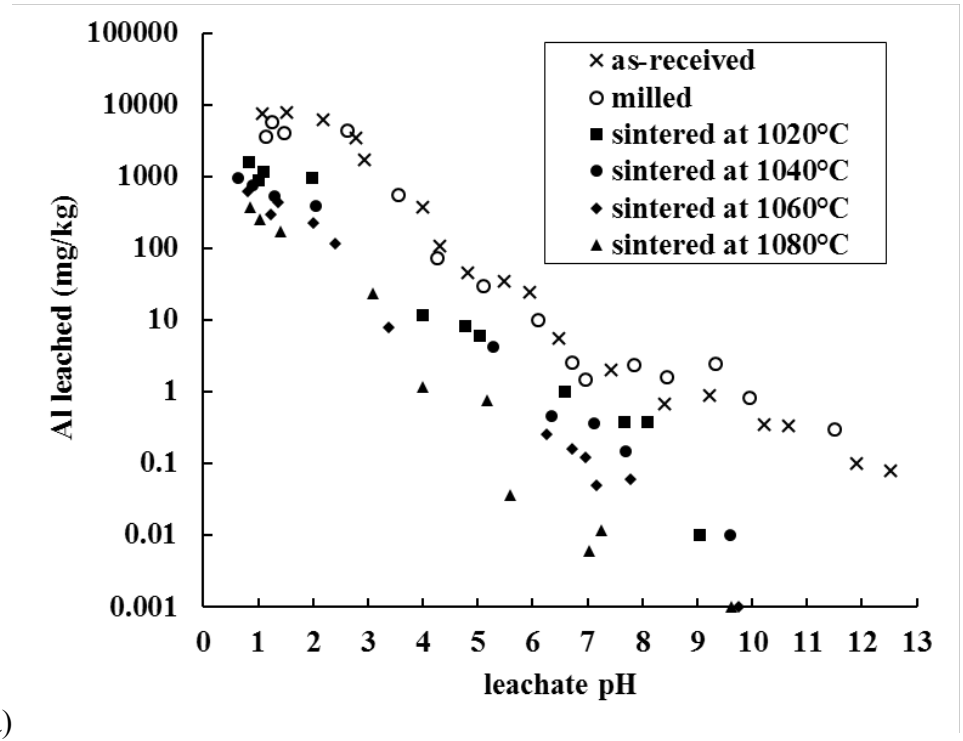

(a)

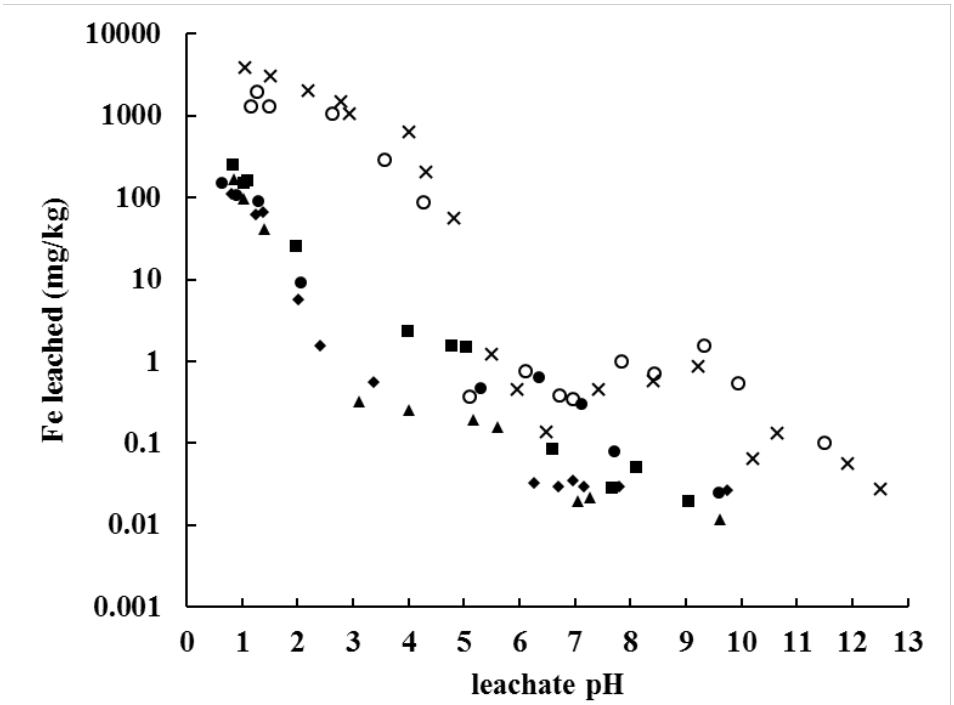

(b)

Figure 4.19: Leaching data for (a) Al and (b) Fe as a function of leachate pH for aged dry discharged fine IBA dust, 80wt. % fine IBA dust: 20wt. % glass milled and sintered fine IBA dust: glass powders

4.5 CONCLUSIONS

The fine dust of incinerator bottom ash (IBA) generated from dry discharge systems has been processed using conventional ceramic processing. This involved mixing with glass, wet ball milling, drying and sieving the produced powder to less than 500 μm and sintering. The effects of changing the processing parameters and the glass addition have been evaluated and the materials produced have been fully characterised.

Ceramic materials have been produced from the fine IBA dust derived from dry discharge system, for which there are currently limited options for the reuse and up-cycling. It has been found that sintering control the physical, chemical, mineralogical and leaching properties and this is dominated by the particle size distribution of the milled powders and the addition of glass.

Liquid phase sintering is the responsible mechanism for the relatively high-density of the materials obtained. The addition of glass accelerates liquid phase sintering and the densification

point is subsequently reduced as the glass content increases. Maximum densities between 2.20 and 2.40 g/cm^3 were obtained when sintering between 1020 and 1040 °C for mixtures containing 20 wt. % and 30 wt. % glass. These samples exhibited high (~20%) linear shrinkage and this tended to cause deformation and warping of tile samples. Dry discharged fine IBA dust samples containing 10 wt. % glass and no glass produced significant lower maximum densities of 1.9 and 1.8 g/cm^3, respectively. Sintering above 1060 °C resulted in a rapid decrease in the density of the materials produced containing 20 wt. % and 30 wt. % glass. This is associated with the isolated, spherical pores observed in the microstructural analysis of these samples, formed from the entrapment of gases decomposed within the glassy matrices obtained after sintering. Increasing the firing temperature reduces the density due to the formation of internal closed porosity, but the skeletal density increases and this improves the appearance of the ceramic body formed. These samples indicated minimum water absorption and better appearance. In addition, since the objective of the project is to utilise the dry discharged fine IBA dust, the addition of 20 wt. % glass was decided as the optimum composition, and this was subject to further characterisation.

Sintering dry discharged fine IBA dust: glass revealed that the as-received dry discharged fine IBA dust can be transformed into ceramic materials containing pyroxene group minerals. The major crystalline phases present in the dry discharged fine IBA dust are quartz (SiO_2), calcite ($CaCO_3$), gehlenite ($Ca_2Al_2SiO_7$) and hematite (Fe_2O_3), and these are transformed into the pyroxene group minerals diopside ($CaMgSi_2O_6$), clinoenstatite ($MgSi_2O_6$), wollastonite ($CaSiO_3$) together with some albite ($NaAlSi_3O_8$) and andradite ($Ca_3Fe_2Si_3O_{12}$).

Sintering has the effect to reduce the acid neutralisation capacity of the as-received dry discharged fine IBA dust. This is mainly due to the decomposition of calcite and the encapsulation of Ca ions into the glassy matrices and the new crystalline phases formed during sintering. Sintering dry discharged fine IBA dust: glass samples at 1080 °C produced samples with significantly lower leached concentrations for Ca, Mg, Na and K under all pH conditions examined, compared to the as-received dry discharged fine IBA dust. This is believed to be due to the well sintered structure of the produced materials and the incorporation of these metals within the new, less insoluble crystalline phases formed. However, sintering at 1020 °C resulted in relatively high concentrations of Ca and Na under acidic conditions, associated with the partial sintering of the material and the formation of soluble phases containing these ions at this temperature.

The sintered at 1080 °C ceramics exhibit low leaching of heavy metals (Cd, Cr, Cu, Ni, Pb, Zn) compared to the as-received dry discharged fine IBA dust down to very aggressive acid leachate pH conditions. These metals are incorporated within the phases formed during sintering. The most concentrated heavy metals of environmental concern found in the as-received dry discharged fine IBA dust that have the potential to leach under highly acidic conditions are Zn, Pb and Cu. Processing of dry discharged fine IBA dust and sintering at 1080 °C resulted in minimal leaching of these heavy metals due to the incorporation in newly formed minerals or in less structured amorphous phases during sintering.

The produced material obtained with the optimum mixture composition (20 wt. % glass) and sintered at optimum firing temperatures (1080 °C) exhibited high shrinkage, creating warping and deformation during processing. The presence of volatile components in the as-received material, responsible for the pore formation of the sintered ceramics, is responsible for this effect. This is also supported from the 16 wt. % weight loss observed when heated the as-received material at 1100 °C. The combination of these effects, densification, pore formation and crystalline phase changes, results in sintering that is difficult to control and this makes the production of ceramic tiles from uncalcined dry discharged fine IBA dust powder problematic. High shrinkage causes distortion and warping effects and as a result tile production using a pressing sintering route for the uncalcined dry discharged fine IBA dust material is unlikely to be feasible.

Therefore, the effect of calcining the processed materials to eliminate the evolution of these gases has to be investigated.

CHAPTER 5 EFFECT OF CALCINING ON THE PRODUCTION OF CERAMICS FROM DRY DISCHARGED INCINERATOR BOTTOM ASH DUST

5.1 INTRODUCTION

In the previous chapter the potential of producing ceramic materials from the fine IBA dust derived from a dry discharge system have been evaluated. The processing involved mixing dry discharged fine IBA dust with glass, wet ball milling, drying and sieving to less than 500 μm, and sintering. The effects of glass addition and processing parameters have been studied. Glass addition and sintering temperature controls the physical, mechanical, mineralogical, microstructural and leaching behaviour properties. Effective sintering is associated with the particle size distribution of the milled material and the addition of glass.

The optimum materials (80 wt. % dry discharged fine IBA dust and 20 wt. % glass sintered at 1080 °C) exhibited relatively high density, low water absorption and high Vickers micro hardness. However, the high linear shrinkage (~20 %) obtained was responsible for product warping and high levels of fired scrap. This phenomenon is associated with the 16 wt. % weight loss observed when heated the as-received dry discharged fine IBA dust at 1100 °C, making clear the presence of volatile compounds in the as-received material. Therefore, there is a need to remove the volatile compounds before sintering and the effect of calcining the powder after wet ball milling, drying and sieving was investigated.

In this chapter the effect of calcining temperature on the properties of sintered materials has been evaluated. A series of dry discharged fine IBA dust samples mixed with different amounts of glass have been processed and the produced materials have been characterised in terms of the physical, chemical, mechanical, mineralogical, microstructural and leaching properties obtained.

5.2 OBJECTIVES

The main objective of this part of the research was to examine the effect of calcining temperature in the processing of dry discharged fine IBA dust for the production of ceramics materials with minimal linear shrinkage. In order to achieve this a series of ceramic samples with

dry discharged fine IBA dust mixed with varying the glass addition and varying calcining temperature have been produced and their properties have been fully characterised. Once the optimum calcining temperature has been decided, the effect of sintering temperature on the properties of the ceramic materials produced from powders calcined at optimum temperatures has been determined and discussed.

5.3 MATERIAL PROCESSING AND CHARACTERISATION

5.3.1 Materials and processing

A representative 50 kg batch of the <1 mm fine fraction of IBA was obtained from the Monthey EfW facility in Switzerland. The flow diagram of the process is presented in Figure 5.1.

Fine IBA dust was mixed with waste glass and wet ball milled using high-density alumina milling media, a water to charge ratio of 2 and a milling media to charge ratio of 5. Milled slurries were dried overnight at 105 °C and passed through a 500 μm sieve to remove the coarse particles, mainly consisting of coarse glass and stones. The obtained powder was subject to subsequent heating in an alumina crucible to temperatures between 600 and 1200 °C. The calcined powders were then lightly ground using a mortar and pestle and 1 wt. % of polyethylene glycol (PEG-8000) was added as a binder to aid pressing. The produced powders were uniaxial pressed at 48 MPa (Nannetti S hydraulic press) in steel dies to form tile samples (110 m × 55 mm × 20 mm) and disc samples (40 mm diameter). Pressed samples were then sintered in an electric furnace (Lenton Thermal Design Ltd., ECF 12/45) at a heating rate of 6 °C·min^{-1} to temperatures between 1020 and 1100 °C with a dwell time of 1 hour at peak temperature.

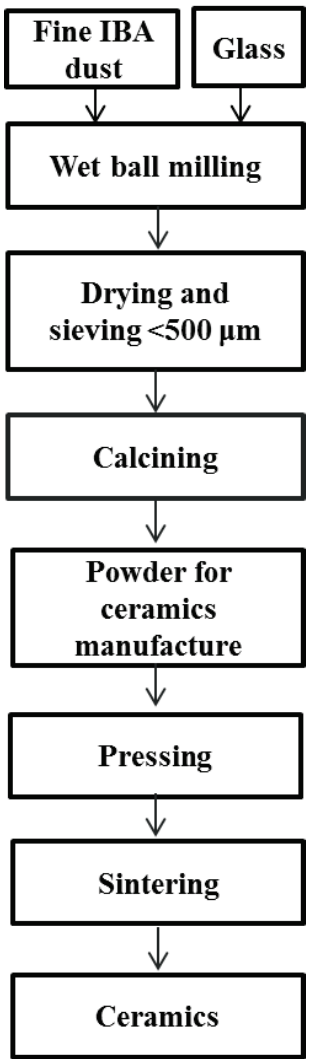

Figure 5.1: Flow diagram of ceramic processing of dry discharged fine IBA dust. In this process a calcining stage has been introduced to remove the volatiles present in the as-received fine IBA dust, responsible for the high linear shrinkage observed in the conventional ceramic manufacturing route.

5.3.2 Characterisation of sintered samples

The produced samples were characterised in terms of their density, linear shrinkage and water absorption. Calcined and sintered samples were ground to <150 µm to determine the crystalline phases by XRD. Gold coated fracture surfaces of IBA: glass samples calcined at

different temperatures were analysed by SEM. Polished surfaces of the ceramics produced with powders calcined at different temperatures were compared by optical microscopy. The optimum ceramics produced were further characterised for the Vickers micro hardness, Young's modulus and thermal conductivity. The obtained values were compared to the values of traditional terracotta ceramics.

5.3.3 Metal leaching from as-received and processed dry discharged fine IBA dust

The leaching characteristics of the as-received dry discharged fine IBA dust, the calcined at different temperatures powders and the optimum ceramic have been evaluated using the pH dependence leaching test using a liquid to solid (L/S) ratio of 10 (CEN/ TS 14429). Samples were ground to < 150 μm sieve and digests were analysed by ICP-AES.

5.4 RESULTS AND DISCUSSION

5.4.1 Effect of calcining on the 'green' density

The 'green' density of the materials produced with uncalcined and calcined at 1080 °C is presented in Figure 5.2.

The calcined at 1080 °C powder produced pressed samples with higher 'green' density compared to the samples produced with uncalcined powders. This is associated with the improved packing of the materials produced with calcined powders. 'Green' bodies produced with uncalcined powders exhibited a 'green' density of approximately 1.5 g/cm^3. Samples produced with calcined at 1080 °C powders indicated significant higher 'green' density of about 2.0 to 2.2 g/cm^3. Increasing the compaction pressure had negligible effect on 'green' densities of samples produced with the uncalcined and calcined at 1080 °C powders.

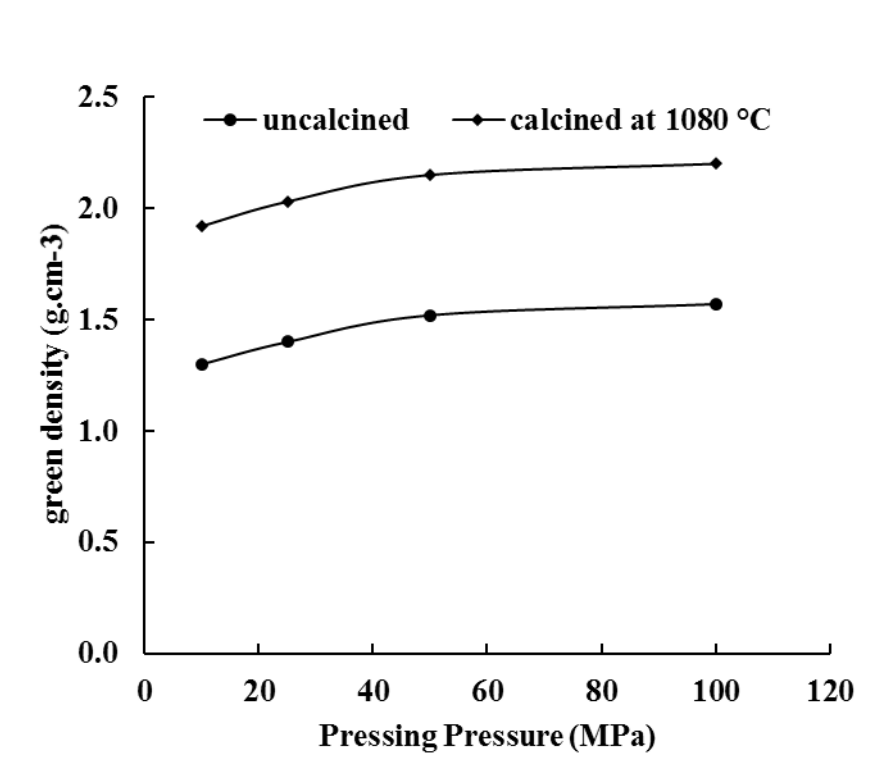

Figure 5.2: Effect of calcining temperature on the 'green' density of mixtures containing 80 wt. % dry discharged fine IBA dust and 20 wt. % glass. Samples calcined at 1080 °C exhibited higher 'green' density associated with improved packing of powders.

5.4.2 Effect of calcining temperature on the density and linear shrinkage of samples sintered at 1080 °C

The effect of calcining temperature on the density and firing linear shrinkage of samples sintered at 1080 °C with varying glass additions are shown in Figure 5.3 and 5.4. The 1080 °C sintering temperature was constant in this set of experiments, since this was the optimum temperature obtained from the analysis in the effect of sintering temperature on the properties of the uncalcined samples, explained in the previous chapter. Calcining the ball milled powder significantly improves the properties of the ceramics produced and causes a marked reduction in shrinkage during firing. The green density of the calcined samples increases due to improved particle packing and as a result the linear shrinkage decreases from 20 % for uncalcined powder

to less than 7% for calcined powder. This is similar or slightly below the shrinkage observed during sintering of typical clay ceramics and lower shrinkage reduces the potential for warping and unwanted deformation of products during sintering. Shrinkage during sintering and the associated increase in density is driven by the elimination of surface area in the powder compact and this is also significantly aided by the fluxing effect of the added waste glass which promotes liquid phase sintering.

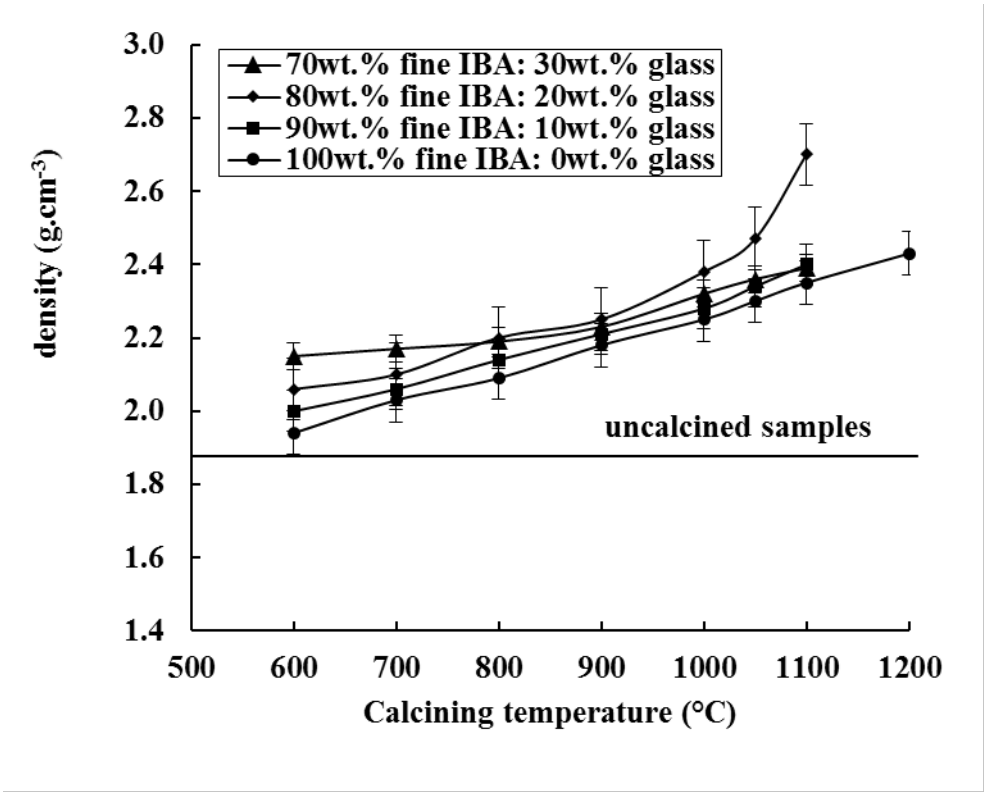

Figure 5.3: Effect of calcining temperature on the density of samples sintered at 1080 °C. Calcined samples achieve higher densities than samples produced with uncalcined powders. Error bars: +/- 1 std

Significantly higher densities between 2.30 and 2.80 g/cm^3 are achieved by calcining powders above 1000 °C. Calcining powders below 1000 °C produced ceramic samples with densities between 1.50 to 2.30 g/cm^3. The linear shrinkage that occurs during sintering decreased with increasing calcining temperature for all mix compositions. Higher density and lower shrinkage results from reducing the volatiles present in the dry discharged fine IBA dust by

calcining at temperatures above 1000 °C and this also improves the packing of calcined powders during pressing to give higher pressed densities. Samples containing more than 10 wt. % glass tended to melt and distort when calcined at temperatures above 1100 °C and measurements were not possible.

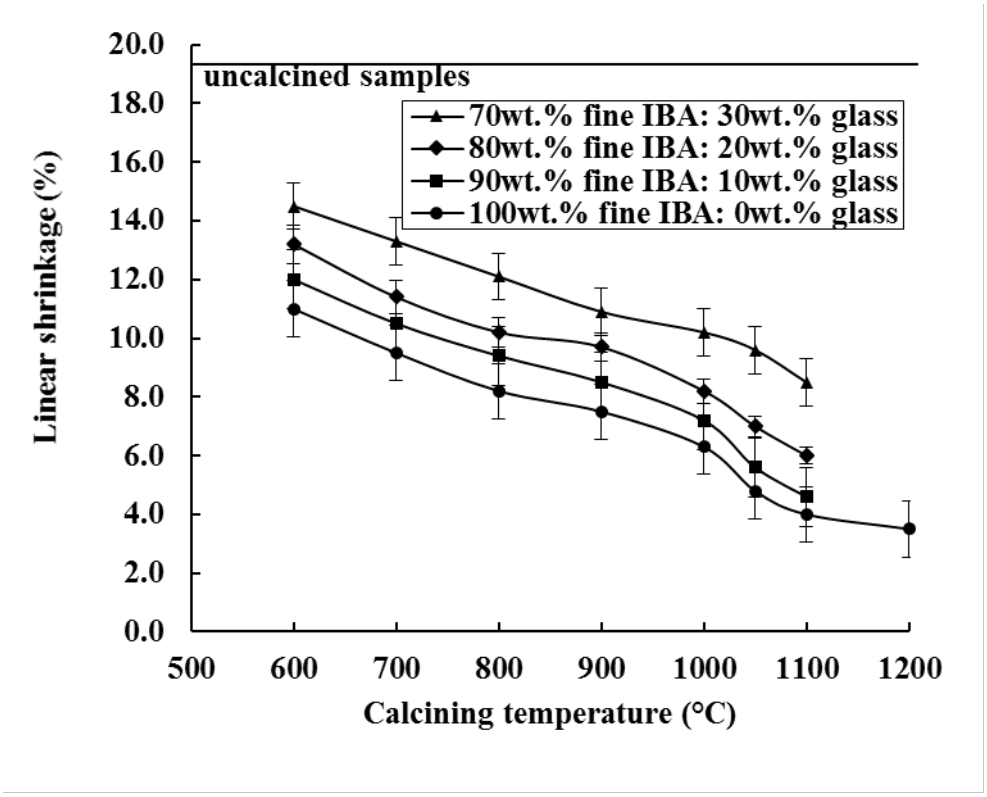

Figure 5.4: Effect of calcining temperature on the linear shrinkage of samples sintered at 1080 °C.Calcined samples achieve significantly lower linear shrinkage than samples produced with uncalcined powders, associated with the higher 'green' densities achieved for the calcined powders. Error bars: +/- 1 std

5.4.3 Effect of calcining temperature on water absorption of samples sintered at 1080 °C

The effect of calcining temperature on the water absorption of samples sintered at 1080 °C is presented in Figure 5.5.

The water absorption of samples prepared from calcined powders containing 20 wt. % glass was negligible for almost all calcining temperatures examined. Samples prepared with 10 wt. % and no glass achieved approximately 1% water absorption, when calcined at 1100 and 1200 °C, respectively, and fired at 1080 °C. Water absorption rapidly decreases with increasing calcining temperature, and this is due to the elimination of pores, associated with the gradual decrease of the volatiles gases decomposed at these temperatures.

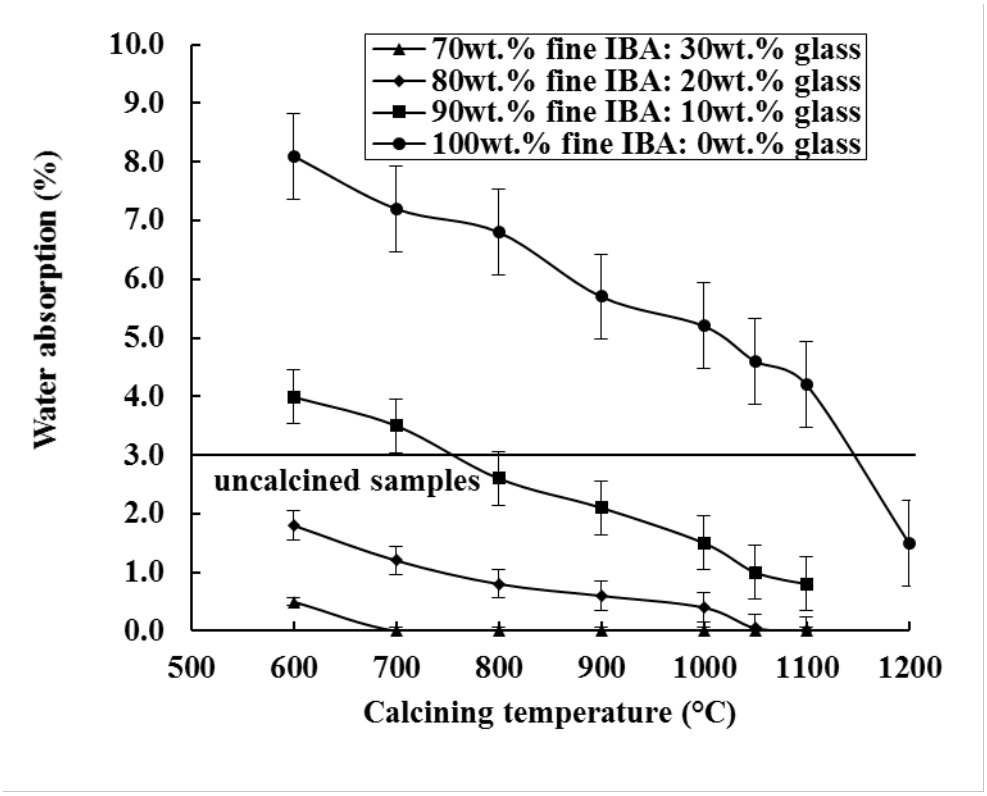

Figure 5.5: Effect of calcining temperature on water absorption of samples sintered at 1080 °C. Calcined samples achieve lower water absorption than samples produced with uncalcined powders. Error bars: +/- 1 std

Strong interdependencies between the linear shrinkage, the density and the water absorption were observed, and this is in accordance with the observations of other researchers (Barbieri et al., 2002; Cheeseman et al., 2003; Aloisi et al., 2006; Velis et al., 2014). However, samples containing more than 10 wt. % glass and calcined at 1080 °C, appeared to have

properties within the defined limits for the desired ceramic materials and this calcining temperature was subject to further investigation.

5.4.4 Effect of sintering temperature on the density and linear shrinkage of samples produced with powders calcined at 1080 °C

The density and linear shrinkage of samples calcined at 1080 °C and sintered at different temperatures is presented in Figures 5.6 and 5.7, respectively.

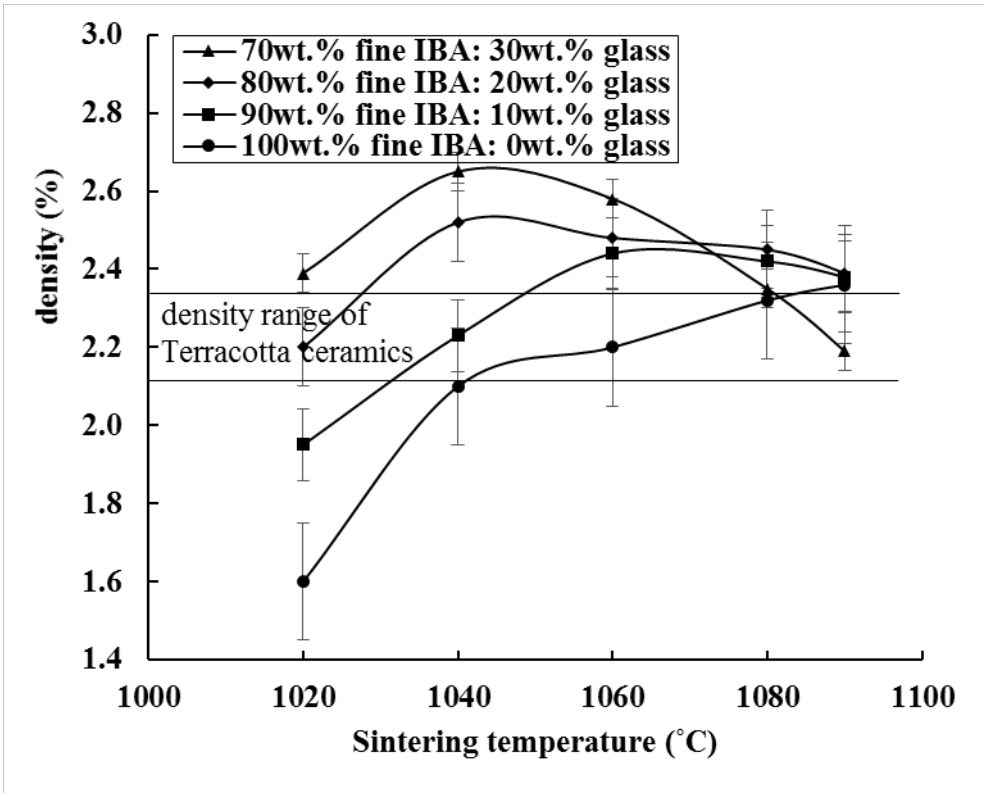

Figure 5.6: Effect of sintering temperature on the density of samples calcined at 1080 °C. Error bars: +/- 1 std.

Increasing sintering temperature from 1020 to 1100 °C tends to increase the density of the materials containing less than 20 wt. % glass, associated with the reduction of pore volume that occurs during sintering. Samples containing 30 wt. % glass exhibit an increase in the density when fired to 1040 °C, and the density decreased when fired above 1040 °C. This is due to

sintering at temperatures where the powder compact starts to melt and soften, producing a lower density material.

Maximum fired densities between 2.40 and 2.80 g/cm^3 were obtained for compositions containing 20 and 30 wt. % of glass calcined at 1080 °C and sintered at temperatures between 1040 and 1080 °C. Linear shrinkage was significantly reduced (<10%) compared to un-calcined samples for all mix compositions. This benefit of reaching higher densities with much lower shrinkage is due to the improved pressing behaviour of powders calcined at high temperatures. Ceramic samples produced from optimum uncalcined and calcined powders are shown in Appendix A.

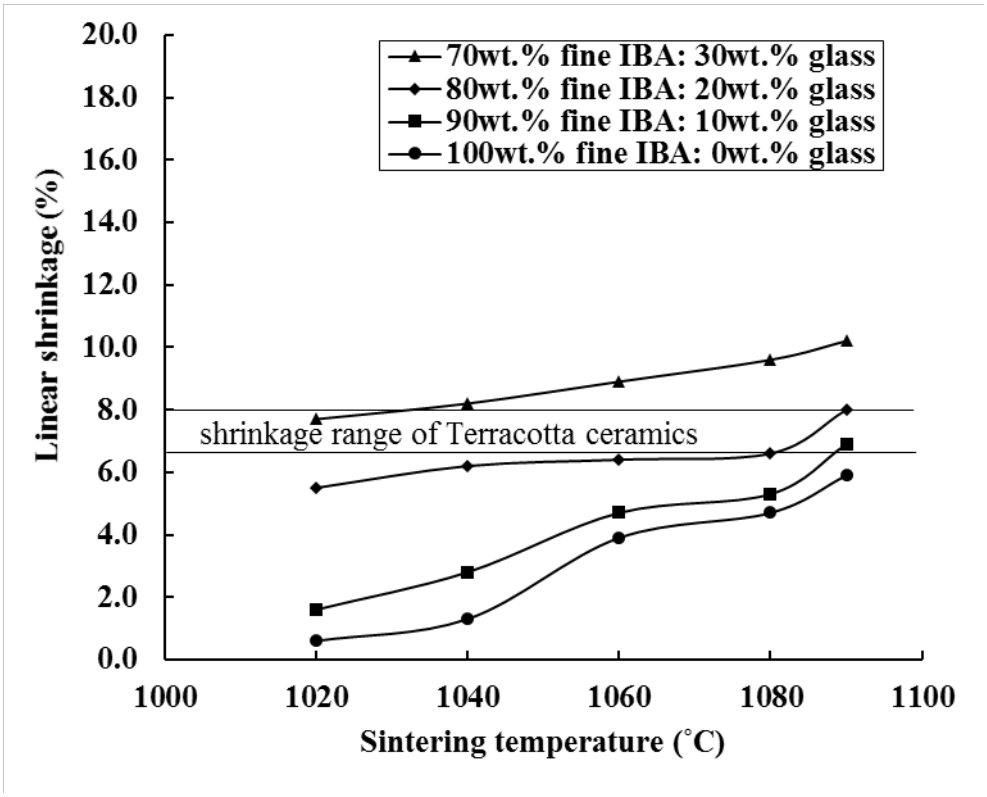

Figure 5.7: Effect of sintering temperature on the linear shrinkage of samples calcined at 1080 °C. Error bars: negligible

5.4.5 Effect of sintering temperature on water absorption of samples produced with powders calcined at 1080 °C

The water absorption of samples calcined at 1080 and sintered at different temperatures is presented in Figure 5.8. Increasing sintering temperature leads to a decrease in water absorption for all mixture compositions examined. This is associated with the elimination of open pores, responsible for the accessibility to water. The water absorption was negligible for samples containing > 10 wt. % glass sintered between 1080 and 1100 °C and samples containing 10 wt. % and no glass exhibited water absorption of about 1.0% and 5.0%, respectively.

Samples containing 20 wt. % glass, calcined at 1080 °C and sintered at 1080 °C, exhibited properties within the defined limits and improved appearance compared to the optimum samples produced with uncalcined powders and other samples produced with calcined powders. Therefore, samples containing 20 wt. % glass and calcined at different temperatures were subject to further characterisation.

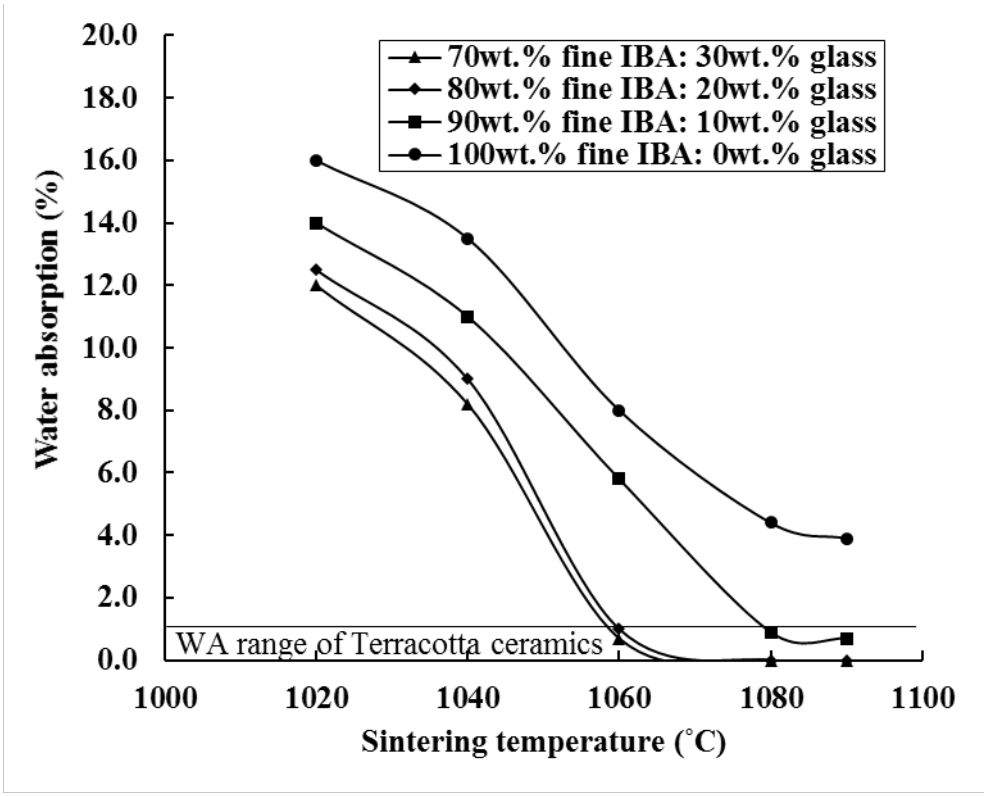

Figure 5.8: Effect of sintering temperature on water absorption of samples calcined at 1080 °C.WA refers to water absorption. Error bars: negligible

5.4.6 Mechanical properties and thermal conductivity of sintered ceramics

The density, Young's modulus, Vickers micro hardness and thermal conductivity of the optimum sintered ceramic produced by milling 80 wt.% dry discharged fine IBA dust with 20 wt.% glass, calcining the produced powder at 1080 °C and sintering at 1080 °C have been compared with typical values of a terracotta ceramic are presented in Table 5.1 .

It is clear that the ceramic manufactured from fine dry-discharged IBA dust exhibit improved properties in comparison to terracotta ceramics (Acchar et al., 2006). In addition, ceramics produced with calcined at 1080 °C indicated improved properties than the optimum ceramics derived from uncalcined powders.

Table 5.1: Mechanical properties and thermal conductivity of optimum ceramics (80 wt. % dry discharged fine IBA dust: 20 wt. % glass) produced with calcined at 1080 °C and uncalcined powder and the corresponding values for the commercial Terracotta ceramics

Property	**Sintered ceramic with calcined at 1080 °C powder**	**Terracotta ceramics**	**Sintered ceramic with uncalcined powder**
Density (g/cm^3)	2.7	2.3	1.9
Young's modulus (GPa)	76.2	71.0	52.3
Vickers microhardness (GPa)	4.4	3.1	3.8
Thermal conductivity (W/m*K)	0.6	0.6	0.6

5.4.7 Mineralogy of processed dry discharged fine IBA dust: glass samples

The XRD analysis of samples containing 20 wt. % glass, calcined at different temperatures and the optimum ceramic obtained calcined at 1080 °C and sintered at 1080 °C are presented in Figure 5.9.

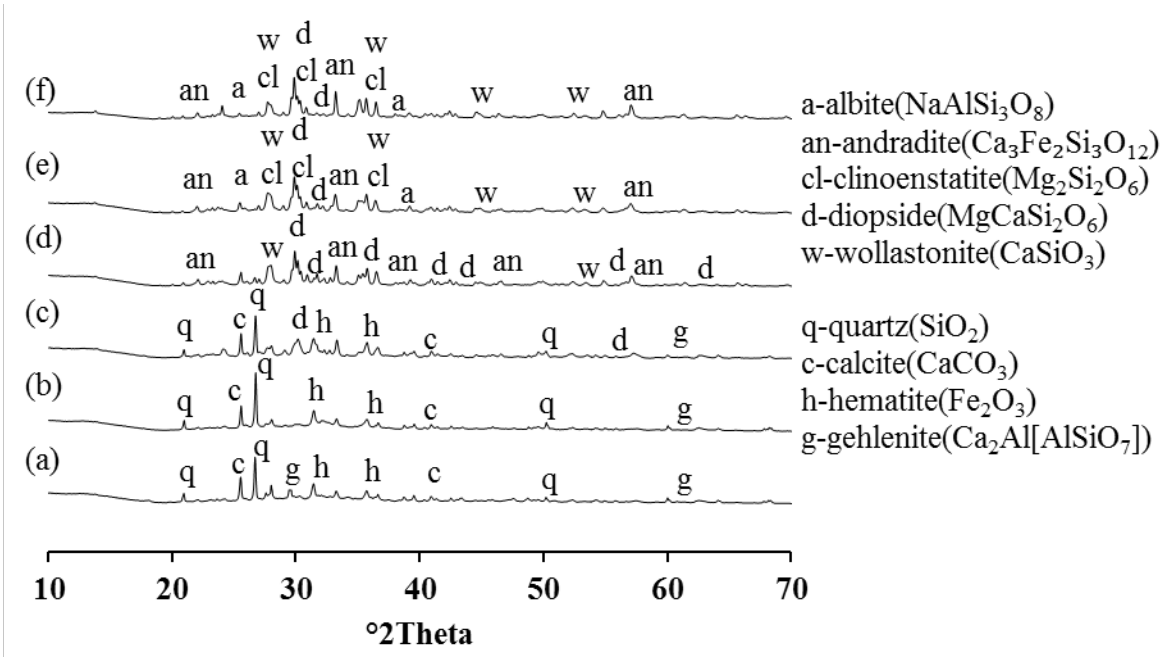

Figure 5.9: XRD data of the : (a) milled 80 wt.% dry discharged fine IBA dust: 20 wt.% glass, calcined at (b) 600 °C, (c) 800 °C, (d) 1000 °C, (e) 1080 °C and (f) calcined at 1080 °C and sintered at 1080 °C. This indicates that the amount of quartz (SiO_2), calcite ($CaCO_3$), gehlenite ($Ca_2Al_2SiO_7$) and hematite (Fe_2O_3) decrease on calcining and these crystalline phases are no longer present after calcining at 1080 °C.

While quartz (SiO_2), calcite ($CaCO_3$), hematite (Fe_2O_3) and ghelenite ($Ca_2Al_2SiO_7$) are the major crystalline phases in the as-received dry discharged fine IBA dust, new crystalline phases are formed in powders calcined above 800 °C. The pyroxene minerals diopside ($CaMgSi_2O_6$) and clinoenstatite ($MgSi_2O_6$) together with some andradite ($Ca_3Fe_2Si_3O_{12}$) are the major crystalline phases in powders calcined at 1080 °C. Figure 5.9 also shows that sintering of calcined powder does not introduce additional changes in the crystalline phases present.

XRD analysis of dry discharged fine IBA dust: glass calcined at increasing temperatures indicates that the amount of quartz (SiO_2), calcite ($CaCO_3$), gehlenite ($Ca_2Al_2SiO_7$) and hematite (Fe_2O_3) decrease on calcining and these crystalline phases are no longer present after calcining at 1080 °C. The dominant phases formed are diopside ($CaMgSi_2O_6$), clinoenstatite ($MgSiO_3$) and wollastonite ($CaSiO_3$) together with some garnet group and plagioclase feldspar crystalline phases such as andradite ($Ca_3Fe_2Si_3O_{12}$) and albite ($NaAlSi_3O_8$). Diopside was the principal crystalline phase, with clinoenstatite and andradite also present when calcining at 1000 °C, with small amounts of hematite and augite. The main crystalline phases in dry discharged fine IBA dust: glass mix calcined at 1080 °C were diopside ($CaMgSi_2O_6$), clinoenstatite ($MgSiO_3$) and andradite ($Ca_3Fe_2Si_3O_{12}$). Diopside and wollastonite are calcium pyroxenes, while clinoenstatite is a magnesium pyroxene. Pyroxenes are an important group of rock-forming silicate minerals of variable composition typically containing Ca, Mg and Fe. They occur as stable phases in almost every type of igneous rock and are found in rocks of widely different composition (Deer et al., 1992).

Wollastonite and clinoenstatite have also been reported to form in other waste derived ceramics. Augite and clinoenstatite were identified in ceramics obtained from vitrification of incinerator bottom and fly ash. Augite has also been reported in crystalline phases formed from the vitrification of electric arc dust (Romero et al., 2001; Rawlings et al., 2006).

5.4.8 Microstructure of processed dry discharged fine IBA dust: glass samples

SEM images of fracture surfaces of samples containing 20 wt. % glass, calcined at different temperatures and sintered at 1080 °C are presented in Figure 5.10.

The effect of calcining temperature on the microstructure of the produced samples is in agreement with the density data. Samples prepared with calcined at 600 and 800 °C powders and sintered at 1080 °C, appeared with an extensive volume of isolated, irregular shaped dispersed pores. The development of this microstructure is associated with the partial decomposition of volatile compounds, such as alkaline metal sulphates. The evolution of these gases, such as SO_2, and the subsequent melting of glass, which has the ability to entrap these gases within the glassy matrix, are associated with the formation of the foamed microstructure observed (Stern and Weise, 1996; Cheeseman et al., 2003).

Increasing the calcining temperature to 1000 °C resulted in a more uniform closed porosity microstructure, although some open pores were also present, in accordance with the water absorption data. Firing the calcined at 1080 °C powders at 1080 °C, produced samples with reduced porosity, since calcining the samples at 1080 °C have resulted to the complete decomposition of volatile compounds, associated with the spherical closed pores observed in the optimum uncalcined samples. This can be further explained by the TGA data, since heating the dry discharged fine IBA dust: glass powders at 1080 °C, results in the reduction in mass by 16 wt. %, mainly associated with the volatile gases.

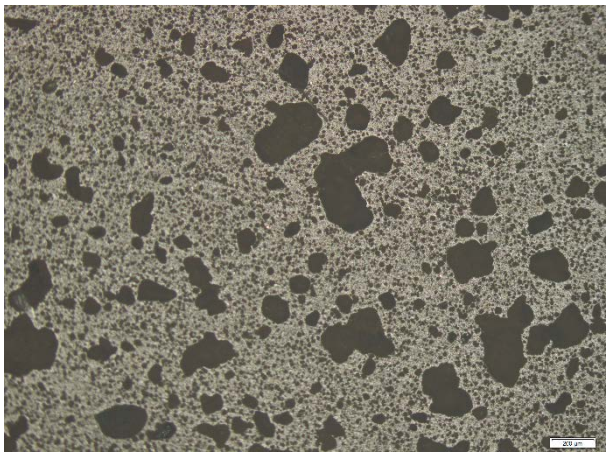

(a)

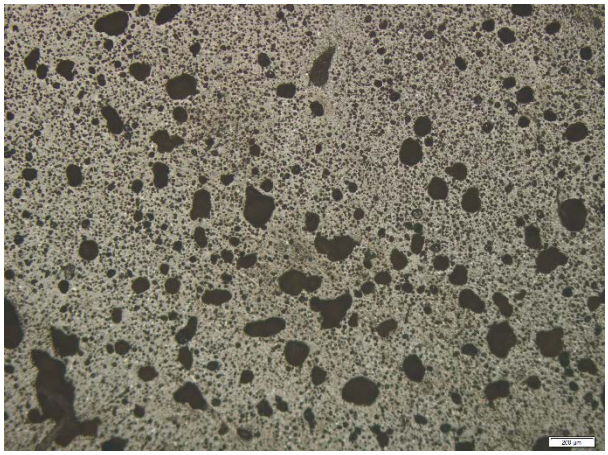

(b)

(c)

(d)

Figure 5.10: SEM images of samples sintered at 1080 °C and prepared with 80 wt.% dry discharged fine IBA dust: 20 wt.% glass milled powders calcined at (a) 600 °C, (b) 800 °C, (c) 1000 °C and (d) 1080 °C. Firing the calcined at 1080 °C powders at 1080 °C, produced samples with reduced porosity. Calcining the samples at 1080 °C have resulted to the complete decomposition of volatile compounds, associated with the spherical closed pores observed in the calcined at lower temperatures samples.

5.4.9 Leaching behaviour during processing

Acid Neutralisation Capacity

Figure 5.11 shows the ANC test results for the as-received dry discharged fine IBA dust, the milled material and the powders calcined at different temperatures. The results are presented in terms of final leachate pH after 48 hours contact as a function of the amount of nitric acid added to the sample, in equivalents of acid per kg of solid.

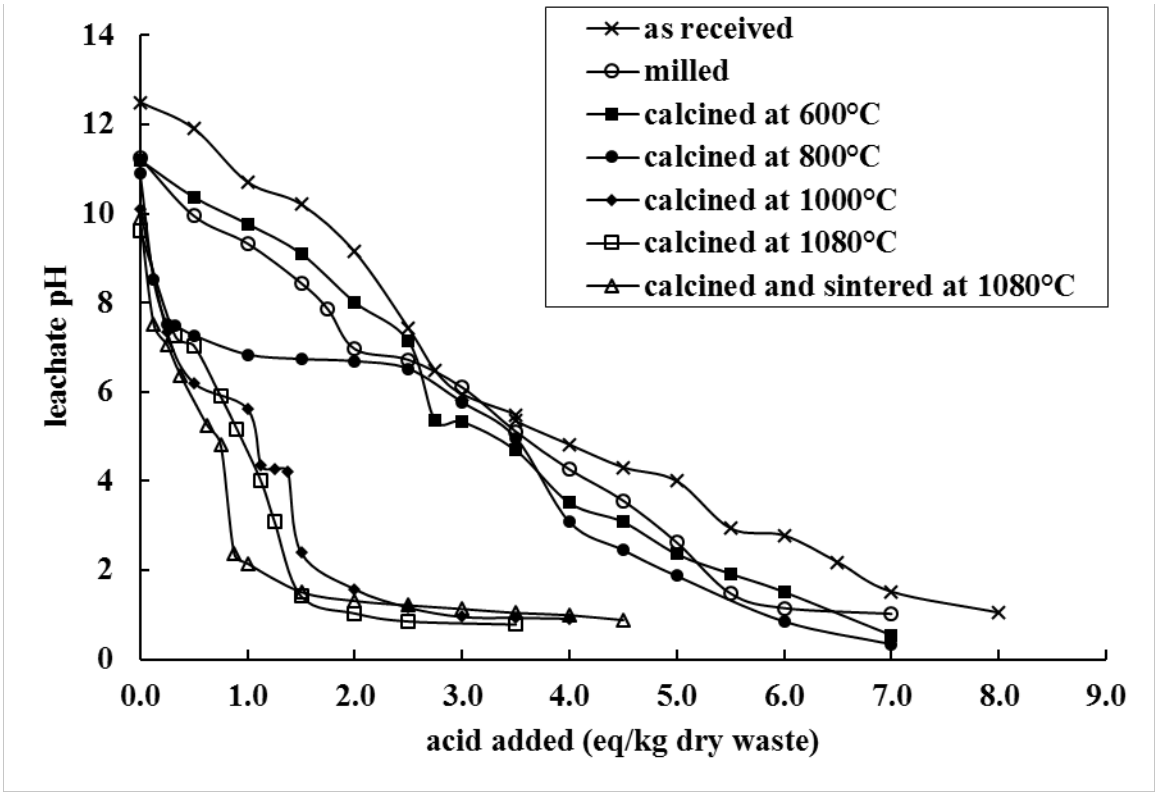

Figure 5.11: Acid Neutralisation capacity of the as-received dry discharged fine IBA dust, milled 80 wt.% dry discharged fine IBA dust: 20 wt.% glass, calcined milled powders at 600 °C, 800 °C, 1000 °C, 1080 °C and calcined milled powders at 1080 °C and sintered at 1080 °C. Increasing the calcining temperature resulted in a decrease in ANC curve.

Calcining the milled powders to 600 °C resulted in a material that showed similar ANC to the milled powder. This is associated with the relatively low calcining temperature, which

does not allow the milled powder to activate the decomposition reactions, mainly of $CaCO_3$, and therefore the buffering capacity of the powder produced with calcining at 600 °C remains similar to the capacity of the milled powder.

Increasing the calcining temperature to 800 °C produces powders with initial similar ANC curve with the powders produced with calcining the powder at 1000 °C and 1080 °C. However, the ANC curve tended to be similar to the calcined at 600 °C powders at pH < 6, associated with the partial decomposition of $CaCO_3$.

Increasing the calcining temperature to 1000 °C and 1080 °C, resulted in a rapid decrease in ANC curve, associated with the gradual decomposition of $CaCO_3$ to CaO and CO_2, combined with subsequent encapsulation and incorporation of Ca^{2+} in both amorphous and crystalline phases present in the calcined powders (Van der Sloot et al., 2001; Bethanis et al., 2004; Van der Sloot et al., 2012). The minimum ANC was achieved for the optimum ceramic (calcined at 1080 °C and sintered at 1080 °C), since the two-stages heating has resulted in the complete elimination of volatile gases, associated with an increase in buffering capacity.

Leachate analysis data

Concentrations of selected alkali and alkali-earth metals and heavy metals leached from the as-received dry discharged fine IBA dust, the powders produced from milling 20 wt. % glass: 80 wt. % dry discharged fine IBA dust, the powders calcined at different temperatures and the optimum ceramic are presented in Figure 5.12 to 5.17.

(a) Leaching of alkali metals and alkali metal earth ions

Leaching data for Ca, Mg, Na and K in mg/kg are presented in Figure 5.12 and 5.13.

The addition of acid leads to similar concentrations of Ca releases for powders calcined at 600 and 800 °C at pH < 6. The calcined at 600 °C powders followed the same trend as the as-received dry discharged fine IBA dust and the milled material for pH > 6. Powders calcined at 800 °C exhibited rapid decrease in Ca leached concentrations for pH > 6, associated with the partial decomposition of $CaCO_3$ occurred in this temperature and the formation of less-soluble calcium silicates, such as diopside, that encapsulate Ca in the crystalline phases formed (Selinger et al., 1997; Van der Sloot et al., 2001; Bethanis et al., 2004; Van der Sloot et al., 2012). Powders calcined at 1000 °C exhibited intermediate Ca leached concentration at pH < 6, while the Ca

leached concentration decreases at pH > 6. This is associated with the formation of insoluble stable crystalline phases at this temperature, which incorporate Ca in the new crystalline phases formed. Increasing the calcining temperature to 1080 °C results in a rapid decrease in Ca leached concentration, since at this temperature $CaCO_3$ has completely decomposed and Ca ions have been encapsulated into the new crystalline insoluble, stable phases formed, such as andradite, diopside and wollastonite. Ca showed the lowest release for the ceramic produced with optimum processing parameters under all pH conditions examined.

Mg leached concentration curve for the as-received, milled, and calcined at 600 and 800 °C powders are similar to the curve produced for Ca leached concentration, and this supports the possible role of calcite in controlling Mg leaching (Van der Sloot et al., 2012). Calcining at temperatures above 1000 °C significantly reduces the Mg leached concentration under all pH conditions examined, associated with the formation of new less soluble crystalline phases.

Na leached concentration of the calcined at 600 °C and 800 °C powders exhibited an increase compared to the as-received and the milled materials at pH < 7. This indicates the formation of readily soluble phases containing this ion at this calcining temperature. Na leached concentration of the calcined at 800 °C powders rapidly decreases at pH > 7, indicating the partial decomposition of volatile components containing this ion. This is also supported by the behaviour of Na leached concentration of powders calcined at 600 °C at pH > 7, which are similar to the as-received and milled materials. Calcining at 1000 °C produced powders with intermediate Na leached concentration, while increasing the calcining temperature at 1080 °C produced powders with maximum resistance against leaching and this was further increased for the optimum ceramic obtained. This is also associated with the formation of stable insoluble phases, encapsulating Na ions into the crystalline phases formed, such as albite.

K leached concentration for powders calcined at different temperatures indicated similar curves as for the other alkali metals examined. Calcining at 600 and 800 °C produced powders with K leached concentration slightly lower than the as-received and the milled materials at pH < 7. This was rapidly decreased at pH > 7 for powders calcined at 800 °C, but remained similar to the as-received and the milled materials for powders calcined at 600 °C. Calcining the powders to 1000 and 1080 °C, gradually decreases K leached concentration for all pH examined. Maximum resistance against K leaching was observed for the optimum ceramics produced.

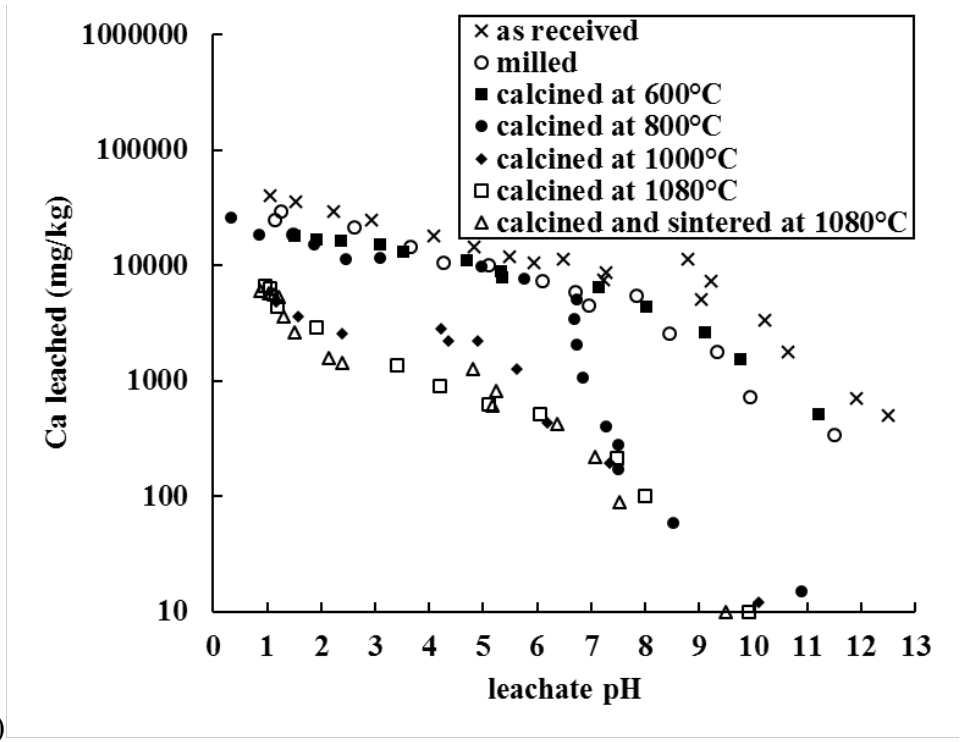

(a)

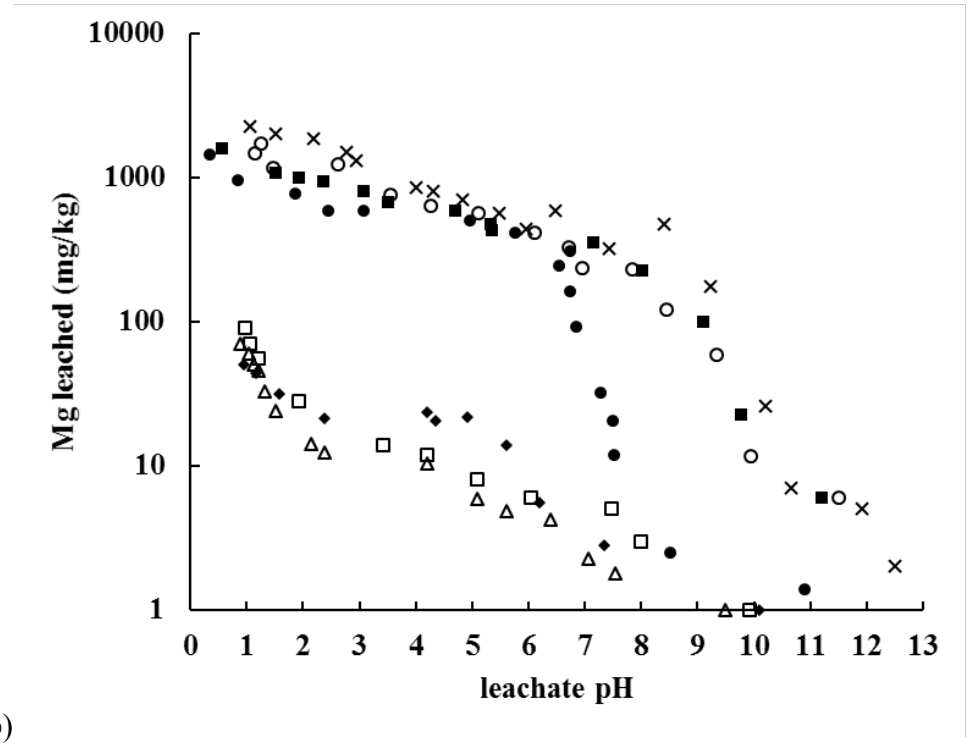

(b)

Figure 5.12: Leaching data for (a) Ca and (b) Mg as a function of leachate pH for the as-received dry discharged fine IBA dust, milled 80 wt.% dry discharged fine IBA dust: 20 wt.% glass, calcined milled powders at 600 °C, 800 °C, 1000 °C, 1080 °C and calcined milled powders at 1080 °C and sintered at 1080 °C.

(b) Leaching of heavy metals

Leaching data for Cr, Cu, Ni, Zn, Cd and Pb in mg/kg are presented in Figures 5.14 and 5.15 for the as-received dry discharged fine IBA dust, the milled material, the calcined at different temperatures powders and the optimum ceramics.

There is no significant leaching of Cr for the powders calcined above 1000 °C and the optimum ceramic at pH > 4. Cr is effectively bound into these materials and is not available for leaching (Wunsch et al., 1996; Bethanis et al., 2004). There is also relatively low leaching from powders calcined above 1000 °C down to very aggressive acid leachate pH conditions. The leaching behaviour of Cr from powders calcined at 600 and 800 °C is very different at pH > 4. Calcining at 600 and 800 °C has clearly made a proportion of the Cr leached much more available. Similar observations have been made by other researchers, where a significant increase in Cr mobility has been identified when thermal treatment is performed under oxidising atmosphere at sintering temperatures above 600 °C. This is associated with the transformation of the relatively soluble trivalent state of Cr into the readily soluble and more mobile hexavalent form (Wang et al., 2001; Bethanis et al., 2004; Van der Sloot et al., 2012). Calcining the powders above 1000 °C has the effect to convert the hexavalent form into the initial trivalent state and Cr is incorporated into non-leachable crystalline phases.

Cu leaching is typically below 1 mg/ kg at pH > 4, for all the powders calcined at the different temperatures examined. Calcining at 600 and 800 °C produces powders with high availability in Cu leaching, similar to the as-received and the milled materials, at pH < 5. However, Cu leached concentration is significantly reduced at pH > 5 with the calcined at 600 °C powders exhibiting higher availability in Cu than the powders calcined at 800 °C. This is believed to be associated with the decomposition of Cu-containing sulphate salts, also responsible for the isolated porosity observed when sintered these powders at 1080 °C (Cheeseman et al., 2003; Bethanis et al., 2004). Calcining the powders above 1000 °C produces materials that gradually decrease their resistance in leaching of Cu, with the optimum ceramic produced indicating the lowest Cu leached availability.

Ni leached concentration is at low levels for all the powders calcined at different temperatures over the range of leachate pH values examined. Calcining at 600 °C produces powders with similar leaching behaviour to the as-received and milled materials at pH < 5. Calcining the powders at 800 °C decreases the Ni leaching availability and this is significantly

reduced for powders calcined above 1000 °C for all pH conditions examined. The optimum ceramic produced indicated the lowest availability in Ni leaching.

As reported earlier, Zn solubility has the tendency to be very sensitive with pH changes. Calcining at 600 and 800 °C produces powders with similar Zn leached concentration at pH < 6, compared to the as-received and the milled materials. Zn solubility is reduced for powders calcined at 600 and 800 °C at pH > 6. Calcining the powders above 1000 °C produces powders with significant lower Zn leached concentration under all pH conditions examined. This is associated with the inertization of Zn to compounds of low solubility, as suggested by other researchers (Selinger et al., 1997; Bethanis et al., 2004; Van der Sloot et al., 2012).

There is no detectable Pb leaching for powders calcined at 1080 °C and the optimum ceramic produced at pH > 4. Pb leached concentration is significantly reduced for powders calcined above 1000 °C by a factor of 10 compared to the powders calcined at 600 and 800 °C. Calcining the milled material to 600 °C produces a powder with similar Pb leaching behaviour to the as-received and the milled material for all pH conditions examined. Calcining the powders to 800 °C produces a material with slightly lower Pb leached concentration than the calcined at 600 °C powders at pH < 5. However, at pH > 5 powders calcined at 800 °C exhibited reduced Pb leaching concentration than the calcined at 600 °C, similarly to the other metals examined.

Cd leached concentration is gradually decreases with increased calcining temperature. The calcined at 600 °C materials exhibited similar Cd leaching behaviour for all pH conditions examined to the as-received and the milled material, since the low temperature does not allow the activation of the decomposition reactions. Calcining the powders at 800 °C produces materials with slightly lower leaching potential than the calcined at 600 °C powders at pH < 5. However, this is significantly reduced at pH > 5, associated with the partial activation of the decomposition reactions. Calcining the milled powders above 1000 °C significantly reduces the Cd leached concentration under all pH conditions examined, since Cd ions have been incorporated into the new stable crystalline phases formed. The lowest Cd leached concentration was observed for the optimum ceramic produced.

The values of the heavy metals leached from the as-received, the calcined at 1080 °C powder and the optimum ceramic produced under aggressive leachate conditions (pH 3) have been summarised in Table 5.2. The total concentration of the heavy metals contained in the as-received dry discharged fine IBA dust are also reported and the percentage reduction of these

heavy metals during processing is presented. Cu, Zn and Pb are the most readily available heavy metals from the as-received dry discharged fine IBA dust. Approximately 30% of Cu is available for leaching for the as-received material and about 35 % of Zn and 38% of Pb are available for leaching from the as-received dry discharged fine IBA dust. This is significantly reduced for the processed materials, with above 95% reduction for all heavy metals examined for the calcined at 1080 °C calcined pyroxene powder and above 96% for the optimum ceramic produced with most heavy metals indicating above 99% reduction.

(c) Leaching of Al and Fe

Leaching data for Al and Fe for the as-received, milled and calcined at different temperatures materials in mg/ kg are presented in Figure 5.16.

Increasing the calcining temperature has the effect to significantly reduce the Al leached concentration under all pH conditions examined for powders calcined above 1000 °C. This is believed to be due to fixation to the new crystalline phases formed, such as albite. Calcining at 800 °C results in a material that has reduced Al leached concentration at pH > 6, associated with the partial decomposition of $Al(OH)_3$ and amorphous aluminosilicates present in the as-received material and the subsequent formation of less soluble phases (Bethanis et al., 2004; Van der Sloot et al., 2012). The optimum ceramic obtained exhibit the lowest concentration of Al leaching.

Similar behaviour is observed for Fe leached concentration. Calcining at 600 and 800 °C produces materials with reduced Fe leaching concentration than the as-received and the milled materials. This is believed to be due to the low temperatures that does not allow the activation of decomposition reactions, mainly from the ferrihydrates present in the as-received ash, and therefore the formation of crystalline phases that have the ability to encapsulate Fe ions within their matrices. Calcining above 1000 °C produces powders with significantly lower Fe leached concentration at all pH conditions examined, associated with the encapsulation of Fe ions into the new stable crystalline phases formed, such as andradite. The lowest Fe leached concentration was observed for the optimum ceramic produced.

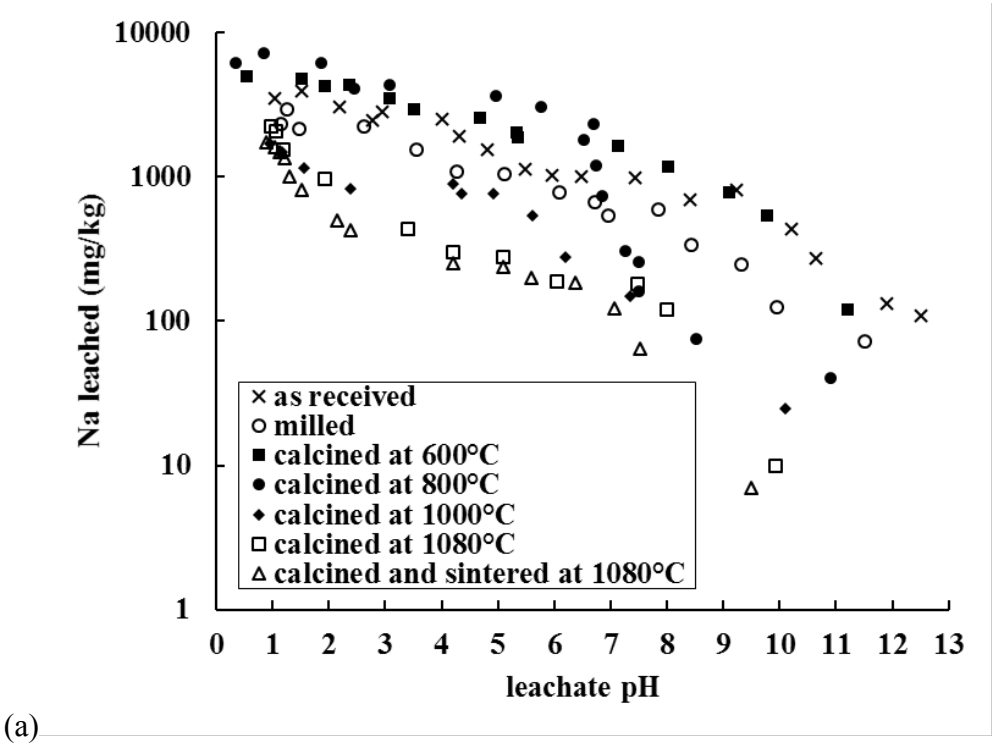

(a)

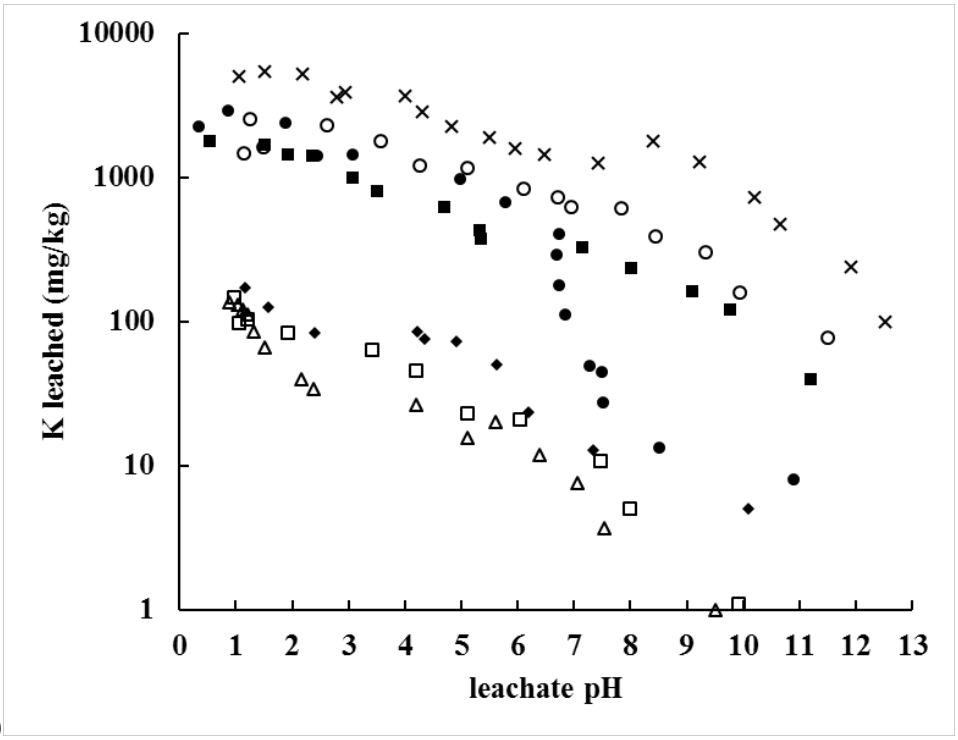

(b)

Figure 5.13: Leaching data for (a) Na and (b) K as a function of leachate pH for the as-received dry discharged fine IBA dust, milled 80 wt.% dry discharged fine IBA dust: 20 wt.% glass,

calcined milled powders at 600 °C, 800 °C, 1000 °C, 1080 °C and calcined milled powders at 1080 °C and sintered at 1080 °C.

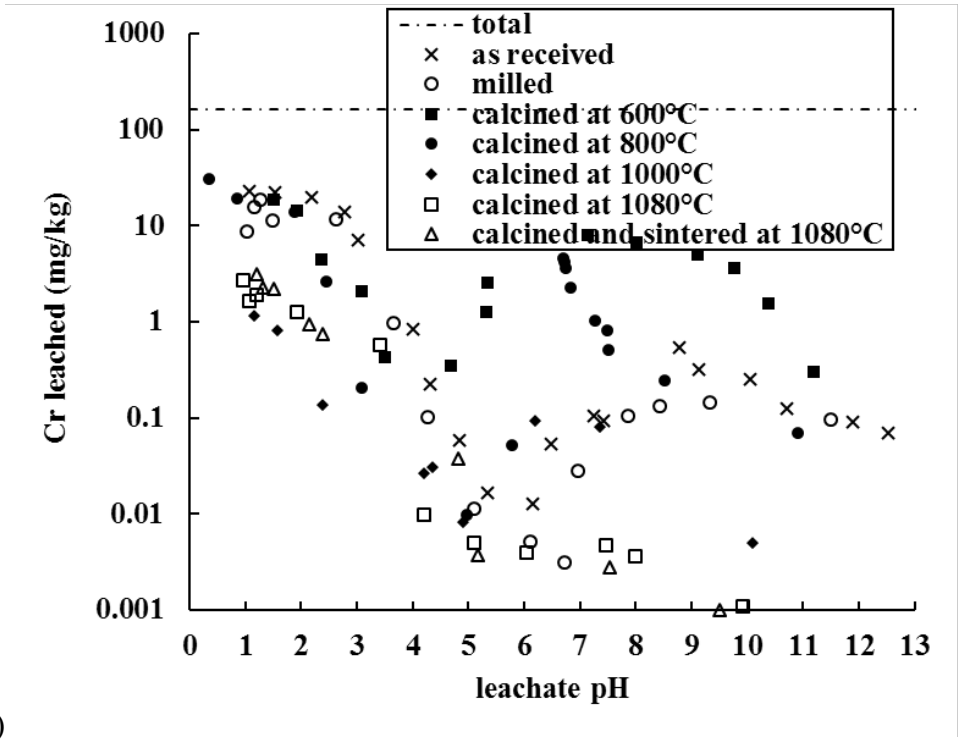

(a)

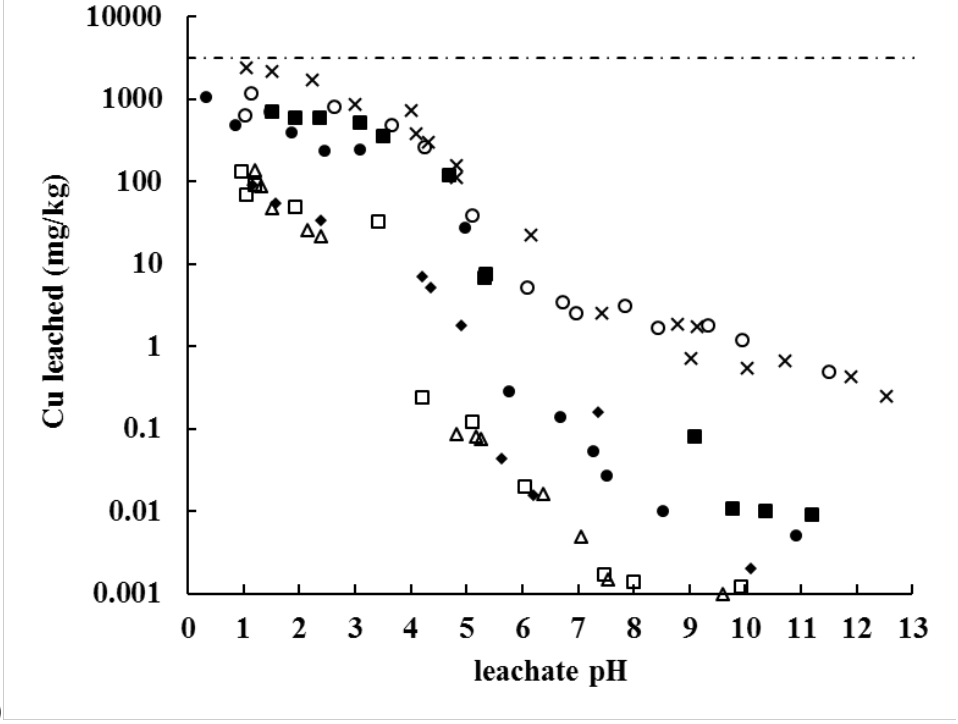

(b)

Figure 5.14: Leaching data for (a) Cr and (b) Cu as a function of leachate pH for the as-received dry discharged fine IBA dust, milled 80 wt.% dry discharged fine IBA dust: 20 wt.% glass, calcined milled powders at 600 °C, 800 °C, 1000 °C, 1080 °C and calcined milled powders at 1080 °C and sintered at 1080 °C.

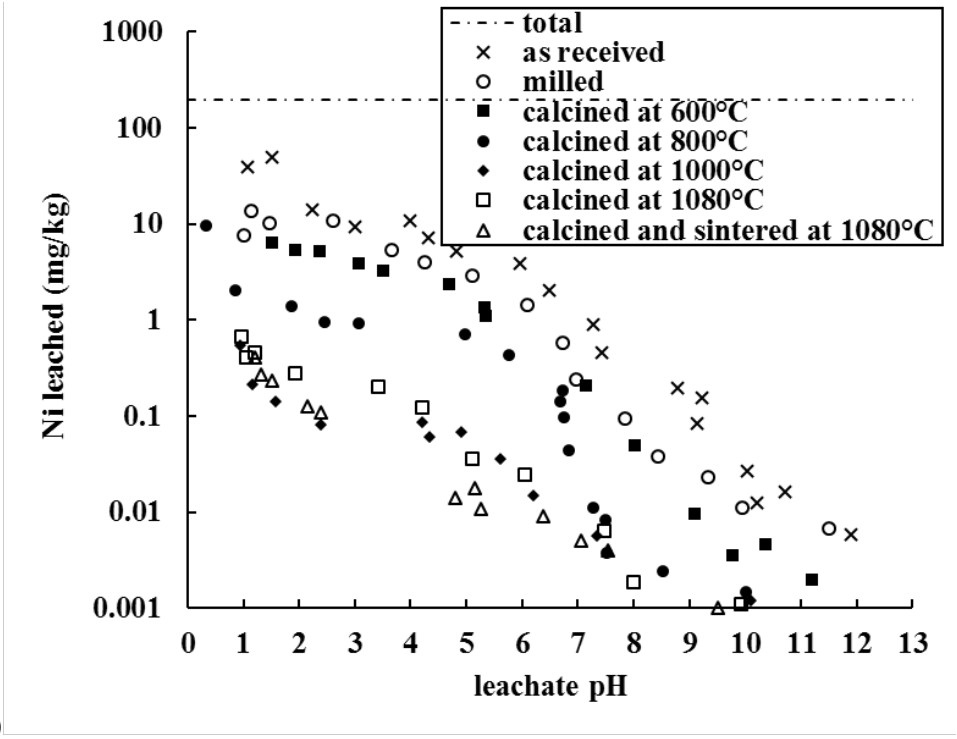

(a)

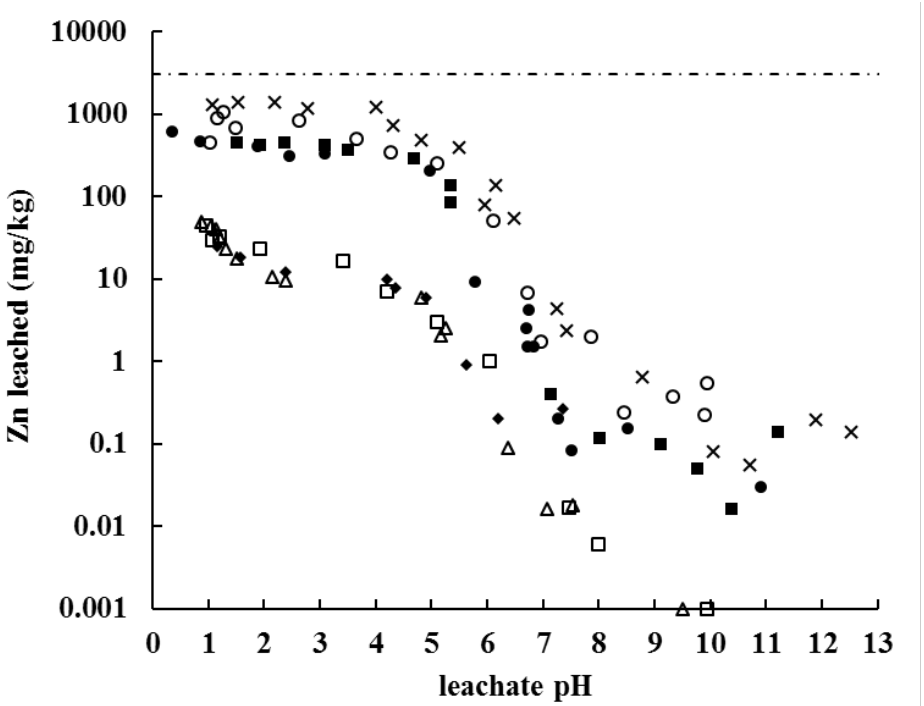

(b)

Figure 5.15: Leaching data for (a) Ni and (b) Zn as a function of leachate pH for the as-received dry discharged fine IBA dust, milled 80 wt.% dry discharged fine IBA dust: 20 wt.% glass, calcined milled powders at 600 °C, 800 °C, 1000 °C, 1080 °C and calcined milled powders at 1080 °C and sintered at 1080 °C.

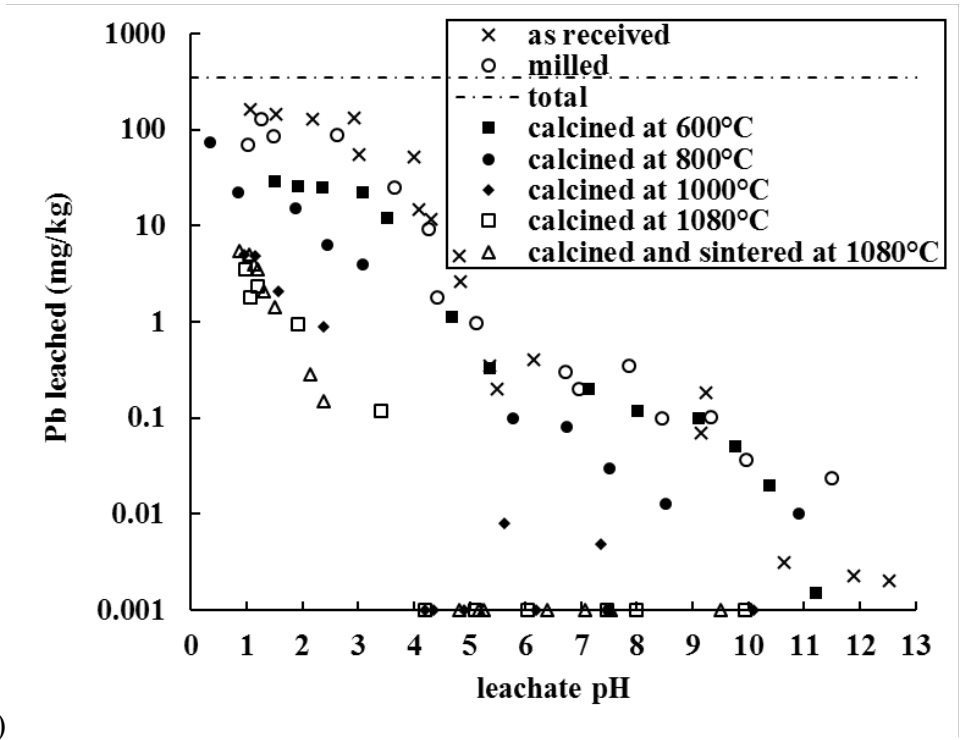

(a)

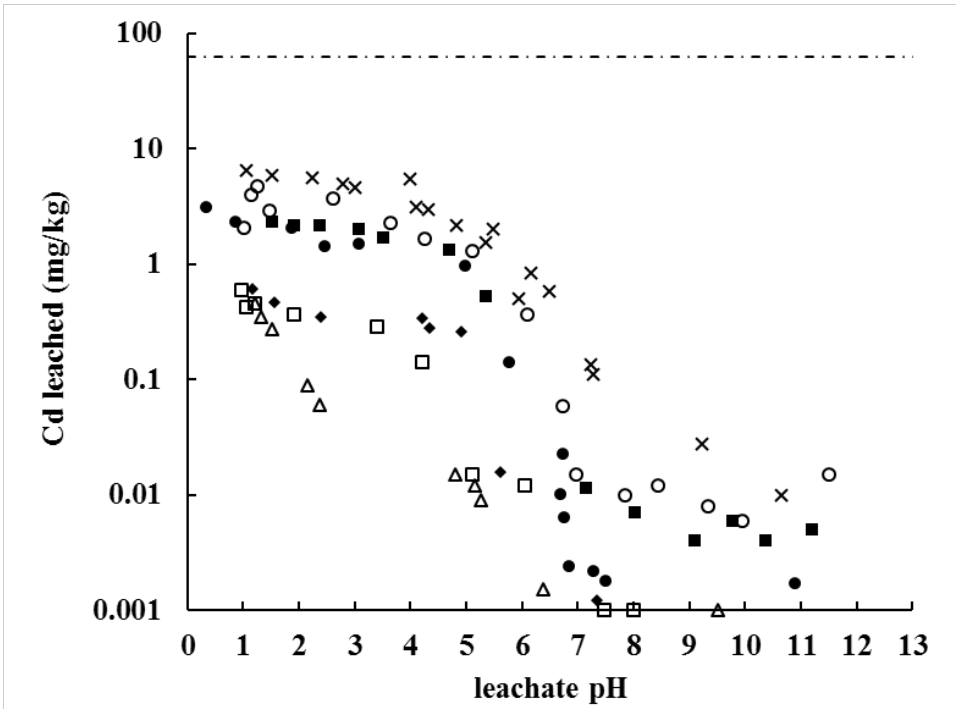

(b)

Figure 5.16: Leaching data for (a) Pb and (b) Cd as a function of leachate pH for the as-received dry discharged fine IBA dust, milled 80 wt.% dry discharged fine IBA dust: 20 wt.% glass, calcined milled powders at 600 °C, 800 °C, 1000 °C, 1080 °C and calcined milled powders at 1080 °C and sintered at 1080 °C

Table 5.2: Effect of processing on leaching of selected heavy metals under aggressive leachate conditions (pH 3).The total concentration of heavy metals in the as received wet discharged IBA were obtained by ICP-AES. Leaching data are reported for the as-received dry discharged fine IBA dust, calcined milled powder containing 80 wt.% dry discharged fine IBA dust: 20 wt.% glass at 1080 °C and calcined milled powders at 1080 °C and sintered at 1080 °C. The % reduction in leaching of heavy metals after calcining at 1080 °C and after calcining and sintering at 1080 °C is also reported and presented with bold letters in the corresponding columns.

			Amount leached (leachate pH 3)			
	Concentration in dry discharged fine IBA dust	**As-received dry discharged fine IBA dust**	**Powder calcined at 1080 °C**		**Powder calcined at 1080 °C and sintered at 1080 °C**	
	mg/kg	**mg/kg**	**mg/kg**	**% reduction**	**mg/kg**	**% reduction**
Cr	163	17.9	0.75	**95.8**	0.6	**96.7**
Cu	3200	887.6	21.8	**97.5**	19.5	**97.8**
Ni	197.5	9.3	0.13	**98.6**	0.05	**99.5**
Cd	63	4.6	0.16	**96.5**	0.09	**98.1**
Zn	3100	1139.4	9.4	**99.2**	8.2	**99.3**
Pb	350	133.1	0.15	**99.9**	0.07	**99.7**

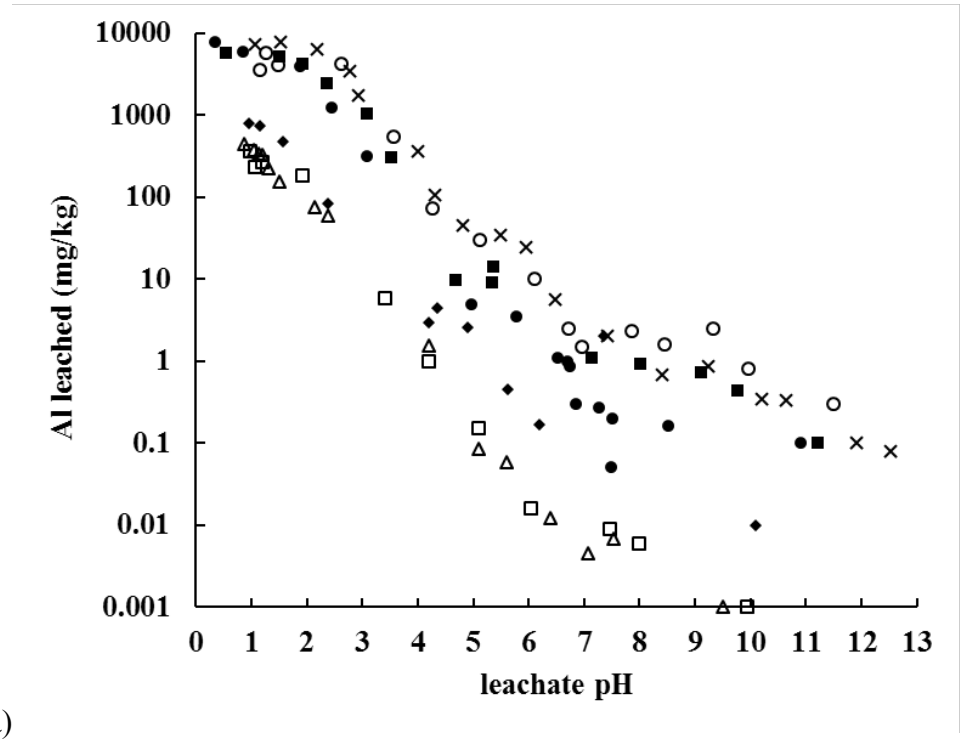

(a)

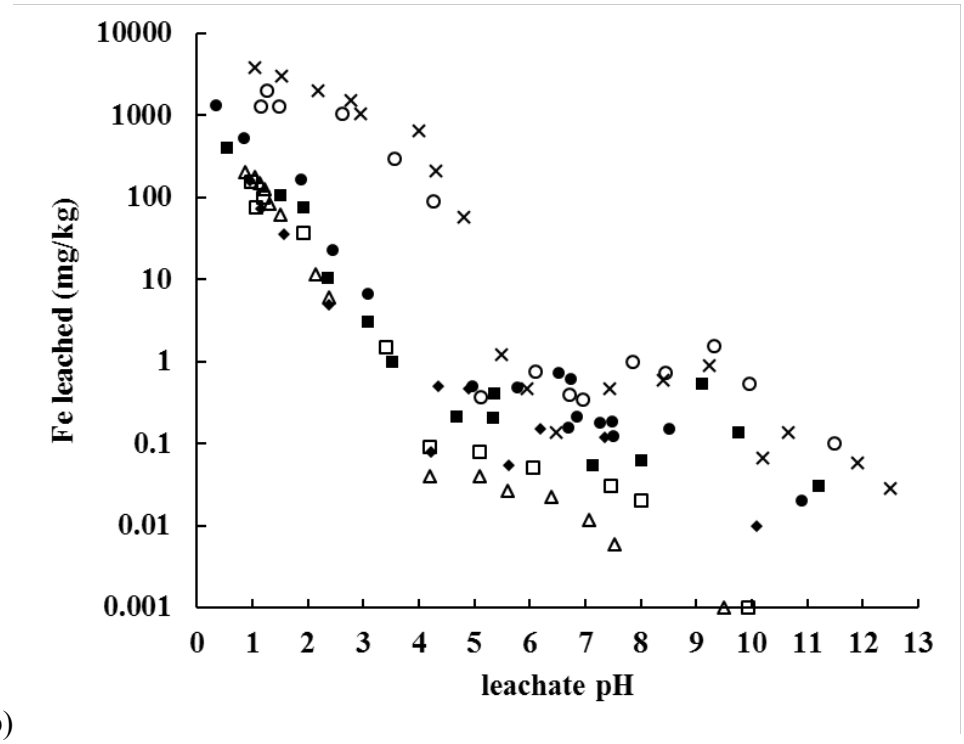

(b)

Figure 5.17: Leaching data for (a) Al and (b) Fe as a function of leachate pH for the as-received dry discharged fine IBA dust, milled 80 wt.% dry discharged fine IBA dust: 20 wt.% glass, calcined milled powders at 600 °C, 800 °C, 1000 °C, 1080 °C and calcined milled powders at 1080 °C and sintered at 1080 °C.

5.4.10 Fate of sulphates and chlorides

Sulphate and chloride concentrations in the as-received dry discharged fine IBA dust, the milled material, the calcined at 1080 °C powder and the optimum ceramic are presented in Table 5.3.

There is a 27% by weight reduction in the sulphate concentration after mixing 80 wt. % dry discharged fine IBA dust and 20 wt. % glass and wet milling the mixture for 24 hours. This is believed to be due to the presence of soluble sulphate compounds, such as anhydrite ($CaSO_4$), in the as-received material, which are removed after milling. Calcining the powder at 1080 °C produces a material that exhibits a significant reduction in the sulphate concentration by approximately 95% by weight and the optimum ceramic indicates a 96% by weight reduction. This is associated with the evaporation of alkali metal sulphates at temperatures above 1000 °C (Chimenos et al., 1999; Bethanis et al., 2004).

Similar reduction was observed for the chloride concentration during processing. After milling the chloride concentration was reduced by approximately 68% by weight. Chlorides are typically present as soluble salts in the as-received dry discharged fine IBA dust (Kirby and Rimstidt, 1994; Vehlow et al., 2006) that dissolve easily when the material contacts water. Chloride concentration is further reduced by 95% and 96% by weight for the calcined at 1080 °C powder and the optimum ceramic produced, accordingly. This is associated with the evaporation of metal chlorides at temperatures normally above 900 °C, as suggested by other researchers (Belevi and Langmeier, 2000; Sorensen et al., 2001).

Table 5.3: Effect of processing on sulphate and chloride concentration. Data are reported for the as-received dry discharged fine IBA dust, milled 80 wt.% dry discharged fine IBA dust: 20 wt.% glass, calcined milled powder at 1080 °C and calcined milled powders at 1080 °C and sintered at 1080 °C. Chloride and sulphate concentration is reduced by 96% by weight for the calcined at 1080 °C powder and sintered at 1080 °C ceramic.

	Sulphate (weight %)	**Chloride (weight %)**
As-received fine IBA	2.19	1.42
Wet milled 80wt.% dry discharged fine IBA dust: 20wt.% glass	1.58	0.45
Calcined at 1080 °C milled powder	0.12	0.07
Calcined at 1080 °C milled powder and sintered at 1080 °C	0.08	0.06

5.5 CONCLUSIONS

The effect of calcining the milled powders and the effect of sintering materials produced from these powders have been investigated. The aim was to produce ceramics from the dry discharged fine IBA dust with minimum linear shrinkage, since high shrinkage is associated with warping and deformation after sintering, and also ceramic materials with high density and hardness and negligible water absorption.

It has been found that the fine fraction of dry-discharged IBA dust can be processed to produce pyroxene group ceramics. Optimum processing involve mixing 80 wt. % dry discharged fine IBA dust with 20 wt.% glass which is added to aid liquid phase sintering, wet ball milling to reduce the particle size distribution and homogenise the mix, calcining at 1080 °C to transform the crystalline phases present and enable volatilisation of gases responsible for pore-forming. The produced powder was uniaxial pressed and sintered at 1080 °C to produce a high quality ceramic with improved properties than the ceramic produced with uncalcined powders and the commercial terracotta ceramics. It has been found that calcining significantly improves the pressing and sintering behaviour of dry discharged fine IBA dust. Optimum sintered ceramics exhibit low firing shrinkage (< 7%), high densities (> 2.7 g/cm^3), negligible water absorption and improved mechanical properties. Quartz and calcite are the major crystalline phases present in the as-received dry discharged fine IBA dust. The pyroxene group minerals, diopside ($CaMgSi_2O_6$), clinoenstatite ($MgSiO_3$) and wollastonite ($CaSiO_3$) are the major crystalline phases present in calcined powders and ceramics sintered at 1080 °C.

Calcining and sintering at optimum processing temperatures significantly reduces the ANC compared to the as-received dry discharged fine IBA dust, associated with the inertization of the metals present in the as-received dry discharged fine IBA dust and the incorporation and encapsulation within the new less soluble crystalline phases formed. Calcining above 1000 °C resulted in a significant and gradual reduction in all metals examined under all pH conditions investigated compared to the as-received material. Minimum metals leached concentration was observed for the calcined at 1080 °C powder and the optimum ceramic derived. However, calcining at 600 and 800 °C indicated similar metals leached concentration for most metals examined under aggressive pH conditions, compared to the as-received dry discharged fine IBA dust. This was reduced at normal pH conditions due to the low temperature applied, which

results in the partial activation of the decomposition reactions. However, Cr leached concentration exhibited higher concentration than the as-received materials, associated with the transformation of the relatively soluble trivalent state of Cr into the readily soluble and more mobile hexavalent form.

The research presented in this chapter demonstrates the potential to beneficially up-cycle the fine fraction of dry-discharged IBA dust into a raw material suitable for the production of ceramic tiles that have potential for use in a range of industrial applications. However, the process envelopes need to be identified in order to further optimise the process, and determine the interrelations between the processing conditions and the desired properties of the produced ceramics. For this reason, Response Surface Methodology and the Design Expert software have been used.

CHAPTER 6 PROCESS ENVELOPES

6.1 INTRODUCTION

In the previous chapter the effect of calcining the dry discharged fine IBA dust: glass powders prior sintering have been investigated. In addition, the effect of sintering samples produced with calcining powders at different temperatures have been examined. The processing involves mixing dry discharged fine IBA dust with glass to promote liquid phase sintering, milling to change the particle size distribution and calcining to transform the crystalline phases present and allow pre-sintering volatilisation of gas generating phases. This significantly alters the pressing and sintering behaviour of dry discharged fine IBA dust. Sintering dry discharged fine IBA dust powders without calcining results in excessive shrinkage and samples tend to deform during firing, making the production of tiles difficult with volatilisation reactions producing excessive porosity. Calcined dry discharged fine IBA dust: glass powders compact to give higher green densities, have low firing shrinkage (~5%) and produce sintered ceramics with high densities (2.78 g/cm^3), negligible water absorption and high Vickers micro hardness (4.5 GPa). While quartz and calcite are major crystalline phases present in as-received dry discharged fine IBA dust, diopside ($CaMgSi_2O_6$), clinoenstatite ($MgSiO_3$) and andradite ($Ca_3Fe_2Si_3O_{12}$) are the pyroxene group crystalline phase present in calcined powders and ceramics sintered at 1080 °C. However, due to the strong interrelations observed between density, water absorption and linear shrinkage a further investigation to the factors affecting the process and subsequently affecting the properties of the produced materials is needed. These factors have been identified in the previous chapters and include the glass addition, sintering temperature and calcining temperature.

Response Surface Methodology (RSM) is a statistical method that describes the relationships between several input variables and one or more response properties, and allows the achievement of an optimum point (Box and Wilson, 1951). RSM has been used to optimise the production of lightweight aggregates from mixtures of fly ash, bentonite and glass powder (Kockal and Ozturan, 2011) and waste glass and clay (Velis et al., 2014), to design, model and predict the physical and engineering properties of ceramics derived from mixes of coal fly ash, lime and water (Nardi et al., 2004) and kaolin processing and granite sawing wastes (Menezes et

al., 2008).It has also been used to identify the parameters influencing manufacturing processes and properties of aggregates using coal pond ash (Vasugi and Ramamurthy, 2014). In this project, RSM has been applied using the software Design-Expert 9. The input variables are glass addition, calcining temperature, sintering temperature, and the response properties are density, water absorption and linear shrinkage as shown in Figure 6.1.

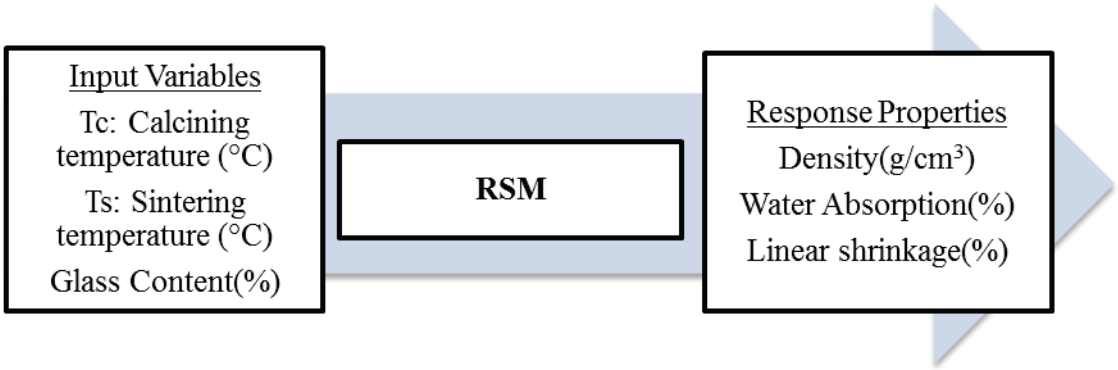

Figure 6.1: Input variables and response (output) properties of the model developed. RSM refers to Response Surface Methodology

6.2 OBJECTIVES

The aim of this chapter is to identify the optimum points for each mixture composition by the use of Response Surface Methodology. In order to do so, the Design Expert 9 software is used, which has the ability to identify optimum points in a process with defined inputs. For the purpose of this research glass addition, calcining and sintering temperature has been defined as inputs to the software, and the corresponding outputs were derived from the experimental work reported in Chapters 4 and 5. The outputs include the density, linear shrinkage and water absorption of the samples.

6.3 ANALYSIS METHODS

RSM usually involves four steps: model fitting, validation of the model, response surface and optimization.

ANNOVA and Model fitting

To check the adequacy of the model polynomials i.e. how well the model fits the data, statistical rules of Analysis of Variance (ANOVA) are used: p-value describes the importance of the effect that the terms in the polynomial have on the response. A very small value (less than 0.05) indicates a significant effect on the response, and therefore the adequacy of the model. R-squared is the coefficient of determination, which describes from 0 to 1 the agreement between the calculated and the observed results. Diagnostics plots such as the predicted versus actual value plot are also used (Banks, 1998; Myers et al., 2009).

The best fitting model as identified by ANOVA was selected and validated by a sequence of steps (Cook, 1977; Box and Cox, 1982; Banks, 1998; Myers et al., 2009):

1. Selecting the highest ordered model from all the potentially fitting models meeting the criteria of: (i) P-value <0.0001 and >0.8 predicted coefficient of determination R^2 pred, (ii) absence of lack-of-fit, (iii) reasonable agreement between predicted and adjusted R^2 (R^2 pred - R^2 adj <0.2), and iv) adequate model precision, which measures the signal to noise ratio. It establishes how well the model can navigate through the design space and predicts the response. A ratio greater than 4 is desirable;

2. Terms (mixture components, process factors or any non-linear blending and curvature) not significant at $\alpha = 0.1$ were removed from the model. The relatively high α was chosen to avoid rejecting potentially significant terms too early in the model selection process. In all cases hierarchy was respected, i.e., all lower level terms were retained, irrespective of significance;

3. The detailed ANOVA statistics were computed for the model and evaluated;

4. The ANOVA underlying assumptions were checked against a comprehensive series of diagnostic plots: plot of internally studentized residuals (ISR), residuals vs. predicted values, residuals vs. runs, predicted vs. actually measured values, ISR for each factor. The data points should be evenly split by a 45-degree line;

5. Box-Cox transformation .Where a transformation was beneficial, the best Lamda (λ) value was computed, the transformation applied and model fitting exercise repeated;

6. The influence of each experimental run on the model was evaluated by plotting relevant statistics (difference in fits - DFFITs, difference in Betta coefficients - DFBETAS, leverage vs. runs, Cook's distance). Where potential model outlier runs were identified and a special case was established, these were removed from the model and the model fitting exercise was repeated.

The data for the input variables were derived from the experimental work presented in chapters 4 and 5. Design Expert software applies polynomial models to the input variables (linear, quadratic and cubic) based on statistical criteria, as shown in Table 6.1.

Table 6.1: Main statistical rules to evaluate model adequacy.p-value describes the importance of the effect that the terms in the polynomial have on the response. R-squared is the coefficient of determination, which describes from 0 to 1 the agreement between the calculated and the observed results (Montgomery, 2008).

Parameter	**Criteria for validation**
p-value of the terms in the model	<0.0001 model is significant
Adj.R^2 and Pred. R^2	(Adj.R^2 - Pred. R^2)< 0.2

Model Validation

The validation was undertaken to establish if the models that were fitted for each response data were accurately able to predict a response. It is done by comparing results of additional experiments with the prediction responses of the software (using point prediction feature). Experiments in the lab and point prediction on the software are conducted. Residuals below 10% indicate that the model is valid, and can now be used to draw response surfaces and optimize the process.

Response surface

A contour response graph is plotted. It depicts the change of a response with the input variables, thus identifying the process envelopes.

Optimization

The optimization module searches for a combination of input variables that simultaneously satisfy the criteria placed on each of the response. In this study we are looking for the input variables that will maximize the density and minimize the linear shrinkage and water absorption values. These were defined as density typically > 2.1 $g.cm^{-3}$, linear shrinkage< 8% and water absorption < 2%.

Input and output variables

The glass addition, the calcining and the sintering temperature have been defined as input to the system. Glass addition ranges from 0 to 30 wt. %, calcining temperature is between 600 and 1200 °C and the sintering temperature is between 1020 and 1100 °C. The output variables included density, linear shrinkage and water absorption of the produced ceramics. Optical microscopy was used to characterise the microstructure of the optimum samples for each mixture composition.

6.4 RESULTS AND DISCUSSION

6.4.1 RSM Model Fitting to ceramics properties

The p-values and the adjusted and predicted R^2 for the cubic models of the properties developed with the use of DesignExpert are summarized in Table 6.2.

Table 6.2: Statistical values of models used for density, linear shrinkage and water absorption of sintered ceramics

	p-value	Adjusted R^2	Predicted R^2
Density	< 0.0001	0.8429	0.7709
Linear shrinkage	< 0.0001	0.8953	0.8427
Water Absorption	< 0.0001	0.8869	0.7662

The ANOVA values derived from the software are presented in Table 6.3.

Table 6.3: Analysis of variance for density, linear shrinkage and water absorption of sintered ceramics. Df refers to degrees of freedom, which is the number of values in the final calculation of the response properties that are free to vary. F ratio is the ratio of two mean square values. p-value describes the importance of the effect that the terms in the polynomial have on the response.

	Sum of squares	**df**	**Mean square**	**F-Value**	**p-value**	**Prob >F**
Density	2.43	19	0.13	19.35	<0.0001	significant
Linear shrinkage	628.82	19	33.10	30.27	<0.0001	significant
Water absorption	2055.05	12	170.92	28.12	<0.0001	significant

Statistically significant models were fitted for all the dependent variables under examination. All the ANOVA underlying assumptions and model selection criteria were met. A logarithmic (base10) Box-Cox transformation was applied to all properties, with the exception of ρ_{rd} (no transformation), to best meet the ANOVA prerequisites of normality and homogeneity of variance. Thus, the predicted values refer to the median, rather than the arithmetic mean of the properties modeled. The calcining temperature is the critical factor affecting the density and linear shrinkage of sintered ceramics. This demonstrates that the density increases and the linear shrinkage decreases as the calcining temperature increases. Glass addition and sintering temperature have a much less significant influence in the density and linear shrinkage of the produced samples, however these are the most significant factors in determining the water absorption of the ceramic samples.

The adjusted R^2 was > 0.85 for all input-output functions, indicating strong correlations between the variables examined. The wide range of density and water absorption properties achieved suggests this system can deliver products customized for a wider range of ceramic applications. At each temperature the highest density is always observed for mixes with the

highest glass content, suggesting that glass addition promotes liquid phase sintering, as anticipated.

6.4.2 System boundaries

The response surface methodology contour graphs for the density data for each mixture composition are presented in Figure 6.2. Ceramics samples exhibiting high density, low linear shrinkage and low water absorption resulted from sintering and calcining at high temperatures for all mixture compositions.

The highest density was always observed for mixes with the highest glass content (30 wt. %) associated with the effect of glass that aids liquid phase sintering, as described in chapters 4 and 5. Mixes containing 30 wt. % glass and sintered between 1020 and 1080 °C, exhibited densities > 2.1 $g.cm^{-3}$ for all calcining temperatures examined, which is within the desirable specification. Sintering between 1040 and 1080 °C mixes containing 20 wt.% glass for all calcining temperatures, produced ceramic samples with densities > 2.1 $g \cdot cm^{-3}$. For mixes containing 10 wt.% glass, calcining above 800 °C and sintering between 1040 and 1100 °C produced samples within the defined limits, while mixture compositions containing no glass achieved densities> 2.1 $g \cdot cm^{-3}$ when calcined above 850 °C and sintered between 1040 and 1080 °C. Sintering temperature and glass content are significant ($p < 10^{-7}$) in explaining the most of the variation in ρ_{rd}. Calcining temperature is less significant ($p< 10^{-5}$) in determining ρ_{rd}.

The contour graphs of linear shrinkage of samples produced with varying glass addition are presented in Figure 6.3. Linear shrinkage typically decreases with calcining temperature and increases with sintering temperature. Calcining at 700 °C and sintering at 1020 °C mixes containing 30 wt. % glass, produced ceramic samples with linear shrinkage of about 8%, which gradually decreases with increasing calcining temperature. Samples with 30 wt. % glass calcined above 1100 °C exhibited linear shrinkage < 8% for all sintering temperatures. Similarly, mixture compositions containing 20 wt.% glass calcined above ~1100 °C indicated linear shrinkage < 8% for all sintering temperatures. The calcining temperature limit to achieve desired linear shrinkage values decreases with glass addition and samples containing 10 wt. % or no glass indicated calcining temperature above 1050 and 1000 °C for all sintering temperatures, accordingly. Calcining temperature is the most significant factor in determining the linear shrinkage ($p< 10^{-7}$). Sintering temperature and glass addition are less significant ($p < 10^{-5}$).

The response surface contour graphs of the Water Absorption obtained from samples containing different amount of glass is presented in Figure 6.4. Mixes containing 20 and 30 wt. % glass exhibited water absorption within the desired limits when sintered above 1060 °C for all calcining temperatures. Mixture compositions of 10 wt. % and no glass indicated water absorption within the defined limits when sintered and calcined at temperatures >1100 °C. Sintering temperature and glass content are both significant ($p < 10^{-7}$) in determining water absorption. Calcining temperature is much less significant ($p < 10^{-4}$).

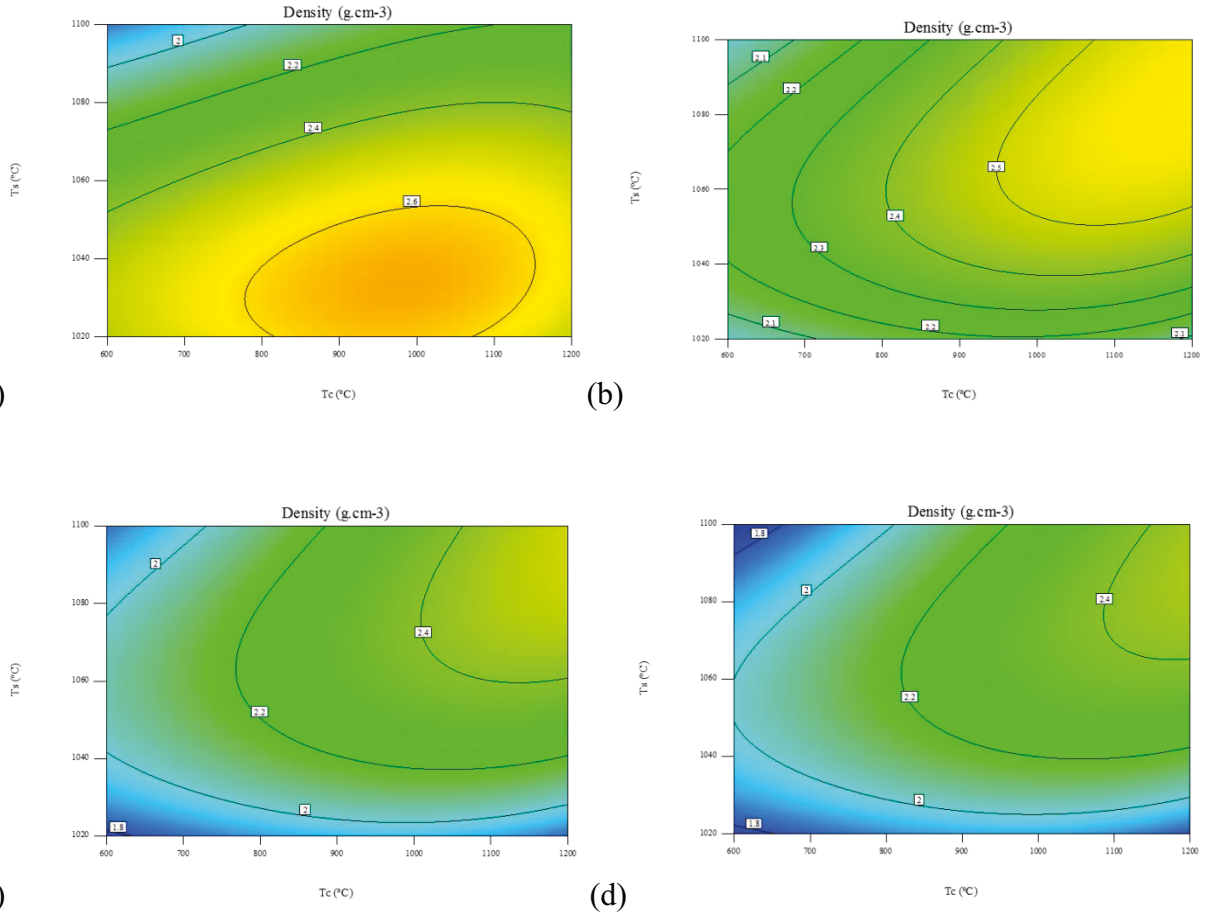

Figure 6.2: Response Surface Methodology for density of dry discharged fine IBA dust: glass samples containing: (a) 30 wt. %, (b) 20 wt. %, (c) 10 wt. % and (d) no glass. Yellow to orange colour corresponds to densities higher than 2.5 $g.cm^{-3}$. Green colour corresponds to densities between 2.1 and 2.5 $g.cm^{-3}$. Light blue to blue corresponds to densities lower than 2.1 $g.cm^{-3}$.

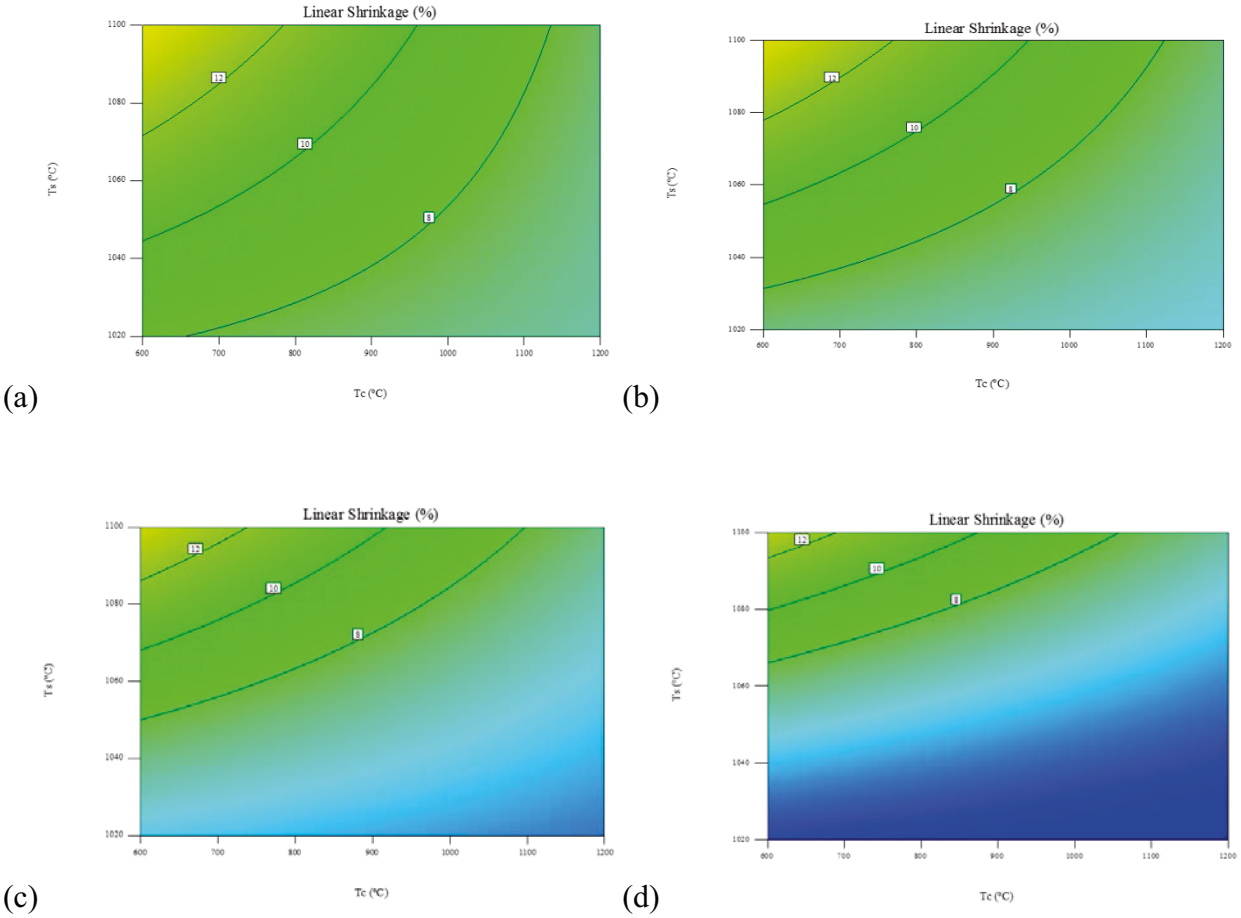

(a) (b)

(c) (d)

Figure 6.3: Response Surface Methodology for linear shrinkage of dry discharged fine IBA dust: glass samples containing: (a) 30 wt. %, (b) 20 wt. %, (c) 10 wt. % and (d) no glass. Green colour corresponds to linear shrinkage higher than 6 %. Light blue to blue colour corresponds to linear shrinkage lower than 6%.

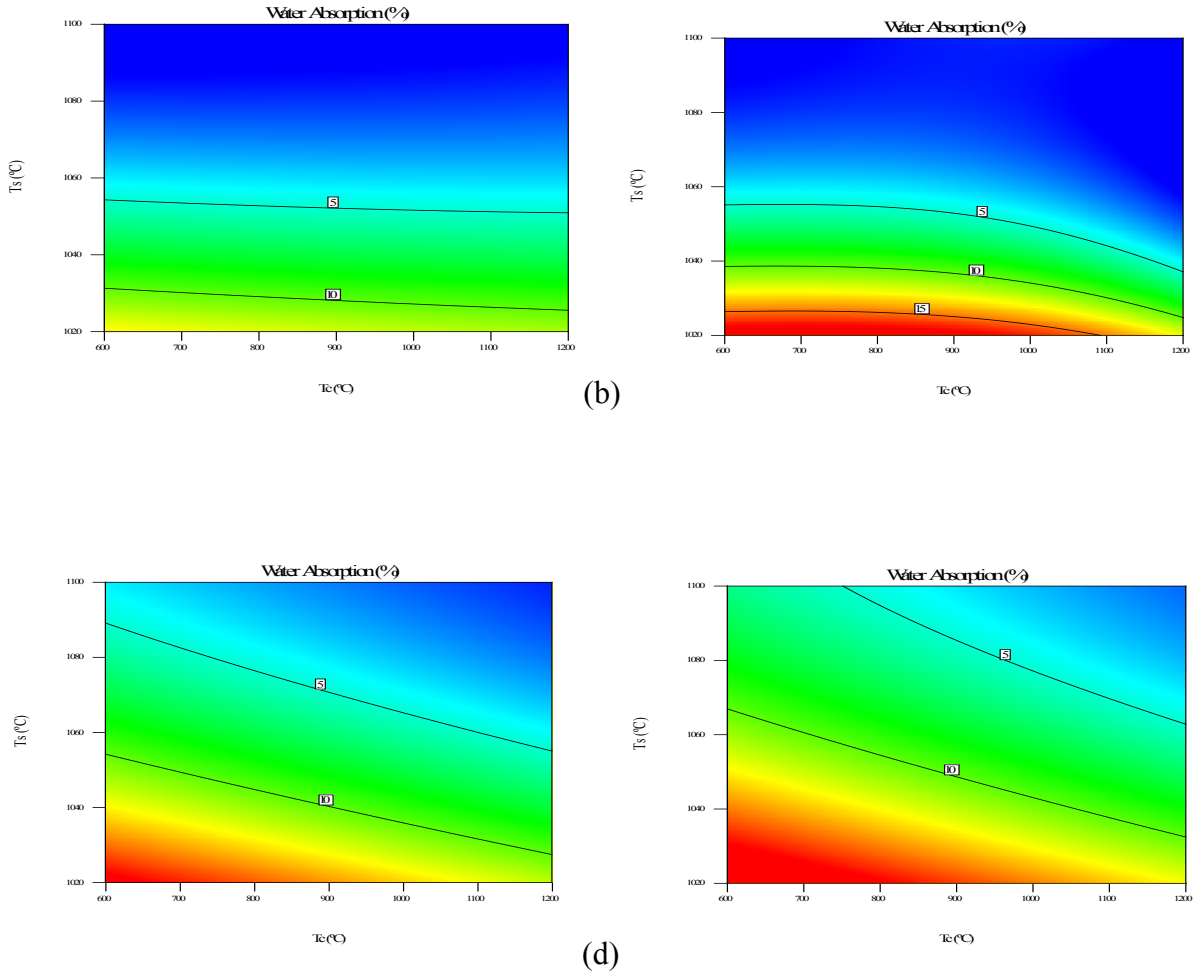

Figure 6.4: Response Surface Methodology for water absorption of dry discharged fine IBA dust: glass samples containing: (a) 30 wt. %, (b) 20 wt. %, (c) 10 wt. % and (d) no glass. Light blue to blue colour corresponds to water absorption lower than 5%. Green colour corresponds to water absorption between 5 and 12 %. Yellow colour corresponds to water absorption between 12 and 14%. Red colour corresponds to water absorption higher than 14%.

6.4.3 Optimal points and microstructural characterization

Solutions for optimal ceramic production as identified by the optimization algorithms are shown in Table 6.4.

Table 6.4: Optimum processing conditions to achieve maximum density, minimal water absorption and linear shrinkage of mixture compositions containing 70 wt. % to 100 wt. % dry discharged fine IBA dust and glass.Data for the clay ceramics are reported in the last row. Tc: calcining temperature; Ts: sintering Temperature.

Dry discharged fine IBA dust (%)	Tc (°C)	Ts (°C)	Density (g/cm^3)	Water absorption (%)	Linear Shrinkage (%)
100	**1200**	**1130**	**2.4**	**0.9**	**5.1**
90	**1100**	**1100**	**2.5**	**0.1**	**5.3**
80	**1080**	**1080**	**2.7**	**0.0**	**5.4**
70	**1060**	**1040**	**2.7**	**0.0**	**5.5**
Clay Ceramics			**2.1-2.3**	**0.0-5.0**	**7.0-14.0**

The results were produced and confirmed in the laboratory. For mixture compositions containing 100 wt.% dry discharged fine IBA dust, optimum calcining and sintering temperatures were identified as 1200 and 1130 °C respectively. For powders containing 90 wt. % dry discharged fine IBA dust optimum firing conditions were 1100 °C for both calcining and sintering temperatures. For mixture compositions containing 20 wt.% glass the optimum conditions were 1080 °C for both temperatures and for mixes containing 30 wt.% glass the optimum temperatures were identified at 1060 °C for the calcining and 1040 °C for the sintering temperature. Optical micrographs of polished surfaces of sintered ceramics prepared at optimum

firing conditions are shown in Figure 6.5. All samples produced contain small pores but ceramics produced with 10 wt. % and no glass addition contain larger pores consistent with lower density. Mixture compositions containing 20 wt. % and 30 wt. % glass exhibited the denser microstructure and improved appearance than mixes with 10 wt. % or no glass. The densities of samples produced with 20 wt. % and 30 wt. % glass were similar at ~2.7 g/cm^3 and these samples had a linear shrinkage of < 7%, which is lower than the shrinkage of typical terracotta ceramics. Optimum calcining temperatures for the processing of milled powders containing 20 wt. % and 30wt. % glass was reduced by 20 and 40 °C compared to samples prepared with 10 wt. % glass, respectively. The calcining temperature is 120 to 140 °C lower for samples containing 20 and 30 wt. % glass, accordingly, compared to ceramics produced with no glass addition. The research, however, deals with the resource efficiency of the fine IBA, therefore, the 20 wt. % glass addition was chosen as the optimum mixture composition. These were reaffirmed in the laboratory and the results were in accordance with the Design Expert values. The mixture composition containing 20 and 30 wt. % glass were the optimum, since these exhibited the highest density, lowest water absorption and linear shrinkage within the acceptable limits.

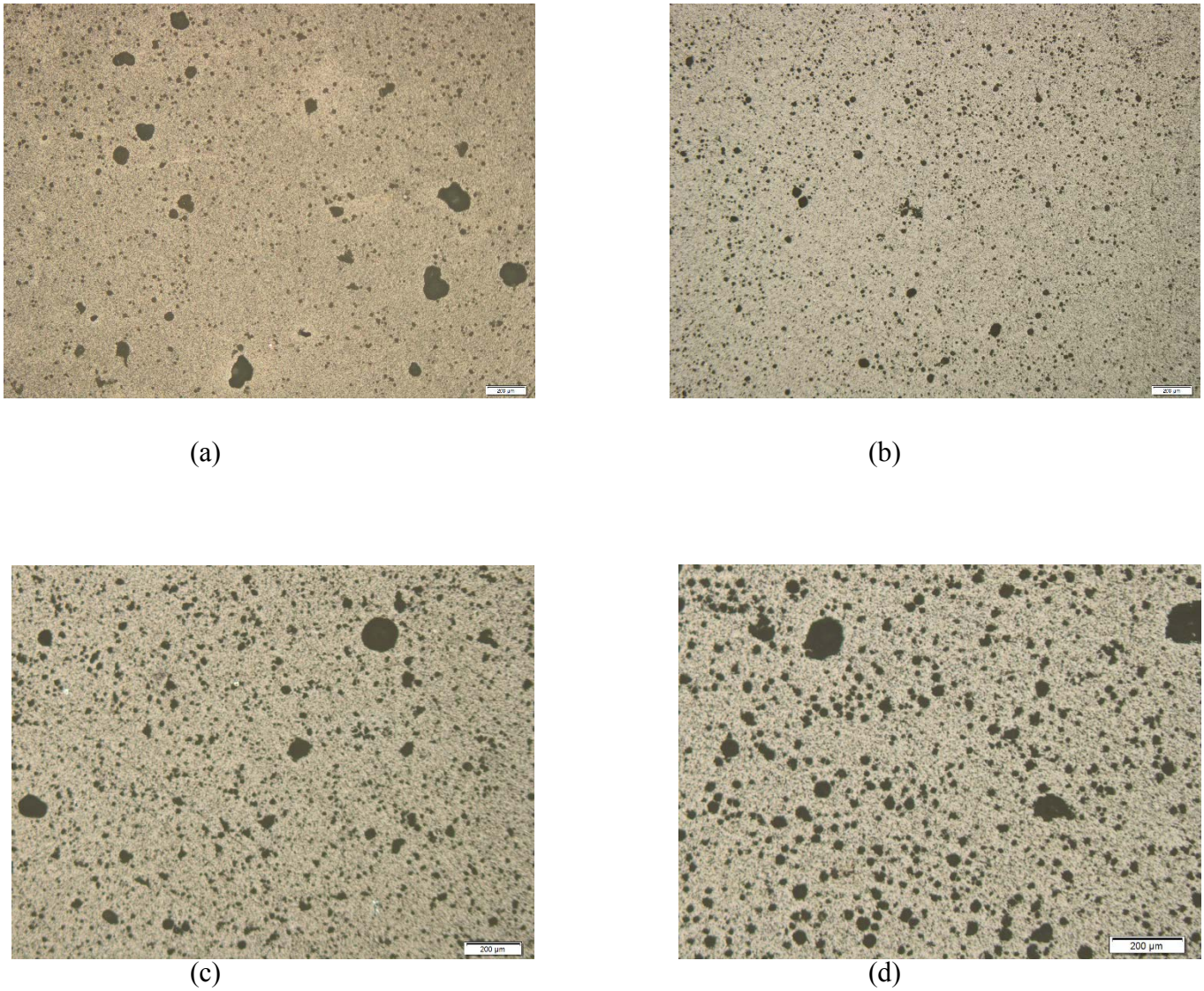

(a) (b)

(c) (d)

Figure 6.5: Optical microscope images of ceramic samples containing dry discharged fine IBA dust and (a) 30 wt. %, (b) 20 wt. %, (c) 10 wt. % and (d) no glass and produced with optimum conditions.Ceramic samples containing 30 and 20 wt. % (a and b, respectively) exhibited the denser microstructure and improved appearance than mixes with 10 wt. % or no glass (c and d, respectively). The research, however, deals with the resource efficiency of the dry discharged

fine IBA dust, therefore, the 20 wt. % glass addition was chosen as the optimum mixture composition.

6.5 CONCLUSIONS

The boundaries of the process developed and the optimum processing parameters were identified. Composition and processing were optimized using response surface methodology (RSM) modelling, and specifically (i) a combined process-mixture dual RSM, and (ii) multi-objective optimization functions. RSM is a statistical design of experiments methodology, increasingly used to develop and optimize products and model processes within the environmental sciences and engineering. It has not previously been used for ceramics production from the fine fraction of incinerator bottom ash. RSM is particularly useful when properties depend on variables such as composition and sintering temperature, for which the under- lying physical mechanisms are unclear, and where complex nonlinear interdependencies exist. In addition, dual RSM can produce a statistically validated predictive empirical model able to optimize both the average (target) values and the variability. Concurrent multiple factor optimization is applied here, benefiting from advances in desirability optimization methodology (DOM).

For the purposes of this research, the Design Expert 9.0 software was used. Input variables include glass addition, sintering and calcining temperature and response variables involve density, linear shrinkage and water absorption. These values were derived from the experimental work and plugged into the software in order to identify the boundaries of the system for which input variables the desired properties can be achieved. The sintering temperature ranged from 1020 to 1100 °C and the calcining temperature between 600 and 1200 °C. Glass addition was between 30 wt. % and no glass. The DOM was set according to the properties of Terracotta ceramics. Therefore, density was set at > 2.1 $g.cm^{-3}$, linear shrinkage <8% and water absorption < 2%.

The results indicated that calcining temperature is the most significant process parameter affecting the linear shrinkage of sintered ceramics. Density and water absorption is mainly controlled by the sintering temperature and the glass addition. Mixes containing 20 and 30 wt. %

glass exhibited densities > 2.1 $g.cm^{-3}$ for all calcining temperatures examined, when sintered between 1040 to 1080 °C and 1020 to 1080 °C, respectively. Mixture compositions containing 10 wt. % or no glass, calcined above 800 °C and sintered between 1040 and 1100 °C and 1040 and 1080 °C, accordingly, produced samples within the defined limits.

Linear shrinkage typically decreases with calcining temperature and increases with sintering temperature. Samples containing 20 and 30 wt.% glass calcined above 1100 °C exhibited linear shrinkage < 8% for all sintering temperatures. Mixes containing 10 wt. % or no glass achieved linear shrinkage within the defined limits when calcined above 1050 and 1000 °C for all sintering temperatures, accordingly.

Water absorption decreases with increasing sintering temperature and increasing glass addition, since these factors promote liquid phase sintering. Mixes containing 20 and 30 wt. % glass, sintered above 1060 °C for all calcining temperatures, exhibited water absorption within the defined limits. Higher sintering temperatures (>1100 °C) for all calcining temperatures are needed to achieve minimal water absorption for mixes containing 10 wt. % and no glass.

The optimum points derived from the software were confirmed in the laboratory and the microstructure was subject to optical microscopy. Significant higher sintering and calcining temperatures are needed to achieve desired properties for samples containing no or 10 wt. % glass. Mixes containing 20 and 30 wt. % glass produced maximum density, minimum linear shrinkage and water absorption, when calcined at 1040 and 1080 °C and sintered at 1060 and 1080 °C, accordingly. These samples indicated closed, uniform porosity. However, the aim of the project is the utilization of the fine fraction of IBA, and therefore, the mixture composition containing 20 wt. % glass and 80 wt. % dry discharged fine IBA dust was chosen as the optimum.

Incinerator bottom ash is a heterogeneous material, associated with the variability of waste feedstock combusted for the production of energy. In addition, the wet discharge process greatly affects the properties of IBA, and therefore, the chemical and physical behavior of the processed materials using IBA. For this reason, the process developed and optimized in the previous chapters needs to be testified by the use of fine IBA derived from a different location and discharge technique.

CHAPTER 7 EFFECT OF WET DISCHARGED FINE INCINERATOR BOTTOM ASH ON THE PRODUCTION OF CERAMICS

7.1 INTRODUCTION

In the previous chapters ceramic materials with improved properties than the traditional Terracotta ceramics have been produced from the fine fraction of IBA dust derived from a dry discharge process. The process involved the addition of glass, wet ball milling, calcining and sintering. The process was optimised by the use of Response Surface Methodology and the results were confirmed in the laboratory. It has been found that calcining temperature is the dominant process parameter affecting the linear shrinkage of sintered ceramics, while sintering temperature and glass are the dominant factors affecting the density and water absorption of ceramic samples. Optimum processing conditions involve the addition of 20 wt.% glass, wet ball milling for 24 hours to produce a homogeneous powder suitable for further processing, calcining at 1080 °C to eliminate the volatiles present in the dry discharged fine IBA dust, pressing to form samples suitable for firing and sintering at 1080 °C. The produced ceramic exhibited high density (~ 2.7 $g.cm^{-3}$), low linear shrinkage (~5.5%) and negligible water absorption.

However, IBA is a heterogeneous material and its properties are directly related to the MSW feedstock, seasonal and topographical variations, and from the IBA discharge technique applied. Wet discharged IBA has typically coarser particles, since contact with water is associated with strong agglomerations. Reactions with water also affect the physical and chemical properties of the IBA produced and subsequent the properties of the materials produced using IBA (KEZO, 2011; Morf et al., 2013). The variability of IBA in terms of location and composition have been the subject of numerous studies (Chandler et al., 1997; ISWA, 2006). In

addition, Morf et al., (2013), compared the characteristics and metal extraction potential of IBA produced from wet and dry discharge processes, as explained in chapter 1.

In this chapter the effect of fine IBA produced from a wet discharged technique on the process developed for the dry discharged fine IBA dust has been investigated. The material was characterized in terms of physical and chemical behavior, and the produced ceramics were characterized in terms of physical, chemical, mineralogical and microstructural behavior. The acid neutralization capacity and leaching behavior of the raw and processed materials have been studied and discussed. The effect of wet discharged fine IBA on the process developed would allow the validation and therefore the repeatability of the process.

7.2 OBJECTIVES

The primary objective of this research is to develop a processing technology for the production of ceramic tiles from the fine fraction of incinerator bottom ash. The objective of the work reported in this chapter is to investigate the effect of IBA discharge technique on the optimum process developed for the dry discharged fine IBA dust. The effect of calcining and sintering temperature on the wet discharged fine IBA have been investigated and the produced materials were characterised in order to validate the process developed for the dry discharged fine IBA dust.

7.3 MATERIAL PROCESSING AND CHARACTERISATION

7.3.1 Characterisation of wet discharged fine IBA

A representative 50 kg batch of <4 mm wet discharged processed IBA was obtained from a major supplier of secondary IBA aggregate in SE England (Day Group, Brentford facility). This had previously been aged in the environment for approximately 2 months and the ferrous and non-ferrous metals extracted with the remaining mineral components size sorted for use as secondary aggregate. The challenging less than 4 mm fraction of wet discharged IBA represents about 45 wt. % of the total IBA received at the processing plant. Representative samples were dried at 105 ºC and disc milled (Gy–Ro, Glen Creston Ltd., UK) to form powders with a mean particle size of 35 μm and pressed into discs for analysis by X-ray fluorescence (XRF, Spectro

2000 Analyser). The crystalline phases in the milled powder were characterised by X-ray diffraction (Philips PW 1830 diffractometer with PW1820 goniometer using CuK radiation with an accelerating voltage of 40 kV). The effect of temperature on mass loss was investigated using thermogravimetric analysis (TG/DTA, Stanton Redcroft, STA-1500 Series) on 25µg samples of milled powder using a ramp rate of 10 °C.min^{-1}.

7.3.2 Ceramic processing

The optimum process developed for the dry discharged fine IBA dust demonstrated that the addition of 20 wt. % of recycled soda lime silica glass significantly improved liquid phase sintering of fine IBA. 500 g sample batches consisting of 400 g of wet discharged fine IBA and 100 g glass were therefore prepared with 1 wt. % of polyethylene glycol (PEG-8000) added as binder. This was wet milled for 24 hours in a porcelain ball mill using high-density alumina milling media, a water to charge ratio of 2 and a milling media to charge ratio of 5. The particle size distribution of the milled slurry was determined by laser diffraction (Beckman Coulter, LS-100 Series). Milled slurries were dried overnight at 105 °C and passed through a 500 µm sieve to form powder suitable for pressing. Tile samples (110 m × 55 mm × 20 mm) and disc samples (40 mm diameter) were formed by uniaxial pressing at 48 MPa (Nannetti S hydraulic press) in a steel die. Pressed samples were then sintered in an electric furnace (Lenton Thermal Design Ltd., ECF 12/45) at a heating rate of 6 °C·min^{-1} to temperatures between 1020 and 1100 °C using a dwell time of 1 hour at peak temperature. After wet ball milling, drying and sieving, the wet discharged fine IBA: glass powder was heated in an alumina crucible to temperatures between 600 and 1100 °C to investigate the effect of calcining temperature. The powders were then lightly ground using a mortar and pestle to produce calcined powders suitable for processing into ceramics using the same procedures as for un-calcined powders.

7.3.3 Characterisation of sintered samples

The density, linear shrinkage and water absorption of sintered samples were characterised as explained in section 3.4. X-ray diffraction used the same procedures as for the as-received wet discharged fine IBA fraction to determine the crystalline phases present in milled and sintered samples. Polished surfaces of selected sintered samples were examined by SEM and optical microscopy (section 3.3.8).

7.3.4 Metal leaching from as-received and processed materials

The acid neutralisation capacity and leaching characteristics of the as-received wet discharged fine IBA, and the processed wet discharged fine IBA have been evaluated using the pH dependence leaching test using a liquid to solid (L/S) ratio of 10 (section). Samples for leaching were dried and ground to pass through a 150 μm sieve.

7.4 RESULTS AND DISCUSSION

7.4.1 As-received wet discharged fine IBA

The chemical composition of the as-received wet discharged fine IBA have been determined and the results are presented in Table 7.1.

Table 7.1: Chemical composition of the as-received wet discharged fine IBA obtained from Day Group facility in England. Representative samples were dried at 105 ºC and disc milled (Gy–Ro, Glen Creston Ltd., UK) to form powders with a mean particle size of 35 μm. The powders were then pressed into discs and analysed by XRF. Results are expressed as oxides.

Oxide	Major elements % (dry basis)	Minor and trace elements (mg/kg)	
SiO_2	30.4	Ba	680
Fe_2O_3	13.0	Be	2.3
CaO	26.8	Cd	85
Al_2O_3	11.5	Co	32
K_2O	1.3	Cr	240
MgO	2.6	Mn	35
Na_2O	3.3	Ni	215
P_2O_5	2.2	Pb	420
ZnO	0.9	Sr	390
CuO	0.4	V	45
TiO_2	1.4	Y	9
		Zr	100

Approximately 80% w/w of the wet discharged fine fraction of IBA consists of oxides of Si, Ca, Fe and Al. (IAWG, 1994; Cheeseman et al., 2003; Bethanis et al., 2004; ISWA, 2006;

Qiao et al., 2008b; Hjelmar et al., 2010; Yiao et al., 2010; Onori et al., 2011; Cheng, 2012; Lin et al., 2012;Schabbach et al., 2011; Schabbach et al., 2012; Morf et al., 2013; Liu et al., 2014). The wet discharged fine IBA contains significant amounts of potassium, sodium, magnesium, titanium, zinc, copper and phosphate. Heavy metals of environmental concern present in the as-received wet discharged fine IBA at high concentrations, include Ba (650-700 mg/ kg), Ni (210-230 mg/kg) and Pb (400-450 mg/kg).

The moisture content of the wet discharged fine IBA was 22.2 %, since the material when discharged from the combustion chamber has been in contact with water. The as-received wet discharged fine IBA indicated a pH ranged from 10.5 to 11.5, associated with the presence of alkali and alkali-earth elements, responsible for the alkaline nature of the material (ISWA, 2006). The pH value of the wet discharged fine IBA is lower than the dry discharged material, associated with the reaction of the wet discharged material with water and the longer period that has been aged.

XRD data given in Figure 7.1 shows that the major crystalline phases present in the < 4mm wet discharged IBA fraction are quartz (SiO_2), calcite ($CaCO_3$), gehlenite ($Ca_2Al_2SiO_7$) and hematite (Fe_2O_3). These phases were similar to the as-received dry discharged fine IBA dust. The crystalline pattern of five as-received wet discharged fine IBA samples from different batches was reproducible, indicating that the as-received wet discharged fine IBA was homogeneous.

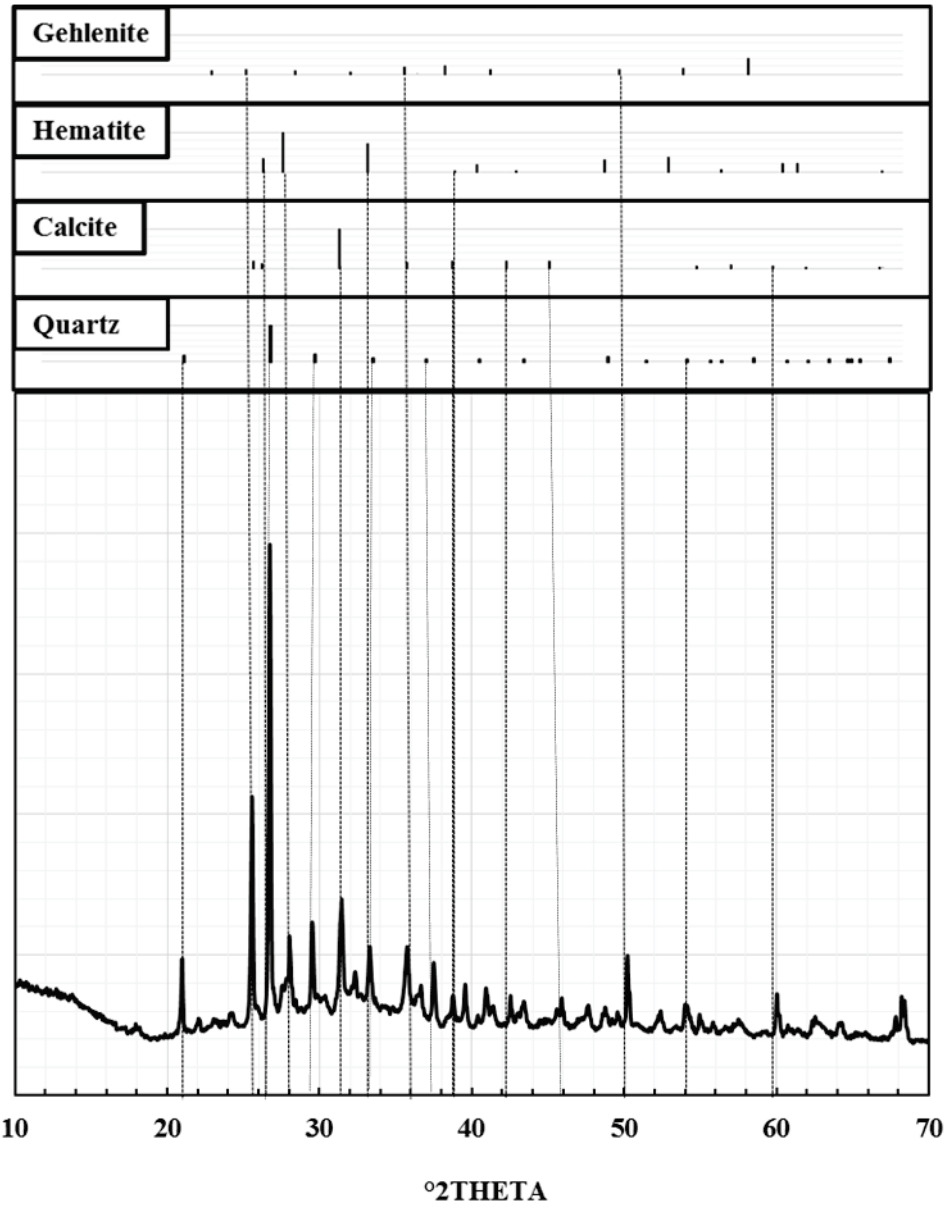
Gehlenite
Hematite
Calcite
Quartz
10
20
30
40
50
60
70
°2THETA

Figure 7.1: X-ray diffraction traces for the as-received less than 4 mm wet discharged fine IBA. Representative samples were dried at 105 ºC and disc milled (Gy–Ro, Glen Creston Ltd., UK) to form powders with a mean particle size of 35 μm. Schematic X-ray powder diagrams are included for relevant phases. Quartz (SiO_2), Hematite (Fe_2O_3), Gehlenite (Ca_2 Al[$AlSiO_7$]) and Calcite (CaO) are the major crystalline phases present.

Thermogravimetric analysis data in Figure 7.2 shows that from ambient temperature to 120 °C weight loss occurs due to evaporation of residual moisture. Significant weight loss occurs between 600 and 770 °C from decomposition of calcite ($CaCO_3$) to CaO and CO_2 (Slavo et al., 2000; Bethanis et al., 2004; Qiao et al., 2008b). Weight loss between 1020 and 1100 °C (~1.7%) is due to the decomposition of alkali metal sulphates with the evolution of SO_2 (Stern and Weise, 1966; Mangialardi et al., 1998).

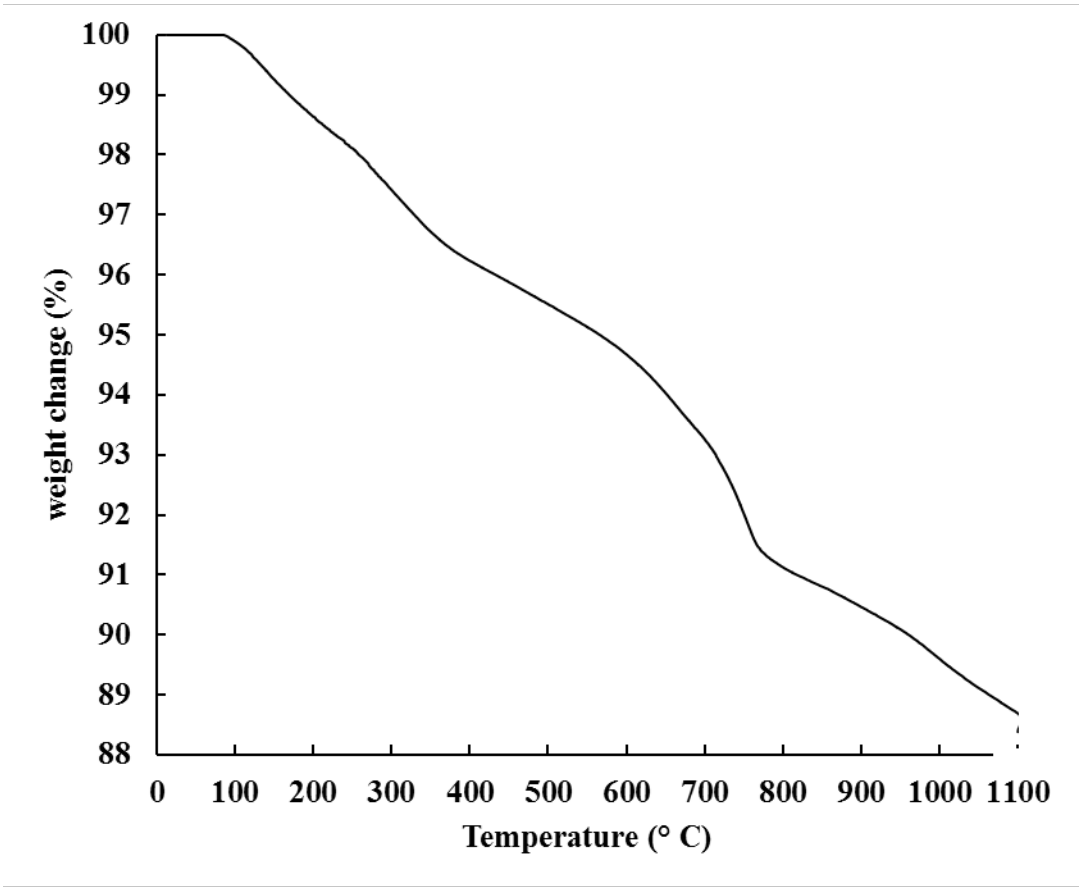

Figure 7.2: Thermogravimetric curve for the as-received fine fraction of wet discharged IBA heated to 1100 °C with a 10 °C.min-1 ramp rate. TGA was conducted on 25µg samples of milled powders using a ramp rate of 10 °C.min^{-1}.

7.4.2 Effect of milling time on wet discharged fine IBA

The effect of milling time on the particle size distribution of the 80 wt. % wet discharged fine IBA and 20 wt. % glass mixture is shown in Figure 7.3. The average particle size (d_{50}) of samples milled for 2, 8 and 24 hours milled samples were 15 µm, 6 µm and 3 µm respectively, and 24 hour milling was selected for use in subsequent experiments, similarly to the milling time used for the dry discharged fine IBA dust.

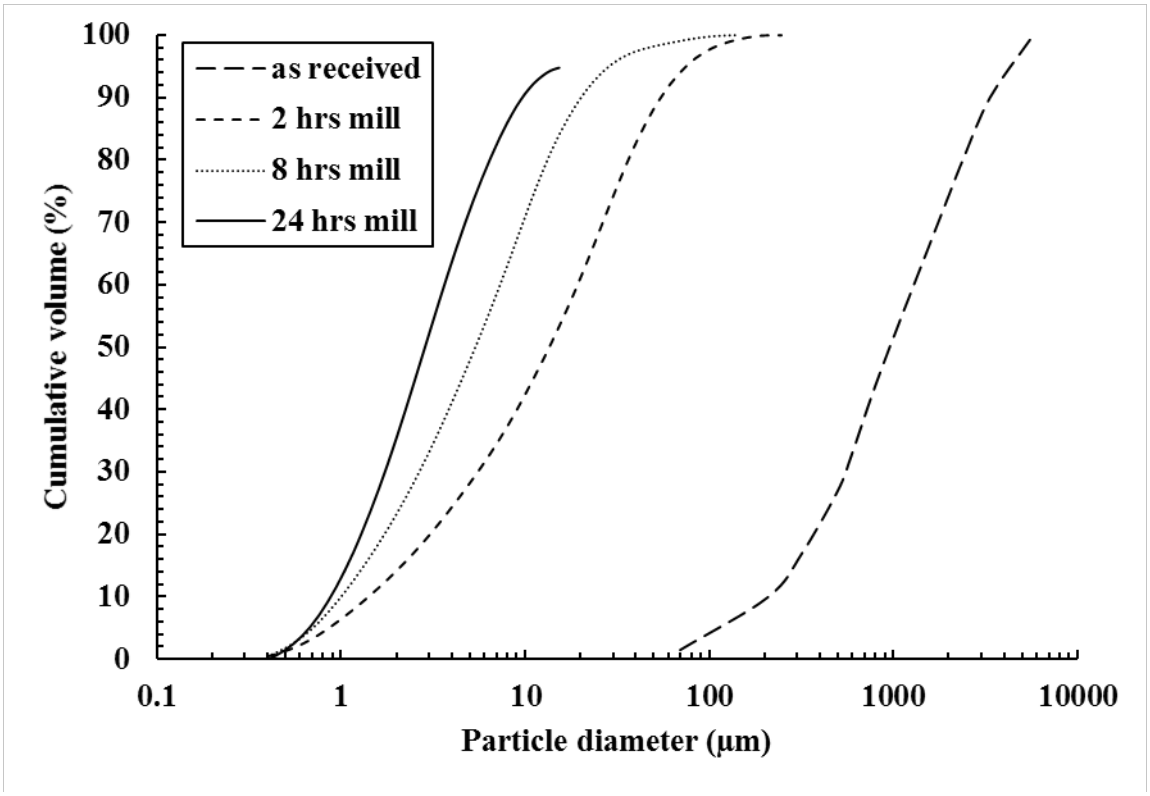

Figure 7.3: Effect of milling time on the particle size of the as-received wet discharged fine IBA. The 24 hours milling seems to give reasonable particle size.

7.4.3 Effect of calcining on the 'green' density

The 'green' density of the materials containing 20 wt. % glass and produced with uncalcined and calcined at 1080 °C is presented in Figure 7.4.

Samples produced with powder calcined at 1080 °C, exhibited higher 'green' density compared to the materials produced with uncalcined powders. The maximum 'green' density of the materials prepared with uncalcined powders was about 1.53 g/cm^3 when pressed at 100 MPa while the calcined powders achieved green densities of 2.15 g/cm^3, indicating that calcined powders have improved packing and compaction properties. Increasing the compaction pressure had negligible effect on 'green' densities of samples produced with the uncalcined and calcined at 1080 °C powders.

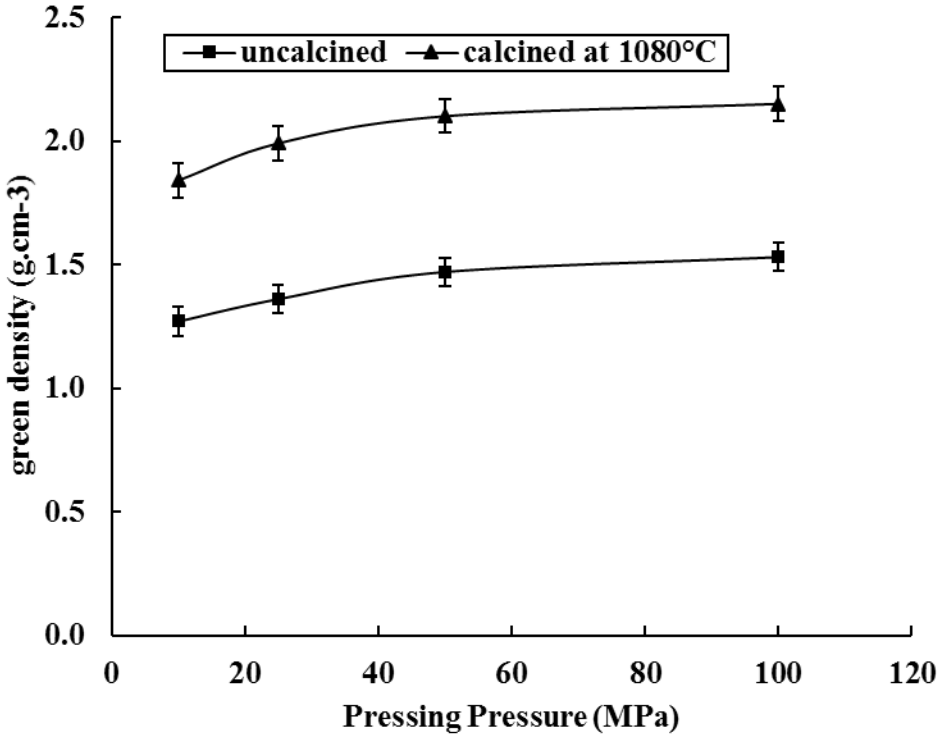

Figure 7.4: Effect of pressing pressure on the 'green density' of samples containing 80 wt.% wet discharged fine IBA and 20 wt. % glass and produced with uncalcined and calcined at 1080 °C powders. Samples produced with calcined at 1080 °C powder exhibited higher 'green' density.

7.4.4 Effect of sintering temperature on the density and linear shrinkage of samples produced with calcined powders

Figure 7.5 and 7.6 shows the effect of sintering temperature on the density and linear shrinkage, accordingly, of samples containing 20 wt. % glass and calcined at different temperatures. The results indicate that the wet discharged fine IBA when processed for the production of ceramics has similar behaviour compared to the dry discharged material. Maximum average densities of approximately 2.5 g/cm^3 were obtained by sintering uncalcined powders at 1040 °C, although the appearance of these samples indicates these are not properly sintered. Sintering at 1080 °C uncalcined powders resulted in an additional mass loss of 16 wt. %. Linear shrinkage was ~20% for samples sintered above 1040 °C and this tended to cause deformation and warping of tile samples, as was the case for samples produced with the dry discharged fine IBA dust.

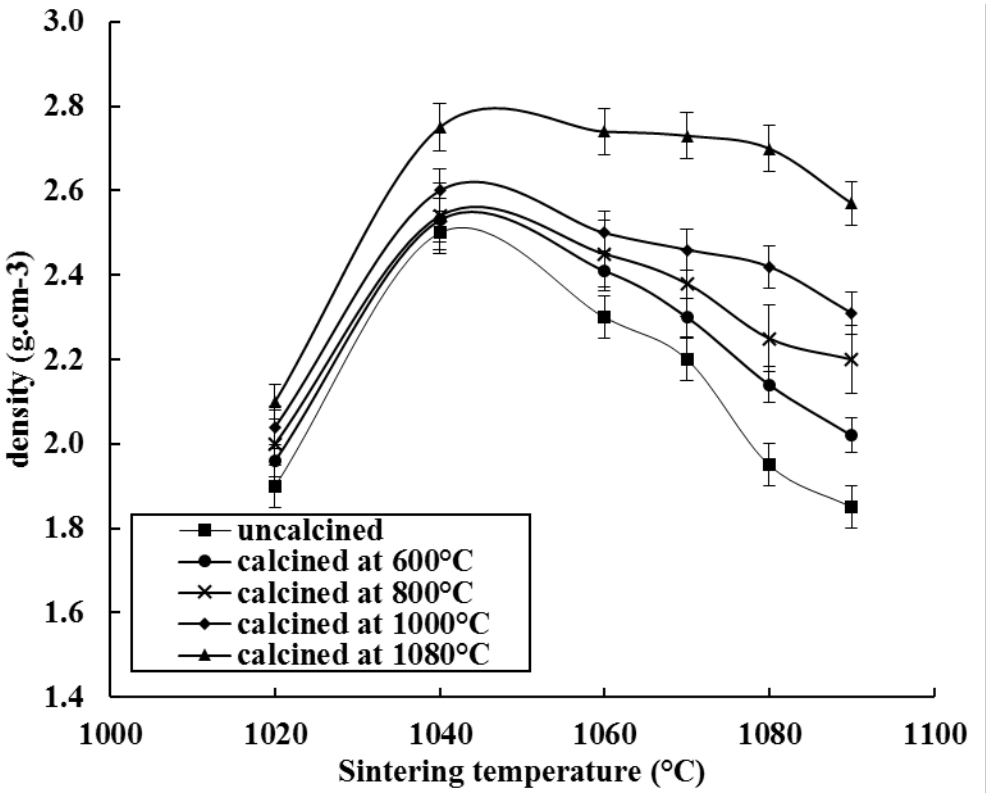

Figure 7.5: Effect of sintering temperature on the density of samples containing 80 wt. % wet discharged fine IBA and 20 wt. % glass and calcined at different temperatures. Error bars: +/- 1 std.

Increasing the firing temperature reduces the density due to the formation of internal closed porosity, but the skeletal density increases and this improves the appearance of the ceramic body formed. The microstructure contains an extensive network of spherical pores formed from decomposition of volatile phases present such as alkali metal sulphates, at temperatures where simultaneous softening of the glassy phase occurs so that the gasses generated remain trapped as pores in the microstructure. Firing at 1080 °C therefore causes liquid phase sintering and pore formation due to gas evolution. Therefore, the materials exhibited similar effects as the dry discharged fine IBA dust, and the effect of calcining the wet discharged fine IBA: glass powders prior processing was investigated, similarly to the optimum process developed for the dry discharged material. Powder samples calcined at temperatures between 600 and 900 °C had linear shrinkages between 9.5 and 13.0% and had densities of around 2.00 g/cm^3. Significantly higher densities of 2.35 g/cm^3 and 2.8 g/cm^3 were achieved by calcining at 1000 °C and 1080 °C and shrinkage was reduced. This benefit of reaching higher densities with much lower shrinkage is due to the improved pressing behaviour of powers calcined at high temperatures. The maximum average density of 2.80 g/cm^3 was obtained using milled wet discharged fine IBA/glass powder calcined at 1080 °C and these samples had a linear shrinkage of only 5.4%, which is lower than the shrinkage of typical clay ceramics, typically in the range of 7 to 8%. The results showed that the wet discharged fine IBA has similar behaviour compared to the dry discharged fine IBA dust, when processed for the production of ceramics.

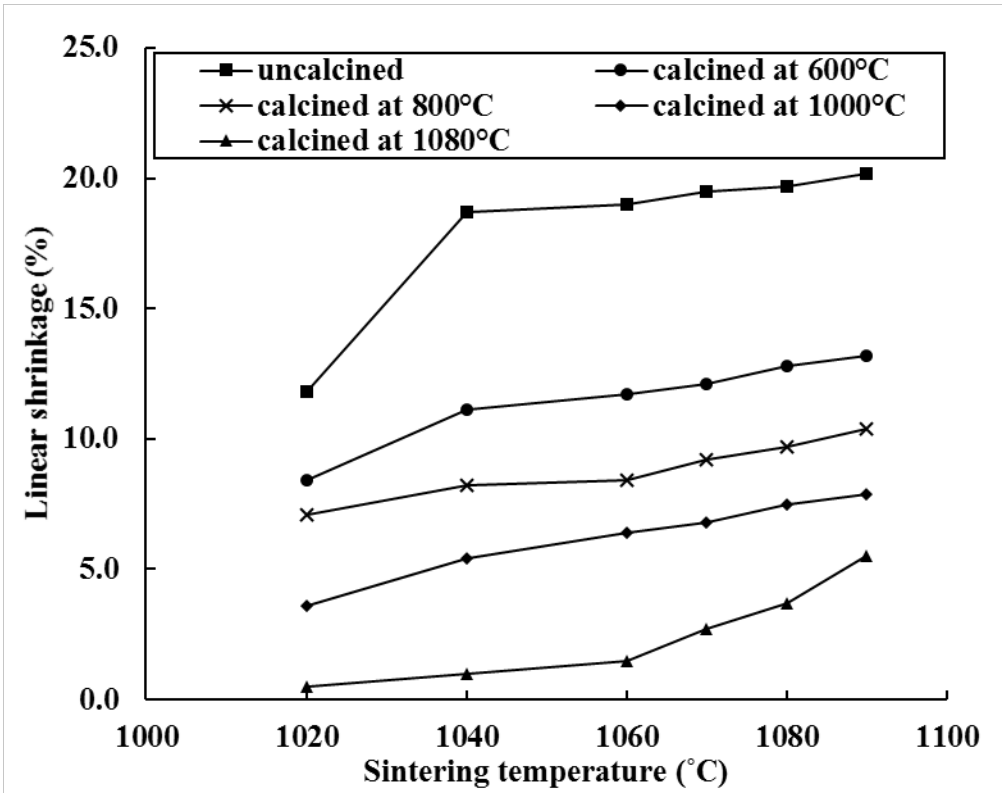

Figure 7.6: Effect of sintering temperature on the linear shrinkage of samples containing 80 wt. % wet discharged fine IBA and 20 wt. % glass and calcined at different temperatures. Error bars: negligible

7.4.5 Effect of sintering temperature on water absorption of samples produced with calcined powders

The effect of sintering temperature on the water absorption of samples containing 20 wt. % glass and calcined at different temperatures is shown in Figure 7.7. Water absorption is approximately 17% for samples produced with uncalcined powders and sintered at 1020 °C. This gradually decreases with increasing calcining and sintering temperature. The water absorption of the produced ceramics was negligible for samples sintered at temperatures above 1070 °C and calcined at different temperatures.

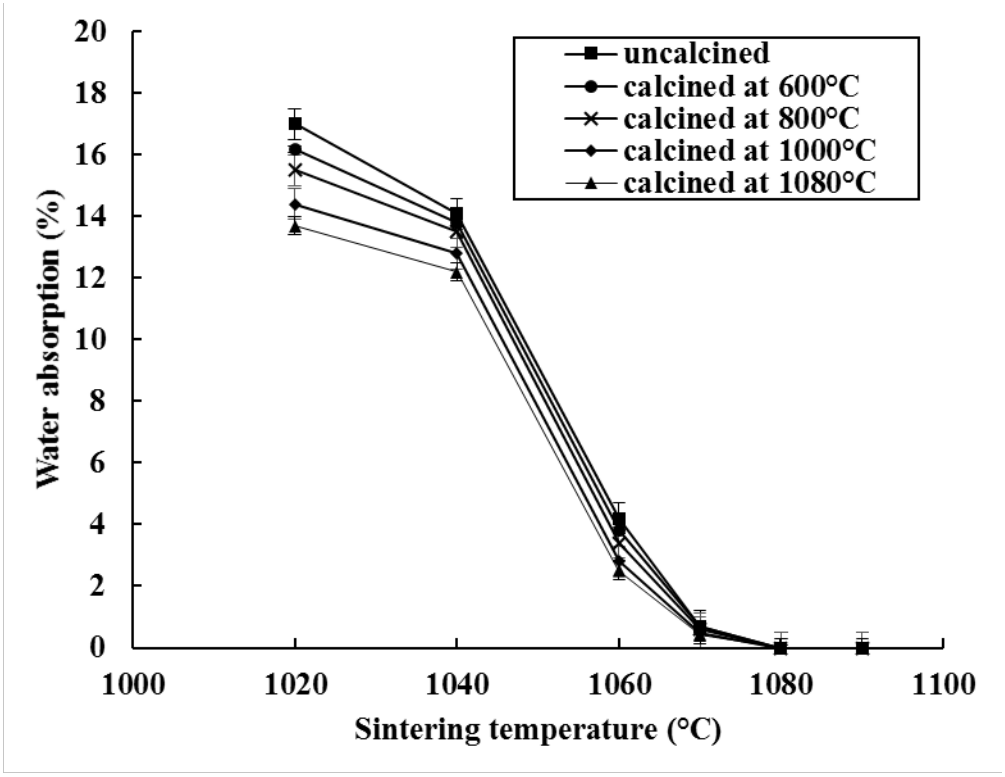

Figure 7.7: Effect of sintering temperature on the water absorption of samples containing 80 wt. % wet discharged fine IBA and 20 wt. % glass and calcined at different temperatures. Error bars: negligible.

7.4.6 Effect of sintering temperature on the Vickers micro hardness of samples produced with calcined powders

The average micro-hardness data for ceramics produced from uncalcined and calcined powders sintered at temperatures between 1020 and 1100 °C is shown in Figure 7.8. Sintering uncalcined samples at 1080 °C produced a Vickers micro-hardness of 4.1 GPa. Ceramics prepared at the same temperature from calcined powder had a hardness of 4.5 GPa. Terracotta ceramics have Vickers micro-hardness between 3.3 to 3.5 GPa.

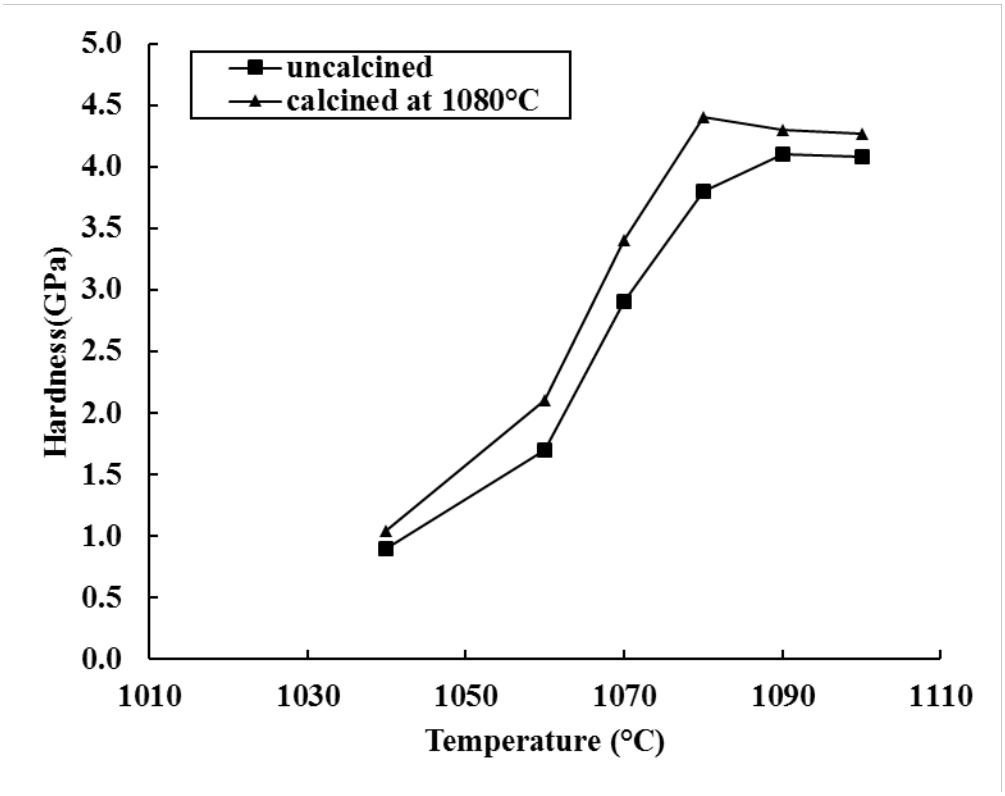

Figure 7.8: Effect of sintering temperature on the Vickers micro hardness of samples containing 80 wt. % wet discharged fine IBA and 20 wt. % glass and calcined at different temperatures. Error bars: negligible.

7.4.7 Mineralogy of processed wet discharged fine IBA: glass samples

X-ray diffraction data for 24 hour milled wet discharged fine IBA: glass mixes calcined at 600, 800, 1000 and 1080 °C are shown in Figure 7.9. Quartz (SiO_2), calcite ($CaCO_3$), hematite (Fe_2O_3) and ghelenite ($Ca_2Al_2SiO_7$) are the major crystalline phases in the as-received wet discharged fine IBA. Calcining above 800 °C produces powders with new crystalline phases, similarly to the processed dry discharged fine IBA dust. Calcining at 1080 °C forms powders mainly consisting of the pyroxene minerals diopside ($CaMgSi_2O_6$) and clinoenstatite ($MgSi_2O_6$) together with some andradite ($Ca_3Fe_2Si_3O_{12}$). Sintering of calcined at 1080 °C powders does not introduce additional changes in the crystalline phases present.

XRD data indicates that extensive changes in the crystalline phases present also occur during the calcining process. The original wet discharged fine IBA fraction contains quartz (SiO_2), calcite ($CaCO_3$) gehlenite ($Ca_2Al_2SiO_7$) and hematite (Fe_2O_3) while the sintered ceramic contain predominantly diopside ($CaMgSi_2O_6$), clinoenstatite ($MgSiO_3$) and andradite ($Ca_3Fe_2Si_3O_{12}$). Similarly to the processing of the dry discharged fine IBA dust, XRD analysis of wet discharged fine IBA: glass calcined at increasing temperatures reveals that the amount of quartz (SiO_2), calcite ($CaCO_3$), gehlenite ($Ca_2Al_2SiO_7$) and hematite (Fe_2O_3) decrease on calcining and these crystalline phases are no longer present for powders calcined at 1080 °C. The principal crystalline phase present when calcining at 1000 °C was diopside, together with some clinoenstatite, andradite and small amounts of hematite and albite. The main crystalline phases in wet discharged fine IBA: glass mix calcined at 1080 °C were diopside ($CaMgSi_2O_6$), clinoenstatite ($MgSiO_3$) and andradite ($Ca_3Fe_2Si_3O_{12}$). Diopside is calcium pyroxenes, while clinoenstatite is a magnesium pyroxene.

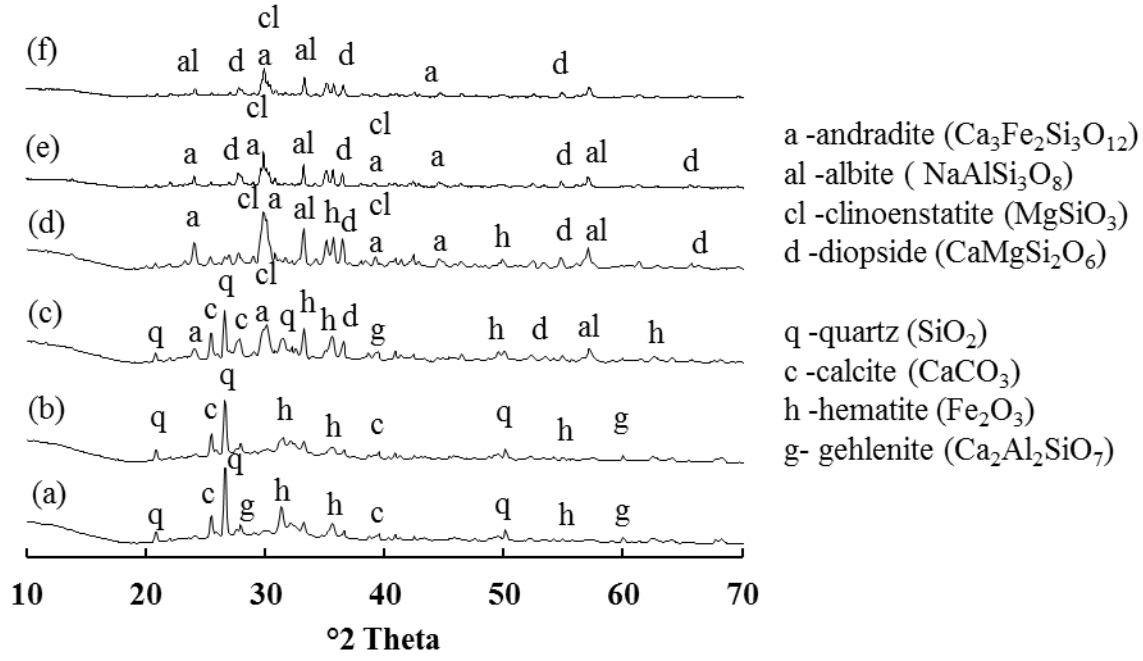

Figure 7.9: XRD data of the : (a) milled 80 wt.% wet discharged fine IBA: 20 wt.% glass, milled powder calcined at (b) 600 °C, (c) 800 °C, (d) 1000 °C, (e) 1080 °C and (f) powder calcined at 1080 °C and sintered at 1080 °C. This indicates that the amount of quartz (SiO_2), calcite

($CaCO_3$), gehlenite ($Ca_2Al_2SiO_7$) and hematite (Fe_2O_3) decrease on calcining and these crystalline phases are no longer present after calcining at 1080 °C.

7.4.8 Microstructure of processed wet discharged fine IBA: glass samples

Optical micrographs of polished surfaces of ceramics prepared from calcined and uncalcined powders sintered at 1080 °C are shown in Figure 7.10. Both types contain small pores but ceramics produced from uncalcined powder additionally contain large pores consistent with lower density. Figure 7.11 shows image analysis data from the optical photomicrograph images confirming that the number of fine pores per unit area is similar in both samples and that the coarse pores (up to 400 μm) are present only in the uncalcined samples. The SEM micrographs of fracture surfaces in Figure 7.12 confirm the reduced porosity resulting from calcining.

The influence of the calcining temperature on the evolution of the pore structure is in agreement with the density measurements. Pyroxene ceramics produced from wet discharged fine IBA/glass powder calcined at 1080 °C exhibit pores within a denser ceramic matrix that have a much finer and more consistent size distribution compared to ceramics manufactured from uncalcined powder.

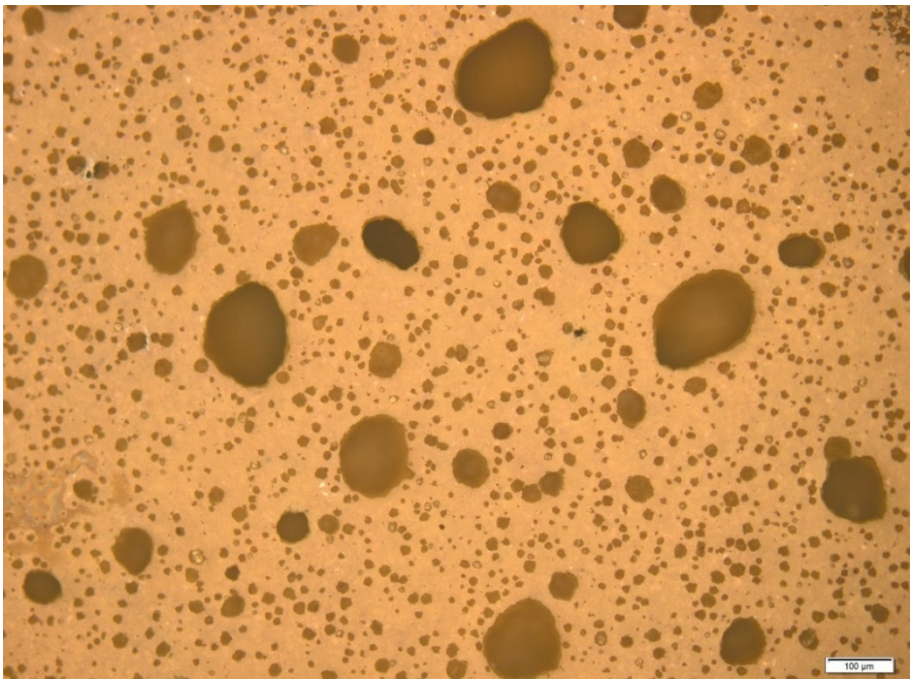

(a)

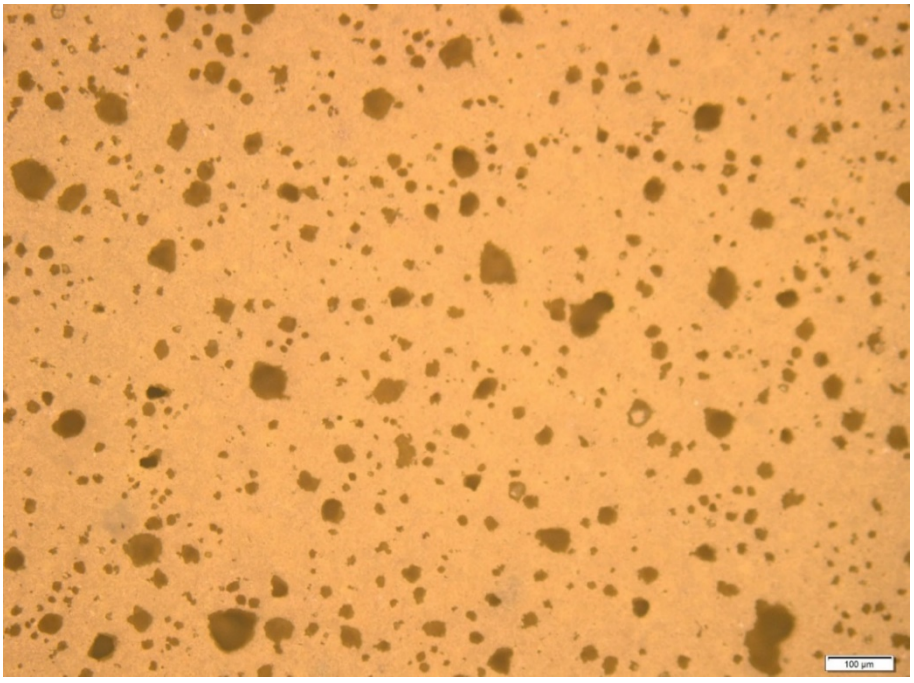

(b)

Figure 7.10: Optical micrographs of polished surfaces of ceramics containing 80 wt. % wet discharged fine IBA and 20 wt. % glass sintered at 1080 °C: (a) without calcining, (b) calcined at 1080 °C powder.

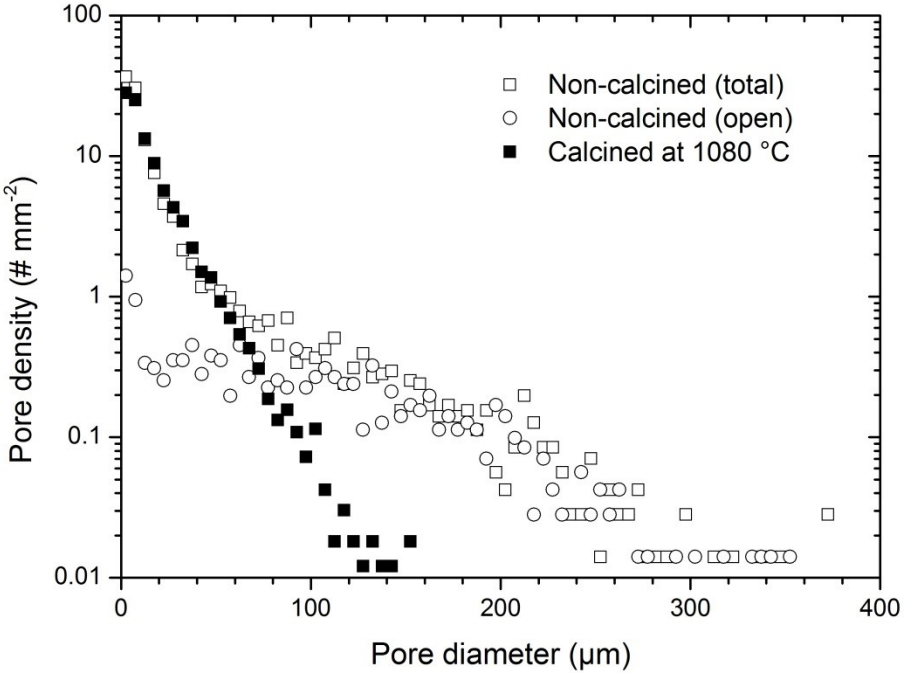

Figure 7.11: Pore size distributions after sintering at 1080 °C of un-calcined and calcined at 1080 °C samples containing 80 wt. % wet discharged fine IBA and 20 wt. % glass. The number of fine pores per unit area is similar in both samples and that the coarse pores (up to 400 µm) are present only in the uncalcined samples.

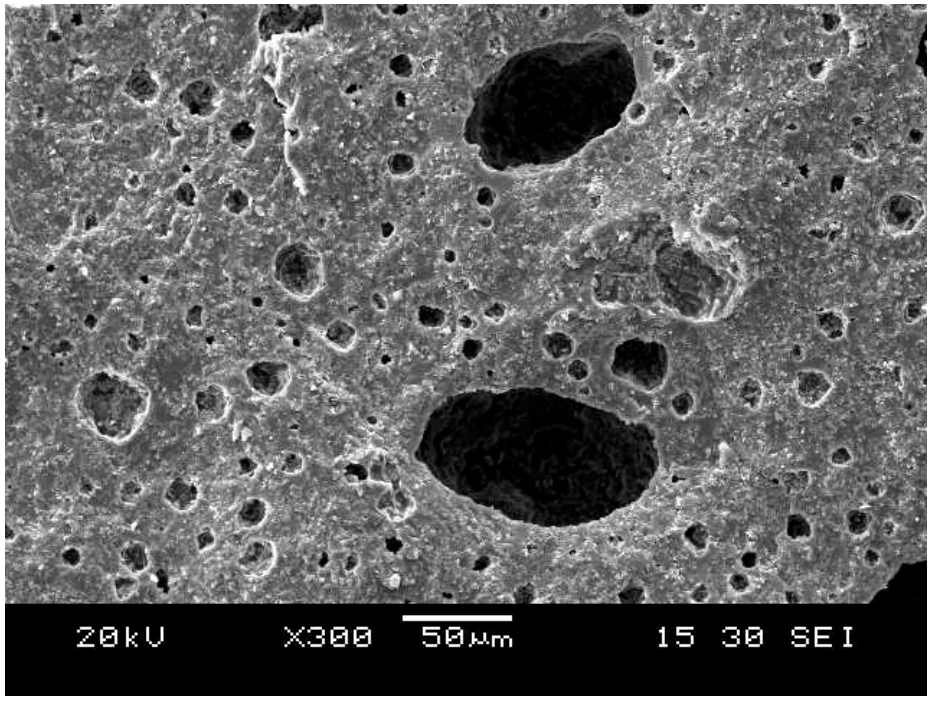

(a)

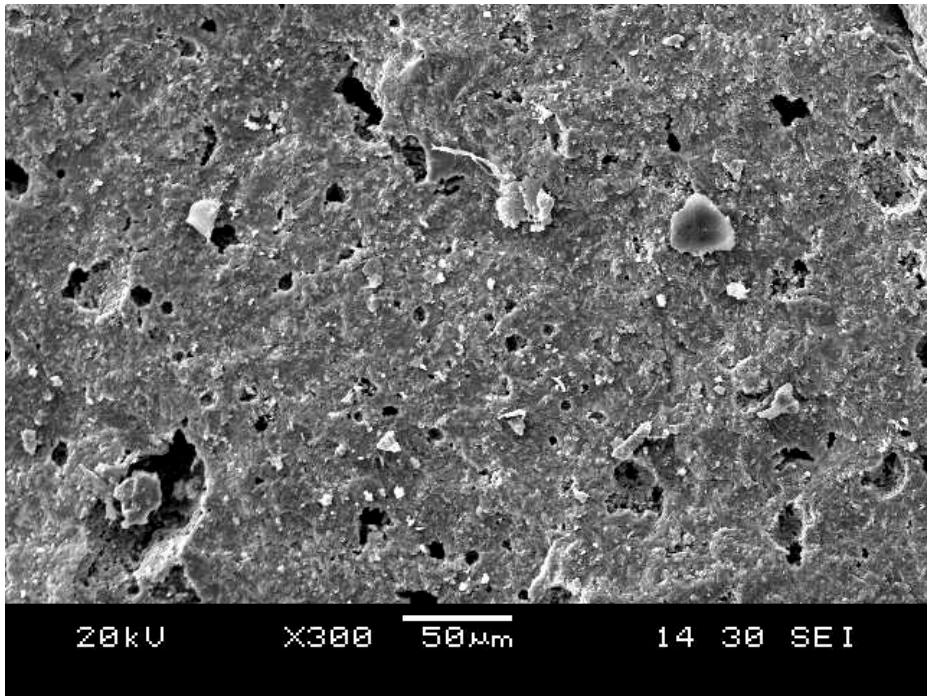

(b)

Figure 7.12: SEM micrographs of fracture surfaces of ceramics containing 80 wt. % wet discharged fine IBA and 20 wt. % glass sintered at 1080 °C: (a) without calcining, (b) calcined at 1080 °C powder.

7.4.9 Leaching behaviour during processing

Acid Neutralisation Capacity

Figure 7.13 shows final leachate pH data as a function of acid addition. Ceramic sintered at 1080°C produced with wet discharged fine IBA: glass powder calcined at 1080°C exhibit a rapid decrease in pH compared to the as-received wet discharged fine IBA, corresponding to significantly reduced Acid Neutralisation Capacity (ANC). Results are reported as equivalents of acid per kg of solid.

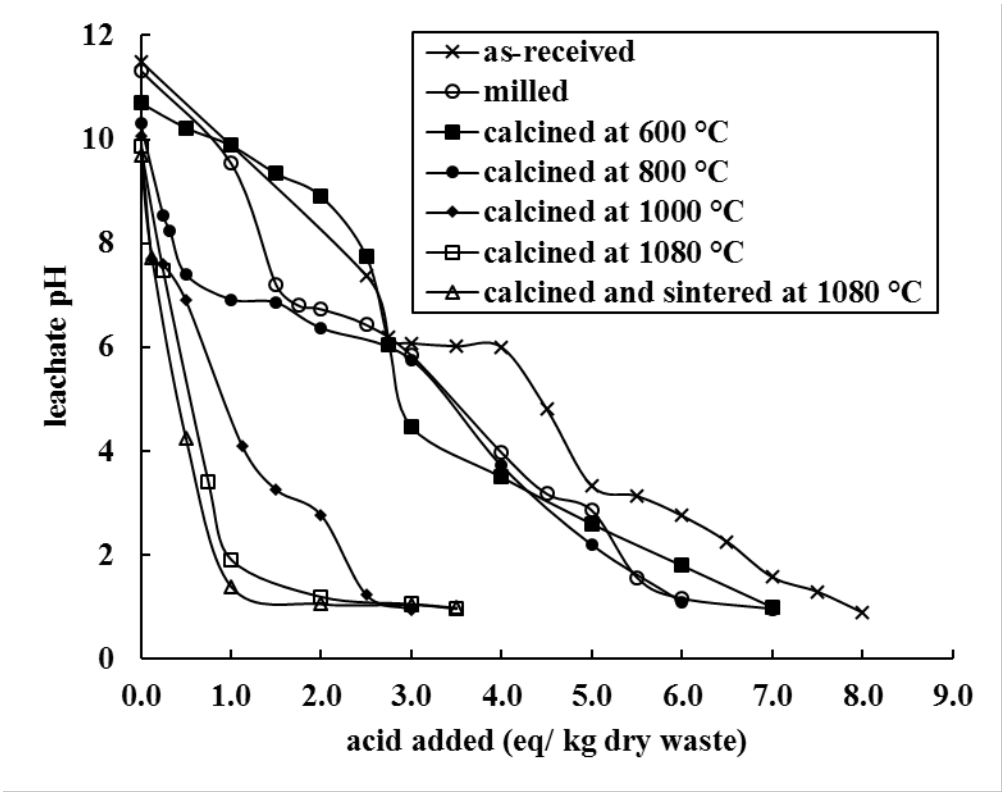

Figure 7.13: Acid Neutralisation capacity of the as-received wet discharged fine IBA, milled 80 wt.% wet discharged fine IBA: 20 wt.% glass, calcined milled powders at 600 °C, 800 °C, 1000 °C, 1080 °C and calcined milled powders at 1080 °C and sintered at 1080 °C. Increasing the calcining temperature resulted in a decrease in ANC curve.

The carbonated as-received wet discharged fine IBA displayed a fairly constant rate of pH decrease with acid addition. $CaCO_3$ is present in the as-received wet discharged fine IBA and as a result of carbonation during ageing. This provides significant buffering capacity to acid addition due to the formation of Ca^{2+}, HCO^{3-} and OH^- ions when water is added (Guimaraes et al, 2006; Van der Sloot et al, 2012).

While the as-received wet discharged fine IBA show significant ANC at pH 5 to 6, calcined wet discharged fine IBA: glass powder above 1000 °C and sintered ceramics exhibit a rapid decline in leachate pH with acid addition through this pH range, indicating reduced ANC. This reduction in ANC from calcining wet discharged fine IBA: glass is primarily due to the decomposition of $CaCO_3$ to CaO and CO_2 that occurs during calcining, combined with subsequent encapsulation and incorporation of Ca2+ in both amorphous and crystalline phases present in the processed wet discharged fine IBA (Guimaraes et al, 2006; Van der Sloot et al, 2012). The ANC results of the wet discharged fine IBA indicate the similarity in the ANC behaviour compared to the as received and processed dry discharged fine IBA dust.

Metal leaching from as-received and processed wet discharged fine IBA

The concentrations of selected alkali and alkali earth metals and heavy metals leached from the as-received wet discharged fine IBA, calcined at different temperatures and sintered ceramic at 1080°C produced with wet discharged fine IBA: glass powder calcined at 1080°C are shown in Figure 7.14,7.15, 7.16, 7.17, 7.18 and 7.19. Ceramic processing significantly reduced leaching of all elements contained in as-received wet discharged fine IBA.

(a) Leaching of alkali metals and alkali metal earth ions

Leaching data for Ca, Mg, Na and K in mg/kg are presented in Figure 7.14 and 7.15. The Ca leaching curves follow similar trends as the processing of the dry discharged fine IBA dust. The aged as-received wet discharged fine IBA releases high concentrations of Ca with acid addition, associated with the presence of soluble mineral phases such as $CaCO_3$, $CaSO_4$, $CaCl_2$, CaO and Ca-silicates present. Calcining above 1000 °C produces materials with less-soluble calcium silicates phases, such as diopside or andradite, that encapsulate Ca in the crystalline

phases formed, and subsequent significantly reduce Ca leached concentration with acid addition (Guimaraes et al, 2006; Van der Sloot et al, 2012). Calcining at 600 and 800 °C produces powders with similar Ca leached concentration at pH < 6 compared to the as-received and the milled materials. The calcined at 600 °C powders do not induce any change at pH > 6 compared to the as-received wet discharged fine IBA, however, the calcined at 800 °C powders exhibit significant reduction in Ca leached concentration over that pH range. This is associated with the partial decomposition reactions when the wet discharged fine IBA: glass mixture is heated at this temperature, as was the case for the dry discharged material (Selinger et al., 1997; Van der Sloot et al., 2001; Bethanis et al., 2004; Van der Sloot et al., 2012). Ca showed the lowest release for the ceramic produced with optimum processing parameters under all pH conditions examined.

The similarity in the leaching curves of Mg and Ca of fine as-received wet discharged fine IBA supports the possible role of calcite in controlling Mg leaching, as was the case of the dry discharged material and also observed by other researchers (Van der Sloot et al, 2012). Mg leached concentration is significantly reduced for powders calcined at temperatures above 1000 °C under all pH conditions examined, due to the formation of new less soluble crystalline phases. Sintered ceramic with calcined at 1080 °C powder exhibit the lowest concentration in Mg leaching.

Na is released from the aged as-received wet discharged fine IBA over a wide pH range. Calcined at 600 and 800 °C powders indicated higher Na leached concentration at pH < 7 compared to the as-received and the milled material. The calcined at 600 °C powders exhibited an increase in Na leached concentration at pH > 7, associated with the presence of this ion in readily soluble phases at this calcining temperatures. Powders calcined at 800 °C indicated similar or slightly higher Na leached concentration compared to the as-received material, linked with the partial decomposition reactions of components containing Na ions. Powders calcined at 1000 °C exhibited intermediate Na leached concentration and powders calcined at 1080 °C had increased leaching resistance with acid addition. There is significantly reduced Na leaching from the sintered at 1080°C ceramic produced with calcined at 1080°C powder under alkaline conditions, associated with the encapsulation and incorporation of Na ions into stable insoluble crystalline phases formed, such as albite.

K leached concentration for the as-received and the calcined at different temperatures powders indicated similar curves as the dry discharged material. Powders calcined at 600 and

800 °C indicated slightly lower K leached concentration than the as-received and the milled materials at pH < 7. Powders calcined at 600 °C exhibited similar K leaching behaviour with acid addition at pH > 7 compared to the as-received wet discharged fine IBA, but this was rapidly decreased for powders calcined at 800 °C under similar alkaline conditions. Calcining the wet discharged fine IBA: glass powders to 1000 and 1080 °C, decreases K leached concentration for all pH examined. The lowest K leached concentration was observed for the optimum ceramics produced, similarly to the processing of the dry discharged fine IBA dust.

(b) Leaching of heavy metals

Leaching data for Cr, Cu, Ni, Zn, Cd and Pb in mg/kg are presented in Figures 7.16, 7.17 and 7.18 for the as-received wet discharged fine IBA, the milled material, the calcined at different temperatures powders and the optimum ceramics.

Calcining at 600 and 800 °C produces powders with increased Cr leached concentration at pH > 4 compared to the as-received wet discharged fine IBA. This is associated with the presence of the more mobile Cr hexavalent form, which has been transformed from the initial trivalent form when heated at these temperatures. Powders calcined at 1000 °C indicated similar or slightly higher Cr leached concentration compared to the as-received material under all pH conditions examined. Calcining powders at 1080 °C resulted in a relatively low Cr leaching down to very aggressive conditions, associated with the encapsulation of this metal into more stable, less soluble crystalline phases. The optimum ceramic derived exhibited the lowest Cr leached concentration for all pH conditions examined.

Cu leached concentration is below 1 mg/ kg at pH > 4, for the as-received, milled and the powders calcined at different temperatures. Powders calcined at 600 °C indicated similar Cr leaching behaviour to the as-received and the milled powders for all pH conditions examined. Calcining at 800 °C produces powders with similar or slightly lower Cu leached concentration compared to the as-received wet discharged fine IBA down to very aggressive pH conditions. However, at pH > 7 powders calcined at 800 °C indicated a significant reduction in Cu leached concentration, associated with the decomposition of Cu-containing sulphate salts. Powders calcined above 1000 °C exhibited a gradually decrease in Cu leached concentration. The lowest Cu leached availability was observed for the optimum ceramic.

Powders calcined at 600 °C indicated similar Ni leached concentration compared to the as-received and milled materials. Calcining the powders at 800 °C decreases the Ni leaching availability by approximately an order of magnitude. This is significantly reduced for powders calcined above 1000 °C for all pH conditions examined. The lowest Ni leached concentration was observed for the optimum ceramic produced.

Zn leached concentration for powders calcined at 600 and 800 °C is lower than the as-received material by about an order of magnitude at pH < 5. Powders calcined above 1000 °C indicated significantly reduced Zn leached concentration under all pH conditions examined. Heating the material at these temperatures results to the inertization of Zn to compounds of low solubility, as observed for the dry discharged fine IBA dust and other researchers (Selinger et al., 1997; Bethanis et al., 2004; Van der Sloot et al., 2012).

Pb leached concentration is reduced by approximately an order of magnitude for powders calcined at 600 and 800 °C compared to the as-received fine IBA at pH < 4. Powders calcined at 800 °C indicated a significant reduction in Pb leached concentration at pH > 4. Calcining powders above 1000 °C resulted in materials with significantly lower Pb leached concentration than the as-received wet discharged fine IBA and the powders calcined at 600 and 800 °C, under all pH conditions examined. Powders calcined at 1080 °C and the optimum ceramic produced exhibited no detectable Pb leached concentration at pH > 7.

Powders calcined at 600 °C indicated similar or slightly lower Cd leached concentration compared to the as-received wet discharged fine IBA, under all pH conditions examined. Increasing the calcining temperature at 800 °C resulted in significant lower Cd leached concentration than the as-received material at pH > 6, but similar to the as-received wet discharged fine IBA at pH < 6. Powders calcined above 1000 °C exhibited significant lower Cd leached concentration and the optimum ceramic produced indicated the lowest Cd leached concentration for all pH conditions examined.

The values of the heavy metals leached from the as-received, the calcined at 1080 °C powder and the optimum ceramic produced under aggressive leachate conditions (pH 3) have been summarised in Table 21. The total concentration of the heavy metals contained in the as-received wet discharged fine IBA are also reported and the percentage reduction of these heavy metals during processing is presented. Cu, Zn and Pb are the most readily available heavy metals from the as-received wet discharged fine IBA, as was the case for the dry discharged fine

IBA dust. Approximately 30% of Cu is available for leaching for the as-received material and about 25% of Zn and 26% of Pb are available for leaching from the as-received wet discharged fine IBA. Calcining at 1080 °C resulted in a significant reduction in leached concentration of these metals, with above 95% reduction for all heavy metals examined. The optimum ceramic indicated the highest reduction in all heavy metals examined with above 96% reduction compared to the leaching values obtained for the as-received material.

(c) Leaching of Al and Fe

Leaching data for Al and Fe for the as-received, milled and calcined at different temperatures materials in mg/ kg are presented in Figure 7.19. Powders calcined at 800 °C indicated reduced Al leached concentration at pH > 6, mainly associated with the partial decomposition of Al $(OH)_3$ and amorphous aluminosilicates, typically present in the as-received wet discharged fine IBA. Powders calcined above 1000 °C resulted in a significant reduction in Al leached concentration under all pH conditions examined. This is associated with the fixation to the new crystalline phases formed and the incorporation and encapsulation of Al in less soluble, more stable crystalline phases, such as albite. The lowest Al leached concentration was observed for the optimum ceramic.

Powders calcined at 600 and 800 °C resulted in materials with reduced Fe leached concentration compared to the as-received wet discharged fine IBA. At this temperatures, the ferrihydrates typically present in the as-received material does not have the capacity to decompose, and therefore, encapsulated within the new stable crystalline phases formed. Powders calcined above 1000 °C resulted in materials with much lower Fe leached concentration than the as-received wet discharged fine IBA. This is associated with the incorporation and encapsulation of Fe ions into the less soluble crystalline phases formed, such as andradite. The optimum ceramic exhibited the lowest Fe leached concentration for all pH conditions examined, as attenuated.

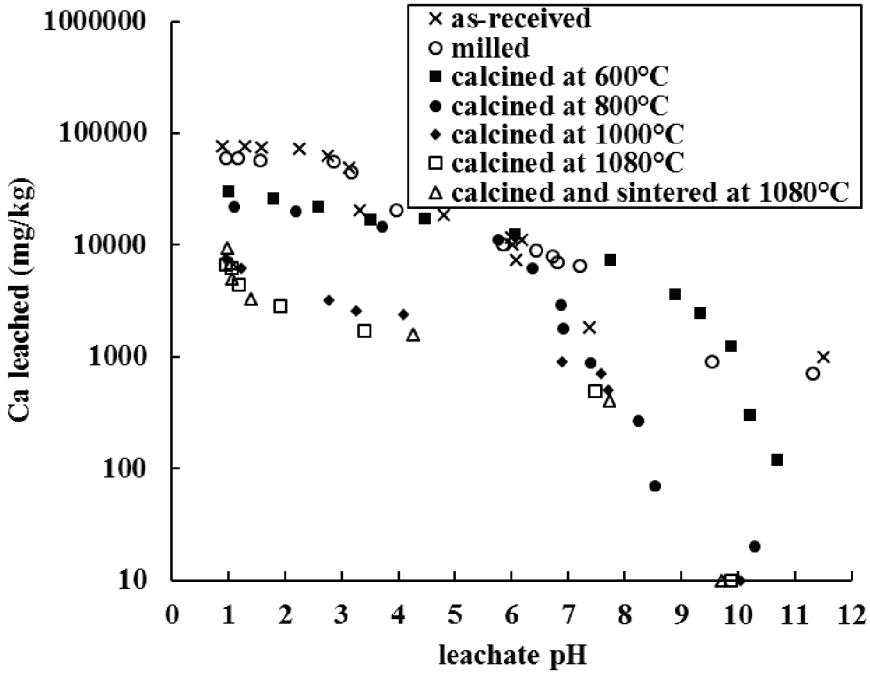
as-received
milled
calcined at 600°C
calcined at 800°C
calcined at 1000°C
calcined at 1080°C
calcined and sintered at 1080°C
Ca leached (mg/kg)
1000000
100000
10000
1000
100
10
0 1 2 3 4 5 6 7 8 9 10 11 12
leachate pH

(a)

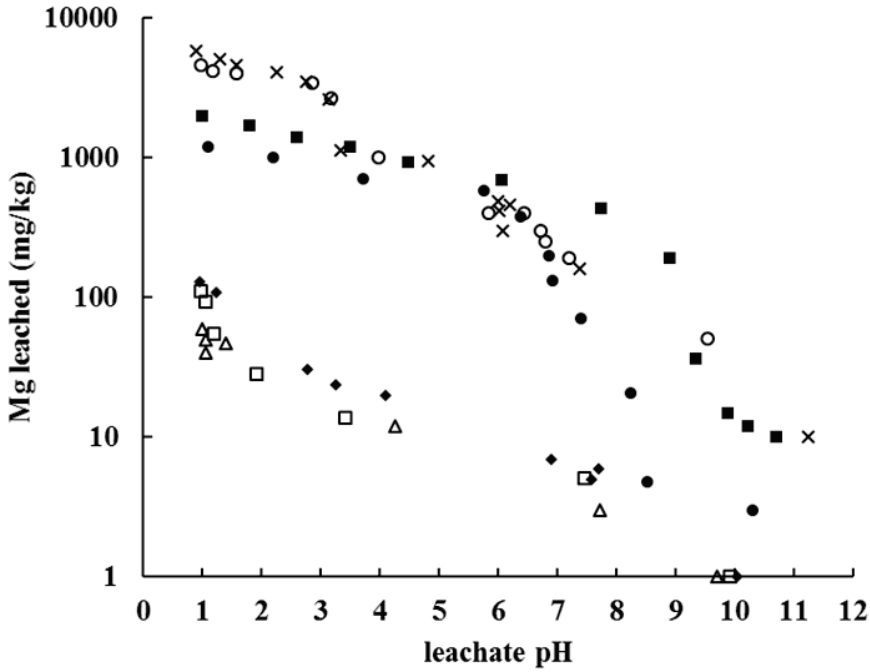
Mg leached (mg/kg)
10000
1000
100
10
1
0 1 2 3 4 5 6 7 8 9 10 11 12
leachate pH

(b)

Figure 7.14: Leaching data for (a) Ca and (b) Mg as a function of leachate pH for the as-received wet discharged fine IBA, milled 80 wt.% wet discharged fine IBA: 20 wt.% glass, calcined milled powders at 600 °C, 800 °C, 1000 °C, 1080 °C and calcined milled powders at 1080 °C and sintered at 1080 °C.

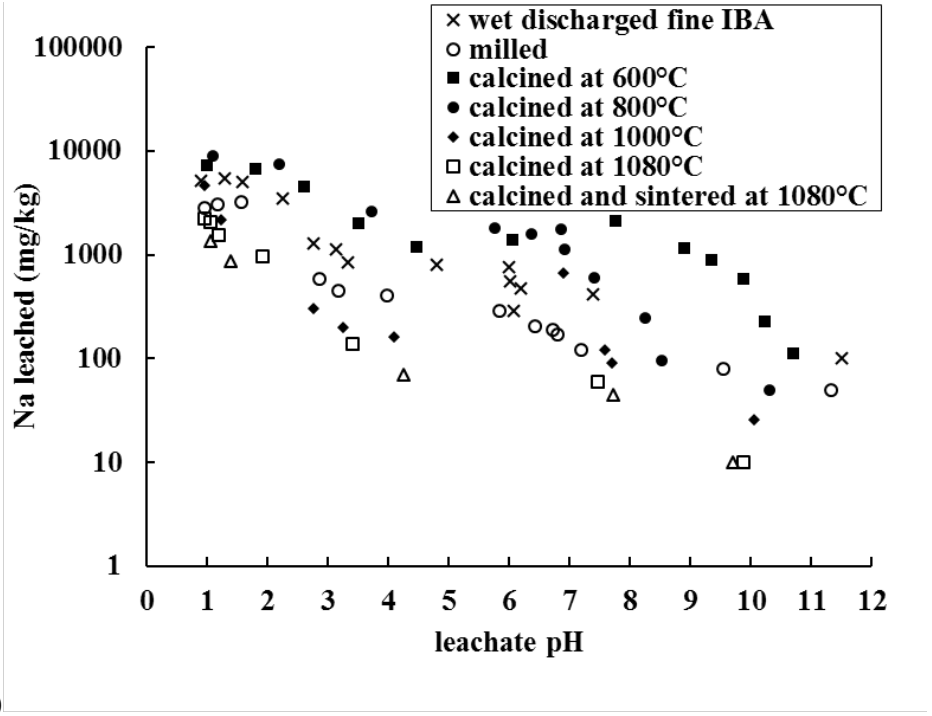

(a)

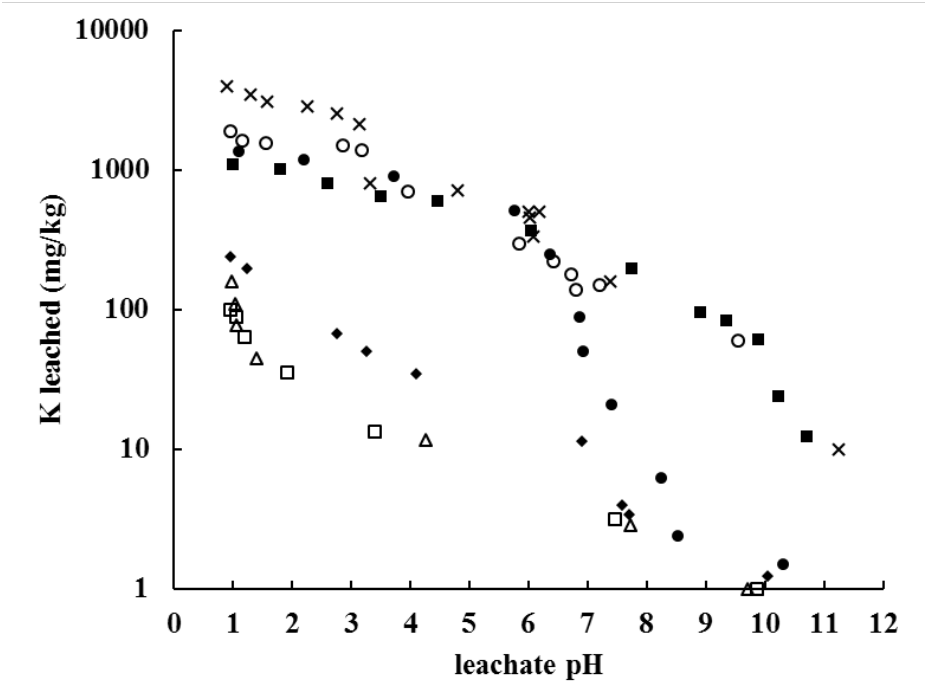

(b)

Figure 7.15: Leaching data for (a) Na and (b) K as a function of leachate pH for the as-received wet discharged fine IBA, milled 80 wt.% wet discharged fine IBA: 20 wt.% glass, calcined milled powders at 600 °C, 800 °C, 1000 °C, 1080 °C and calcined milled powders at 1080 °C and sintered at 1080 °C.

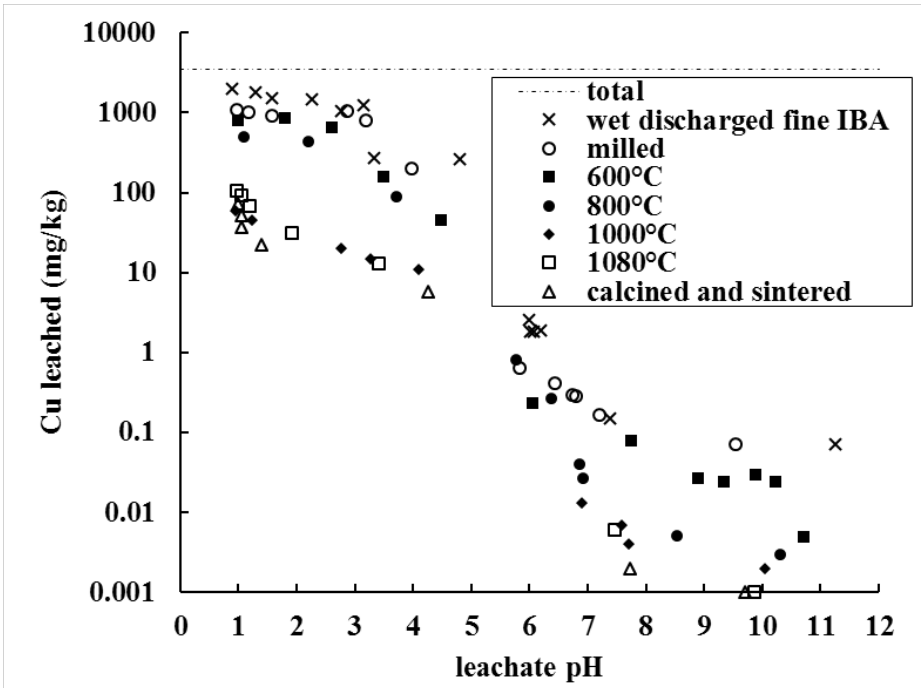

(a)

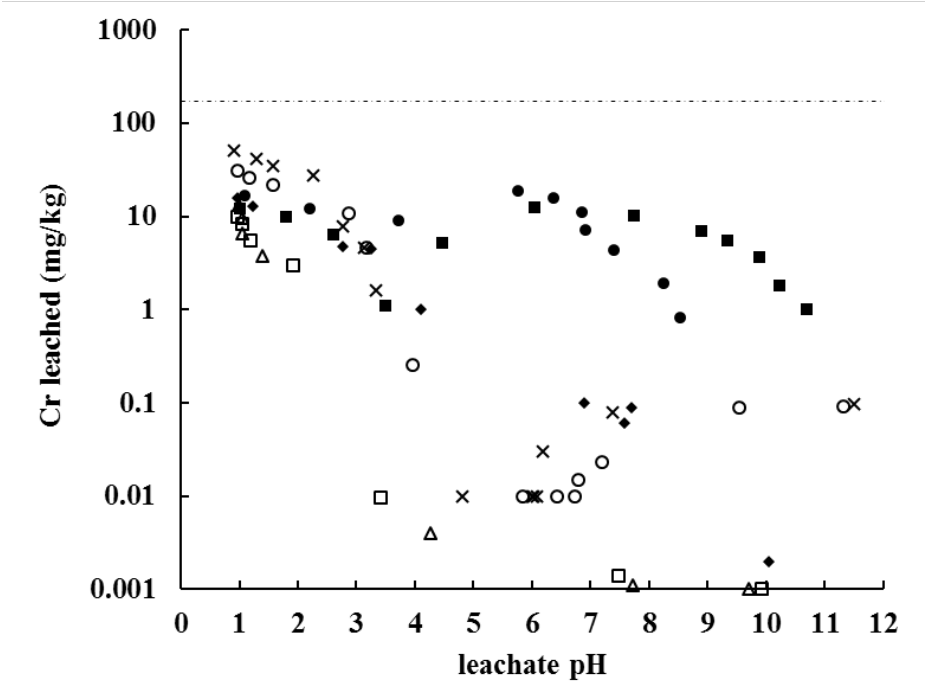

(b)

Figure 7.16: Leaching data for (a) Cu and (b) Cr as a function of leachate pH for the as-received wet discharged fine IBA, milled 80 wt.% wet discharged fine IBA: 20 wt.% glass, calcined milled powders at 600 °C, 800 °C, 1000 °C, 1080 °C and calcined milled powders at 1080 °C and sintered at 1080 °C.

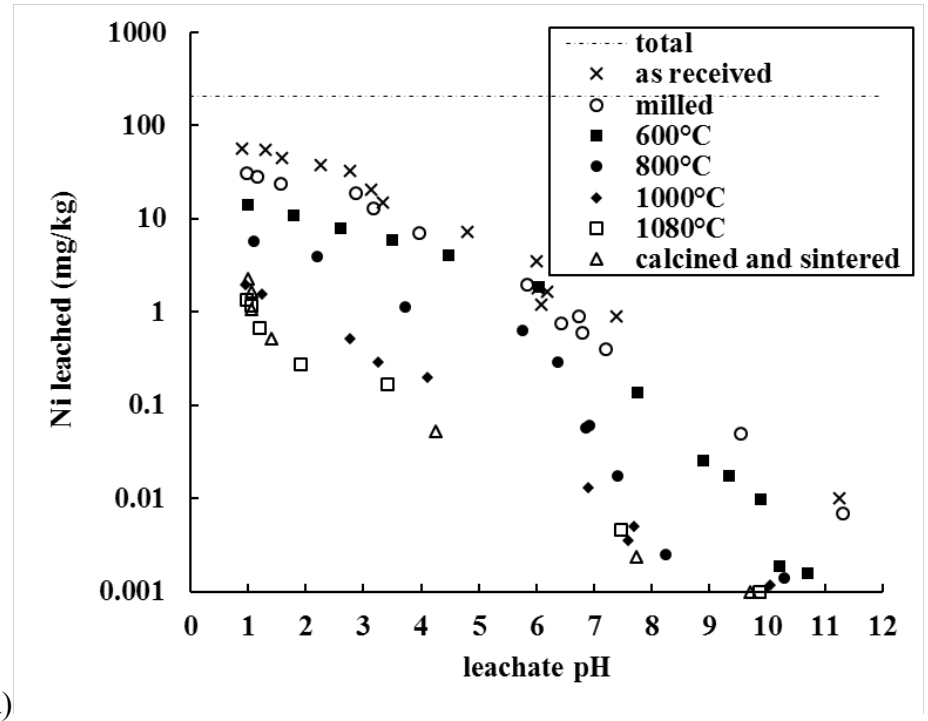

(a)

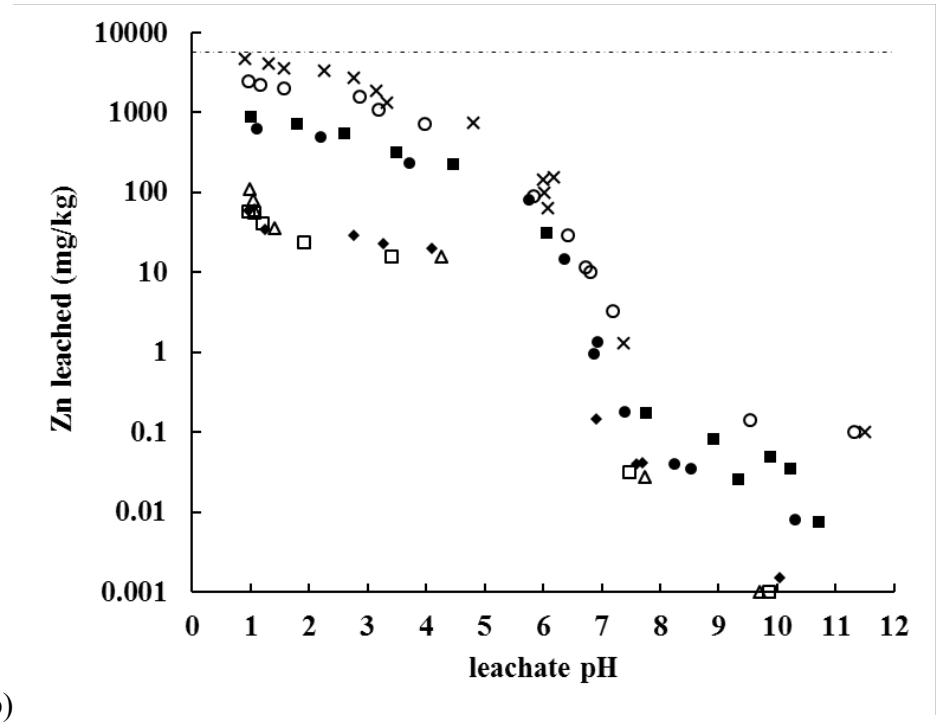

(b)

Figure 7.17: Leaching data for (a) Cu and (b) Cr as a function of leachate pH for the as-received wet discharged fine IBA, milled 80 wt.% wet discharged fine IBA: 20 wt.% glass, calcined milled powders at 600 °C, 800 °C, 1000 °C, 1080 °C and calcined milled powders at 1080 °C and sintered at 1080 °C.

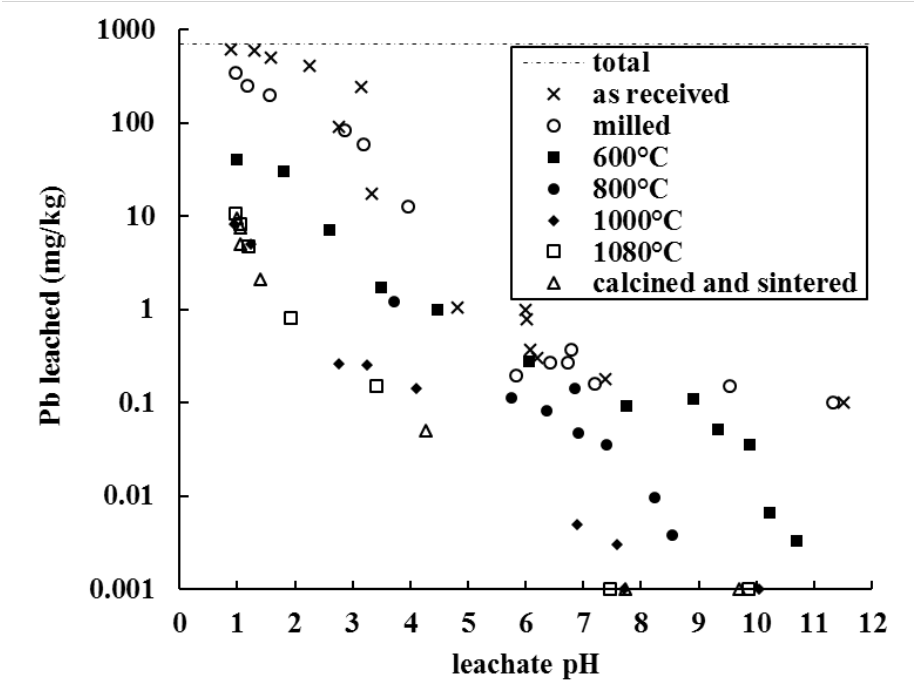

(a)

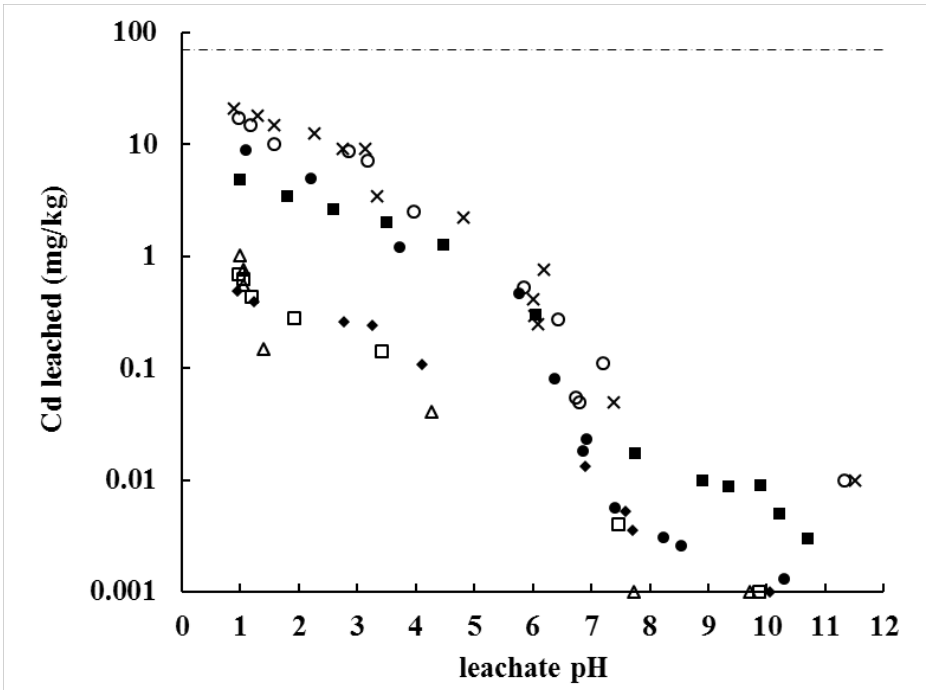

(b)

Figure 7.18: Leaching data for (a) Pb and (b) Cd as a function of leachate pH for the as-received wet discharged fine IBA, milled 80 wt.% wet discharged fine IBA: 20 wt. % glass, calcined milled powders at 600 °C, 800 °C, 1000 °C, 1080 °C and calcined milled powders at 1080 °C and sintered at 1080 °C

Table 7.2: Effect of processing on leaching of selected heavy metals under aggressive leachate conditions (pH 3).The total concentration of heavy metals in the as received wet discharged IBA were obtained by ICP-AES. Leaching data are reported for the as-received wet discharged fine IBA, calcined milled powder containing 80 wt.% wet discharged fine IBA: 20 wt.% glass at 1080 °C and calcined milled powders at 1080 °C and sintered at 1080 °C. The % reduction in leaching of heavy metals after calcining at 1080 °C and after calcining and sintering at 1080 °C is also reported and presented with bold letters in the corresponding columns.

		Amount leached (leachate pH 3)				
	Concentration in wet discharged fine IBA	**As-received wet discharged fine IBA**	**Powder calcined at 1080 °C**		**Powder calcined at 1080 °C and sintered at 1080 °C**	
	mg/kg	**mg/kg**	**mg/kg**	**% reduction**	**mg/kg**	**% reduction**
Cr	240	75	3.6	**95.2**	1.9	**97.5**
Cu	6,850	940	32	**96.6**	26	**97.2**
Ni	215	22	0.7	**96.8**	0.12	**99.4**
Cd	85	10.2	0.21	**97.9**	0.11	**98.9**
Zn	9,100	2,230	14.6	**99.3**	11.2	**99.5**
Pb	420	110	1.8	**98.3**	0.9	**99.2**

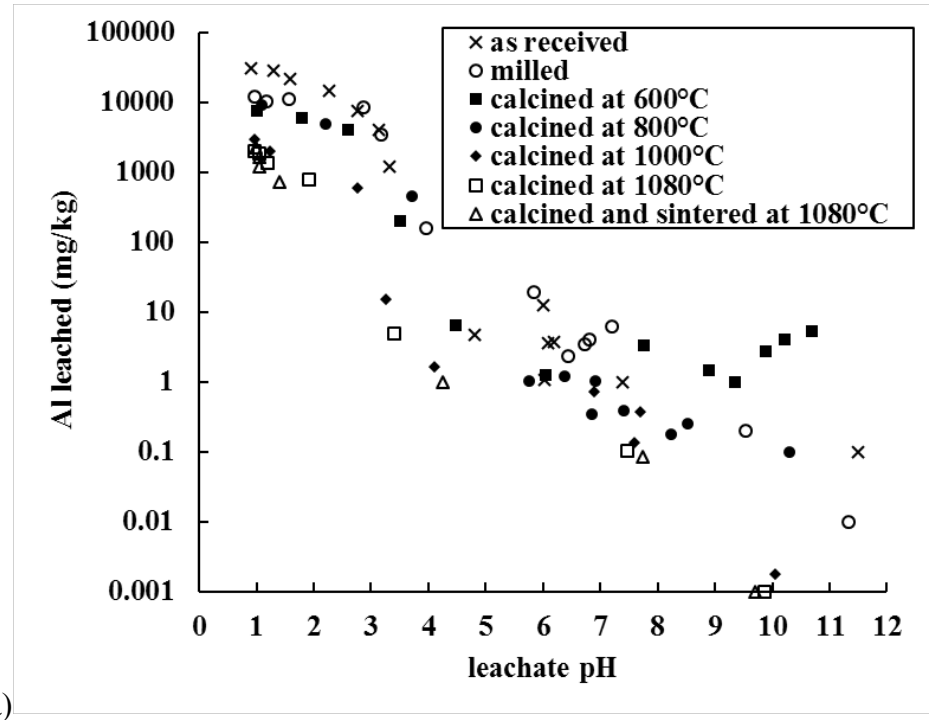

(a)

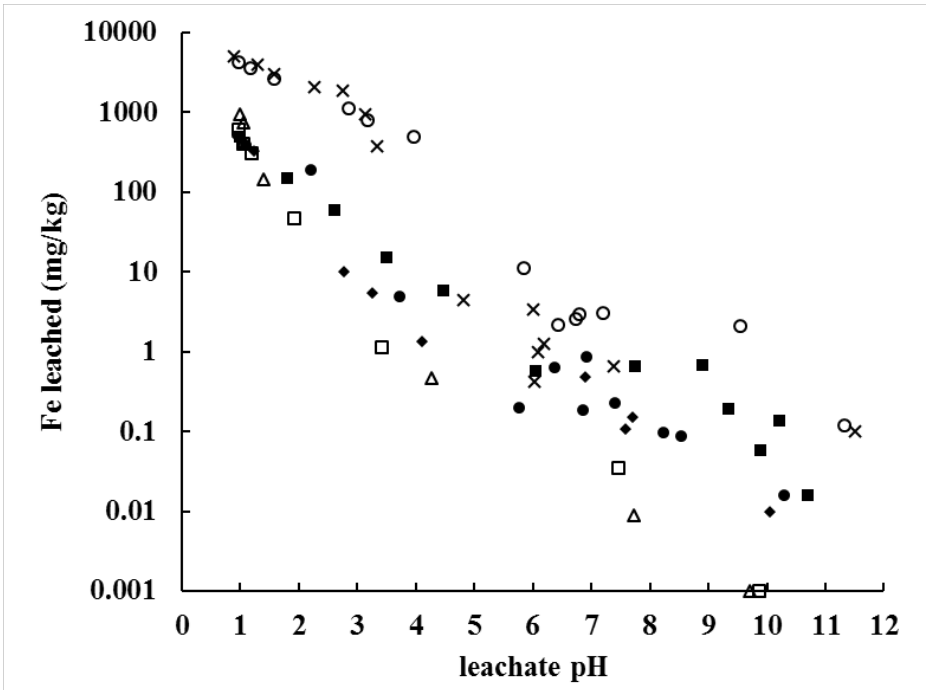

(b)

Figure 7.19: Leaching data for (a) Al and (b) Fe as a function of leachate pH for the as-received wet discharged fine IBA, milled 80 wt.% wet discharged fine IBA: 20 wt.% glass, calcined milled powders at 600 °C, 800 °C, 1000 °C, 1080 °C and calcined milled powders at 1080 °C and sintered at 1080 °C.

7.4.10 Fate of sulphates and chlorides of the wet discharged fine IBA and processed material

Sulphate and chloride concentrations in the as-received wet discharged fine IBA, the milled material, the calcined at 1080 °C powder and the optimum ceramic are presented in Table 7.3.

Mixing wet discharged fine IBA with 20 wt. % glass and wet milling, produced a powder with 23.4% reduction in the sulphate concentration and 62.5 wt. % reduction in the chloride concentration. This is associated with the presence of sulphates and chlorides as soluble salts in the as-received material, which are removed after contact with water. Powders calcined at 1080 °C exhibited a 94 wt.% reduction in sulphates concentration and about 95 wt.% reduction in chlorides concentration, associated with the evaporation of metal sulphates and chlorides normally above 1000 and 900 °C, accordingly (Sorensen et al., 2001; Belevi and Langmeier, 2000; Morf et al., 2000; Bethanis et al., 2004). The optimum sintered ceramic exhibited the lowest sulphate and chloride concentration with approximately 96 wt. % reduction in both elements compared to the as-received material.

Table 7.3: Effect of processing on sulphate and chloride concentration. Data are reported for the as-received dry discharged fine IBA dust, milled 80 wt.% dry discharged fine IBA dust: 20 wt.% glass, calcined milled powder at 1080 °C and calcined milled powders at 1080 °C and sintered at 1080 °C. Chloride and sulphate concentration is reduced by 96% by weight for the calcined at 1080 °C powder and sintered at 1080 °C ceramic.

	Sulphate (weight %)	**Chloride (weight %)**
As-received fine IBA	2.35	1.71
80wt.% IBA: 20wt.% glass wet milled	1.80	0.64
Calcined at 1080 °C IBA: glass powder	0.14	0.09
Sintered ceramic	0.09	0.07

7.5 CONCLUSIONS

The less than 4 mm fine IBA fraction obtained from a wet discharge process has been used for the production of ceramics using the optimised process developed for the dry discharged fine IBA dust.

It has been found that the challenging wet discharged fine fraction of IBA can be processed to produce pyroxene group ceramics, with similar properties compared to the ceramics produced with the dry discharged material. Calcined wet discharged fine IBA/glass powders compact to give higher green densities, have low firing shrinkage (~6 %) and produce sintered ceramics with high densities (2.78 g/cm^3), negligible water absorption and high Vickers micro hardness (4.5 GPa). While quartz and calcite are major crystalline phases present in as-received wet discharged fine IBA, diopside ($CaMgSi_2O_6$), clinoenstatite ($MgSiO_3$) and andradite ($Ca_3Fe_2Si_3O_{12}$) are the pyroxene group crystalline phases present in calcined powders and ceramics sintered at 1080 °C. Calcining and sintering significantly reduces the ANC compared to the as-received wet discharged fine IBA. The wet discharged fine IBA during processing exhibit reduced leaching in all metals examined under all pH conditions due to encapsulation and incorporation into glassy and crystalline phases.

CHAPTER 8 DISCUSSION

The objective of this research was to develop a manufacturing process for the production of an inert material suitable for the production of ceramic tiles containing a significant amount of the fine fraction of IBA. It also aimed to understand the properties of the fine fraction of IBA and fine IBA behaviour during processing and potential utilisation.

The fine fraction of IBA is a million tonnes waste material that currently sustainable utilisation techniques are not available. The disposition of IBA strongly depends on national legislations. For example, in the UK, wet discharged fine IBA is landfilled as-received, while in Switzerland the dry discharged fine IBA is mixed with cement and filter ashes and disposed of in hazardous landfills.

The research examined two different materials, derived from dry and wet discharge process. XRF data showed that the two materials are different since the composition was different. The TGA showed that the dry and wet discharged fine IBA fraction decompose at different rates with increasing temperature. The fine as-received IBA samples exhibited similar crystalline phases, as the XRD analysis showed. Ceramics produced from the fine fraction of IBA derived from a wet discharged process exhibit similar properties as the ceramics produced from the dry discharged fine IBA fraction. However, the < 4 mm wet discharged material after wet milling and sieving produced 10 to 15 wt.% > 500 μm fraction and this cannot be processed. This fraction mainly consists of rounded glass and other difficult to mill materials, such as rock, bone, wood, some plastic and metal. The dry discharged material had negligible loses after milling and sieving, associated with the more efficient air separated dry discharge Martin system used for the production of this material (Appendix B). However, the processing of these materials for the production of an inert powder suitable for ceramic manufacturing was similar.

The fine fraction of IBA derived from a dry discharge process was subjected to ceramic processing using conventional ceramic technology. This involved wet milling, drying and sieving to less than 500 μm, powder compaction and sintering. The addition of glass to the initial mixture was also investigated. The aim of this part of the research was to a better understanding of the dry discharged fine IBA dust fraction characteristics and its behaviour during processing. The produced materials were characterised in terms of physical, chemical, mineralogical and

microstructural properties. The leaching behaviour during processing of the optimum mixture composition was also investigated.

This part of the research has demonstrated that the fine fraction of dry discharged IBA dust can be combined with ~20 wt. % glass and processed to form pyroxene mineral containing ceramics. The addition of glass has the effect to aid liquid phase sintering and resulted in lower sintering temperatures than the materials containing little or no glass. Milling produces homogeneous powders suitable for further processing. The 24 hours milling time was the most effective and this was chosen as the optimum milling time.

The properties and microstructure of the produced ceramics are controlled by sintering. Dry discharged fine IBA dust: glass mixtures sintered at 1040 °C produce ceramics with maximum density, although the appearance of these samples indicated that these were not properly sintered. Samples fired at higher temperatures exhibited reduced density associated with the formation of internal closed porosity, responsible for increased skeletal density and subsequent improvement of the appearance of the ceramic body formed. Samples fired at 1080 °C exhibited the lowest water absorption and the highest hardness, but indicated high linear shrinkage (~20%) associated with deformation and warping after sintering. However, these conditions were chosen as the optimum on the basis of the produced properties and appearance.

The microstructure of samples fired at 1080 °C indicated an extensive volume of isolated, spherical pores, associated with the decomposition of volatile gases present, such as alkali metal sulphates, and the entrapment of the gases within the glassy phase formed. Therefore, sintering at 1080 °C causes liquid phase sintering and pore formation due to gas evolution.

Analysis of XRD data indicates sintering is responsible for extensive changes in the crystalline phases present. The original dry discharged fine IBA dust contains quartz (SiO_2), calcite ($CaCO_3$) gehlenite ($Ca_2Al_2SiO_7$) and hematite (Fe_2O_3) while the sintered ceramic contain predominantly diopside ($CaMgSi_2O_6$), clinoenstatite ($MgSiO_3$) and andradite ($Ca_3Fe_2Si_3O_{12}$). The combination of these effects, densification, pore formation and crystalline phase changes, are associated with sintering that is difficult to control and subsequently the production of ceramic tiles from dry discharged fine IBA dust using a pressing sintering route is unlikely to be feasible.

The acid neutralisation capacity of sintered dry discharged fine IBA dust is significantly reduced compared to the as-received dry discharged fine IBA dust. This is typically associated

with the solubilisation of alkali and alkali earth metals when the material contacts water during milling, the decomposition of $CaCO_3$ to CO_2 and CaO, and the subsequent encapsulation and incorporation of CaO into the glassy matrices formed.

Increasing the sintering temperature has the effect to significantly reduce Ca, Mg and K leached concentrations of the IBA: glass mixes under all pH conditions examined. The similarity in the leaching curves of Mg and Ca of as-received dry discharged fine IBA dust supports the possible role of calcite in controlling Mg leaching. Na leached concentration was also significantly reduced for materials sintered above 1040 °C. Sintering dry discharged fine IBA dust: glass mixes at 1020 °C resulted in materials with similar Na leaching behaviour compared to the as-received material, associated with the partial sintering of these materials. Sintering at 1080 °C produced materials with maximum resistance against leaching compared to the other sintering temperatures investigated under all pH conditions examined.

Sintering had similar effect to the leaching behaviour of heavy metals investigated under all pH conditions (Cr, Cu, Ni, Zn, Cd and Pb).Increasing the sintering temperature resulted in a reduction in heavy metals leached concentration for all pH conditions examined. Sintering has the effect to incorporate these heavy metals within the stable matrices of the silicate and alumino-silicate minerals formed.

The effect of calcining the dry discharged fine IBA dust: glass powders before sintering, in order to remove the volatile elements responsible for the high firing shrinkage, was investigated. Calcining the ball milled powder produced samples with improved properties and significantly reduced linear shrinkage during sintering. The green density of the samples produced with calcined powders increased due to improved particle packing and subsequently the firing linear shrinkage decreased from 20 % for uncalcined powder to less than 7% for powders calcined at optimum temperatures, which is similar or slightly lower than the shrinkage observed during sintering of typical clay ceramics.

Calcining between 1000 and 1080 °C produces samples that indicated significant increase in density, associated with a reduction in pore volume, also in agreement with the density measurements. XRD analysis of dry discharged fine IBA dust: glass calcined at increasing temperatures indicates that the amount of quartz (SiO_2), calcite ($CaCO_3$), gehlenite ($Ca_2Al_2SiO_7$) and hematite (Fe_2O_3) decrease on calcining and these crystalline phases are no longer present after calcining at 1080 °C. The dominant phases formed are diopside ($CaMgSi_2O_6$),

clinoenstatite ($MgSiO_3$) and andradite ($Ca_3Fe_2Si_3O_{12}$) with some garnet group crystalline phases such as andradite ($Ca_3Fe_2Si_3O_{12}$). XRD analysis of powders calcined at 1000 °C revealed that diopside was the principal crystalline phase, with clinoenstatite and andradite also present and small amounts of hematite and augite. Calcining at 1080 °C produces powders with main crystalline phases as diopside ($CaMgSi_2O_6$), clinoenstatite ($MgSiO_3$) and andradite ($Ca_3Fe_2Si_3O_{12}$). Diopside is calcium pyroxenes, while clinoenstatite is a magnesium pyroxene. Pyroxenes are an important group of rock-forming silicate minerals of variable composition typically containing Ca, Mg and Fe. They occur as stable phases in almost every type of igneous rock and are found in rocks of widely different composition. Pyroxene ceramics produced from dry discharged fine IBA dust/glass powder calcined at 1080 °C exhibit pores within a denser ceramic matrix that have a much finer and more consistent size distribution compared to ceramics manufactured from uncalcined powder.

The densification of the material is associated with the elimination of surface area in the powder compact, also responsible for the firing shrinkage. The last stage of liquid phase sintering involves liquid movement from efficiently packed regions into pores and causes grain growth and densification. There is an extensive change in the crystalline phases and decomposition reactions that produce pore forming gasses occur during calcining rather than during sintering. This results in the transformation of the dry discharged fine fraction of IBA dust powder into a ceramic raw material that is not associated with the detrimental effects observed for uncalcined powders.

The carbonated as-received dry discharged fine IBA dust displayed a fairly constant rate of pH decrease with acid addition. $CaCO_3$ is present in the as-received dry discharged fine IBA dust and as a result of carbonation during ageing. This provides significant buffering capacity to acid addition due to the formation of Ca^{2+}, HCO_3^- and OH^- ions when water is added.

While the as-received dry discharged fine IBA dust show significant ANC at pH 5 to 6, calcined dry discharged fine IBA dust: glass powder and sintered ceramics exhibit a rapid decline in leachate pH with acid addition through this pH range, indicating reduced ANC. This reduction in ANC from calcining dry discharged fine IBA dust: glass is primarily due to the decomposition of $CaCO_3$ to CaO and CO_2 that occurs during calcining, combined with subsequent encapsulation and incorporation of Ca^{2+} in both amorphous and crystalline phases present in the processed fine IBA

The addition of acid releases high concentrations of Ca from soluble mineral phases such as $CaCO_3$, $CaSO_4$, $CaCl_2$, CaO and Ca-silicates present in the aged as-received dry discharged fine IBA dust. Calcining at 1080 °C and sintering at 1080 °C significantly reduced Ca leaching and this is believed to be related to the formation of less-soluble calcium silicates, such as diopside or andradite, that encapsulate Ca in the crystalline phases formed. Na and K are released from the aged as-received fine IBA over a wide pH range. There is significantly reduced Na and K leaching from the sintered at 1080 °C ceramic produced with calcined at 1080 °C powder under alkaline conditions. Sintered ceramic with calcined at 1080 °C powder exhibit significant reduction in Mg leaching.

There is no significant leaching from dry discharged fine IBA dust: glass powder calcined at 1080°C and sintered at 1080°C down to very aggressive acid leachate pH conditions. Calcining of as-received dry discharged fine IBA dust and glass significantly reduced Cu leaching to very low levels. The Zn solubility is very sensitive to pH and the metal is reported to be present in IBA as zinc silicates or aluminates. Calcining and sintering dry discharged fine IBA dust at 1080°C substantially improved Zn leaching at extreme pH conditions, due to inertization of Zn to compounds of low solubility, as reported by other researchers. The Pb leaching rapidly reduced with calcining and sintering at 1080 °C. The most readily available heavy metals are Pb, Zn and Cu and are considered as being potentially leachable from the dry discharged fine IBA dust. Approximately 30 to 35% is potentially available for leaching under aggressive leachate conditions. This reduces to less than 0.5% on calcining and sintering at the optimum conditions. The percentage reduction in leaching resulting from calcining and sintering dry discharged fine IBA dust and glass at 1080 °C was greater than 99% for all heavy metals examined.

The Al leaching curve for the aged as-received dry discharged fine IBA dust is generally characterised by a V-shaped pH-leaching curve. During carbonation of IBA, $Al(OH)_3$ and amorphous aluminosilicates are formed. Sintering at 1080 °C with calcined at 1080 °C powder reduced Al leaching, due to fixation to crystalline phases.

Strong interdependencies between the linear shrinkage, the density and the water absorption were observed, and this is in accordance with the observations of other researchers (Velis et al., 2014; Aloisi et al., 2006; Cheeseman et al., 2003; Barbieri et al., 2002). The next step of the research involved the optimization and the identification of the boundaries of the process developed. Response Surface Methodology was therefore used, which allows the

identification of the optimum processing conditions with defined input and outputs. The inputs included glass addition, sintering temperature and calcining temperature, since these parameters have been identified as critical important and able to control the properties of the final products. The output variables were defined as density, water absorption and linear shrinkage of the produced materials. Sintering temperature and glass content were the most significant parameters ($p < 10^{-7}$) in explaining the most of the variation in the density and were the critical factors in controlling the water absorption and linear shrinkage of the produced materials. Calcining temperature is less significant ($p< 10^{-5}$) in determining density and water absorption, however it plays a critical role in controlling the linear shrinkage of the sintered ceramics.

The mixture composition containing 20 and 30 wt. % glass were the optimum, since these exhibited the highest density, lowest water absorption and linear shrinkage within the acceptable limits. However, since the research dealt with the resource efficiency of the fine fraction of IBA, mixture compositions containing 20 wt. % glass were defined as the optimum mixes. Optimum processing conditions involve the addition of 20 wt.% glass, wet ball milling for 24 hours to produce a homogeneous powder suitable for further processing, calcining at 1080 °C to eliminate the volatiles present in dry discharged fine IBA dust, pressing to form samples suitable for firing and sintering at 1080 °C. The produced ceramic exhibited high density (~ 2.7 $g.cm^{-3}$), low linear shrinkage (~5.5%) and negligible water absorption.

However, IBA is a heterogeneous material and its properties are directly related to the MSW feedstock, seasonal and topographical variations, and from the IBA discharge technique applied. Wet discharged IBA has typically coarser particles, since contact with water is associated with strong agglomerations. Therefore, fine IBA derived from a wet discharged technique was used in order to validate the process developed. The fine fraction of this material represents approximately 40 wt. % of the total IBA discharged, and its size fraction is less than 4 mm.

Ceramics produced using the optimum processing conditions also exhibited significantly reduced linear shrinkage during firing and this was associated with a higher ‘green’ density in the pressed but unfired compacted sample. High shrinkage during firing of ceramics tended to be associated with warping and deformation of sintered products, as was the case of processing the dry discharged fine IBA dust. The percentage shrinkage of the optimum ceramics were similar or slightly lower than the shrinkage measured for the ceramics produced from the dry discharged

sample. Shrinkage during sintering and the associated increase in density is driven by the elimination of surface area in the powder compact and this is also significantly aided by the fluxing effect of the added waste glass which promotes liquid phase sintering.

The calcining stage involved heating the milled wet discharged fine IBA and glass to above 1000 ºC and this transformed the crystalline phases present in the IBA so that post calcining the powder formed is no longer the original wet discharged fine IBA. XRD data indicate that the original wet discharged fine IBA fraction contains quartz (SiO_2), calcite ($CaCO_3$) gehlenite ($Ca_2Al_2SiO_7$) and hematite (Fe_2O_3) as the major crystalline phases. Post calcining the crystalline phases present are predominantly the pyroxene-group minerals diopside ($CaMgSi_2O_6$), clinoenstatite ($MgSiO_3$) and wollastonite ($CaSiO_3$) together with some albite ($NaAlSi_3O_8$) and andradite ($Ca_3Fe_2Si_3O_{12}$). Heating the milled wet discharged fine IBA: glass mix also volatilises trace phases that would otherwise cause problems during sintering. As a result a much denser ceramic microstructure was formed from sintering the calcined powder in comparison to the as milled powder.

The as-received wet discharged fine IBA exhibited a fairly constant rate of pH decrease with acid addition, similarly to the processing of the dry discharged sample. Carbonation during ageing of IBA, leads to the formation of $CaCO_3$, which provides significant buffering capacity (Van der Sloot et al, 2013; Guimaraes et al, 2006). The sintered ceramics show rapid decline in leachate pH with acid addition, indicating reduced ANC compared to the as-received wet discharged fine IBA. Calcining decomposes $CaCO_3$ to CaO and CO_2 and the CaO then forms new amorphous and crystalline phases in the processed wet discharged fine IBA: glass mix (Guimaraes et al., 2006; Van der Sloot et al, 2012).

Leaching of Ca occurs from soluble minerals phases present in the as-received wet discharged fine IBA, such as $CaCO_3$, $CaSO_4$, $CaCl_2$, CaO and Ca-silicates. The ceramics produced using optimum processing leach much less Ca due to the formation of low solubility calcium silicates, such as diopside, wollastonite or andradite. Na, K and Mg leach from the as-received wet discharged fine IBA over a wide pH range and this is also significantly reduced from optimum sintered ceramics.

The optimum processed ceramics exhibited low leaching down to very aggressive acid leachate pH conditions. Cu, Zn and Pb are incorporated within the phases forming during sintering. Cu leaching was reduced to very low levels after processing the as-received wet

discharged fine IBA and glass. Zn is present in the wet discharged fine IBA: glass mix as zinc silicates and aluminates, which are highly soluble. Pb is also readily leached from the as-received wet discharged fine IBA. The percentage reduction in leaching resulting from processing wet discharged fine IBA and glass under optimum conditions was greater than 99% for all the metals examined.

Therefore, processing wet discharged fine IBA by using similar conditions as the optimised process for the dry discharged material, produced ceramic materials with similar properties and behaviour as the dry discharged fine IBA dust.

The process developed can be used for the inertization and sustainable utilisation of the fine fraction of IBA. The main barrier of the process is the two stage heating, calcining and sintering, which is an energy intense process for the production of a low cost ceramic. However, the environmental burden and high cost of disposal associated with the utilisation of the fine IBA fraction counterbalance this barrier. Therefore, the potential for scaling up the process is strongly recommended. In doing so, a detailed cost-benefit analysis and a Life Cycle Assessment (LCA) is recommended, where all the inputs of the system should be taken into account. The process developed should be compared to the current method of disposal, i.e. landfilling, and with the traditional ceramic manufacturing processes. The use of recycled glass should be evaluated and the use of additives in the processing, such as the use of organic binder, PEG, and the use of water should be also taken into account.

CHAPTER 9 CONCLUSIONS AND RECOMMENDATIONS

9.1 CONCLUSIONS

The key conclusions from the research are:

- The research examined two different fine IBA fractions, derived from dry and wet discharge process. However, the processing of these materials for the production of an inert powder suitable for ceramic manufacturing was similar. Compositions contained 70 wt. % fine IBA: 30 wt. % glass and 80 wt. % fine IBA: 20 wt. % glass formed ceramics with improved properties than the commercial Terracotta ceramics. However, since the aim of the research was the utilisation of the fine IBA fraction, the 80 wt. % fine IBA: 20 wt. % glass was chosen as the optimum mixture composition. The successful processing of this significant amount of fine IBA fraction has not previously been achieved and is considered a significant achievement from this research.

- Inertization of the optimum mixture composition was achieved when the fine IBA: glass mixture was calcined at 1080 °C. This material was suitable for the manufacture of ceramics when pressed and sintered at 1080 °C. The research has also presented, for the first time, an evaluation of the leaching behaviour of metals present in the fine IBA fraction when heated at different temperatures.

- Calcining at optimum temperatures had the effect of transforming the crystalline phases of the as-received fine IBA fraction. The produced ceramics indicated significantly reduction in the linear shrinkage and increase in the density compared to ceramics produced with uncalcined powders and to the commercial Terracotta ceramics. The development of a process able to transform the problematic fine fraction of IBA into an inert material suitable for the production of ceramics with high density and minimal linear shrinkage is a significant contribution.

9.1.1 Physical properties and microstructure of produced samples

- Liquid phase sintering is the responsible mechanism for the relatively high-density of the materials obtained. The addition of glass accelerates liquid phase sintering and the densification point is subsequently reduced as the glass content increases.

- Sintering fine IBA: glass powders without calcining results in excessive shrinkage and samples tend to deform during firing, making the production of tiles difficult with volatilisation reactions producing excessive porosity.

- Firing at 1080 °C causes liquid phase sintering and pore formation due to gas evolution. Samples produced with uncalcined powders exhibited a microstructure that contains an extensive network of spherical pores formed from decomposition of volatile phases present in the fine IBA fraction, such as alkali metal sulphates. This is observed at temperatures where softening of the glassy phase occurs and the gasses generated remain trapped as pores in the microstructure.

- Calcining fine IBA: glass powders produces powders that can be pressed to give higher green densities. These have low firing shrinkage (~4%) and produce sintered ceramics with high densities (2.78 g/cm^3), negligible water absorption and high Vickers micro hardness (4.5 GPa). Calcining removes the volatile compounds present in the fine IBA and is associated with weight loss of about 14 wt.%.

9.1.2 Leaching behaviour and crystalline phases transformations

- Calcining and sintering significantly reduces the ANC compared to the as-received fine IBA due to decomposition of calcite ($CaCO_3$) to CaO and CO_2 during processing and incorporation of CaO into the new more stable crystalline structures formed.

- The fine IBA fraction during processing exhibit reduced leaching in all metals examined under all pH conditions due to encapsulation of these ions within the glassy phases present in the calcined and sintered materials. The optimum ceramic exhibited negligible leaching of heavy metals of environmental concern under extreme acidic conditions.

- The sulphates and chlorides concentration was reduced by about 99% for the optimum ceramics produced by the two different fine IBA fractions examined. This is associated with the evaporation of metal sulphates and chlorides above 1000 and 900 °C, respectively.

- Processing of the fine fraction of IBA derived from a wet discharged process had similar effect on the transformation of the crystalline phases present in the as-received material as the processing of the dry discharged fine IBA dust. While quartz and calcite are major crystalline phases present in the as-received fine IBA, diopside ($CaMgSi_2O_6$), clinoenstatite ($MgSiO_3$) and andradite ($Ca_3Fe_2Si_3O_{12}$) are the pyroxene group crystalline phases present in calcined powders produced from the fine IBA and ceramics sintered at 1080 °C. This is due to calcining above 1000 °C produces materials with less-soluble calcium silicates phases, such as diopside or andradite, that encapsulate Ca in the crystalline phases formed.

9.1.3 Process envelopes of the technique developed

- The addition of glass together with suitable calcining and sintering temperatures controls the processing of the fine IBA fraction for the manufacture of ceramics. The process developed can be adjusted according to the needs of the final product, therefore, a variety of materials can be produced with respect to the required properties of the final product, creating multiple benefits for the EfW industry.

- Response Surface Methodology indicated that calcining temperature is the most significant process parameter affecting the linear shrinkage of sintered ceramics. Density and water absorption is mainly controlled by the sintering temperature and the glass addition. Mixes containing 20 and 30 wt. % glass exhibited densities > 2.1 $g.cm^{-3}$ for all calcining temperatures examined, when sintered between 1040 to 1080 °C and 1020 to1080 °C, respectively. Linear shrinkage typically decreases with calcining temperature and increases with sintering temperature. Samples containing 20 and 30 wt. % glass calcined above 1100 °C exhibited linear shrinkage < 8% for all sintering temperatures.

Mixes containing 10 wt. % or no glass when calcined above 1050 and 1000 °C for all sintering temperatures achieved linear shrinkage within the defined limits, accordingly.

- Sintering temperature and glass content promote liquid phase sintering. Increased liquid phase sintering increases density and reduces connected porosity and therefore water absorption. Mixes containing 20 and 30 wt. % glass, sintered above 1060 °C for all calcining temperatures, exhibited water absorption within the defined limits. Higher sintering temperatures (>1100 °C) for all calcining temperatures are needed to achieve minimal water absorption for mixes containing 10 wt. % and no glass.

9.2 CONTRIBUTIONS TO KNOWLEDGE

1. A novel treatment technique for transforming the problematic fraction of IBA into an inert material suitable for the production of ceramics has been developed.
2. The crystalline phase transformations that occurs during this processing of fine IBA have been characterised.
3. The effect of adding glass has been evaluated. This promotes liquid phase sintering and produces hard dense ceramics with improved appearance.
4. The effect of calcining IBA: glass mixes has been investigated and found to minimize linear shrinkage during sintering to form ceramic samples.
5. The research has demonstrated that thermal treatment reduces the leaching of metals present in fine IBA by over 95%.

9.3 RECOMMENDATIONS FOR FURTHER WORK

- The potential for scaling up the process should be examined, since the innovative process developed shows great potential to alleviate the unsustainable disposal of the millions of tonnes of fine IBA generated annually in over 450 EfW plants in Europe. The fine fraction is defined as the IBA fraction that remains after ferrous, non-ferrous separation and sorting of the medium and coarse secondary aggregates. For which alternative uses are not currently available. In each case, the variability of the fine fraction of IBA should

be investigated. The study will examine the variance in the composition of the fine IBA with time, location and different types of combustion chambers. In addition, differences between the laboratory process developed and the pilot scale should be identified. These may include the milling time and the production of a spherical powder after calcining suitable for pressing and sintering. The later could be developed by spray drying the calcined powder.

- A detailed cost-benefit analysis assessing the potential of scaling-up the process is strongly recommended. The costs of collection, transportation and disposal of the fine fraction of IBA, together with the clay extraction costs should be compared with the costs of utilizing the fine IBA fraction for ceramic tile production. In addition, the market of the ceramic tiles that can be produced should be identified and the barriers to commercial exploitation should be determined. These could be the two stage heating of the process developed, however, the benefits of sustainable utilizing the fine IBA fraction should be considered.

- In order to further assess the sustainability of the ceramic tiles produced from the fine IBA fraction, the leaching potential should be further evaluated. The use of other leaching tests, such as batch, column and compacted granular leaching tests should be considered.

- The environmental considerations of the process developed throughout the Life Cycle of the product is recommended. A cradle-to-cradle approach is needed in order to evaluate the environmental risks and identify the bottlenecks of the process throughout its life cycle. These maybe associated with the use of waste glass, the organic binder and the use of water during processing.

REFERENCES

Acchar W., Vieira F., Segadães A.M., 2006. Using ornamental stone cutting rejects as raw materials for red clay ceramic products: Properties and microstructure development. Mater Sci Eng A. 435-436, 606-610.

Alkemade M.M.C, 1994. How to prevent expansion of MSWI Bottom Ash in road construction, in: Environmental Aspects of Construction with Waste Materials (Goumans J.J.J.M. et al. eds), Elsevier, Amsterdam, pp.863-877.

Allegrini E., Butera S., Kosson D.S., van Zomeren A., Van der Sloot H.A., Astrup T.F., 2015. Life cycle assessment and residue leaching: The importance of parameter, scenario and leaching data selection

Allegrini E., Maresca A., Olsson M.E., Holtze M.S., Boldrin A., Astrup T.F., 2014. Quantification of the resource recovery potential of municipal solid waste incineration bottom ashes. Waste Management 34(9), 1627-1636.

Aloisi M., Karamanov A., Taglieri G., Ferrante F., Pelino M., 2006. Sintered glass ceramic composites from vitrified municipal solid waste bottom ashes. J. Hazard Mater. 137 (1), 138-143.

American Public Health Association- American Water Works Association- Water Environment Federation (APHA- AWWA-WEF), 1992. Standard methods for examination of water and wastewater, 18th ed., Washington DC, PP. 1-57.

Andreola F., Barbieri L., Hreglich S., Lancellotti I., Morselli L., Passarini F., Vassura I., 2008. Reuse of incinerator bottom and fly ashes to obtain glassy materials. Journal of Hazardous Materials 153(3), 1270-1274.

Ansari S., Munir K., Gregg T., 2012. Impact at the 'bottom of the pyramid': the role of social capital in capability development and community empowerment. J Manage Stud 49 (4): 813-842.

Appendino P., Ferraris M., Matekovits I., Salvo M., 2004. Production of glass-ceramic bodies from the bottom ashes of municipal solid waste incinerators. J. Eur. Ceram. Soc. 24 (5), 803-810.

Arickx S., De Borger V., Van Gerven T., Vandecasteele C., 2010. Effect of carbonation on the leaching of organic carbon and of copper from MSWI bottom ash. Waste Management 30 (7), 1296-1302

Astrup T., Jakobsen R., Christensen T.H., Hansen J.B., Hjelmar, O., 2006. Assessment of long-term pH developments in leachate from waste incineration residues. Waste Management Research 24, pp. 491-502.

Astrup F.T, Pedersen A.J., Hyks J., Frandsen J.F., 2010. Residues from Waste Incineration. PSO-5784.

Banks J., 1998. Handbook of simulation: modelling, estimation and control. John Wiley and Sons Inc., US.

Barbieri L., Corradi A., Lancellotti I., Manfredini T., 2002. Use of municipal incinerator bottom ash as sintering promoter in industrial ceramics. Waste Manag. 22 (8), 859-863.

Barbieri L., Karamanov A., Corradi A., Lancellotti I., Pelino M., Rincon J.M., 2008. Structure, chemical durability and crystallization behaviour of incinerator-based glassy systems. Journal of non-crystalline solids. 354(2-9), 521-528.

Baruzzo D., Minichelli D., Bruckner S., Fedrizzi L., Bachiorrini A., Maschio S., 2006. Possible production of ceramic tiles from marine dredging spoils alone and mixed with other waste materials. J. Hazard Mater. 134 (1-3), 202-210.

Belevi H. and Langmeier M., 2000. Factors determining the element behaviour in municipal solid waste incinerators. 2. Laboratory experiments, Environmental Science and Technology 34, 2507-2512.

Berg E.R. and Neal J.A., 1998. Municipal solid waste bottom ash as Portland cement concrete ingredient. Journal of Materials in Civil Engineering 10, 168-173.

Bertolini L., Carsana M., Cassago D., Quadrio Curzio A., Collepardi M., 2004. MSWI ashes as mineral additions in concrete. Cement Concrete Resources. 34(10), 1899-1906.

Bethanis, S., Cheeseman, C.R., Sollars, C.J., 2002. Properties and microstructure of sintered incinerator IBA. Ceram Int. 28 (8) 881-886.

Bethanis S., Cheeseman C.R., Sollars C.J., 2004. Effect of sintering temperature on the properties and leaching of incinerator IBA. Waste Manag. Res. 22 (4), 225-264.

Beylot A., Villeneuve J., 2013. Environmental impacts of residual Municipal Solid Waste incineration: A comparison of 110 French incinerators using a life cycle approach. Waste Management, 33(12), 2781-2788.

Bio Intelligence Service, 2012. Use of economic instruments and waste management performances, Contract ENV.G.4/FRA/2008/0112, European Commission (DG ENV). Available at: http://ec.europa.eu/ environment/waste/use.htm

Birgisdottir H., Bhander G., Hauschild M.Z, Christensen T.H., 2007. Life Cycle Assessment of disposal of residues from municipal solid waste incineration: Recycling of bottom ash in road construction or landfilling in Denmark evaluated in the ROAD-RES model. Waste Management. 27, S75-S84

Blengini G.A., Garbarino E., Solar S., Shields D.J., Hamor T, Vinai R., Agioutantis Z., 2012. Life Cycle Assessment guidelines for sustainable production and recycling of aggregates: the Sustainable Aggregates Resource Management project (SARMa). Journal of Cleaner Production. 27, 177-181

Boccaccini A. R., Bücker M., Bossert J., 1996. Glass and Glass-Ceramics from Coal Fly ash and Waste Glass, Tile and Brick International 12, 515-518.

Boccaccini A.R., Bücker M., Bossert J., Marszalek K., 1997. Glass matrix composites from coal fly ash and waste glass, Waste Management 17(1), 39-45.

Boccaccini A.R., 1999. Fabrication, microstructural characterisation and mechanical properties of glass compacts containing controlled porosity of spheroidal shape, Journal of Porous Materials 6, 369-379.

Boccaccini A.R., Schawohl J., Kern H., Schunck B., Rincon J.M., Romero M., 2000. Sintered glass ceramics from municipal incinerator fly ash, Glass Technology 41(3), 99-105.

Boccaccini A.R., Veronesi P., Leonelli C., 2001. Microwave processing of glass matrix composites containing controlled isolated porosity, Journal of the European Ceramic Society 21, 1073-1080.

Boesch M., Vadenbo C., Saner D., Huter C., Hellweg S., 2014. An LCA model for waste incineration enhanced with new technologies for metal recovery and application to the case of Switzerland. Waste Management, 378-389.

Bourtsalas A., Vandeperre L., Grimes S., Themelis N., Koralewska R., Cheeseman C., 2015. Beneficial reuse of the fine fraction of incinerator bottom ash from a dry discharge system in the manufacture of pyroxene ceramics. *Waste Manage Res.,* In Press.

Bowen D.K. and Hall C.R., 1975. Microscopy of materials- Modern imaging methods using electron, X-Ray and ion beams. The MacMillan Press Ltd. Great Britain.

Box, G. E. P. and Wilson, K. B., 1951. On the Experimental Attainment of Optimum Conditions. Journal of the Royal Statistical Society. Series B (Methodological), 13, 1-45.

Box, G. E. P. and Cox, D. R., 1982. An analysis of transformations revisited, rebutted. Journal of the American Statistical Association, 77, (377), 209-210.

Bruder-Hubshcer V., Lagarde F., Leroy M.J., Coughanowr C., Enguehard F., 2001. Utilisation of bottom ash in road construction: evaluation of the environmental impact, Waste Management and Research 19(6), 545-556.

Brunner P., Rechberger H., 2015. Waste to energy – key element for sustainable waste management. Waste Management, 37, 3-12.

BS EN ISO 10545-3:1997, Ceramic tiles- Part 3: Determination of water absorption, apparent porosity, apparent relative density and bulk density.

BS EN ISO 10545-8: 1998, Ceramic tiles – Part 8: Determination of linear thermal expansion.

BS EN ISO 12680-1:2007 Methods of test for refractory products. Determination of dynamic Young's modulus (MOE) by impulse excitation of vibration.

BS EN 14411:2012, Ceramic tiles. Definitions, classification, characteristics, evaluation of conformity and marking.

BS EN 15169:2007, Characterization of waste. Determination of loss on ignition in waste, sludge and sediments.

BS ISO 14869-2:2002, Soil quality- Dissolution for the determination of total element content- Part 2: Dissolution by alkaline fusion.

CEN/TS 14429: 2005, Characterisation of waste- Leaching behaviour tests- Influence of pH on leaching with initial acid/ base addition.

Cerame-unie: The European Ceramic Industry Association, 2013. Paving the way to 2050: The ceramic industry roadmap.

Chandler A.J., Eighmy T.T., Hartlen J., Hjelmar O., Kosson D.S., Sawell S.E., Van der Sloot H.A., Vehlow J., 1997. Municipal solid waste incinerator residues, in: Studies in Environmental Science vol. 67, Elsevier, Amsterdam.

Cheeseman C.R., Makinde A., Bethanis S., 2005. Properties of lightweight aggregate produced by rapid sintering of incinerator bottom ash. Resources, Conservation and Recycling, 43(2), 147-162.

Cheeseman C.R., Monteiro da Rocha S., Sollars C.J., Bethanis S., Boccaccini A.R., 2003. Ceramic processing of incinerator bottom ash. Waste Management 23 (10), 907-916.

Cheng A., 2012. Effect of incinerator bottom ash properties on mechanical and pore size of blended cement mortars. Materials and Design 36, 859-864.

Cheng T.W., Huang M.Z., Tzeng C.C., Cheng K.B., Ueng T.H., 2007. Production of coloured glass–ceramics from incinerator ash using thermal plasma technology. Chemosphere 68(10), 1937-1945.

Chimenos J.M., Segarra M., Femández M.A., Espiell F., 1999. Characterization of the bottom ash in municipal solid waste incinerator, J. Hazard. Mater. 64 (3), 211-222.

Cicek B., Tucci A., Bernardo E., Will J., Boccaccini A.R., 2014. Development of glass-ceramics from boron containing waste and meat bone ash combinations with addition of waste glass. Ceramics International 40(4), 6045-6051.

Cleary J., 2009. Life cycle assessments of municipal solid waste management systems: A comparative analysis of selected peer-reviewed literature. Environ Int., 35 (8), 1256-1266.

Communication from the Commission to the European Parliament, the Council, the European Economic and Social Committee and the Committee of the regions towards a circular economy: a Zero Waste Programme for Europe.

Cook, R. D., 1977. Detection of influential observation in linear-regression. Technometrics 19(1), 15-18.

Cornelis G., Van Gerven T., Vandecasteele C., 2012. Antimony leaching from MSWI bottom ash: Modelling of the effect of pH and carbonation. Waste Management 32(2), 278-286.

Council Directive 1999/31/EC of 26 April 1999 on the landfill of waste (Waste Landfill Directive)

Day A., 2012. Advances in the Processing and Use of Incinerator Bottom Ash. Society of Chemical Industries. Presentation available at:

http://www.soci.org/~/media/Files/Conference%20Downloads/2012/Lightweight%20and%20Recyclable%20Aggregates%202012/SCI_Presentation_Nov_2012__Adam_Day.ashx

Department for Environment Food and Rural Affairs (Defra), 2013. Incineration of Municipal Solid Waste. Available from https://www.gov.uk/government/uploads/system/uploads/attachment_data/file/221036/pb13889-incineration-municipal-waste.pdf

Deer W.A., Howie R.A., Zussman J., 1992. An introduction to the rock-forming minerals, Longman Group, England.

Dijkstra J.J., van der Sloot H.A., Comans R.N.J., 2006. The leaching of major and trace elements from MSWI bottom ash as a function of pH and time. Applied Geochemistry, 21 (2), 335–351

Directive 2000/76/EC of the European Parliament and of the Council of 4 December 2000 on the incineration of waste (Waste Incineration Directive)

Directive 2008/98/EC of the European Parliament and of the Council of 19 November 2008 on waste and repealing certain Directives (Waste Framework Directive)

Ducman V., Mladenovič A., Šuput J.S., 2002. Lightweight aggregate based on waste glass and its alkali–silica reactivity. Cement and Concrete Research, 32(2), pp. 223-226.

Dugenest S., Casabianca H., Grenier-Loustalot M.F., 1999. Municipal solid waste incineration bottom ash: Physicochemical characterisation of organic matter, Analysis 27(1), 75-81.

Environment Agency, 2013. Waste Sampling and Testing for Disposal to Landfill

European Commission BREF, 2007. Reference document on Best Available Techniques in the Ceramic Manufacturing Industry.

European Waste Catalogue, 2000/532/EC

Eusden J.D., Eighmy T.T., Hockert K., Holland E., Marsella K., 1999. Petrogenesis of municipal solid waste combustion bottom ash, Applied Geochemistry 14, 1073-1091.

Eymael M.M.Th., de Wijs W. and Mahadew D., 1994. The use of bottom ash in asphalt concrete, in: Environmental Aspects of Construction, Studies in Environmental Science vol. 60, Elsevier, Amsterdam.

Fan C.S., Li K.C., 2014. Glass-ceramics produced from thin-film transistor liquid-crystal display waste glass and blast oxygen furnace slag. Ceramics International 40(5), 7117-7123.

Ferrandiz-Mas V., Bond T., Garcia-Alcocel E., Cheeseman C.R., 2014. Lightweight mortars containing expanded polystyrene and paper sludge ash, Construction and Building Materials, 61, 285-292.

Ferraris M., Salvo M., Ventrella A., Buzzi L., Veglia M., 2009. Use of vitrified MSWI bottom ashes for concrete production. Waste Management, 29(3), 1041-1047

Ferraris M., Salvo M., Smeacetto F., Augier L., Barbieri L., Corradi A., Lancellotti I., 2001. Glass matrix composites from solid waste materials, J. Eur. Ceram. Soc., 21 (4), 453-460.

Ferrari S., Belevi H., Baccini P. Chemical speciation of carbon in municipal solid waste incinerator residues. Waste Management 22(3), 303-314.

Francis A.A., Abdel Rahman M.K., Daoud A., 2013. Processing, structures and compressive properties of porous glass-ceramic composites prepared from secondary by-product materials. Ceramics International 39(6), 7089-7095.

Furlani E., Tonello G., Maschio S., 2010. Recycling of steel slag and glass cullet from energy saving lamps by fast firing production of ceramics. Waste Management 30(8-9), 1714-1719.

Garrick N.W. and Chan K.-L., 1993. Evaluation of domestic incinerator ash for use as aggregate in asphalt concrete, Transportation Research Record 1418, 30-34.

German R.M., 1985. Liquid phase sintering. Plenum Press, New York.

Gertsakis J. and Lewis H., 2003. Sustainability & the Waste Management Hierarchy; a discussion paper on the waste management hierarchy and its relationship to sustainability. Melbourne, Australia: Eco recycle Victoria

Giegrich J, and Vogt R., 2005. The contribution of Waste management to sustainable development in Germany. Umweltbundesamt Report FKZ 203 92 309, Berlin

Green D.J., 1998. An introduction to the mechanical properties of ceramics. Cambridge Solid State Science Series, Cambridge, UK.

Guimaraes A.L., Okuda T., Nishijima W., Okada M., 2006. Organic carbon leaching behaviour from incinerator bottom ash, J. Hazard. Mater. 137(2), 1096-1101.

He F., Fang Y., Xie J., Xie J., 2012. Fabrication and characterization of glass–ceramics materials developed from steel slag waste. Materials and Design 42, 198-203.

Hjelmar O., Holm P.E., Lehmann N.K.L., Asmussen O., Rose N., 1998. Background for utilisation of contaminated soil and residues. Miljoprojekt nr. 415, Danish Environmental Protection Agency, Copenhagen, Denmark.

Hjelmar O., Johnson A., Comans, R., 2010. Incineration: Solid Residues. In Christensen, T.H. (Ed.), Solid Waste Technology and Management, Chapter 8.4. John Wiley & Sons, Ltd, Chichester (ISBN: 978-1-405-17517-3).

Hoornweg D. and Bhada-Tata P., 2012. What a Waste? A Global Review of Solid Waste Management, Urban Development Series Knowledge Papers, No. 15

Hoornweg D., Bhada-Tata P., Kennedy C., 2013. Waste production must peak this century. Nature 502. pp. 615-617.

Hu B., Rem P., van de Winckel T., 2008. Fine Heavy Non-Ferrous and Precious Metals Recovery in Bottom Ash Treatment. ISWA knowledge database, paper 38.

Ingamells C.O., 1970. Lithium metaborate flux in silicate analysis. Analytica Chimica Acta 52(2), 323-334.

International Ash Working Group (IAWG) (1994). An international perspective on characterisation and management of residues from municipal solid waste incineration: Summary Report, International Conference Environmental Implications of Construction Materials and Technology Developments, Maastricht.

International Solid Waste Association Working Group on Thermal Treatment of Waste (ISWA-WGTT), Subgroup Bottom Ash from WTE- Plants, 2006. Management of Bottom Ash from WTE Plants: An overview of management options and treatment methods.

Jing Z., Fan X., Zhou L., Fan J., Zhang Y., Pan X., Ishida E.H., 2013. Hydrothermal solidification behaviour of municipal solid waste incineration bottom ash without any additives. Waste Management, 33(5), 1182-1189

Johnson K.E. and Knights B., 1995. Leaching testing of MSWI bottom ash and stabilised products. Journal of Waste Management and Resource Recovery 2(3), 123-131.

Kaplan, P.O., J. Decarolis, and S. Thorneloe, 2009. Is it better to Burn or Bury Waste for Clean Electricity Generation? Environmental Science Technology, 43, 1711-1717.

Karamanov A., Schabbach L.M., Karamanova E., Andreola F., Barbieri L., Ranguelov B., Avdeev G., Lancellotti I., 2014. Sinter-crystallization in air and inert atmospheres of a

glass from pre-treated municipal solid waste bottom ashes. Journal of non-crystalline solids 389, 50-59.

Kaufman, S.M., N.J. Themelis, 2009. Using a direct method to characterize and measure flows of Municipal Solid Waste in the United States. Journal Air & Waste Management. Assoc. 59: 1386-1390.

KEZO facility Zurich Annual Report, 2011. Waste and Resource Management: Practical, Economic, Innovative.

Kockal N.U., Oztruan T., 2011. Optimization of properties of fly ash aggregates for high-strength lightweight concrete production. Materials and Design 32(6), 3586-3593.

Kourti I., Cheeseman C.R., 2010. Properties and microstructure of lightweight aggregate produced from lignite coal fly ash and recycled glass. Resources, Conservation and Recycling 54(11), 769-775.

Koralewska R., Cheeseman Ch., Bourtsalas A.C., 2014. Metal Recovery and Reuse of the Mineral Fine Fraction from dry-discharged bottom ashes. International VDI Conference – Metals and Minerals Recovery from IBA, Düsseldorf October 14-15.

Kosson D.S. and Garrabrants A.C. 2002. An integrated framework for evaluating leaching in waste management and utilization of secondary materials. Environmental Engineering Science. 19(3): p. 159-204.

Koster R. and Vehlow J., 1998. Organische und anorganishce Kontaminaten in Mullverbrennungsschlacken. FZK-Nachrichten, 30, 139.

Kumar S., Singh K. K., Ramachandrarao, 2000. Synthesis of Cordierite from Fly Ash and Its Refractory Properties, Journal of Materials Science Letters 19, 1263-1265.

Kuo W., Liu C., Su D., 2013. Use of washed municipal solid waste incinerator bottom ash in pervious concrete. Cement and Concrete Composites, 37, 328-335.

Lancellotti I., Cannio M., Bollino F., Catauro M., Barbieri L., Leonelli C., 2015. Geopolymers: An option for the valorization of incinerator bottom ash derived “end of waste”. Ceramics International, 41(2), Part A, 2116-2123.

Lancellotti I., Ponzoni C., Barbieri L., Leonelli C., 2013. Alkali activation processes for incinerator residues management. Waste Management 33(8), 1740-1749.

Lin C., Chang W.K., Chang T.C., Lee C.H., Lin C.H., 2009. Recycling thin film transistor liquid crystal display (TFT-LCD) waste glass produced as glass–ceramics. Journal of Cleaner Production 17(16), 1499-1503.

Lin C., Weng M., Chang C., 2012. Effect of incinerator bottom-ash composition on the mechanical behaviour of backfill material. Journal of Environmental Management, 113, 377-382.

Lin C., Wu C., Ho H., 2006. Recovery of municipal waste incineration bottom ash and water treatment sludge to water permeable materials, Waste Management, 26 (9), 970-978.

Liu H., Lu H., Chen D., Wang H., Xu H., Zhang R., 2009. Preparation and properties of glass–ceramics derived from blast-furnace slag by a ceramic-sintering process. Ceramics International 35(8), 3181-3184.

Liu Z.-S., Li W.-K., Huang C.Y., 2014. Synthesis of mesoporous silica materials from municipal solid waste incinerator bottom ash. Waste Management 34(5), 893-900.

Manfredi S., Tonini D., Christensen T.H., 2009. Landfilling of waste: accounting of greenhouse gases and global warming contributions. Waste Manage Research. 27, 825-836

Matthews, E. and N.J. Themelis, 2007. "Potential for reducing global methane emissions from landfills". Proceedings Sardinia 2007, 11th International Waste Management and Landfill Symposium, Cagliari, Italy, 1–5 October 2007, pp. 2000-2030.

Meima J.A. and Comans R.N.J., 1997. Geochemical modelling of weathering reactions in municipal solid waste incinerator bottom ash. Environmental Science and Technology, 31(5), 1269-1275.

Meima J.A., van der Weijden R.D., Eighmy T.T., Comans R.N.J., 2002. Carbonation processes in municipal solid waste incinerator bottom ash and their effect on the leaching of copper and molybdenum. Applied Geochemistry, 17, 1503–1513.

Menezes R.R., Malzac Neto H.G., Santana L.N.L., Lira H.L., Ferreira H.S., Neves G.A., 2008. Optimization of wastes content in ceramic tiles using statistical design of mixture experiments. Journal of the European Ceramic Society 28 (16), 3027-3039.

Morf L.S., Di Lorenzo F., Skutan S., Böni D., Haupt M., Haag O., Gloor R., 2013. Precious metals and rare earth elements in municipal solid waste – sources and fate in a Swiss incineration plant. Waste Manage. 33, 634–644

Morrell R., 1985. Handbook of properties of technical and engineering ceramics. Part 1: An introduction for the engineer and designer, HMSO, London, pp. 126-134.

Muchova L., 2010. Wet Physical Separation of MSWI Bottom Ash. (PhD thesis) Technical University of Delft, Delft, the Netherlands.

Muller U., Rubner K., 2006. The microstructure of concrete made with municipal waste incinerator bottom ash as an aggregate component. Cement and Concrete Research, 36(8), 1434-1443.

Myers R.H., Montgomery D.C., Anderson-Cook C.M., 2009. Response Surface Methodology: process and product optimisation using designed experiments (3rd edition). John Wiley and Sons, New Jersey.

Nardi J.V., Acchar W., Hotza D., 2004.Enhancing the properties of ceramic products through mixture design and response surface analysis. Journal of European Ceramic Society, 24, 375-379.

Nixon J.D., Wright D.G., Dey P.K., Ghosh S.K., Davies P.A., 2013. A comparative assessment of waste incinerators in the UK. Waste Management 33, 2234-2244.

Nzihou A., Themelis N., Kemiha M., Benhamou Y., 2012. Dioxin emissions from municipal solid waste incinerators (MSWIs) in France. Waste Management, 32(12), 2273-2277.

Olsson S., Karrmann E., Gustafsson P.J., 2006. Environmental system analysis of the use of bottom ash from incineration of municipal waste for road construction. Resource Conservation Recycling, 48, 26-40

Onori R., Polettini A., Pomi R., 2011. Mechanical properties and leaching modelling of activated incinerator bottom ash in Portland cement blends. Waste Management 31 (2), 298-310.

Park J.S., Park Y.J., Heo J., 2007. Solidification and recycling of incinerator bottom ash through the addition of colloidal silica (SiO_2) solution. Waste Management, 27(9), 2007, 1207-1212.

Pavasars I., 2000. Composition of organic matter in bottom ash from MSWI, in: Waste Materials in Construction (Wooley G.R. *et al.* eds.), Elsevier, Amsterdam, pp. 241-246.

Pecqueur G., Crignon C., Quénée B., 2001. Behaviour of cement-treated MSWI bottom ash. Waste Management. 21, 229–233

Pelino M., Karamanov A., Pisciella P., Crisucci S., Zonetti D., 2002. Vitrification of electric arc furnace dusts. Waste Management 22(8), 945-949.

Pfrang- Stotz G., Schneider J., 1995. Comparative studies of waste combustion bottom ashes from various grate and firing systems, conducted with respect to mineralogical and geochemical methods of examination, Waste Management Resources 13, 273-292.

Pfrang- Stotz G., Reichelt J., Roos R., 2000. Chemical- mineralogical valuation of the leachate potential of municipal solid waste incineration (MSWI) bottom ashes, in: Waste Materials in Construction (Wooley G.R. *et al.* eds.), Elsevier, Amsterdam, pp 975-983.

Polettini A., Polettini S., Pomi R., Sirini P., 2000. Physical properties and acid neutralisation capacity of incinerator bottom ash- Portland cement mixtures, in: Waste Materials in Construction (Wooley G.R. et al. eds.), Elsevier, Amsterdam, pp.791-802.

Polettini A., Pomi R., Fortuna E., 2009. Chemical activation in view of MSWI bottom ash recycling in cement-based systems. Journal of Hazardous Materials, 162(2–3), 1292-1299.

Polettini A., Pomi R., 2004. The leaching behaviour of incinerator bottom ash as affected by accelerated ageing. Journal of Hazardous Materials, 113(1-3), 209-215.

Ponsot I., Bernardo E., 2013. Self-glazed glass ceramic foams from metallurgical slag and recycled glass. Journal of Cleaner Production 59, 245-250.

Porteous A., 2005. Why energy from waste incineration is an essential component of environmentally responsible waste management. Waste Management 25(4), 451-459.

Qiao X.C., Ng B.R., Tyrer M., Poon C.S., Cheeseman C.R., 2008a. Production of lightweight concrete using incinerator bottom ash. Construction and Building Materials 22(4), 473-480.

Qiao X.C., Tyrer M., Poon C.S., Cheeseman C.R., 2008b. Novel cementitious materials produced from incinerator bottom ash. Resources, Conservation and Recycling, 52(3), 496-510.

Quenee B., Li G., Siwak J.M. and Basuyau V., 2000. The use of MSWI bottom ash as aggregates in hydraulic concrete, in: Waste Materials in Construction, Elsevier, Amsterdam, pp. 422-437.

Quinn G.D., 1998. Hardness testing of ceramics. Advanced materials and processing 8. 23-27.

Rambaldi E., Esposito L., Andreola F., Barbieri L., Lancellotti I., Vassura I., 2010. The recycling of MSWI bottom ash in silicate based ceramics. Ceram Int., 36 (8), 2469-2476.

Rani A., Boccaccini A.R., Deegan D., Cheeseman C.R., 2008. Air pollution control residues from waste incineration: Current UK situation and assessment of alternative technologies. Waste Management, 28(11), 2279-2292.

Rawlings R.D., Wu J.P., Boccaccini A.R., 2006. Glass ceramics: Their production from wastes - A review. J Mater Sci., 41 (3), 733-761.

Reich J., Pasel C., Herbell J-D, Luckas M., 2002. Effects of limestone addition and sintering on heavy metal leaching from hazardous waste incineration slag, Waste Management 22, 315-326.

Reijinders, L., 2005. Disposal, uses and treatment of combustion residues: a review. *Resources Conservation Recycling*.43, 313-336.

Reitman, D.O., 2013. "CEWEP Energy Report II (Status 2007-2010)". Available from, http://www.cewep.eu/m_1069

Richerson D.W., 1982. Modern Ceramic Engineering. Properties, processing and use in design, M. Dekker, USA.

Rivard-Lentz D.J., 1998. Incinerator bottom ash as a soil substitute: physical and chemical behavior, Fuel and Energy Abstracts 39 (1), 28.

Romero M., Rawlings R.D., Rincσn J.M., 1999. Development of a new glass-ceramic by means of controlled vitrification and crystallisation of inorganic wastes from urban incineration, Journal of European Ceramic Society 19, 2049-2058.

Romero M., Rincσn J.M., Rawlings R.D., Boccaccini A.R., 2001. Use of vitrified urban incinerator waste as raw material for production of sintered glass-ceramics, Mater Res Bull. 36 (1-2), 383-395.

Rozenstrauha I., Lodins E., Krage L., Drille M., Balode M., Putna I., Filipenkov V., Chinnam R.K., Boccaccini A.R., 2013. Functional properties of glass–ceramic composites containing industrial inorganic waste and evaluation of their biological compatibility. Ceramics International 39(7), 8007-8014.

Sabbas T., Polettini A., Pomi R., Astrup T., Hjelmar O., Mostbauer P., Cappai G., Magel G., Salhofer S., Speiser C., Heuss-Assbichler S., Klein R., Lechner P., 2003. Management of municipal solid waste incineration residues, Waste Management, 23 (1), 61-88.

Santos R., Mertens G., Salman M., Cizer O., van Gerven T., 2013. Comparative study of ageing, heat treatment and accelerated carbonation for stabilization of municipal solid waste

incineration bottom ash in view of reducing regulated heavy metal/metalloid leaching. Journal of Environmental Management, 128,807-821.

Schabbach L.M., Andreola F., Karamanova E., Lancellotti I., Karamanov A., Barbieri L., 2011. Integrated approach to establish the sinter-crystallization ability of glasses from secondary raw material. Journal of non-crystalline solids 357, 10-17.

Schabbach L.M., Andreola F., Barbieri L., Lancellotti I., Karamanova E., Ranguelov B., Karamanov A., 2012. Post-treated incinerator bottom ash as alternative raw material for ceramic manufacturing. Journal of the European Ceramic Society, 32 (11), 2843- 2852.

Schabbach L.M., Bolelli G., Andreola F., Lancellotti L., Barbieri L., 2012. Valorisation of MSWI bottom ash through ceramic glazing process: a new technology. Journal of Cleaner Production, 23(1), 147-157.

Schneider J., Vehlow J. and Vogg H., 1994. Improving the MSWI bottom ash quality by simple in-plant measures, in: Environmental Aspects of Construction with Waste Materials, (Goumans J.J.J.M. et al. eds.), Elsevier, Amsterdam, pp. 605-620.

Schreurs J.P.G.M., van der Sloot H.A., Hendriks Ch., 2000. Verification of laboratory field leaching behaviour of coal fly ash and MSWI bottom ash as a road base material, Waste Manag. 20 (2-3), 193-201.

Selinger A., Schmidt V., Bergfeldt B., Vehlow J. And Simon F.-G., 1997. Investigation of sintering processes in bottom ash to promote their reuse in civil construction. Parts 1&2, in: Waste Materials in Construction: Putting theory into practice (Goumanns J.J.J. et al eds.), Elsevier, Amsterdam, pp. 41-58.

Song Y., Li B., Yang E., Liu Y., Ding T., 2015. Feasibility study on utilization of municipal solid waste incineration bottom ash as aerating agent for the production of autoclaved aerated concrete. Cement and Concrete Composites, 56, 51-58.

Sorensen M.A., Mogensen E.P.B., Lundtrop K., Jensen D.L., Christensen T.H., 2001. High temperature co-treatment of bottom ash and stabilised fly ashes from waste incineration, Waste Management 21, 555-562.

Stern K.H., Weise E.L., 1966. High temperature properties and decomposition of inorganic salts, Part 1: Sulphates, NSRDS- National Bureau of Standards 7, USA.

Summary of the Clean Air Act, 42 U.S.C. §7401 et seq., 1970.

Summary of the Resource Conservation and Recovery Act, 42 U.S.C. §6901 et seq., 1976.

Tang B., Lin J., Qian S., Wang J., Zhang S., 2014. Preparation of glass–ceramic foams from the municipal solid waste slag produced by plasma gasification process. Materials Letters 128, 68-70.

Tchobanoglous G., Theisen H., and Vigil S., 1993. lntegrated Solid Waste Management", Chapter 4, McGraw-Hill, New York.

Themelis N.J., Diaz Barriga M.E., Estevez P., Velasco M. G., 2012. Guidebook for the Application of Waste to Energy technologies in Latin America and the Caribbean. Inter-American Development Bank. Earth Engineering Centre, Columbia University. Available from http://www.seas.columbia.edu/earth/wtert/pressreleases/Guidebook_WTE_v5_July25_2013.pdf

Themelis N., Bourtsalas A., 2013. UK Waste Management: Growing old or growing clean? Waste Management World, 14(3).

Themelis N., Ulloa P., 2007. Methane generation in landfills. Renewable Energy 32, 1243-1257.

Thompson M. and Walsch J.N., 1989. Handbook of Inductively Coupled Plasma Spectrometry (2nd edition), Blackie, London, pp. 316.

Toller S, Karrman E, Gustafsson J.P, Magnusson Y., 2009. Environmental assessment of incinerator residue utilisation. Waste Management. 29(7), 2071- 2077.

Ullner C., Germak A., Le Doussal H., Morrel R., Reich T. , Vandermeulen W., 2001.Hardness testing on advanced technical ceramics. Journal of the European Ceramic Society 21(4), 439-451.

Valle-Zermeño R., Formosa J., Prieto M., Nadal R., Niubó M., Chimenos J.M., 2014. Pilot-scale road subbase made with granular material formulated with MSWI bottom ash and stabilized APC fly ash: Environmental impact assessment. Journal of Hazardous Materials, 266,132-140.

Van der Sloot H.A., 1990. Leaching behaviour of waste and stabilised waste materials; characterisation from environmental assessment purposes, Waste Management and Research 8(3), 215-228.

Van der Sloot H.A., Heasman L., Quevauviller Ph., 1997. Harmonisation of leaching/ extraction tests, in: Studies in Environmental Science, vol. 70, Elsevier Science B.V: Amsterdam.

Van der Sloot H.A., Kosson D.S., Hjelmar O., 2001. Characteristics, treatment and utilisation of residues from municipal waste incineration, Waste Management 21, 753-765.

Van der Sloot H.A. and Kosson D.S., 2012. Use of characterisation leaching tests and associated modelling tools in assessing the hazardous nature of wastes. Journal of Hazardous Materials, 207-208, 36-43

Van Gerven T., Van Keer E., Arickx S., Jaspers M., Wauters G., Vandecasteele C., 2005. Carbonation of MSWI bottom ash to decrease heavy metal leaching, in view of recycling. Waste Management 25, 291–300.

Van Haaren R. and Themelis N., 2010. "Columbia/BioCycle U.S. survey". BioCycle. Available from, http://www.seas.columbia.edu/earth/wtert/sofos/SOG2010.pdf

Vasugi V., Ramamurthy K., 2014. Identification of admixture for palletisation and strength enhancement of sintered coal pond ash aggregate through statistically designed experiments. Materials and Design 60, 563-575.

Vehlow J., Bergfeldt B., Hunsinger H., 2006. PCDD/F and related compounds in solid residues from municipal solid waste incineration- a literature review. Waste Management and Research 24. 404-420.

Vehlow J., 2015. Air pollution control systems in WtE units: An overview. Waste Management, 37, 58-74.

Velis C., Franco-Salinas C., O' Sullivan C., Najorka J., Boccaccini A.R., Cheeseman C.R., 2014. Up-Cycling Waste Glass to Minimal Water Adsorption/Absorption Lightweight Aggregate by Rapid Low Temperature Sintering: Optimization by Dual Process-Mixture Response Surface Methodology. Environ Sci Technol, 48, 7527-7535.

Virta R.L., 2003. Clay and Shale. U.S. Geological Survey Minerals yearbook.

Xiao Y., Oorsprong O., Yang Y., Voncken J.H.L., 2008. Vitrification of bottom ash from a municipal solid waste incinerator. Waste Management, 28(6), 1020-1026.

Wang K.-S., Chiang K.-Y., Perng J.-K., Sun C.-J., 1998. The characteristics study on sintering of municipal solid waste incinerator ashes. Journal of Hazardous Materials 59 (2-3), 201-210.

Wang K.-S., Sun C.-J., Liu C.-Y., 2001. Effects of the type of sintering atmosphere on the chromium leachability of thermal-treated municipal solid waste incinerator fly ash. Waste Management 21, 85-92.

Wang Z., Ni W., Jia Y., Zhu L., Huang X., 2010. Crystallization behaviour of glass ceramics prepared from the mixture of nickel slag, blast furnace slag and quartz sand. Journal of non-crystalline solids 356(31-32), 1554-1558.

Whiston C., 1987. X-Ray Methods, J. Whiley and Sons, UK.

Wiles C.C. (1996), Municipal solid waste combustion ash: State-of-the-knowledge, Journal of Hazardous Materials 47, 325-344.

Wiles C. and Shepherd P., 1999. Beneficial use and recycling of municipal waste combustion residues- A comprehensive resource document, NREL/ BK-570-25841, National Renewable Energy Laboratory, Golden, Co.

World Commission on Environment and Development (WCED), 1987. Our Common Future. Oxford University Press.

World Economic Forum, 2015. Global Risks 2015, 10th edition. Available at: http://www.academia.edu/10310304/World_Economic_Forum_Global_Risks_2015

Wunsch P., Greilinger C., Bieniek D., Kettrup A., 1996. Investigation of the binding of heavy metals in thermally treated residues from waste incineration, Chemosphere 32 (11), 2211-2218.

Yang J., Zhang D., Hou J., He B., Xiao B., 2008. Preparation of glass-ceramics from red mud in the aluminium industries. Ceramics International 34(1), 125-130.

Yao J., Li W.B., Tang M., Feng C.R., Shen D.S., 2010. Effect of weathering treatment on the fractionation and leaching behaviour of copper in municipal solid waste incinerator bottom ash. Chemosphere 81(5), 571-576.

Yoon S.D., Lee J.U., Lee J.H., Yun Y.H., Yoon W.J., 2013. Characterization of Wollastonite Glass-ceramics Made from Waste Glass and Coal Fly Ash. Journal of Materials Science and Technology 29(2), 149-153.

Zevenbergen C., Comans R.N.J., 1994. Geochemical factors controlling the mobilisation of major elements during weathering of bottom ash, in: Environmental Aspects of Construction with Waste Materials, Elsevier, Amsterdam, pp.179-194.

Zhang J., Dong W., Li J., Qiao L., Zheng J., Sheng J., 2007. Utilization of coal fly ash in the glass–ceramic production. Journal of Hazardous Materials 149(2), 523-526.

References

Zhang H., He P.-J., Shao L.-M., Li X-J., 2008. Leaching behaviour of heavy metals from municipal solid waste incineration bottom ash and its geochemical modelling. Journal of Materials Cycle and Waste Management 10, 7-13.

Zhang Z., Zhang L., Li A., 2015. Development of a sintering process for recycling oil shale fly ash and municipal solid waste incineration bottom ash into glass ceramic composite. Waste Management 38, 185-193.

Zhao Y., Chen D., Bi Y., Long M., 2012. Preparation of low cost glass–ceramics from molten blast furnace slag. Ceramics International 38(3), 2495-2500.

References from web

Confederation of Waste-to-Energy Plants (CEWEP):
http://cewep.eu/information/data/studies/m_1224

CEWEP: Information for landfill tax:
http://www.cewep.eu/media/www.cewep.eu/org/med_557/955_2012-04-27_cewep_-_landfill_taxes__bans_website.pdf

Day Group official website: Information for Incinerator Bottom Ash Aggregates:
http://www.daygroup.co.uk/incinerator-bottom-ash-aggregate.php

Day Group official website: Information for EcoSand
http://www.daygroup.co.uk/eco-sand.php

Dow Chemical Company official website: Information on Polyethylene Glycol-8000 binder:
http://msdssearch.dow.com/PublishedLiteratureDOWCOM/dh_0887/0901b80380887913.pdf?filepath=polyglycols/pdfs/noreg/118-01806.pdf&fromPage=GetDoc

Ellen MacArthur Foundation, 2014-last update, Principles of the circular economy:
http://www.ellenmacarthurfoundation.org/circular-economy/circular-economy.

Environmental Protection Agency (EPA), 'Air Emissions from MSW Combustion Facilities':
http://www.epa.gov/wastes/nonhaz/municipal/wte/airem.htm

References

Environmental Protection Agency website. ‘MSW statistics’:
http://www.epa.gov/ttnatw01/eparules.html

Eurostat (2013), ‘Municipal Solid Waste Statistics: Generation and treatment of MSW in the European Union’:
http://ec.europa.eu/eurostat/statistics-explained/index.php/Municipal_waste_statistics

FEVE, 2014-last update, Glass recycling statistics:
http://www.feve.org/index.php?option=com_content&view=article&id=10&Itemid=11.

FEVE, 2014-last update, Glass statistics Europe 1990 to 2012:
http://www.feve.org/FEVE-Glass-Recycling-Stats-Year-2012/Decoupling-1990-to-2012.pdf.

Hitachi Zosen Inova official website: Information for Newhaven EfW plant:
http://www.hz-inova.com/cms/images/stories/pictures/download/hzi_ref_newhaven_en.pdf

Leaching test description (H. Van der Sloot, 2015):
http://www.leaching.net/leaching/test-methods/

Lenntach, 2014-last update, Glass:
http://www.lenntech.com/glass.htm

Martin Gmbh official website: ‘Dry discharge system’:
http://www.martingmbh.de/en/dry-discharge-system.html

SATOM Monthey Energy from Waste plant:
http://www.satom-monthey.ch/Satom/

SELCHP plant in East London:
http://www.selchp.co.uk/energy-recovery/combined-heat-and-power/

References

Viridor official website: Information for Lakeside EfW plant:
http://www.viridor.co.uk/our-operations/recovery/energy-from-waste/lakeside-efw/

WRAP, 2014-last update, Glass:
http://www.wrap.org.uk/content/glass-3

Appendix A: Images of samples produced with uncalcined and calcined powders

Images of samples produced with uncalcined and calcined powders are presented in Figures A1 and A2, accordingly. Samples produced with calcined powders exhibited minimal linear shrinkage compared to samples produced with uncalcined powders. In addition, samples produced with uncalcined powders tend to deform during sintering, making the production of tile s difficult to control.

Figure A1. Photograph of sample produced with uncalcined 80 wt. % dry discharged fine IBA dust: 20 wt. % glass and sintered at 1080 °C

Figure A2. Photograph of sample produced with calcined at 1080 °C 80 wt. % dry discharged fine IBA dust: 20 wt. % glass and sintered at 1080 °C (optimum ceramic)

Appendix B: Effect of discharge technique on the milling of the fine materials

After milling for 8 h the slurry was passed through 500 µm sieve and the residue collected on the sieves washed and dried. The amount greater than 500 µm is shown for each fine fraction used in Figure A1. This typically represents about 10 to 15% of the original <4 mm wet discharged fraction and mainly consists of rounded glass and other difficult to mill materials, such as rock, bone, wood, some plastic and metal, mainly Copper. The dry discharged fine IBA fraction exhibited negligible loses after milling and sieving to less than 500 µm, and this is believed to be due to the more efficient air separated technique used for the production of this material.

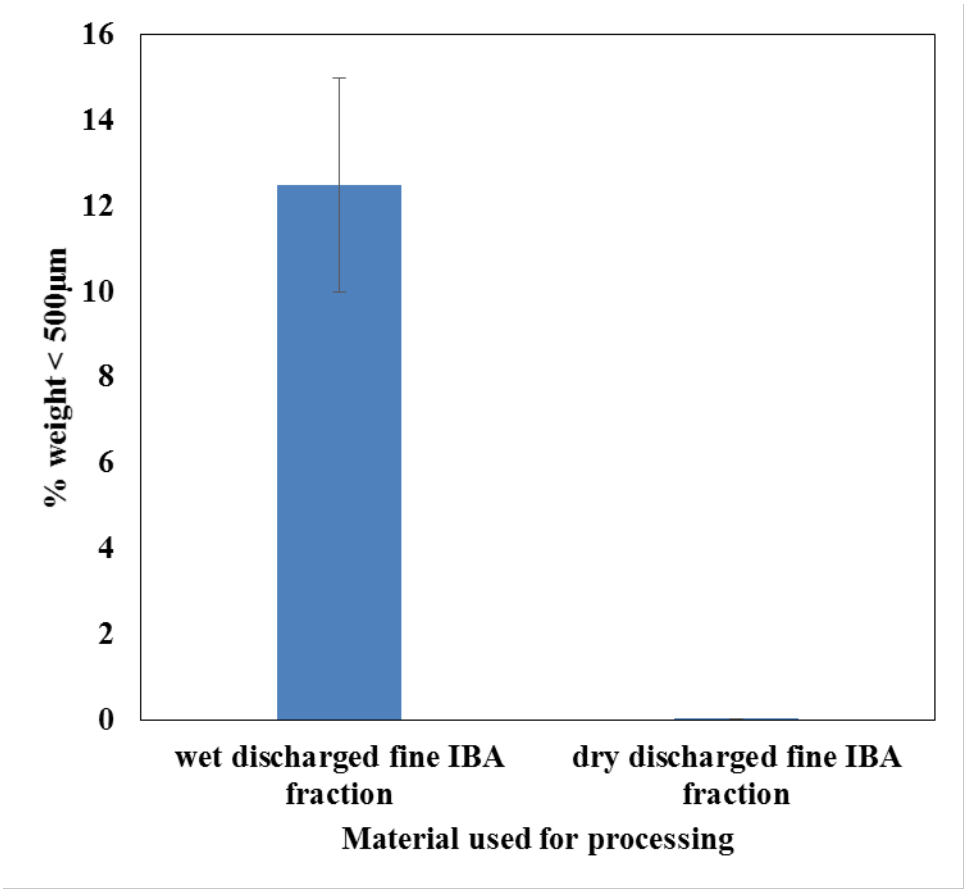

Figure B1. Percentage weight of coarse material retained on a 500 µm sieve after 24 h wet ball milling of the fine IBA fractions.